

TECTONO-STRATIGRAPHIC AND THERMAL EVOLUTION OF THE
HAYMANA BASIN, CENTRAL ANATOLIA, TURKEY

A THESIS SUBMITTED TO
THE GRADUATE SCHOOL OF NATURAL AND APPLIED SCIENCES
OF
MIDDLE EAST TECHNICAL UNIVERSITY

BY

ERHAN GÜLYÜZ

IN PARTIAL FULFILLMENT OF THE REQUIREMENTS
FOR
THE DEGREE OF DOCTOR OF PHILOSOPHY
IN
GEOLOGICAL ENGINEERING

OCTOBER 2015

Approval of the thesis:

**TECTONO-STRATIGRAPHIC AND THERMAL EVOLUTION OF THE
HAYMANA BASIN, CENTRAL ANATOLIA, TURKEY**

submitted by **ERHAN GÜLYÜZ** in partial fulfillment of the requirements for the degree of **Doctor of Philosophy in Geological Engineering Department, Middle East Technical University** by,

Prof. Dr. Gülbin Dural Ünver

Dean, Graduate School of **Natural and Applied Sciences**

Prof. Dr. Erdin Bozkurt

Head of Department, **Geological Engineering**

Prof. Dr. Nuretdin Kaymakcı

Supervisor, **Geological Engineering Dept., METU**

Examining Committee Members:

Prof. Dr. Erdin Bozkurt

Geological Engineering Dept., METU

Prof. Dr. Nuretdin Kaymakcı

Supervisor, Geological Engineering Dept., METU

Prof. Dr. Kadir Dirik

Geological Engineering Dept., HÜ

Prof. Dr. Bora Rojay

Geological Engineering Dept., METU

Assist. Prof. Dr. Erman Özsayın

Geological Engineering Dept., HÜ

Date: 28.10.2015

I hereby declare that all information in this document has been obtained and presented in accordance with academic rules and ethical conduct. I also declare that, as required by these rules and conduct, I have fully cited and referenced all material and results that are not original to this work.

Name, Surname: Erhan GÜLYÜZ

Signature:

ABSTRACT

TECTONO-STRATIGRAPHIC AND THERMAL EVOLUTION OF THE HAYMANA BASIN, CENTRAL ANATOLIA, TURKEY

Gülyüz, Erhan

Ph.D., Department of Geological Engineering

Supervisor: Prof. Dr. Nuretdin Kaymakçı

October 2015, 173 pages

The Haymana Basin is located on the southernmost tip of the Central Pontides and straddles between the İzmir-Ankara-Erzincan Suture Zone at the north and Intra-Tauride Suture Zone at the south. These suture zones designate the former positions of various branches of the Neotethys Ocean in Turkey, the basins evolved within these zones record the progressive closure of the Neotethys and the collision between Taurides, Kırşehir Block and Pontides during late Cretaceous to Eocene time interval. The Haymana Basin is one of the best area because of its crucial position and continuous Late Cretaceous to Middle Eocene marine deposits to unravel the evolution of the Neotethys.

In addition to Neogene cover units, four upper Cretaceous to Paleogene key sequences are defined based on depositional environments. These sequences grade laterally and vertically into each other and are continuous from the Late Cretaceous to Eocene whereas local progressive syn-sedimentary unconformities and frequent depocenter migrations are common. Additionally, post-middle Paleocene to middle Eocene sequences coarse upwards. These characteristics possibly reflect a response to local uplift and subsidence in front of south-verging thrust faults in a tectonic setting of transition from fore-arc to collisional settings, subsequent to the terminal subduction of the Neotethys at the end of early Paleocene.

The Haymana Basin is represented by two structural segments based on the trends of E–W and WNW–ESE directed structures at the south-eastern and north-western segments, respectively. The balanced cross-sections indicate ~4% and ~25 shortening at the north-western and south-eastern segments, respectively. The differences in amount of shortenings might be result of reduce in the effectiveness zone of Dereköy basin bounding thrust fault towards west and large vertical block rotations controlled by a strike-slip fault which might be the westward extension of Hirfanlar-Hacıbektaş fault zone into the Haymana basin that dissects the Kırşehir Block into two sectors. Fault kinematic analysis, based on 623 fault-slip data from 73 stations, indicates that the basin was subjected to initially N–S extension and then a N–S directed compression and coeval E–W extension during late Cretaceous–early Miocene time interval.

Thermo-chronometric samples collected from the basinfill were analyzed in order to unravel the thermal and exhumation history of the basin by using Apatite-Helium (AHe) dating and fission track length measurement techniques. AHe dating results indicate that the south-eastern segment of the basin started to uplift at least before 35.29 ± 3.5 Ma whereas north-western segment, 21.83 ± 2.2 Ma. Thermal models also show ~14 Ma differences in initiation of uplift in these two structural segments. They also indicate gradual subsidence until late Eocene (9.2m/kyr) and following rapid uplift (14.1m/kyr) until early Miocene for the south-eastern segment.

It is proposed that the Haymana Basin was a fore-arc basin developed at the southern margin of the Pontides along the northward subducted Neotethys Ocean, then after Paleocene, the basin evolved into foreland settings in front of a south-vergent fold and thrust belt developed during continental collision. Additionally the north-westward movement of Kırşehir Block caused the basin to rotate along vertical axes and promoted its exhumation.

Keywords: Haymana Basin, Central Anatolia, continental collision, fore-arc basin, thermo-chronology, paleostress analysis.

ÖZ

HAYMANA HAVZASININ TEKTONO-STRATİGRAFİK VE TERMAL EVRİMİ, ORTA ANADOLU, TÜRKİYE

Gülyüz, Erhan

Doktora, Jeoloji Mühendisliği Bölümü

Tez Yöneticisi: Prof. Dr. Nuretdin Kaymakcı

Ekim 2015, 173 sayfa

Haymana havzası Orta Pontidlerin en güney ucunda yer alır ve kuzeyde İzmir-Ankara-Erzincan kenet kuşağı, güneyde ise İç Torid kenet kuşağı ile sınırlanır. Bu kenet kuşakları Türkiye’de Neotetis Okyanus’unun birçok kolunun önceki konumlarını tanımlar ve bu kuşak içerisinde evrimleşen havzalar, Neotetis’in progresif kapanımını ve Toros-Kırşehir-Pontid blokları arasında geç Kretase–Eosen zaman aralığında gerçekleşen kıtasal çarpışmaya ait bilgileri kendi çökelleri içerisinde kayıt etmişlerdir. Haymana havzasının anahtar nitelikteki konumu ve sahip olduğu kesintisiz geç Kretase–orta Eosen denizsel çökelleri ile Neotetis’in bölgedeki evrimini anlamada yardımcı olabilecek en önemli alanlardan biridir.

Havzada Neojen örtü birimlerine ek olarak, havza birimlerinin depolanma ortamları göz önünde bulundurularak geç Kretase–Paleojen zaman aralığı için dört anahtar stratigrafik sekans tanımlanmıştır. Bu sekanslar arasında lokal olarak sedimantasyonla eş zamanlı gelişen uyumsuzlukların ve beslenme merkezinin hareket etmesinin izlenmesi dışında, sekanslar geç Kretase–Eosen zaman aralığında süreklidirler ve birbirleri arasında yatayda ve düşeyde geçişlidirler. Ek olarak orta Paleosen sonrasında orta Eosen öncesine kadar olan sekanslarda üst seviyelere doğru tane boyları büyümektedir. Bu özellikler erken Paleosen sonunda Neotetis dalma-batma zonunun yitimini takiben gerçekleşen yay-önü ortamdan kıtasal çarpışma ortamına geçişle alakalı olarak aktifleşen ve güneye hareket eden bindirme faylarının önünde meydana gelen lokal yükselim-alçalım olaylarını muhtemelen yansıtmaktadır.

Haymana Havzası sırasıyla kuzeybatısındaki D–B uzanımlı ve güneydoğusundaki BKB–DGD uzanımlı olmak üzere iki yapısal segmentler ile temsil edilir. Balans edilmiş jeolojik kesitlerde, kuzeybatı segmentte ~%4, güneydoğu segmentte ise ~%25 daralma göstermektedir. Bu segmentlerdeki majör değişimler havzayı sınırlayan Dereköy bindirme fayının etki alanının batıya doğru azalması ve Kırşehir bloğunu iki sektöre ayıran Hirfanlar-Hacıbektaş fay zonunun olası batı uzanımı olarak hareket eden doğrultu atımlı bir fayın kontrol ettiği büyük ölçekli dikey blok rotasyonların sonucu ile açıklanabilir. 73 istasyondan alınan 623 fay çiziği verisiyle hazırlanan kinematik analizler havzanın geç Kretase–erken Miyosen zaman aralığında ilksel olarak K–G genişlemeye sonrasında ise K–G sıkışma ve eş zamanlı gelişen D–B genişlemeye maruz kaldığını göstermektedir.

Apatit-Helyum (AHe) yaşlandırma ve fizyon izi boy ölçümü teknikleri kullanılarak havzanın termal ve yükselim geçmişinin aydınlatılması amacıyla havza birimlerinden alınan termo-kronometrik örnekler analiz edilmiştir. AHe yaşlandırma sonuçları havzanın güneydoğu segmentinin en azından 35.29 ± 3.5 milyon yıl önce yükselmeye başladığını gösterirken kuzeybatı segmentte yükselime başlamanın en azından 21.83 ± 2.2 milyon yıldan önce olduğunu göstermektedir. Termal modeller segmentlerdeki yükselimlerin başlamaları arasında yaklaşık 14 milyon yıllık farkın olduğunu göstermektedir. Ek olarak bu modeller havzanın güneydoğu segmentinin geç Eosen'e kadar dereceli olarak gömüldüğünü (9.2m/ky) sonrasında ise erken Miyosen'e kadar hızlı bir şekilde yükseldiğini (14.1m/ky) göstermektedir.

Bu çalışmada, Haymana Havzasının kuzeye dalan Neotetis Okyanusu boyunca Pontid Bloğunun güney marjinde yay-önü havza olarak geliştiği, Paleosen'den itibaren kıtasal çarpışma döneminde gelişen kıvrım-bindirme kuşağının önünde uzak-ülke tektonik koşullarında evrimleştiği önerilmektedir. Ek olarak Kırşehir Bloğunun kuzeybatı hareketi havzanın dikey ekseninde rotasyona uğramasına neden olmuş ve yükselime etki etmiştir.

Anahtar Kelimeler: Haymana Havzası, Orta Anadolu, kıtasal çarpışma, yay-önü havza, termo-kronoloji, paleostres analizi.

To all mothers in my life: Cevriye, Nurcan, Aynur and Nilay

ACKNOWLEDGEMENTS

This thesis could not have been completed without helps and supports of many people.

First of all, I would like to thank my supervisor Dr. Nuretdin Kaymakcı for his inestimable critics and supports. Without his education philosophy which encouraged me to be independent in all steps of the thesis, I could not feel more self-confident for the next projects. I was lucky because I have benefited from the opportunity of his wide knowledge and perspective about geological problems, when I needed.

My Ph.D. committee members, Dr. Erdin Bozkurt, Dr. F. Bora Rojay, Dr. Kadir Dirik and Dr. Erman Özsayın are deeply thanked for their helps, supports, and willingness to improve the quality of my thesis. Their critical comments with external perspectives on research have guided me to stay on the right line.

I would like to express my gratitude to Dr. Cristina Persano and Dr. Finlay Stuart who helped me a lot by spending their valuable times to educate and train me for thermo-chronology studies. I also would like to thank them for opening their laboratories for my research.

A special thanks to Dr. Ercan Özcan, Dr. Demir Altıner, Aynur Hakyemez and Mustafa Yücel Kaya for their helps during paleontological studies.

My hard and long field studies could not have been completed without the help of Murat Özkaptan. A special thanks to Mustafa Kaplan, who helped me a lot during field and office works. Thank you very much my friends.

I would like to gratefully acknowledge the Yüzüncü Yıl University (Van, Turkey) and ÖYP research foundation for their financial supports.

At last but definitely not the least, I would like to express my grateful thanks to my family members; Erdoğan Gülyüz, Nurcan Gülyüz, Şevket Yağcıoğlu, Aynur

Yağcıođlu, and my brother Semih Yağcıođlu for their supports, encouragements and endless patience during this study, and a special thanks go to my wife Nilay Gülyüz for her understanding, patience, love and endless support.

Final thanks go to my son Doruk Gülyüz, who made his appearance into this world at the middle of this study, and has made his Mum and Dad very happy.

TABLE OF CONTENTS

ABSTRACT.....	v
ÖZ	vii
ACKNOWLEDGEMENTS	xi
TABLE OF CONTENTS	xiii
LIST OF TABLES	xviii
LIST OF FIGURES	xix
CHAPTERS	
1 INTRODUCTION.....	1
1.1 Aim of the Study	1
1.2 Methods of the Study	2
1.3 Layout of the Thesis	4
1.4 Tectonic Setting of the Haymana Basin	4
1.4.1 Basement: Crystalline Rocks	5
1.4.1.1 Ophiolites and Ophiolitic Rocks	5
1.4.1.1.1 Central Anatolian Ophiolites (CAO)	6
1.4.1.1.2 Ankara Imbricate Zone (AIZ).....	7
1.4.1.1.3 Tauride Ophiolites	8
1.4.1.2 Metamorphic Rocks around the Haymana Basin.....	8
1.4.1.2.1 Metamorphic Rocks on Pontides	9
1.4.1.2.2 Central Anatolian Metamorphic Rocks	10
1.4.1.2.3 Tauride–Anatolide Platform Metamorphics (TAPM)	11
1.4.1.3 Magmatic Rocks around the Haymana Basin	12

1.4.1.3.1	Northern Magmatic Complex (Pontide Arc Complex)	12
1.4.1.3.2	Southern Margin Magmatic Complex	14
1.4.2	Late Cretaceous–Paleogene Sedimentary Basins Around Haymana Basin	15
1.4.2.1	Basins Located in the Pontides	16
1.4.2.1.1	Albian to Paleocene	16
1.4.2.1.2	Paleocene to Oligocene Period	17
1.4.2.2	Basins Located on the Northern margins of Taurides and Kırşehir Block	18
1.4.2.2.1	Basins Related to İAESZ	20
1.4.2.2.2	Basins Related to ITSZ	22
1.5	Previous Works	24
2	STRATIGRAPHY	27
2.1	Basement Units	30
2.1.1	Metamorphic Rocks	30
2.1.2	Upper Jurassic–Lower Cretaceous Platform Sequences	30
2.1.3	Late Cretaceous Ophiolitic Units	33
2.2	Late Cretaceous to Eocene Basinfill Units	36
2.2.1	First Cycle	37
2.2.1.1	Haymana Formation	37
2.2.1.2	Beyobası Formation	41
2.2.2	Second Cycle	42
2.2.2.1	Kartal Formation	42

2.2.2.2	Çaldağ Formation.....	46
2.2.2.3	Yeşilyurt Formation	47
2.2.3	Third Cycle.....	50
2.2.3.1	Kırkkavak Formation	50
2.2.3.2	İlgınlıkdere Formation	53
2.2.3.3	Eskipolatlı Formation.....	56
2.2.4	Fourth Cycle.....	60
2.2.4.1	Beldede Formation.....	60
2.2.4.2	Çayraz Formation.....	62
2.2.4.3	Yamak Formation	65
2.3	Neogene Units and Quaternary Alluvium.....	68
3	STRUCTURAL CHARACTERISTICS OF THE BASIN	71
3.1	Folds and Bedding.....	72
3.2	Faults	75
3.3	Fault Kinematics (Paleostress Inversion).....	82
3.3.1	Method and Data	82
3.3.2	Spatio-Temporal Characteristics of Paleostress Inversion Solutions.....	90
3.4	Cross-Sections and Balancing.....	98
3.4.1	Methods and Data.....	98
3.4.2	Characteristics of the Balanced Cross-Sections	100
4	THERMO-CHRONOLOGY (AHe DATING)	105
4.1	Method and Data	105
4.1.1	AHe dating	105

4.1.1.1	Sampling Strategies and Separation	107
4.1.1.2	Age Calculation Procedure	108
4.2	Fission Track Lengths and Their Measurements	108
4.3	AHe Age Results.....	110
4.3.1	Spatio-Temporal Characteristics of AHe Ages.....	115
4.4	Results of Fission Track Length Measurements and Time-Temperature Modelling	116
4.4.1	Interpretation of Time–Temperature Models.....	118
5	DISCUSSION.....	121
5.1	Summary of Stratigraphic, Structural and Thermal Characteristics of the Haymana Basin	121
5.1.1	Characteristics of the Stratigraphical Data.....	121
5.1.2	Characteristics of the Structural Data and Paleostress Results	125
5.1.3	Characteristics of Thermo-Chronological Data	128
5.2	Spatio-Temporal Association of Neotethyan Central Pontide and Central Anatolian Basins, and the Haymana Basin	128
5.2.1	The Position of the Haymana Basin with respect to Subduction Along İAESZ	131
5.2.2	The Position of the Haymana Basin with respect to Subduction along ITO	132
5.2.3	The Position of the Haymana Basin with respect to Collision between Pontides and KB or Taurides	134

5.2.4	The Position of the Haymana Basin with respect to Collision between KB and Taurides	135
6	CONCLUSIONS.....	137
	REFERENCES.....	141
	APPENDICES	
	MAPS.....	165
	CURRICULUM VITAE.....	173

LIST OF TABLES

TABLES

Table 2.1: Contact relations between basinfill and the basement units.	37
Table 3.1 Results of fold analyses.	74
Table 3.2: Locations and the results of paleostress analyses (see Figure 3.12 for locations).	84
Table 4.1: Results of AHe age calculations (see Figure 4.1 for sample locations.	113
Table 4.2: Constraints of time–temperature modellings.	117
Table 4.3: Subsidence and uplift rate calculations.	119

LIST OF FIGURES

FIGURES

- Figure 1.1:** Geological setting of the Haymana Basin. (a) Major tectonic divisions of Anatolia (modified Görür *et al.*, 1984); (b) Mesozoic and Cenozoic basins in central and northern Anatolia, (c) simplified version of the basins (modified Görür *et al.* 1984, Özsayın and Dirik, 2007; Kaymakçı 2000; Kaymakçı *et al.* 2009). 1. Mudurnu, 2. Haymana, 3. Tuzgölü, 4. Ulukışla, 5. Ayhan and Çiçekdağı, 6. Sivas and 7. Çankırı basins. Rectangle shows the location of the study area..... 2
- Figure 1.2:** Map of Mesozoic ophiolitic rocks of the Central Anatolia. a: Önen (2013), b: Çelik *et al.* (2006), c: Çelik *et al.* (2011), d and g: Dilek *et al.* (1999), e: Rojay *et al.* (2004), f: Sarıfakıoğlu *et al.* (2013), h: Dilek and Moores (1990), i: Yalınz *et al.* (2000) 6
- Figure 1.3:** Metamorphic rocks around the study area. Red ages represents apatite-helium exhumation ages from the Central Anatolian metamorphic rocks (Whitney *et al.*, 2003). The green age represents syn-to peak metamorphic carphiolite Ar-Ar age from Anatolide-Tauride Platform metamorphic rocks (Pourteau, 2011). The blue age represents youngest subduction-related peak metamorphic muscovite Ar-Ar age from Central Pontide metamorphic rocks (Okay *et al.*, 2013). NM-Niğde Massif, KM-Kırşehir Massif, AM-Akdağ Massif..... 9
- Figure 1.4:** Magmatic rocks around the Haymana Basin. GVP-Galatian Volcanic Province, , KB-Kırşehir Block, TAP-Tauride-Anatolide Platform, MEVSB-Middle Eocene volcano-sedimentary belt, OG-Oymaağaç Granitoid (see text for references). 13
- Figure 1.5:** Geological map of Central Anatolia showing position of the Central Anatolian basins with respect to İzmir-Ankara-Erzincan and Intra-Tauride suture zones. BAB-Büyükkişla-Ayhan Basin, CB-Çankırı basin , HB-Haymana Basin, KBB-Kırıkkale-Bala Basin, TGB-Tuzgölü Basin, UB-Ulukışla Basin, YCB-Yozgat-Çiçekdağı Basin. (modified after MTA 2002 map). 19
- Figure 2.1:** (a) Regional map showing the location of the study area b) Geological map of the Haymana Basin (our own work and partly modified from MTA 2002).

Letters ‘a-b-c-d-e-f-g-h-i-j-k-l-m’ shows the locations of the measured stratigraphic sections.....	28
Figure 2.2: General stratigraphic columnar section of the Haymana Basin (modified after Ünalán <i>et al.</i> , 1976). Fm-Formation	29
Figure 2.3: (a) Angular relationship between Kocatepe formation and platform sequences. View: towards N. Location: North of Haymana town. (b) Contact relationship between Kocatepe and Haymana formations. View: towards W. Location: Haymana-Ankara road, North of Haymana town (see Figure 2.1 for locations).....	33
Figure 2.4: Faulted contact between basin infill and upper Cretaceous ophiolitic mélanges. View: Towards N. Location: south of Dereköy village. (see Figure 2.1 for locations).....	35
Figure 2.5: Interpretation of DD–2203 seismic line indicating sharp contact (onlap) between ophiolitic basement and basinfill units (see Figure 2.1 for locations). Seismic line is gathered from seismic department of T.P.A.O and interpreted in this study. .	35
Figure 2.6: Fault contact between Haymana formation and the basement units. View: towards E; Location: East of Türkşerefli Village (see Figure 2.1 for location).....	38
Figure 2.7: Measured stratigraphic sections of the Haymana formation. See text for explanations and see Figure 2.1 for location.....	39
Figure 2.8: Measured stratigraphic sections of Beyobası formation. See text for explanations. (see Figure 2.1 for location).....	42
Figure 2.9: GoogleEarth image showing vertical transition between Kartal and Kırkkavak formations. Location: South of Eskiköseler village (see Figure 2.1 for location).....	43
Figure 2.10: Measured stratigraphic sections of the Kartal formation. Note the transition between the Kartal and Kırkkavak formations along the line "c". See text for explanations (see Figure 2.1 for locations).	45
Figure 2.11: Measured stratigraphic sections of the Yeşilyurt formation. See text for explanations (see Figure 2.1 for location).....	49
Figure 2.12: Measured stratigraphic sections of the Kırkkavak formation. See text for explanations (see Figure 2.1 for location).....	52

Figure 2.13: Measured stratigraphic section of Ilgınlıkdere formation. See text for explanations (see Figure 2.1 for location).	55
Figure 2.14: GoogleEarth image showing contacts between Ilgınlıkdere, Eskipolatlı, Kırkkavak and Çayraz formations. Note the unmeasured zone of Ilgınlıkdere formation. Location: West of Çayraz village (see Figure 2.1 for location and see text for further explanation).	55
Figure 2.15: Angular relationship between the Çayraz and the Eskipolatlı formations. Location: South of Sarıgöl Village (see Figure 2.1 for location).	57
Figure 2.16: Measured stratigraphic sections of the Eskipolatlı formation. See text for explanations. (see Figure 2.1 for locations).	59
Figure 2.17: Measured stratigraphic sections of the Beldede formation. See text for explanations (see Figure 2.1 for location).	61
Figure 2.18: Measured stratigraphic sections of the Çayraz formation. See text for explanations (see Figure 2-1 for location).....	64
Figure 2.19: Measured stratigraphic sections of the Yamak formation. See text for explanations (see Figure 2.1 for location).	67
Figure 2.20: GoogleEarth image showing angular relationship between the Neogene units and basin infill. Location: East of İner village. Note 3x vertical exaggeration in the image (see Figure 2.1 for location).	69
Figure 3.1: Structural map of the Haymana Basin (see Appendix A for name of the structures)	72
Figure 3.2: (a) rose diagram of strikes of bedding attitudes; (b) histogram of dip amounts of bedding planes	73
Figure 3.3: β - and $-\pi$ diagrams of the major folds of the Haymana basin. See Figure 3.1 for locations of the folds.....	75
Figure 3.4: (a) Length-weighted rose diagram of all structures of the Haymana Basin; (b) length-weighted rose diagram of folds of the Haymana Basin; (c) length-weighted rose diagram of thrust (or reverse) faults of the Haymana Basin; (d) length-weighted rose diagram of strike-slip faults of the Haymana Basin, see text for explanations; (e) left-lateral Riedel shear diagram developed by $\sim 015^\circ\text{N}$ oriented maximum principle	

stress direction (σ_1), indicating possible trends of the structures in the Haymana Basin (see text for explanations).	77
Figure 3.5: (a) GoogleEarth image showing fault contact between basin infill and platform sequences along the İner reverse fault. Location: East of İner village. Note 3x vertical exaggeration in the image; (b) a view of İner reverse fault and affected units. Location: west of İner village (see Figure 3.1 for locations).	78
Figure 3.6: GoogleEarth image showing offset in the Çaldağ formation along Ahırlıkuyu reverse fault. Location: west of Ahırlıkuyu Village. Note 2x vertical exaggeration in the image (see Figure 3.1 for location).....	79
Figure 3.7: (a) Two dimensional view of a GoogleEarth image showing offset in the Çaldağ formation along the Gedik fault. Location: South of Gedik Village; (b) fault plane of the Gedik fault, see Figure 3.7a for the location and view direction of the photo (see Figure 3.1 for location).....	80
Figure 3.8: Cyclographic traces, slickensides and constructed paleostress configurations of the Haymana Basin fault plane measurements.	87
Figure 3.9: Statistical analyses of fault plane measurements. Rose diagrams of strike of the fault planes, histograms of dip amount of fault planes and rake amounts for all fault plane measurements (a,b,c); for strike-slip faults (d,e,f); for normal faults (g,h,i); for reverse/thrust faults (j,k,l). See text for explanation.	90
Figure 3.10: Contour diagrams of the principle stress orientations of deformation phases. Phase 1 group 1 stress orientations (a,b,c); phase 2 group 2 stress orientations (d,e,f); phase 2 group 3 (h,i,j); phase 2 group 4 stress orientations (k,l,m); phase 3 group 5 stress orientations (n,o,p); phase 3 group 6 stress orientations (r,s,t). See text for explanation.	92
Figure 3.11: Overprinting slickensides observed in the deformation zone of the Dereköy thrust fault. View: towards NNW. Note that first movement (blue arrow) is normal indicated by striations, the second movement (red arrow) is reverse as indicated by calcite fibers (see Figure 3.1 for location).	93
Figure 3.12: Major structures and paleostress orientations. (a) Paleostress orientations of group 2, 3, and 5; (b) Paleostress orientations of group 1, 4, and 6. See text for explanation. See Figure 3.1 for legend.....	94

Figure 3.13: Seismic line (88-Hay-01) showing compressional deformation over Miocene units (see Figure 3-1 for location). Seismic line is gathered from seismic department of T.P.A.O and interpreted in this study. Note: The boundaries of the units were assigned by considering deformation phases discussed in this section and Chapter 4 and 5. 97

Figure 3.14: Summary of temporal relationships of the deformation phases. 97

Figure 3.15: Locations of the balanced cross-section lines and results of balanced cross-sections (see Figure 2.1 and 3.1 for legend). 102

Figure 3.16: Shortening ratio calculations. Note that blue lines indicate initial (expected) length of the horizons and the red lines indicate the length of deformed horizons. a) Shortening calculation of cross-section line b-b'; (b) shortening calculation of cross-section line d-d'; (c) shortening calculation of cross-section line e-e'; (d) shortening calculation of cross-section line f-f'. See text for explanation. 103

Figure 3.17: Fence diagram showing the correlation of the balanced cross-sections and increase in deformation towards eastern and southeastern part of the Haymana Basin. 104

Figure 4.1: Geological map of the Haymana Basin, and locations of the thermochronology samples (see Figure 2.1 and 3.1 for legend). 110

Figure 4.2: Pictures of apatite grains used for AHe dating and their dimensions used for calculation of F_T correction parameter. See Figure 4.1 for sample locations. 111

Figure 4.3: Graphics of pooled age calculations. Horizontal axes represent production rate (P) of He (for 1ma) and vertical axes, measured He concentrations (He mol) for each grain. Note that the highest values of P and He mol of each graphics represent the sum of P and He mol values of each sample. 114

Figure 4.4: Graphic showing the relationship between the AHe ages and sedimentation ages. Note that AHe ages obtained from eastern part of the Haymana Basin is older than western part. AHe ages of the eastern part also decrease towards lower stratigraphic levels, which indicates gradual uplift in that part. See text for further explanation. 116

Figure 4.5: Time–temperature models of samples Th2 (a) and Th9 (b). Note that Th2 represents the eastern part of the Haymana Basin while Th9 represents western part of the basin. See text for explanations and Table 4.3 for uplift and subsidence rates calculated from these models.	118
Figure 5.1: Geological map showing distribution of stratigraphic cycles and main younging and sediment transport directions (see Figure 2.1 and 3.1 for legend). Note: Sediment transport directions are representative and mainly based on Çetin <i>et al.</i> (1986) and Çiner <i>et al.</i> (1996).	124
Figure 5.2: Geological map of Central Anatolia showing the elongation of the main structures. Note that orientations of the structures follows the outline of the Kırşehir Block, and westward extension of Hirfanlar-Hacıbektaş fault zone corresponds to Dereköy thrust in the Haymana Basin.	127
Figure 5.3: Correlation of İAESZ and ITSZ related basins and main tectonic events in these basins	130
Figure 5.4: Conceptual model showing tectonic position of the Haymana Basin during late Cretaceous (a) and middle Paleocene (b) with respect to İAESZ and ITSZ.	131
Figure A.1: Geological Map of the Haymana Basin.	167
Figure A.2: Geological map of the Haymana Basin with bedding plane measurements	169
Figure A.3: Structural Map of the Haymana Basin	171

CHAPTER 1

INTRODUCTION

1.1 Aim of the Study

Sedimentary basins are key areas in understanding both opening and closure histories of ancient oceans and subsequent collision histories of continental margins since they record these events in their infill. In order to unravel the coupling between basin evolution and evolution history of related oceanic domain, basically; the geometry, tectonic setting, stratigraphy, structural and tectonic characteristics and their spatio-temporal evolution need to be studied and understood in detail.

In this context, this study aims at understanding the geometry, 3D architecture and geological evolution of Haymana Basin (Central Anatolia) which straddles the Izmir-Ankara-Erzincan and Intra-Tauride Suture zones (İAESZ & ITSZ) in order to shed some light on the late stage evolution of Northern Neotethys (Figure 1.1). The two suture zones are developed in response to the northwards subduction and demise of different branches of the Neotethys Ocean in Turkey during the late Cretaceous to early Tertiary time interval. In this regard, the tectonic significance and relationship of Haymana Basin with the ITSZ is poorly constrained so far. To this end, main problems addressed in this study include;

- Detailed tectono-stratigraphic characteristics of the Haymana Basin,
- Structural characteristics and deformation history of the Haymana Basin ,
- Thermal evolution the Haymana Basin,
- The positions and mutual relationships of İzmir-Ankara-Erzincan and Intra-Tauride sutures,
- Timing of termination of subduction of Neotethys in the region,
- Post-collisional evolution of Haymana Region in the context of İAESZ and ITSZ,

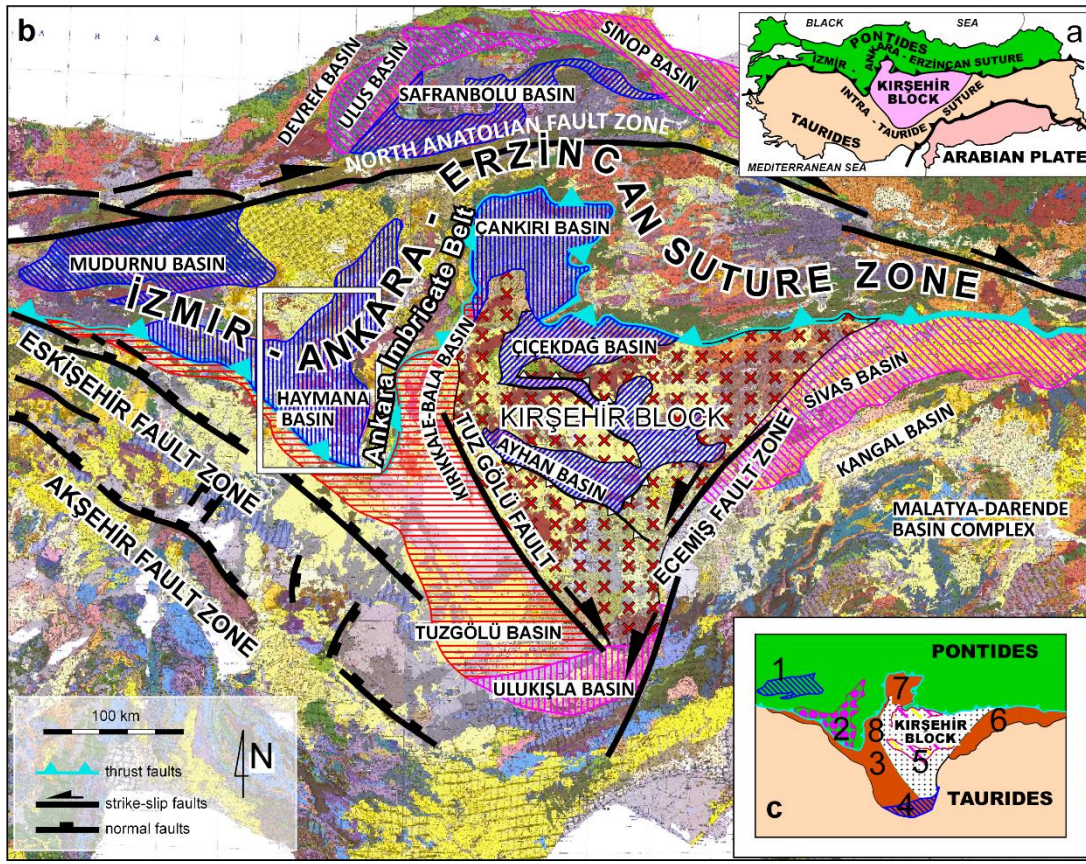


Figure 1.1: Geological setting of the Haymana Basin. (a) Major tectonic divisions of Anatolia (modified Görür *et al.*, 1984); (b) Mesozoic and Cenozoic basins in central and northern Anatolia, (c) simplified version of the basins (modified Görür *et al.* 1984, Özsayın and Dirik, 2007; Kaymakçı 2000; Kaymakçı *et al.* 2009). 1. Mudurnu, 2. Haymana, 3. Tuzgözü, 4. Ulukışla, 5. Ayhan and Çiçekdağı, 6. Sivas and 7. Çankırı basins. Rectangle shows the location of the study area.

1.2 Methods of the Study

The study has been conducted in four stages. These stages comprise, (1) preliminary work, (2) field studies, (3) laboratory studies and (4) office works that include final compilation and integration of all available data.

Preliminary study include a literature survey about Central Anatolia, Central Pontides, Northern Taurides, and reconnaissance survey about the study area. It is noted that there is no published literature information addressing directly deformation and uplift

history of the Haymana Basin, although, the stratigraphy of the basin is relatively well studied.

Field studies represents the second stage. During this stage, three different data sets were obtained: (1) geological mapping, (2) stratigraphic section measurements, and (3) fault-slip data collection.

During geological mapping, published 1/100000 scale geological maps (published by MTA, General Directorate of Mineral Research and Exploration) were used as base maps. If there was any differences between the already drawn boundaries or structures of MTA maps with our observations, they were corrected by using hand GPS and satellite images. Additionally, bedding attitudes were collected systematically in order to create balanced cross-sections and understand the characteristics of the folds during geological mapping.

In order to establish detailed stratigraphy of the basin and understand facies associations, 13 stratigraphic sections representing 10 different formations were measured during the second stage of the field studies.

Collection of the fault-slip data for paleostress analysis is the last stage of the field studies. During this stage, the data collected from the mesoscopic structures include location, attitude of the fault plane, rake of slip lineations, sense of movement, relative timing of sense of movement where overprinting relationships were determined.

In order to unravel the thermal history of the basin, sandstone samples from basinfill units were collected and laboratory studies were conducted as the third stage of the research. These studies comprise two techniques as apatite-helium dating and fission track length measurements. The procedure of the first technique include separation of individual apatite grains from sandstone samples and measuring concentrations of ^4He , ^{38}U , ^{235}U and ^{232}Th from individual apatite grains. Measuring the fission track lengths of α radiations in apatite grains is the main aim of the second technique.

Processing and analysis of the obtained data and thesis writing is the last part of the research.

1.3 Layout of the Thesis

The layout of the thesis is organized as follows.

The first chapter introduces, based on the literature, the thesis by providing information about aim and scope of the thesis, methods of the research, geological background, and the tectonic position of the Haymana Basin.

Understanding the stratigraphy of the basin and facies associations within the basinfill units forms the main subject of the second chapter.

Chapter 3 provides information about the structural characteristics, kinematic evolution and deformation history of the basin and related structures, such as folds and faults. Results of paleostress inversion and balanced cross-section studies are also reported.

Chapter 4 documents information, based on thermo-chronological analysis, about the thermal evolution of the basin in relation to its subsidence and uplift paths.

The Chapter 5 integrates the outcomes of all gathered information provided in the previous chapters and discusses the significance of the Haymana Basin within the frame of spatio-temporal evolution of Tethys Ocean and collision of intervening continental fragments subsequent to its demise.

The last chapter, summarizes the major outcomes of present study and highlights the major conclusions.

1.4 Tectonic Setting of the Haymana Basin

The geological evolution of Turkey is related to the evolutions of Paleo- (largely Paleozoic) and Neo-Tethys (largely Mesozoic) oceans developed between Laurasia in the north and Gondwana in the south. Geologically, Turkey comprises three main tectonic blocks (Ketin, 1966). These include; (1) the Pontides belonging to Laurasia (in the north), (2) The Anatolide-Tauride block (TAB) belonging to Gondwana (in the center), and (3) Arabian platform (AP) (in the southeast). These blocks are

amalgamated between İzmir-Ankara-Erzincan suture zone (İAESZ) in the north, and Bitlis-Zagros suture zone (BZSZ), in south (Figure 1.1). These suture zones contain imbricated stacks of metamorphosed remnants of the Paleotethys and the Neotethys oceans (Şengör and Yılmaz, 1981). Görür *et al.* (1984) proposed another suture zone within the northern branch of the Neotethys separating the Kırşehir Block from the Taurides and named it as Intra-Tauride Suture Zone (ITSZ).

Haymana Basin is located at the junction of the Izmir-Ankara-Erzincan and the Intra-Tauride suture zones in NW Turkey and straddles between the Pontides in the north, Tauride-Anatolide Block (TAB) in the SW and Kırşehir Block (KB) in the East (Figure 1.1). A number of basins have been developed within these continental blocks and in a broad sense, their evolutionary histories are thought to be associated with the northward subduction of the Neotethys Ocean. In the next sections, the origin and major characteristics of these basins in central and north Anatolia and related continental blocks are provided.

1.4.1 Basement: Crystalline Rocks

Crystalline rocks units exposed around the Haymana Basin are designated as the basement. These units comprise ophiolitic and related rocks, metamorphic and magmatic rocks.

1.4.1.1 Ophiolites and Ophiolitic Rocks

Ophiolite belts and ophiolitic mélanges label the suture zones and help to define the former locations of oceanic sedimentary basins formed between continental blocks (e.g., Moores, 1981). Defining their sources and tectonic positions is crucial for paleogeographical reconstructions and understanding the evolution of related sedimentary basins. Based on their geographical positions and associated continental blocks the ophiolitic rocks around the Haymana Basin can be grouped as Central Anatolian Ophiolites (CAO) in the east, Ankara Ophiolitic Mélange (AOM) in the north and Tauride and southern boundary ophiolites in the south (Figure 1.2).

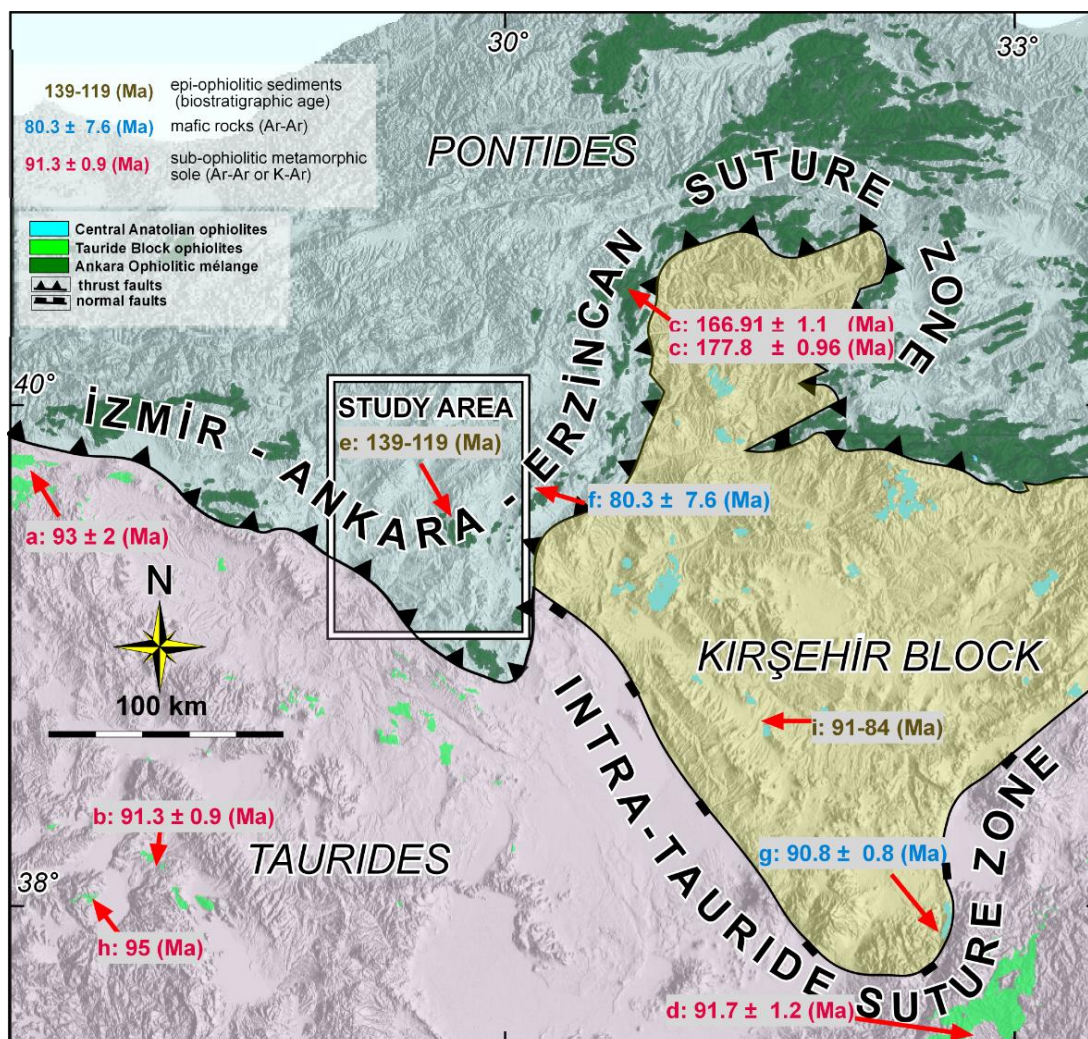


Figure 1.2: Map of Mesozoic ophiolitic rocks of the Central Anatolia. a: Önen (2013), b: Çelik *et al.* (2006), c: Çelik *et al.* (2011), d and g: Dilek *et al.* (1999), e: Rojay *et al.* (2004), f: Sarıfakıoğlu *et al.* (2013), h: Dilek and Moores (1990), i: Yalınz *et al.* (2000)

1.4.1.1.1 Central Anatolian Ophiolites (CAO)

The Central Anatolian ophiolites comprise the ophiolitic rocks within and around the Kırşehir Block. They generally lack the mantle ultramafics (tectonites) and are characterized by cumulates, sheeted dykes, pillow basalts and associated epi-ophiolitic sedimentary rocks (Yalınz *et al.*, 2000). The epi-ophiolitic lower Turonian–lower Santonian pelagic sediments and upper Cretaceous–lower Paleocene intrusions define the time interval for their emplacement (Yalınz *et al.*, 1996). The CAO are developed generally in supra-subduction zone environments but the N-MORB type of ophiolites

are present and generally exposed along the northern margin of the Kırşehir Block within the İAESZ (Göncüoğlu and Türeli, 1993; Tüysüz *et al.*, 1995; Yalınız, 2008).

1.4.1.1.2 Ankara Imbricate Zone (AIZ)

Ankara Imbricate Zone includes the Paleozoic metamorphic rocks, Carboniferous to Triassic mélangé with calcareous blocks and pre-Jurassic ultramafic rocks (Karakaya Complex) and Ankara ophiolitic mélangé (AOM). The AOM defines the northern boundary of the study area but in a broad sense it is exposed and delineates the southern boundary of the Pontides in the Central Anatolia and loosely defines the İAESZ. AOM is generally defined as accretion (or mixture) of different Mesozoic ophiolitic materials including pillow basalts, MORB, intra-oceanic basalts, radiolarites, and upper Jurassic–lower Cretaceous reefal limestones in a scaly matrix (Rojay, 2013). In this study, the Ankara Ophiolitic Mélangé is defined within the Ankara Imbricate Zone for the sake of simplicity of the basement rocks.

Various studies were conducted on the ophiolitic rocks of the İAESZ in order to unravel the opening and closure history of the Neotethys in the region. Early Triassic to Carnian age for the inception age of opening of the Neotethys and Valanginian–early Barremian age for the subduction initiation was proposed, based on radiolarites intercalated with basaltic rocks, by Tüysüz and Tekin (2007). Rojay (2013) suggested northward underthrusting of Tauride-Anatolide Platform beneath Pontides during Early Cretaceous and related thrusting lasted until pre–Miocene. This gave way to progressive emplacement of AOM and imbrication of the older rock fragments derived from the Pontides. Rojay (2013) also noted the absence of Cretaceous magmatic arc related material within the AOM, and it was explained by two possible scenarios: (1) No arc was ever developed, (2) The arc is developed far away further in the north. On the other hand, Dilek and Thy (2006), and Çelik *et al.* (2011) suggested middle–late Jurassic (179–166,9 Ma) ages for the initiation of an intra oceanic subduction within Neotethys in the region based on Ar–Ar hornblende ages of amphibolites around Çankırı and U–Pb zircon crystallization age of plagiogranites cutting the İAESZ ophiolites around Eldivan, respectively.

In the region, Koçyiğit (1991), Koçyiğit *et al.* (2003), Rojay (1995), Rojay and Süzen (1997), and Kaymakcı *et al.* (2009) also noted the development of Upper Cretaceous to Paleocene fore-arc sequences on the AOM.

1.4.1.1.3 Tauride Ophiolites

The Tauride ophiolites are exposed in the southern part of the study area and emplaced on the carbonates of the Tauride-Anatolide Platform units. They are subdivided, based on their relationships with İAESZ and ITO, into two groups. The first group is exposed in the southern margin of the study area and comprises tectonized mantle rocks, mafic ultramafic cumulates, and gabbros. They commonly lack sheeted dike complexes and extrusive rocks of a complete ophiolite sequence. Geochemical characteristics, lithologies and metamorphic sole hornblende Ar-Ar ages of these ophiolites are closely similar and range between 90 to 101 Ma (Harris *et al.*, 1994; Önen and Hall., 2000) (Figure 1.2). According to Önen (2003), and Çelik and Delaloye (2006), this group has intra-oceanic subduction characteristics and are products of the İzmir-Ankara-Erzincan Ocean which are emplaced onto the Taurides from north to south. The second group displays almost same characteristics with the first group, they however, have supra-subduction zone characteristics and are associated with the Intra-Tauride Ocean and thought to be emplaced southwards onto the Tauride platform during Late Cretaceous to Eocene time interval (Lytwyn and Casey, 1995; Dilek *et al.*, 1999; Parlak and Delaloye, 1999; and; Robertson and Andrew, 2002).

1.4.1.2 Metamorphic Rocks around the Haymana Basin

The metamorphic rocks exposed in the study area can be divided into three groups by considering their metamorphic grades, emplacement mechanisms, exhumation ages and locations relative to the İAESZ and ITO: metamorphic rocks of (i) Pontides, (ii) Kırşehir Block and (iii) Tauride-Anatolide Platform (Figure 1.3).

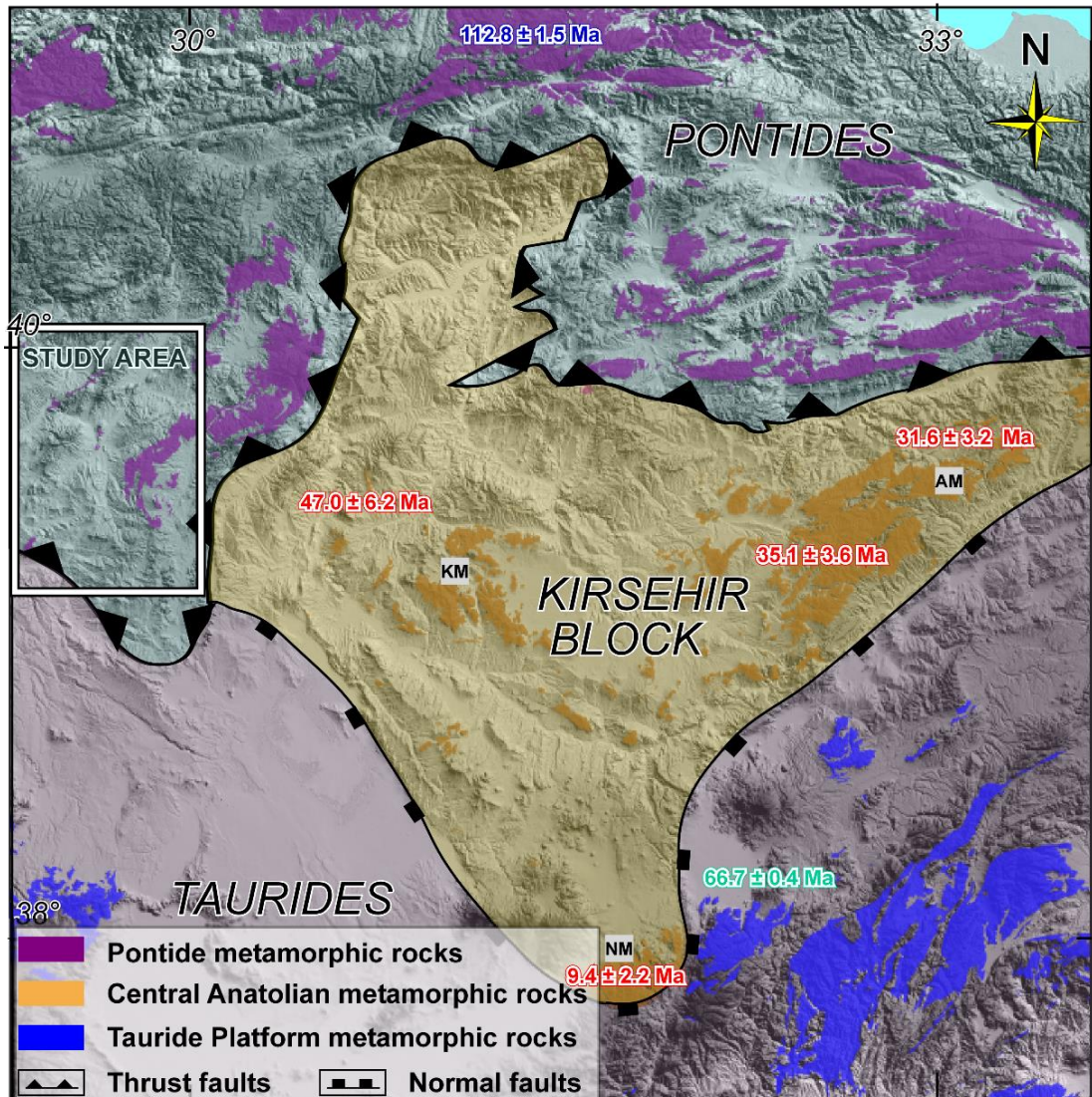


Figure 1.3: Metamorphic rocks around the study area. Red ages represent apatite-helium exhumation ages from the Central Anatolian metamorphic rocks (Whitney *et al.*, 2003). The green age represents syn-to peak metamorphic carphiolite Ar-Ar age from Anatolide-Tauride Platform metamorphic rocks (Pourteau, 2011). The blue age represents youngest subduction-related peak metamorphic muscovite Ar-Ar age from Central Pontide metamorphic rocks (Okay *et al.*, 2013). NM-Niğde Massif, KM-Kırşehir Massif, AM-Akdağ Massif

1.4.1.2.1 Metamorphic Rocks on Pontides

They are exposed in the northern part of the study area (Figure 1.3) and are associated with evolution of Paleotethys and Neotethys oceans.

Late Triassic Karakaya orogeny (closure of Paleotethys) and Alpine orogeny (closure of Neotethys) are the main deformation events in the Pontides (Şengör and Yılmaz, 1981; Okay, 1984; Okay *et al.*, 1996; 1998; 2006; 2013). Karakaya orogeny comprises intensely deformed and partly metamorphosed Permian to Triassic rocks locally set in greywacke matrix. These rocks are exposed around the study area and Ankara region (Bingöl *et al.*, 1974; and Tekeli, 1981). It includes Carboniferous-Permian limestone olistoliths, blocks of Carboniferous (311–331 Ma) high grade metamorphic rocks (Aydın *et al.* 1995; Okay *et al.*, 1996; Topuz *et al.*, 2004a), and early Permian (263–260 Ma) (Topuz *et al.*, 2004) to late Triassic (203–205 Ma) (Okay *et al.*, 2002) low grade metamorphic rocks and pre-Jurassic intrusions (Okay *et al.*, 1996 and 2002; Delaloye and Bingöl, 2000). These rocks are exposed within the Ankara imbricate zone as thrust sheets and also as blocks within the Karakaya complex.

Alpine structures are basically represented by weak deformation with folds and south-vergent thrust faults, possibly due to obduction of Pontides onto the Tauride-Anatolide Platform. HP-LT metamorphic slices with Early Cretaceous (102.1 \pm 1 – 112.8 \pm 1.5 Ma) peak metamorphic ages in the Central Pontides (Okay *et al.*, 2006; 2013) represents the youngest subduction-related metamorphism in the region.

1.4.1.2.2 Central Anatolian Metamorphic Rocks

Central Anatolian metamorphic rocks (CAM) can be observed in the eastern part of the study area (Figure 1.3) and they are exposed in three different locations (Figure 1.3). These outcrops are named as; (1) Kırşehir Massif (Seymen, 1981; 1982), (2) Niğde Massif (Göncüoğlu, 1977) and (3) Akdağ Massif (Pollak, 1958).

According to Whitney *et al.* (2001) and Fayon *et al.* (2001), Central Anatolian metamorphics can be, based on their pressure-temperature-time (P-T-t) paths and tectonic histories, divided into two groups: (1) northern zone which includes Kırşehir and Akdağ massifs. This zone comprises folded, thrust-faulted metasedimentary rocks intruded by gabbro and granitoids. They are related to the final closure of northern Branch of Neotethys during Late Cretaceous time along İzmir-Ankara-Erzincan Suture Zone. (2) southern zone includes Niğde Massif which is a structural dome formed due

to oblique convergence related to closure of the southern Neotethys in the Late Cretaceous along Inner Tauride Suture Zone. Late Cretaceous (91–84 Ma; U-Pb zircon ages) age for syn – to post peak metamorphism and 9.4 ± 2.2 to 47 ± 0.6 Ma apatite–helium ages for exhumation are reported in Central Anatolia by Whitney *et al.* (2001 and 2003). For the exhumation of the Niğde Massif, unlike the previous models, Gautier *et al.* (2002 and 2008) suggest a southerly-dipping detachment fault and > 54 Ma age, based on the presence of a nonconformity between early Eocene clastics and Niğde Massif. They also suggest that the young apatite helium exhumation ages of Whitney *et al.* (2003) must be the reset ages due to the late Miocene volcanic activity in the Central Anatolia.

1.4.1.2.3 Tauride–Anatolide Platform Metamorphics (TAPM)

They are observed at south of the study area and called as Anatolides (Okay, 1984). Northern part of Anatolides is named as Tavşanlı zone. This zone is represented by HP/LT (20–24kbar, 430-500°C) blueschists–eclogites (Okay, 1984, and 2002; Whitney and Davis, 2006; Çetinkaplan *et al.*, 2008; and Okay, 2010) and late Cretaceous (80–88Ma) metamorphism age (Okay *et al.*, 1998; Sherlock *et al.*, 1999; Seaton *et al.*, 2009). Afyon Zone represents southern part of Anatolides. According to Okay (1984), Özgül (1984) and Okay *et al.* (1996); this zone is composed of Precambrian core and Paleozoic to Mesozoic greenschist cover units. On the other hand, Candan *et al.* (2005) and Pourteau (2011) proposed presence of blueschist facies metamorphism in the cover units of this zone and also suggested late Cretaceous to Paleocene (62,8–83,4 Ma; Ar-Ar biotite/muscovite/phyllite ages) peak metamorphic ages for these units.

Decrease in metamorphic grade from north to south is associated with the closure of Neotethys Ocean during late Cretaceous to Paleocene time interval (Şengör and Yılmaz, 1981; Okay, 1984; Candan *et al.*, 2005). Major tectonic events are ordered as northward subduction of Tauride-Anatolide Platform, obduction of ophiolites, accretion and finally collision between Tauride-Anatolide Platform and Pontides (Okay *et al.*, 1996; 2001). However, Pourteau (2011) made a reconstruction indicating

subduction of Anatolides beneath both Kırşehir Block and the Pontides along the Intra Tauride Suture zone.

1.4.1.3 Magmatic Rocks around the Haymana Basin

Magmatic rocks around the study area are divided, based on their locations relative to İAESZ and ITSZ, into two groups; (1) northern margin magmatic complex (Pontide arc complex), 2) southern margin magmatic complex (generally Central Anatolian granitoids) (Figure 1.4).

1.4.1.3.1 Northern Magmatic Complex (Pontide Arc Complex)

Subduction of Neotethys and subsequent collision initiated the magmatism along Pontides and resulted in formation of E–W trending magmatic complex (Figure 1.4). Based on previous studies, magmatism in the Pontides occurred into two periods; (a) subduction, and (b) post-subduction.

(a) Late Cretaceous–Paleocene time interval is represented by magmatic arc related volcanic and coeval intrusive rocks. Alkaline basaltic, trachyandesitic, and andesitic volcanoclastic rocks and lava flows (generally pillow lavas) form the subduction stage (ensimatic arc) volcanic rocks (Rice *et al.*, 2006). Campanian Saraçköy volcanic rocks (Koçyiğit *et al.*, 2003), Coniacian–Campanian Dereköy and Cambu (Yemişliçay) formations (Görür *et al.*, 1997; Tüysüz, 2011), and Campanian–Maastrichtian Yaylaçayı formation (Yoldaş, 1982; Tüysüz *et al.*, 1995; Rice *et al.*, 2006) exposed in the Central Pontides are among this group. Arc-related intrusive bodies in Central Pontides are represented by high K, calc-alkaline, generally I-type and rarely S- or H-type plutons. Although exposures of these rocks with Late Cretaceous to Early Paleocene intrusion ages (Şahin *et al.*, 2004; 2005; Kaygusuz *et al.*, 2009; 2013) are very common in the eastern Pontides, the unique example of this group in the Central Pontides is Upper Cretaceous ($95.4 \pm 4.2 - 70.5 \pm 3.4$ Ma; U-Pb zircon ages) Oymaağaç granitoid (Figure 1.5) (Öztürk *et al.*, 2011; Speciale *et al.*, 2013).

(b) Post subductional period (Paleogene to Miocene) magmatism in the Pontides is represented by sub-alkaline, medium to high-K, calc-alkaline, generally H- rarely I-

type plutonics (Şahin *et al.*, 2004; Boztuğ *et al.*, 2002; Boztuğ and Harlavan, 2007) and dominantly medium to high K, calc-alkaline, rarely tholeiitic volcanic

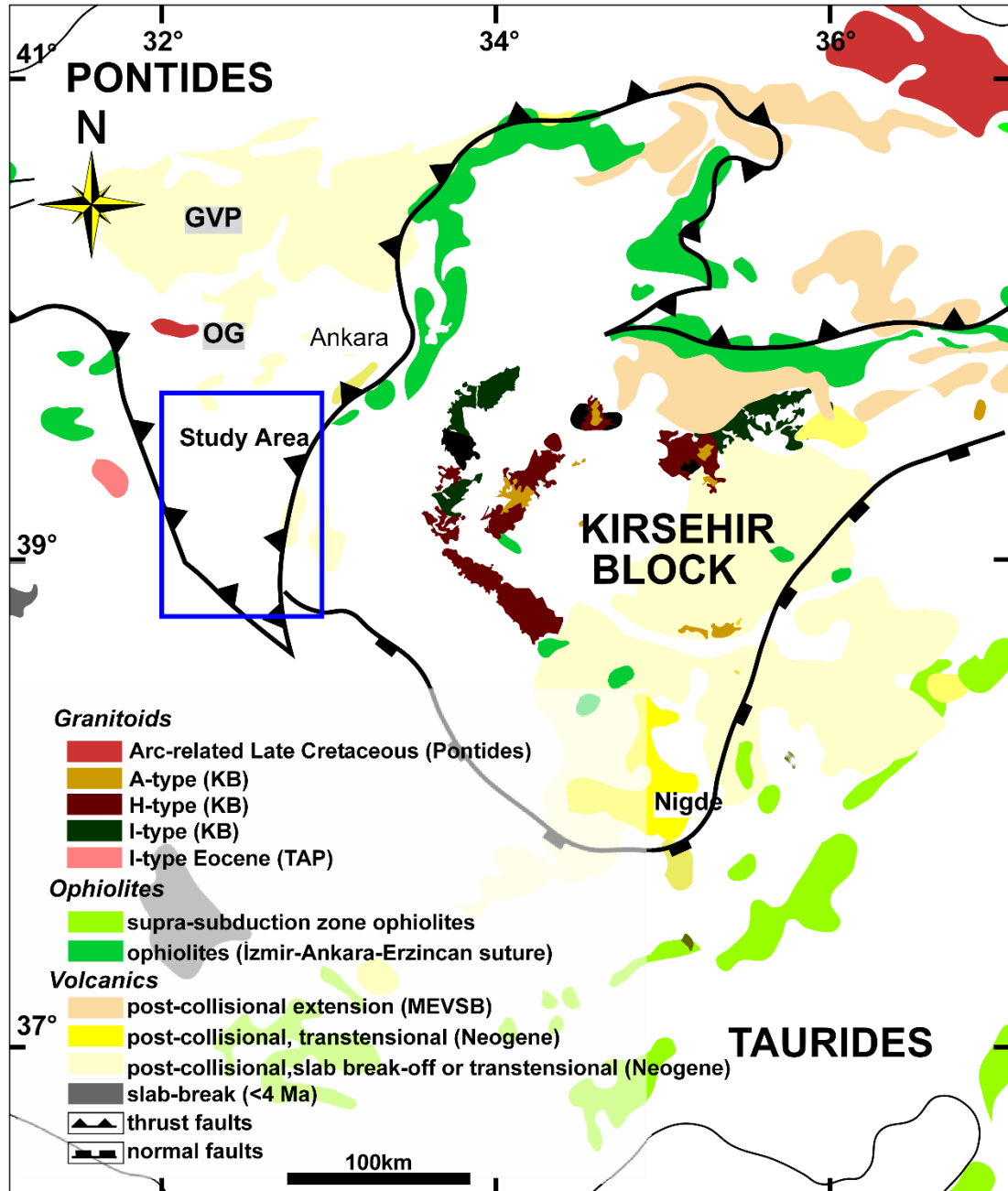


Figure 1.4: Magmatic rocks around the Haymana Basin. GVP-Galatian Volcanic Province, , KB-Kırşehir Block, TAP-Tauride-Anatolide Platform, MEVSB-Middle Eocene volcano-sedimentary belt, OG-Oymaağaç Granitoid (see text for references).

and related volcanoclastic rocks (Arslan *et al.*, 2000; 2013; Keskin *et al.*, 2008; Temizel and Arslan, 2008; Kaygusuz *et al.* 2010).

Various models have been proposed to explain the tectonic settings of the magmatic rocks emplaced during post-subductional period. Collision, slab breakoff, thickening in the crust and post-collisional extension mechanisms are proposed for the Paleogene to Miocene time interval, but these geodynamic events are still under debate.

Galatia Volcanic Complex (GVC) (Tankut *et al.*, 1991) and western extension of the Middle Eocene volcano-sedimentary belt (MEVSB) (Keskin *et al.* 2008) are examples of this group in Central Pontides (Figure 1.4). MEVSB is associated with slab break-off mechanism (Keskin *et al.*, 2008) whereas Koçyiğit *et al.* (2003) propose collisional setting-related development for 44.7–38.8 Ma volcanic rocks of GVC. Following collision (or slab break), extensional setting-related evolution of the GVC is proposed by Toprak *et al.* (1996) and Tankut *et al.* (1998).

1.4.1.3.2 Southern Margin Magmatic Complex

The southern margin magmatic complex comprises Upper Cretaceous to Paleogene plutonic rocks that include Central Anatolian granitoids and granitoids exposed at the northern margin of the Tauride-Anatolide Platform. They are emplaced within collisional to post-collisional tectonic settings, and located on the southern margin of İAESZ. There are also younger volcanic bodies in this zone. They however, postdate the main evolutionary history of the Haymana Basin and subduction-collision processes related to the northern branch of the Neotethys. Therefore, they were not included in this group (Figure 1.4).

There is no unequivocal opinion on the tectono-magmatic setting of the plutonic rocks exposed at the northern margin of the Tauride-Anatolide Platform. Okay and Satır, (2006) proposed that they are arc magmatic rocks of the southerly located Vardar Zone. However, they attributed to with the closure of the northern branch of the Neotethys (Kibici *et al.*, 2008; İlbeyli *et al.*, 2009). They are represented by I-type, medium to high-K, calc-alkaline geochemistry and 53 ± 3.45 Ma Ar-Ar hornblende and

44.7±0.4 Ma Rb-Sr biotite cooling ages (Sherlock *et al.* 1999; and Okay and Satır, 2006).

Central Anatolian granitoids (CAG) intruded the metamorphic and ophiolitic rocks of Kırşehir Block. Their origin is thought to be related to closure of the northern branch of the Neotethys Ocean and also they are considered as the products of the crustal thickening subsequent to arc to arc or arc to continent collision between Pontides and Kırşehir Block (Göncüoğlu *et al.*, 1986; 1992; Kaymakcı *et al.*, 2009). They have generally high-K, calc-alkaline geochemistry and also are generally S-type but both alkaline A-type and calc-alkaline I-type varieties are also reported (Figure 1.4). S-type granitoids represent the syn-collision tectono-magmatic settings and have 95±11 – 84.8±1.4 Ma U-Pb zircon intrusion ages (Göncüoğlu, 1986; Whitney, *et al.*, 2003). This time interval is contemporaneous with the obduction of MORB-type ophiolites onto the Kırşehir Block (Göncüoğlu *et al.*, 1992; Yalınız *et al.*, 1996). The granitoids with both A- and I- or H-type signatures indicate post-collisional and late orogenic origin and are thought to be emplaced in post-collisional extensional setting at the end of Cretaceous to earliest Paleocene (Erler *et al.*, 1991; Göncüoğlu *et al.*, 1992; Erler and Göncüoğlu, 1996). Another model was also proposed to explain the origin of the CAG, and it suggest that they are related to arc magmatism associated with Inner Tauride Ocean located between Tauride Platform and Kırşehir Block (Görür *et al.*, 1984; 1998; Tüysüz *et al.*, 1994; Erdogan *et al.*, 1996; Kadioğlu *et al.*, 2006).

1.4.2 Late Cretaceous–Paleogene Sedimentary Basins Around Haymana Basin

The basins around the Haymana Basin can be classified according to tectonic blocks in which they are involved. Most of the basins, such as the ones surrounding the Kırşehir Block, share relatively similar tectonic history and stratigraphical characteristics while some, such as Mudurnu Basin, has witnessed the opening and closure history of the Neotethys Ocean (Saner., 1980; Altıner *et al.*, 1991). The brief characteristics and evolution of the basins around the Haymana Basin are discussed below. (see Figure 1.1 to see locations of these basins).

1.4.2.1 Basins Located in the Pontides

By considering progressive closure of the Neotethys in the region, tectono-stratigraphic histories of basins located in the Pontides are grouped into three periods; (1) pre–Albian period, (2) Albian to Paleocene period and (3) Paleocene to Oligocene period. The boundary between first two groups is marked by an unconformity starting with Upper Cretaceous arc-related material in the north (Görür, 1997; Tüysüz *et al.*, 1995; 1999; Hyppolyte *et al.*, 2010) and initiation of ophiolitic mélangé development and deposition of the intra-arc to fore-arc sequences in the south (Görür *et al.*, 1984; 1998; Rojay, 1991; 1995; Koçyiğit, 1991; Kaymakçı, 2000; Koçyiğit *et al.* 2003; Rice *et al.*, 2006; 2009). Beginning of compressional tectonic regime, consequent uplift and sedimentation during Paleocene-Eocene in both southern and northern Pontides (Rojay, 1991; 1995; Kaymakçı, 2000; Hyppolyte *et al.*, 2010) defines the boundary of the last two groups. Pre-Albian period predates the evolution of the Haymana Basin. Therefore, last two periods form main concern of this study.

1.4.2.1.1 Albian to Paleocene

By considering the progressive closure of the Neotethys during Late Cretaceous to Tertiary time interval, sedimentary sequences of the basins located in the Pontides are divided into two groups as back-arc sequences in the north or intra- to fore-arc sequences in the south. The boundary between them is designated by Late Cretaceous magmatic arc-related intrusive and volcanic rocks.

Pontide back-arc sequences uncomfortably overlie pre–Albian sequences and include (i) Coniacian–Santonian shallow-marine units that grade upwards into Santonian volcanic and volcanoclastic sequences with limestone intercalations and (ii) onlapping calciturbidites as the last products of the sequence (Görür, 1997; Tüysüz *et al.*, 1999; Hyppolyte *et al.*, 2010). However, Turonian to Maastrichtian time interval in the intra to fore-arc sequences is represented by repetitive ophiolitic mélangé (containing the blocks of pre–Cenomanian platform sequences) development and ensuing fore-arc flysch sequences controlled by northerly dipping thrust faults (Koçyiğit *et al.*, 1988;

Altiner *et al.*, 1991; Rojay, 1995; Rojay and Altiner 1997; Rojay and Süzen, 1997; Koçyiğit *et al.*, 2003; Okay *et al.*, 2006; 2013).

By considering the evolutions of the basins located in the northern and southern Pontides during this period, it is concluded that back-arc extension and arc related deposition dominated the northern margin of the Pontides, however, at the southern margin of the Pontides, main tectonic settings were related to ophiolitic mélangé and fore-arc basin developments.

1.4.2.1.2 Paleocene to Oligocene Period

Collision between TAB-KB and Pontides during Paleocene–early Miocene interval (Koçyiğit *et al.*, 1988; Koçyiğit, 1991; Rojay, 1991; 1995; Kaymakçı, 2000; Kaymakçı *et al.*, 2009; Hippolyte *et al.*, 2010) is the main factor controlling the deposition along Pontides.

Wide exposures of flysch deposits with some continental and shallow-marine sediments along the Black Sea margin represents Paleocene time interval in the northern Pontides (Görür, 1997; Tüysüz *et al.*, 1999; Hippolyte *et al.*, 2010). These units are underlain by Campanian–Maastrichtian sequences, and conformably overlain by Eocene 1000–1500 m-thick siliciclastic turbidities grading upward into Oligocene continental clastics (Tüysüz, 1999; Hippolyte *et al.*, 2010; Espurt *et al.*, 2014). Progressive unconformities and north-vergent thrust faults indicate syn-depositional compression and they are the most common features of the Eocene to Oligocene sequences of northern Pontides (Okay and Şahintürk, 1997; Tüysüz, 1999; Sunal and Tüysüz, 2002; Hippolyte *et al.*, 2010; Espurt *et al.*, 2014).

Paleocene to Eocene stratigraphy of the southern Pontides covers both Upper Cretaceous ophiolitic mélangé and fore-arc sequences (Koçyiğit *et al.*, 1988; Koçyiğit, 1991; Rojay, 1995; Kaymakçı, 2000; Kaymakçı *et al.*, 2009). The contact relationship between fore-arc sequences and Paleocene units varies between conformable and unconformable as a function of proximity to the basin margins. It is difficult to correlate the Paleocene–Eocene stratigraphy of the southern Pontides because it had

been affected by different collision histories of Kırşehir Block, Tauride-Anatolide Platform and Pontides. However, generally it is suggested that Paleocene stratigraphy of this zone starts with a thin deep-marine flysch sequence and grades upwards into thick continental red clastics or shallow-marine carbonates. Also, this alternation is repeated as cycles up to Oligocene units which are commonly continental or lacustrine deposits (Ünalán *et al.*, 1976; Koçyiğit *et al.*, 1988; Koçyiğit, 1991; Rojay, 1995). In analogy to the northern Pontides, Upper Paleocene–Eocene units of this zone was subjected to compressional tectonic regime during this time interval (Koçyiğit *et al.*, 1988; Koçyiğit, 1991; Rojay, 1995; Kaymakcı, 2000).

By considering north-directed subduction, the positions of the pre–Paleocene fore-arc to back-arc sequences, and effects of compressional tectonic regime on basinfills, it is proposed that Paleocene and younger units of northern Pontides were deposited in piggy-back basins developed in retro-arc foreland settings whereas they were deposited on accreted fore-arc sequences in compressional settings in the southern Pontides (Koçyiğit, 1991; Rojay, 1991; 1995; Kaymakcı, 2000; Şen, 2013; Espurt *et al.*, 2014).

1.4.2.2 Basins Located on the Northern margins of Taurides and Kırşehir Block

Basins located on Taurides can be, based on their locations with respect to İAESZ and ITSZ, divided into two groups (Figure 1.5). Tectonic positions of the Cretaceous–Paleogene basins developed on Tauride-Anatolide Platform are debatable and there are numerous previous studies suggesting different models for the association of these basins. Therefore, following sections of this chapter are aimed to summarize the literature and discuss their stratigraphies, structural elements, and possible evolutionary models.

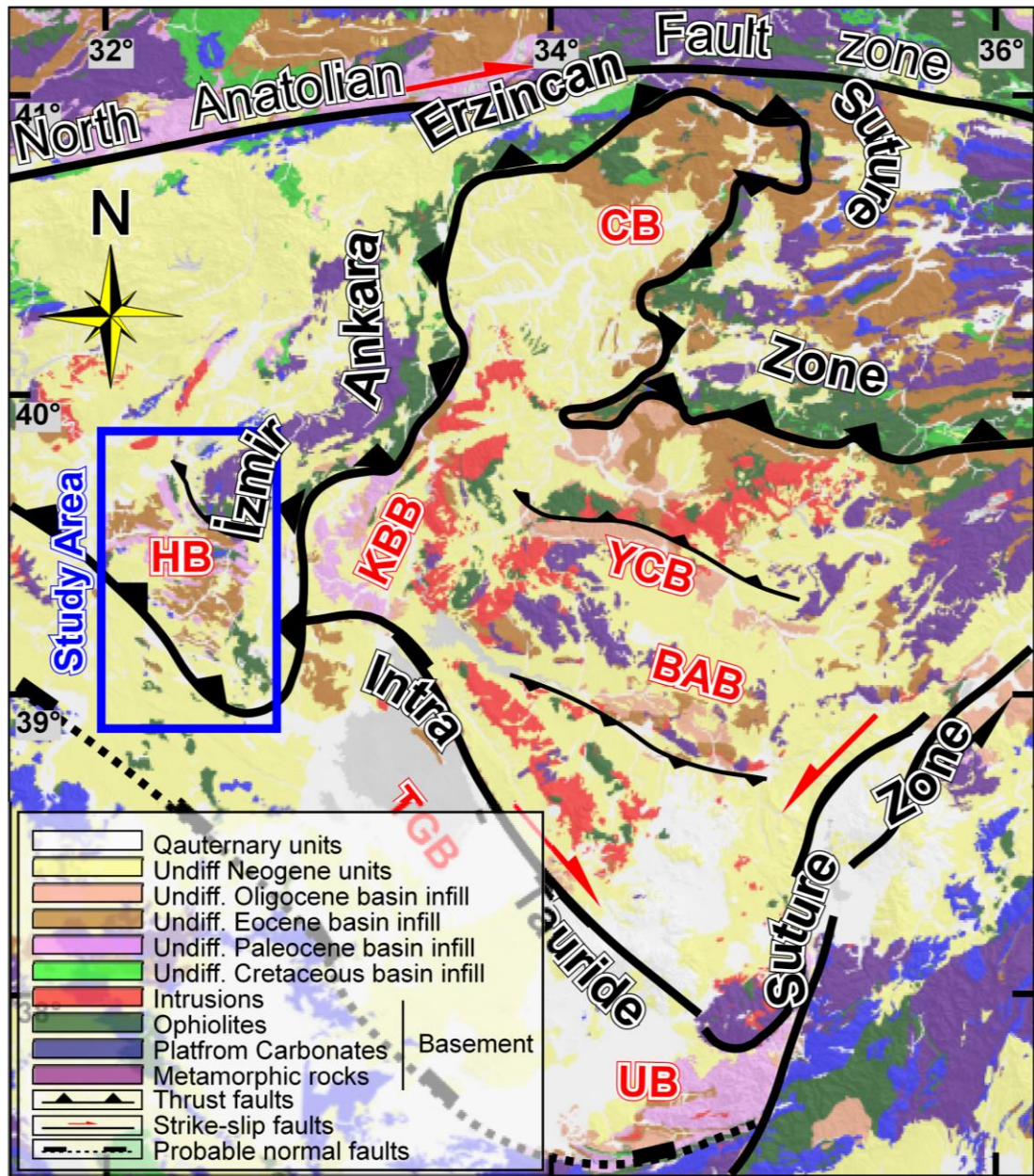


Figure 1.5: Geological map of Central Anatolia showing position of the Central Anatolian basins with respect to İzmir-Ankara-Erzincan and Intra-Tauride suture zones. BAB-Büyükkışla-Ayhan Basin, CB-Çankırı basin , HB-Haymana Basin, KBB-Kırıkkale-Bala Basin, TGB-Tuzgözü Basin, UB-Ulukışla Basin, YCB-Yozgat-Çiçekdağı Basin. (modified after MTA 2002 map).

1.4.2.2.1 Basins Related to İAESZ

Basins located in the collision zone between Pontides, Kırşehir Block and Tauride Platform, are divided into two as; (1) basins evolved between Kırşehir Block and Pontides and (2) basins developed between Pontides and Tauride Platform. The first group comprises Kırıkkale-Bala, Çankırı and Yozgat-Çiçekdağı basins. Mainly, their evolution are associated with the progressive closure of the Neotethys and collision of Kırşehir Block and Pontides (Cater *et al.*, 1991; Poisson *et al.*, 1996; Görür *et al.*, 1998; Kaymakcı, 2000; Gürer and Aldanmaz, 2001; Kaymakcı *et al.*, 2009; Nairn, 2011). In the Central Anatolia, the second group comprises Haymana Basin and it forms the main focus of this study.

Units of Ankara Imbricate zone are exposed at their northern margins, whereas Central Anatolian Crystalline Complex (CACC) (Göncüoğlu *et al.*, 1991) and SSZ-type Central Anatolian ophiolites crop out at the center and southern margins of group 1 basins (Kaymakcı, 2000; Nairn, 2011; Gülyüz *et al.* 2013).

The oldest sedimentary units of these basins are upper Cretaceous to middle–Paleocene volcano-sedimentary turbiditic sequences, namely Ilıcıpınar and Yaylaçayı formations (Norman, 1972; Tüysüz, 1995; Kaymakcı, 2000). They are thought to be deposited in intra- or fore-arc settings (Tüysüz, 1995; Kaymakcı, 2000).

Middle Paleocene to middle Eocene sequences in these basins are represented by various facieses, ranging from continental to deeper marine environment sediments. Mainly fluvial Karabalçık and Baraklı formations (Dellaloğlu *et al.*, 1992; Kara and Dönmez, 1990), shallow-marine to fan delta complex deposits of Dizilitaşlar formation (Norman, 1972; Kaymakcı, 2000) and open marine clastic rocks of Hacıhalil formation (Birgili *et al.*, 1974) are the examples of such lithologies. Presence of intraformational unconformities within these sequences were noted by Kaymakcı (2000) and syn-depositional deformation promoted by southverging thrusts and growth of accretionary prism were considered as the reason for the formation of such unconformities. Additionally, Kaymakcı (2000) reported the presence of CAG-related

fragments within southerly-derived counterparts of these units, which indicates progressive unroofing of CAG during that time interval.

Middle Eocene to early Miocene sequences are represented by (i) shallow marine limestones as Çayraz and Kocaçay formations (Schmidt, 1960; Birgili *et al.*, 1974) which are interpreted as last marine products of these basins (Kaymakcı, 2000) and (ii) Oligocene to lower Miocene continental clastic rocks or evaporites which are signed as last products of foreland settings in the region (Kaymakcı, 2000; Gülyüz *et al.*, 2013).

According to Kaymakcı (2000), deformation history of that region for late Cretaceous to middle Miocene is divided into three periods as pre-late Paleocene, late Paleocene to pre-middle Miocene and middle Miocene. First two phases are associated with the closure of the Neotethys, consequent collision between Pontides and Kırşehir Block and represented by compressional structures as thrust faults or folds. Even though first two phases look similar in terms of structures, there are differences in their stress orientations. The first phase is mainly manifested by NW–SE to NNW to SSE compression while the second phase by compression directions ranging from N–S to E–W. The differences between these phases are explained by N–S shortening due to N–S collision along initially E–W trending trench zone between Kırşehir Block and Pontides and subsequent 30° counterclockwise at the western and 50° clockwise rotations at the eastern margins of the basin due to indentation of the Kırşehir Block into Pontides during the collision (Kaymakcı 2000; Maijers *et al.*, 2011). Phase 3 is represented by multi-directional extensional faults which are thought to be formed as a result of the gravitational collapse following the continental collision and crustal thickening.

Evolution and nature of these basins are discussed in various studies and described as fore-arc basins. They evolved on Ankara Imbricate zone during late Cretaceous to pre-early Paleocene (Tüysüz *et al.*, 1995; Kaymakcı, 2000; Kaymakcı *et al.*, 2009), then started to evolve in a collisional setting as foreland basins during post-early Paleocene to middle Miocene time interval (Kaymakcı, 2000; Kaymakcı *et al.*, 2009). Others suggest a continuous evolution commenced by late Cretaceous collision between

Kırşehir Block and Pontides, then these basins are collisional or piggy-back basins developed on southerly moving nappes (Gürer and Aldanmaz, 2002) or ophiolitic mélanges of İAESZ (Erdoğan *et al.*, 1996) during progressive collisional settings.

1.4.2.2 Basins Related to ITSZ

They comprise the basins developed between Kırşehir Block and Tauride Block and named Tuzgölü, and Ulukışla basins, and the basins within the Kırşehir Block, an unique example is Ayhan-Büyükkişla basin. Evolution of these basins are controversial and mainly attributed either to the closure of Inner Tauride Ocean (Görür *et al.*, 1984, and 1998; Robertson and Dixon, 1984; Robertson, 2002; Clark and Robertson, 2002; and Advokaat *et al.*, 2014) or to extensional tectonic regime subsequent to the collision of Pontides and Tauride-Anatolide Platform (Çemen *et al.*, 1999; Dirik and Erol, 2000; Gautier *et al.*, 2008).

Metasedimentary or ophiolitic basement of the NNW–SSE trending Tuzgölü Basin was determined based on seismic studies (Gürbüz and Evans, 1991; Fernandez-Blanco *et al.*, 2013) and TPAO well logs. Despite the absence of exposures of the contact between the pre–Oligocene basinfill and the basement, it is suggested that the basement display Taurides or Kırşehir Block affinity in the western and eastern parts of the basin, respectively (Görür *et al.*, 1984; 1998; Çemen *et al.*, 1999; Dirik and Erol, 2000). Additionally, the basement of the Ulukışla Basin is defined as The Niğde Massif in the north and southerly obducted Inner Tauride ophiolites and platform sequences of Taurides in the south (Clark and Robertson, 2002) whereas only CACC basement bounds the Ayhan-Büyükkişla Basin (Köksal and Göncüoğlu, 1997; Advokaat *et al.*, 2014).

The oldest sedimentary units of these basins except from Ayhan-Büyükkişla basin are Cretaceous to middle Paleocene continental to deeper marine sequences which are represented by continental Kartal Formation, shallow marine limestone deposits of Asmaboğazı Formation and their deeper marine equivalents of Haymana Formation (Dellaloğlu and Aksu, 1984; Görür *et al.*, 1984; Çemen *et al.*, 1999) in the Tuzgölü Basin and Aktaştepe Formation and its deeper marine counterpart of Halkapınar

Formation in the Ulukışla basin (Demirtaşlı *et al.*, 1973; Clark and Robertson, 2002). Although Görür *et al.* (1984) and Clark and Robertson (2002) suggest a fore-arc setting related environment for the deposition of these units, Çemen *et al.* (1999) and Dirik and Erol (2000) propose extensional tectonic setting deposition. In the Ayhan-Büyükkişla Basin, this time interval is represented by extension-related depositions of volcanoclastics and mainly continental to shallow-marine sequences as Göynük volcanoclastic olistostrome dated as 72.11 ± 1.46 Ma by Advokaat *et al.* (2014) and Yeşilöz Formation (Köksal and Göncüoğlu, 1997; Advokaat *et al.*, 2014).

Middle Paleocene to late Eocene time interval is represented by mainly deep-marine sequences until middle Eocene (Görür *et al.*, 1984; Çemen *et al.*, 1999) whereas volcanoclastic deposits of the Ulukışla Formation dominates this time interval in the Ulukışla Basin. However, deposition of shallow-marine limestones of late Eocene Hasangazi Formation in the Ulukışla Basin corresponds to the shallow-marine sediments in the Tuzgölü Basin (Demirtaşlı *et al.* 1973; Clark and Robertson, 2003). In the Ayhan-Büyükkişla basin, this time interval is represented by development of an unconformity and deposition of Lutetian nummulitic limestones of Mucur formation (Göncüoğlu *et al.*, 1992; Köksal and Göncüoğlu, 1997; Advokaat *et al.*, 2014).

Continental and lacustrine environment-related deposition characterizes the post-late Eocene time interval in these basins (Görür *et al.*, 1984; Köksal and Göncüoğlu, 1997; Çemen *et al.*, 1999; Clark and Robertson, 2003; Advokaat *et al.*, 2014).

Although the deformation histories of Tuzgölü and Ulukışla basins are explained by initial extension up to at least middle Paleocene (Görür *et al.*, 1984) or end of Eocene (Çemen *et al.*, 1999; Dirik and Erol, 2000; Gautier *et al.*, 2008), Clark and Robertson (2002) propose compressional setting for late Cretaceous to Paleocene time interval and subsequent extensional phase until late Eocene for the Ulukışla Basin. Although the studies mentioned above suggest different deformation histories for pre-Eocene time interval, they all agree that post-Eocene time interval is characterized by compressional or strike-slip deformation phases. Initial extension commenced by middle Eocene and following compressional settings characterize the deformation

history of the Ayhan-Büyükkişla basin (Köksal and Göncüoğlu, 1997; Advokaat *et al.*, 2014)

Three different models are suggested for the evolution of these basins. The first one is proposed by Çemen *et al.* (1999), Dirik and Erol (2000), Aydemir and Ateş (2006), and Gautier *et al.* (2002, 2008). They suggest that these basins are an intra continental basins developed on northern promontory of Tauride Block due to extensional/transtensional regime following the collision along İAESZ. However, the second model proposed by Görür *et al.* (1984, 1998) and Advokaat *et al.* (2014) associate the formation of these basins with closure of Intra Tauride Ocean, and also suggest fore-arc and back-arc type basin evolution for Tuzgölü-Ulukışla and Ayhan-Büyükkişla basins, respectively. In addition to these models, Clark and Robertson (2002) suggest progressive evolutionary scenario for the basins. In this respect, consecutive three stages which are latest Cretaceous initial collision (soft collision), early Tertiary extension and Eocene collision (hard collision) were proposed. These stages are also respectively associated with the closure of Inner Tauride Ocean, readjustment of micro plates along suture zone, and ongoing convergence related crustal thickening in Central Anatolia.

1.5 Previous Works

The pioneer studies of the Haymana Basin were conducted by Chaput (1932, 1935a, b and 1936), Rigo de Righi and Cortesini (1959), Reckamb and Özbey (1960), Schmidt (1960). Although the main aim of these studies was to unrevealing the petroleum potential of the basin, they established stratigraphic frame of the region and following studies of Yüksel (1970), Sirel (1975) and Ünalın *et al.* (1976) formed today's stratigraphic nomenclature for the region.

Yüksel (1970) studied around Haymana town and prepared detailed geological map and cross-section of the region. He also defined, based on paleontological dating, the relationships between basin infill units and sedimentological characteristics.

Sirel (1975) worked on micropaleontology of the late Cretaceous –Eocene basin infill and determined foraminiferal biozones for that time interval.

Ünalán *et al.* (1976) studied in Haymana and Polatlı region and determined the stratigraphical frame work and paleogeography of the region. He also defined the facies associations of the basinfill. In this study, nomenclature of Ünalán *et al.* (1976) were followed.

Ünalán *et al.* (1976), Batman (1978, 1981), Dellaloğlu and Aksu (1991), and Rojay *et al.* (2001 and 2004) worked on the basement units of the Haymana Basin. The basement is composed of metamorphic rocks of the Karakaya complex, Jurassic platform carbonates and upper Cretaceous Ankara ophiolitic mélanges.

In addition to these pioneer studies, Gökçen (1978), Gökçen and Kelling (1983), Çetin *et al.* (1986), documented examples of sedimentology studies of the Haymana Basin. They were mainly concerned with sedimentary provenance, paleocurrent directions, petrographical and mineralogical analyses. These authors suggested a single source area with two different lithologies and provided evidence for a N to S feeding direction, except E to W paleoflow direction determined by Çetin *et al.* (1986) for the middle Eocene units. Moreover, cyclicity and sequence stratigraphy of the Eocene shallow-marine carbonates and clastic sequences were studied by Çiner *et al.* (1993 a, b, 1996 a, b). In these studies, existence of nummulitic bank and sub-marine fan deposits in Eocene deposits and tectonic force promoted cyclicity in these units were suggested.

Sirel (1975), Ünalán *et al.* (1976), Sirel and Gündüz (1976), Meriç and Görür (1981), Sirel *et al.* (1986), Dellaloğlu and Aksu (1991), Özcan and Altner (1997), Özcan *et al.* (2001) and Özcan, (2002) documented the results of paleontology studies conducted on upper Cretaceous to Eocene basinfill the Haymana Basin.

Except for the study of Ünalán and Yüksel (1978) which suggests graben origin for the basin, Görür *et al.* (1984, 1998), Koçyiğit *et al.* (1988, 2003), Koçyiğit (1991), Rojay and Süzen (1997), Kaymaccı (2000) suggested, by comparing the tectonic

position and stratigraphic record of the Haymana Basin with other Central Anatolian basins, fore-arc type development for the evolution of the basin

CHAPTER 2

STRATIGRAPHY

Haymana Basin is located in the Central Anatolia (south of Ankara City) and covers about 4000 km². Although the evolutionary history of the basin is directly connected with crystalline rocks of the Pontides, Taurides and Kırşehir blocks, only Pontide basement is exposed in the study area while Kırşehir Block or Tauride Block basement bound the basin in the east and south without any direct contact. The basement units exposing in the study area cover small areas with respect to basinfill and generally have tectonic contact with the younger units in the north and south. In respect to lithological discriminations, basement units are represented by; (1) rocks of the Karakaya complex, which are basically Carboniferous–Permian limestone olistoliths and high-grade metamorphic rocks (Bingöl *et al.*, 1974; Batman, 1978; Tekeli, 1981; Akyürek *et al.*, 1984; Okay *et al.*, 1996; 2002), (2) Upper Jurassic to Lower Cretaceous platform sequences (Ünalán *et al.*, 1976; Altınér *et al.*, 1991; Koçyiğit, 1991) and (3) chaotically distributed ophiolitic fragments or blocks with Cretaceous age (Ünalán *et al.*, 1976; Batman, 1978; Dellaloğlu and Aksu, 1991; Bragin and Tekin, 1996; Rojay *et al.*, 2001;2004; Rojay 2013). In the study area, these units are exposed in a chaotic mélangé as imbricated blocks; they are interpreted in this study as imbricated complex and named Ankara imbricate zone. In contrast to the complex structure of the basement units, basinfill shows continuous sedimentation from late Cretaceous to late Eocene time interval and is basically represented by continental clastic rocks, shallow-marine limestones and turbidites. The basinfill and the basement units are unconformably covered by Neogene continental clastics or evaporites.

Elementarily, units exposing in the Haymana Basin can be grouped as; (1) the basement, (2) late Cretaceous to Eocene basinfill and (3) Neogene cover units. The geological map and the stratigraphic columnar section of the Haymana Basin are given

Figures 2.1 and 2.2, respectively. A large-scale geological map of the Haymana basin is also given in Appendix A.

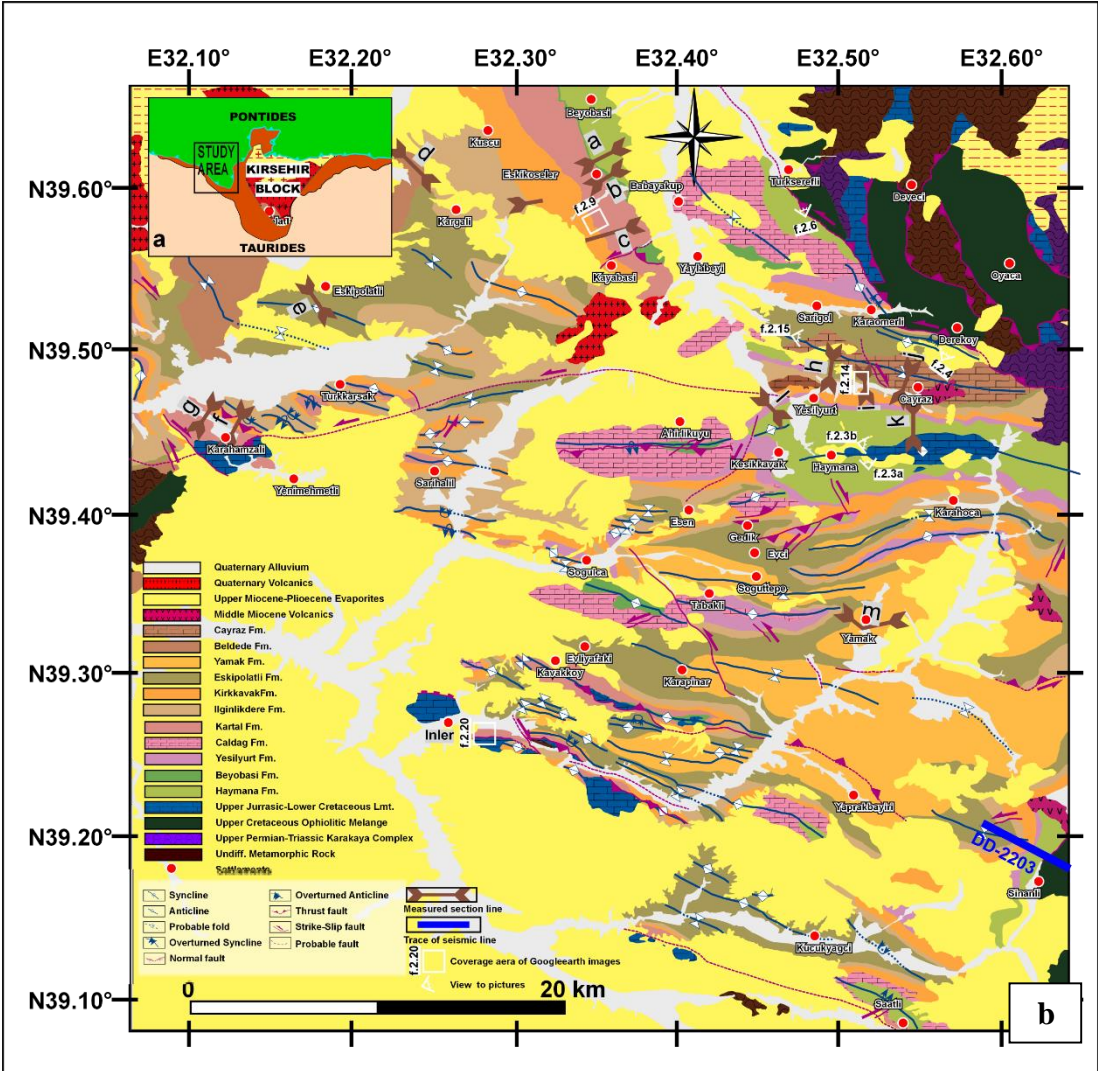


Figure 2.1: (a) Regional map showing the location of the study area b) Geological map of the Haymana Basin (our own work and partly modified from MTA 2002). Letters ‘a-b-c-d-e-f-g-h-i-j-k-l-m’ shows the locations of the measured stratigraphic sections.

System		Thickness (m)	Description	Cycle
Series				
Quaternary			Alluvium	Cover
Neogene	Mio-Pliocene	500	Neogene Units : red beds and evaporites	
Paleogene	Eocene	5000	11- Yamak Fm. : conglomerate, sandstone, mudstone 10- Çayraz Fm. : limestone and marl 9- Beldebe Fm. : continental red clastics	4
	Paleocene		8- Eskipolatli Fm. : marl, sandstone and mudstone 7- Ilgınlıkdere Fm. : conglomerate and sandstone 6- Kirkkavak Fm. : algal limestone and marl	3
L. Cretaceous	Santonian– Maastrichtian	2000	5- Yesilyurt Fm. : marl 4- Çaldag Fm. : reefal limestone 3- Kartral Fm. : continental red clastics	2
			3- Kocatepe member : red pelagic limestone 2- Beyobasi Fm. : sandstone, sandy marl and coal 1- Haymana Fm. : shale and turbiditic sandstone	1
Pre-Upper Cretaceous			3- Platform sequences : recrystallized limestone, limestone 2- Ophiolitic mélange with limestone blocks 1- Metamorphic basement (Pontides)	Basement

Figure 2.2: General stratigraphic columnar section of the Haymana Basin (modified after Ünalán *et al.*, 1976). Fm-Formation

2.1 Basement Units

Basement units exposing in the study area can be grouped as; (1) metamorphic rocks of the Karakaya Complex, (2) Upper Jurassic–Lower Cretaceous platform sequences and 3) Upper Cretaceous ophiolitic units.

2.1.1 Metamorphic Rocks

Carboniferous to Late Triassic time span proposed for the evolution of Karakaya Complex, although there is no radiometric and fossil ages documented from the metamorphic rocks cropping out in the study area.

Batman (1978) is the first study targeting the metamorphic units exposing in the study area. The rocks are named Hisarlıkaya Formation while the other studies dealing with the equivalent of these units in the Ankara region are termed Temirözü Formation (Ünalán *et al.*, 1976), complex of metamorphic rocks and limestone blocks (Norman, 1973), Karakaya Formation (Bingöl *et al.*, 1974) Elmadağ formation (Akyürek *et al.*, 1984) and Karakaya nappes (Koçyiğit, 1987). In this study, Karakaya Complex terminology is preferred in order to simplify grouping of these old rocks and emphasizing their origin. The rocks of Karakaya Complex crop out in the NW part of the study area around Deveci and Boyalık villages and are mainly represented by dark grey to light brownish, highly deformed quartzite, muscovite, chlorite schists, dark meta-ophiolitic rocks and slightly metamorphosed sandstones, conglomerate and mudstone alternations. Presence of Carboniferous to Permian limestone olistoliths sizes ranging from one meter to hundreds of meters dimensions are also common.

2.1.2 Upper Jurassic–Lower Cretaceous Platform Sequences

This group of rock comprise Upper Jurassic to Lower Cretaceous platform carbonates of the Tauride Platform and Pontides. In addition to their fossil assemblages, two group of carbonates are also differentiated on the basis of presence and/or absence of metamorphism. In this sense, metamorphosed rocks are considered as the Tauride Platform carbonates and non-metamorphosed ones, Pontides. In the study area, carbonates of the Pontides crop out in the northern, central, and southern parts of the

region while Tauride Platform carbonates are exposed only in the southernmost part. The contact relationship between basinfill and the Pontide carbonates occur as unconformities and/or faulted contacts. No direct contact between the basinfill and carbonates of Tauride block is, however, not exposed and also any diagnostic fossils belonging to the Tauride platform sequences could not be found in the carbonate pebbles of conglomerates of the basinfill, during field work and thin section studies. Therefore, carbonates of the Pontide block will be main concern of this section.

Outcrops of these units follow N–S trends in the north while it is WNW–ESE direction in the south. These exposures were named as Mollaresul formation (Ünalın *et al.*, 1976), Lalelik formation (Batman, 1978), and Beytepe formation (Dellalođlu and Aksu, 1991). In addition to these local definitions, the equivalent of the units along Pontide belt were defined as Biga-Bursa-Bilecik platform (Altner *et al.*, 1991) and Amasya Group platform carbonates (Rojay, 1995) in the central and western part of the Pontides, respectively.

The carbonates exposed in study area were divided into two members (Batman, 1978) as (I) highly deformed micritic limestone-chert alternations at the base and (ii) reddish to greenish claystone-sandstone alternation with some pre-Jurassic olistostrome blocks at the top (Kocatepe formation of Yüksel, 1970). In addition to these two members, very poorly sorted and graded conglomerate member with ultramafic, radiolarite, chert, metamorphic and magmatic pebbles was also defined at basal part of the unit (Dellalođlu and Aksu, 1991). According to fossil assemblages from northern exposures, Tithonian to Berriasian and Turonian to Santonian ages were proposed (Batman, 1978; Dellalođlu and Aksu, 1991), for the basal and upper levels of the sequence, respectively. In addition to these ages, Kimmeridgian to Valanginian ages were also determined for the basal units of the sequence (D. Altner, personal communication, 2015) based on limestone samples collected within the context of the study from the southern margin of the study area. The fossil assemblages are; *Pseudocyclammına lituus*, *Protopenneroplis striata*, *Mohlerina basiliensis*, *Labyrinthina mirabilis*, *Crescentiella morronnesis*, Miliolidae, Verneulinid foraminifera, and Textularid foraminifera.

In contrast to the previous studies of Ünalın *et al.* (1976), Batman (1978), Dellalođlu and Aksu (1991), an unconformity for the contact of the base and top level of the sequence (Kocatepe formation) was defined during the study. The evidence include; (1) an existence of a time gap for Valanginian to Turonian time interval (maximum gap) for the base and top level of the sequence, (2) their different lithological characteristics as being highly deformed platform sequence at the base and less deformed deeper marine sequence at the top, and (3) angular differences between the sequences (Figure 2-3a). By considering the widespread association of the platform sequence at the bottom, it might be thought that Kocatepe formation forms a part of the basement sequences, the contact relationship between Kocatepe and the oldest unit of the basin (Upper Cretaceous Haymana Formation) around Haymana town (Figure 2-3b) is, however, observed as conformable. This relationship may also be explained as disconformity. In this respect, two different possibilities might be proposed for the association of the Kocatepe formation; (1) Kocatepe formation belongs to basement units and Haymana formation overlies it with a short time gap, (2) Kocatepe formation is the oldest unit of the Haymana Basin covering the basement sequences. For the study, in spite of the widespread association of the Kocatepe formation and platform sequences in the region, it is considered as a part of basinfill due to unproven short-time gap between Haymana-Kocatepe formations, angular relationships and possible dynamic evolution scenarios allowing for being associated with basement units in the some part of the region (proximal) and being conformable with the basinfill units in the central and southern part of the study area (distal).

Although the boundary between Karakaya complex and the platform sequences is tectonic due to imbrication of the basement units, original contact relationship were also determined and interpreted as an unconformity in the study area (Batman, 1978; and Dellalođlu and Aksu, 1991).

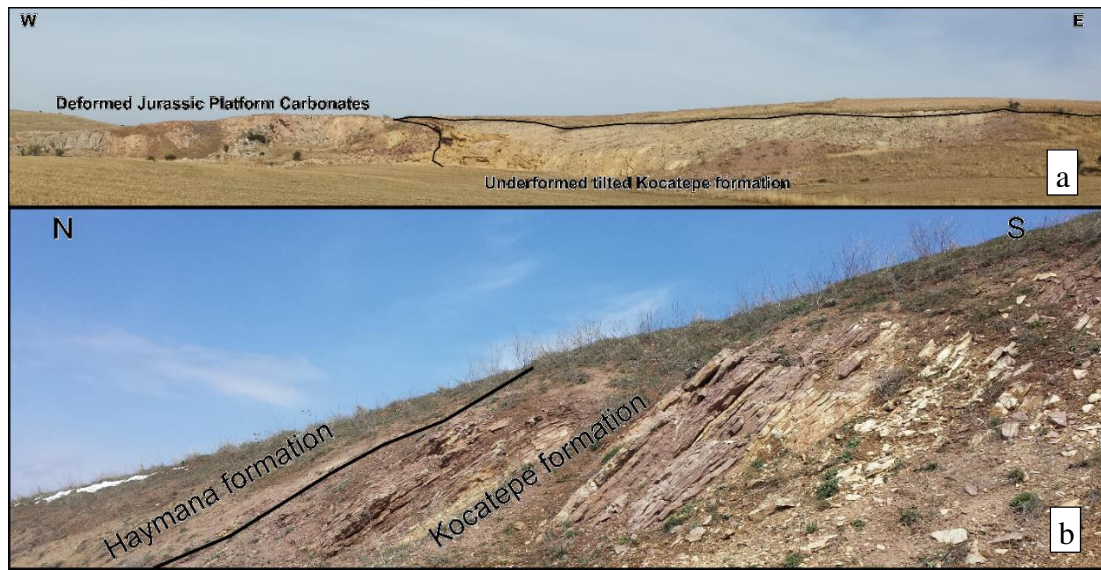


Figure 2.3: (a) Angular relationship between Kocatepe formation and platform sequences. View: towards N. Location: North of Haymana town. (b) Contact relationship between Kocatepe and Haymana formations. View: towards W. Location: Haymana-Ankara road, North of Haymana town (see Figure 2.1 for locations)

2.1.3 Late Cretaceous Ophiolitic Units

Exposures of this group are distributed along the margin of the basinfill units and observed around Dereköy and Oyaca village at the north, Samsam Lake and Sinanlı villages at the southeast, and Yenimehmetli village at the southwest parts of the study area (see Figure 2.1b and Appendix A for locations). Their equivalents in the Ankara region were studied and named as ophiolitic part of Ankara mélangé (Bailey and Mc. Callien, 1950), ophiolitic mélangé (Norman, 1973), Dereköy formation (Ünalán *et al.*, 1976; Batman, 1978), Kılıçlar group (Akyürek *et al.*, 1984), Sinanlı formation (Dellaloğlu and Aksu, 1984) and Samsam group (Dellaloğlu and Aksu, 1991).

Chaotic distribution of different type of variously sized ophiolitic fragments (as pillow basalts, MORB, seamount basalts, OI basalts, radiolarites, mafic-ultramafic rocks and Upper Jurassic –Late Cretaceous reefal origin limestones in a scaly matrix) define the main lithological association of the group. Due to the chaotic and imbricated character of these units, Late Jurassic to late Cretaceous age were proposed for the formation of the ophiolitic units in the region. Except the Callovian–early Aptian age determined

from calcareous intrafills between pillow lavas around Dereköy village (Rojay *et al.* 2004), Norian to late Albian–Turonian radiolaria ages (Bragin and Tekin 1996), and 80.3 ± 7.6 Ma ($^{40}\text{Ar}/^{39}\text{Ar}$, mica) formation age for basaltic pillow lavas (Sarifakioğlu *et al.* 2013) were proposed for the equivalent units exposed at the north of the study area. In addition to the formation ages of the northerly located exposures, Cenomanian to Campanian ages were proposed for pelagic sequences associated with the southerly located equivalents (around Samsam Lake and Sinanlı village) based on fossil assemblages (Dellaloğlu and Aksu, 1991).

The base of the unit is not exposed in the region, however, its contact relationship with the Karakaya Complex and platform sequences might be defined as imbricated and highly deformed contacts. Its contact with the basinfill is observed as a tectonic contact in the north around Dereköy village (Figure 2.4) whereas in the south (around Sinanlı town), this contact relationship is a sharp contact (onlap) based on a seismic line (DD 22–03) crossing that boundary (Figure 2.5). Additionally, fragments of the Late Cretaceous basinfill units are observed within ophiolitic *mélange* at that locality. Although Akıl (2007) and Koçyiğit (1991) suggested faulted (thrust) contacts for the boundary between southern and northern equivalents of the unit, and Neogene cover units, this relationship is not observed within the study area.

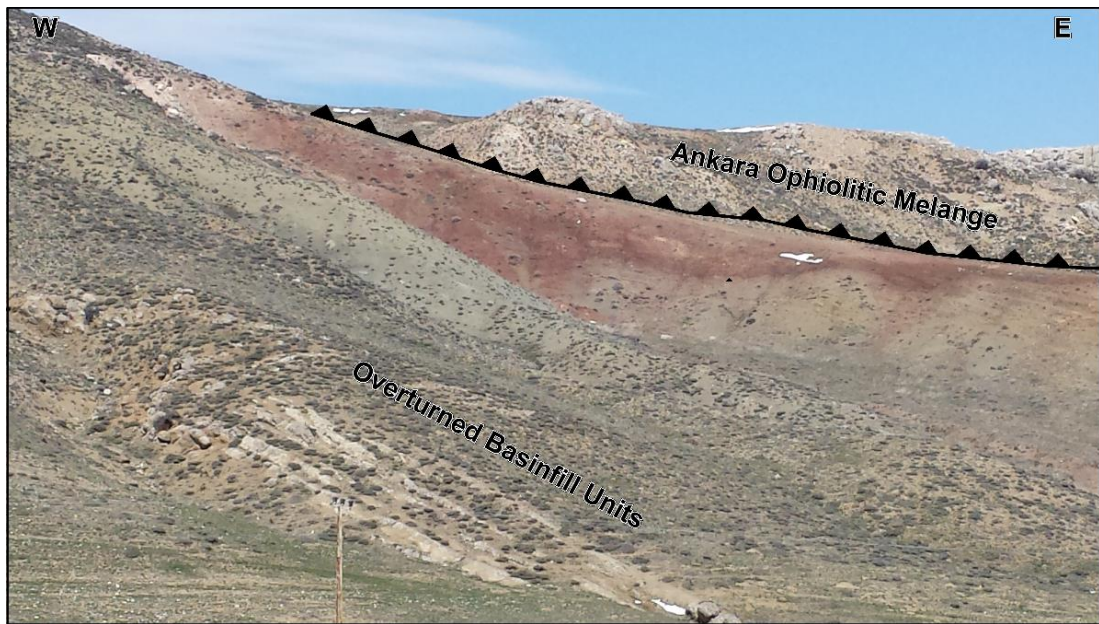


Figure 2.4: Faulted contact between basin infill and upper Cretaceous ophiolitic mélanges. View: Towards N. Location: south of Dereköy village. (see Figure 2.1 for locations)

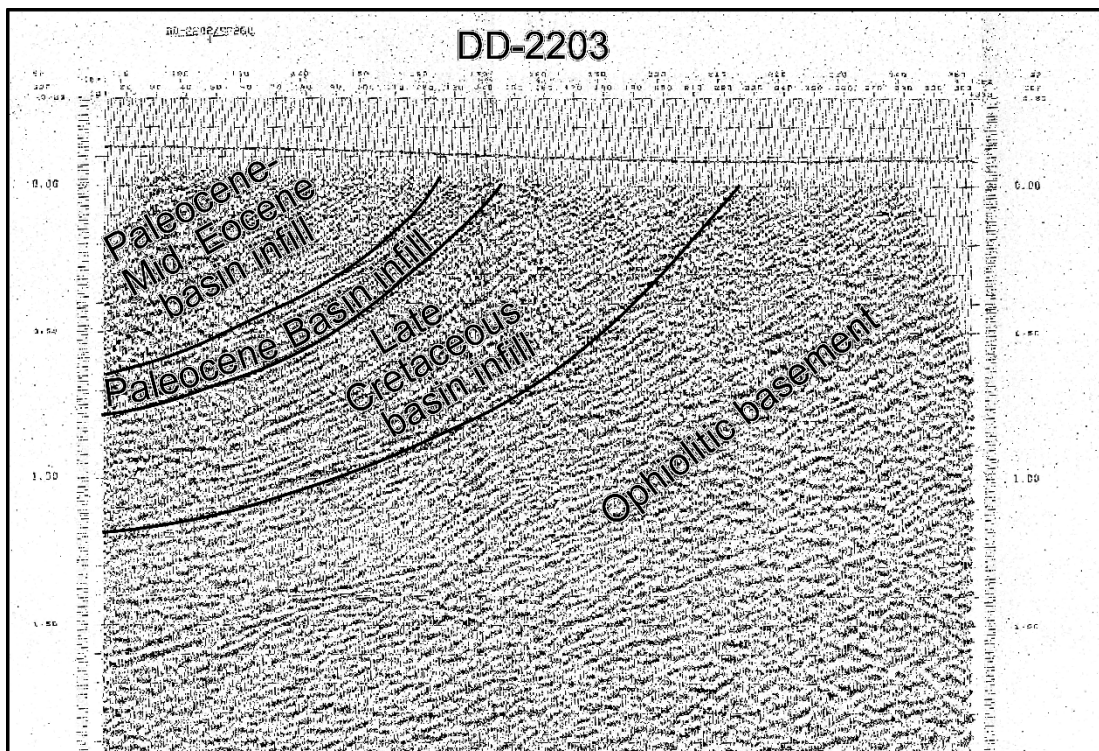


Figure 2.5: Interpretation of DD-2203 seismic line indicating sharp contact (onlap) between ophiolitic basement and basinfill units (see Figure 2.1 for locations). Seismic line is gathered from seismic department of T.P.A.O and interpreted in this study.

2.2 Late Cretaceous to Eocene Basinfill Units

In order to understand characteristics of the basinfill, 13 stratigraphic sections were measured and continuous ~ 7-km-thick sequence of four Upper Cretaceous to late Eocene key stratigraphic sequences (cycles) were determined based on the analysis of the sedimentological facies and depositional environments. The contact relationships between the cycles were described as laterally and vertically gradational with some local syn-sedimentary unconformities. The main criteria for determining the cycles was considered as the depositional environment of the basinfill and their lateral/vertical stratigraphic continuity. As a conclusion each cycle was defined as a group, containing continental clastic rocks, shallow- and deep-marine deposits. Within the scope of stratigraphy studies, a new geological map (Figure 2.1) and stratigraphic columnar section (Figure 2.2) were prepared by mostly adding new field observations on MTA 2002 and Ünalán *et al.* (1976) studies.

Sirel (1975), Ünalán *et al.* (1976), and Gökçen (1976) carried out paleontological, stratigraphical and sedimentological studies, targeting the basinfill and proposed continuous deposition for late Cretaceous to late Eocene time interval, but they all used different terminology for each unit. In this study, definitions of Ünalán *et al.* (1976) will be followed and this forms a basis for determining stratigraphic cycles during this study. In this context, stratigraphic cycles, from older to younger are; (1) Upper Cretaceous Haymana and Beyobası formations, (2) Lower–Middle Paleocene Kartal, Çaldağ and Yeşilyurt formations, (3) Upper Paleocene–Early Eocene Kırkkavak, Iğnınlıkdere and Eskipolatlı formations, and (4) Lower to Middle Eocene Beldede, Çayraz and Yamak formations (Figure 2.2). A matrix chart showing the relationships of these units is given in Table 2.1.

Table 2.1: Contact relations between basinfill and the basement units.

	a	b	c	d	e	f	g	h	i	j	k	l	m	n
Cihanbeyli Fm (a)														
Yamak Fm (b)	U													
Çayraz Fm (c)	U	LVT												
Beldede Fm (d)	U	LVT	LVT											
E.polatlı Fm (e)	U	LVT+U	LVT+U	LVT										
İlgınlıkdere Fm (f)	U	LVT	LVT	N/A	LVT									
Kırkkavak Fm (g)	U	N/A	LVT	N/A	LVT	LVT								
Yeşilyurt Fm (h)	U	N/A	N/A	N/A	LVT	LVT	LVT							
Çaldağ Fm (i)	U	N/A	N/A	N/A	LVT	LVT	N/A	LVT						
Kartal Fm (j)	U	N/A	N/A	N/A	LVT	N/A	LVT+U	N/A	LVT					
Beyobası Fm (k)	U	N/A	N/A	N/A	N/A	N/A	LVT	N/A	N/A	LVT				
Haymana Fm (l)	U	N/A	N/A	N/A	N/A	N/A	N/A	LVT	LVT	LVT	LVT			
Jura Lmt.(m)	U	N/A	T	N/A	N/A	N/A	T	T	T	T	N/A	T+U+LVT		
Cre.Oph. (n)	U	N/A	T	N/A	N/A	T	N/A	T	N/A	N/A	N/A	T+U+LVT	T+U	
Metamorphichs (o)	U	N/A	T	N/A	T	N/A	N/A	N/A	N/A	N/A	N/A	N/A	T+U	T

LVT: lateral and vertical transition U: unconformable N/A: not available T: tectonic contact

2.2.1 First Cycle

The first cycle comprises Upper Cretaceous Haymana and Beyobası formations. Haymana formation is generally represented by turbidity current-related deposits whereas Beyobası formation is characterized by shallow-marine sediments.

2.2.1.1 Haymana Formation

The formation is named for the first time by Rigo de Righi and Cortesini (1959), and same terminology were used by various authors since then. The unit is exposed around Beyobası, Türkşerefli, Sarıgöl, Haymana, Çuluk, Sinanlı and Saatçi villages and cover large areas at the north of the study area (see Figure 2.1b and Appendix A for locations). Its direct contact with the basement units is not observed in the north and the center of the study area. Thin, red, foraminifer-bearing pelagic limestone layers of the Kocatepe formation is, however, conformably overlain by the Haymana formation. The contact between Kocatepe formation and basement units is interpreted as a faulted contact (Figure 2.6) in the north (around Türkşerefli and Sarıgöl villages with ophiolitic units and platform sequences), an unconformity (Figure 2.3a) at the central (around Haymana town with platform sequences), of the study area. In the southernmost part of the area (around Sinanlı village), Haymana formation (or Kocatepe formation) has a sharp contact (onlap) with the ophiolitic basement (Figure 2.5).



Figure 2.6: Fault contact between Haymana formation and the basement units. View: towards E; Location: East of Türkşerefli Village (see Figure 2.1 for location).

The entire sequence of the formation is observed within an anticline, core of which is exposed at east of Haymana town; a stratigraphic section was therefore, measured through the northern limb of this fold whereas a section representing the western continuation of the formation was measured around Beyobası village (Figure 2.7 and see Figure 2.1 for location). The total thickness of the formation is 1045 m and 302 m along the first and second sections, respectively. Although Santonian age (Aynur Hakyemez, Personal communication, 2015), ~100-m-thick, laminated, red pelagic limestone layers of Kocatepe formation were not added to the measured section, and formation is considered as a member at base of the Haymana formation. The first section is represented mainly by three fining-upward sequences (see Figure 2.7 for intervals), composed mainly of conglomerate, sandstone and mudstone alternations. 5-m-thick sandy matrix-supported conglomerate layer forms the base of the formation and contains rounded to semi-rounded, poorly graded, (maximum 20 cm in diameter) pebbles, derived mostly from re-crystallized limestone, chert, basic/acidic volcanic or intrusive and serpentinite. Similar conglomerate horizons (1 to 15-m-thick) occur at the upper levels of the formation but there is a pronounced decrease in pebble size up to 3 cm in diameter. Besides, up to 15-m-thick grey, laminated sandstone layers, monotonous sandstone, mudstone, siltstone, sandy mudstone, and muddy sandstone alternation (turbidites) form the ~ %70 of the section. They are mainly represented by greyish-greenish, thinly-bedded (<50 cm), medium-grained, ungraded, sandstone layers with sole structures like groove/flute casts (locally), and finely laminated (within up to 5-m-thick packages), dark green, bioturbated (locally) mudstone-siltstone layers; slumps are also observed locally. In addition to the dominant deposits of the sequence, even if not a



Figure 2.7: Measured stratigraphic sections of the Haymana formation. See text for explanations and see Figure 2.1 for location.

full sequence, some layers of Bouma sequence are also observed in sandstone horizons. Scattered conglomeratic pebbles (<5 cm in diameter) which are mainly ophiolitic sequence and magmatic or rarely low-grade metamorphic and limestone rooted, are also common in the section. A detailed sedimentology study on sandstone layers of the unit was done by Çetin *et al.* (1986) and they proposed that mainly acidic intrusions related grains, and secondarily ophiolitic and metamorphic fragments are the basic population forming the sandstone layers. They also suggested, based on primary sedimentary structures and tectono-sedimentary classification of the sandstone grains, NNW to SSE dominant paleo-current direction and intra or fore-arc environment for the deposition of the unit. The second section shows similar characteristics with the first one if one considers source and deposition direction. Its layers are, however, represented by thicker conglomerate levels with coarser pebbles and sandstone–sandy mudstone alternations. It is therefore, proposed that deposition of the formation were started in a deep-marine low-energy environment (Kocatepe member) and abrupt shallowing of the basin floor or uplift on the source allowed for the deposition of the thick conglomerate layers at the base; sedimentation was later controlled by turbidity currents with at least two sets of thick (up to 120 m) conglomerate, conglomerate-sandstone alternation at the base of fining-upward sequences (see Figure 2.7 for intervals) possibly resulted from abrupt activities of submarine fans. For this study, it is also inferred that the formation was deposited in fore-arc settings based on its contact with ophiolitic *mélange*, tectono-sedimentary classification of the sandstone grains, and lack of intercalation of volcano-sedimentary sequences.

Based on benthic and pelagic fossil assemblages, the age of the formation is suggested as Maastrichtian (Ünalán *et al.*, 1976), late Campanian–late Maastrichtian (Dellaloğlu and Aksu, 1991) and late Santonian–late Campanian (Özcan and Altınır, 1997). These ages are also conformable with the Santonian age of Kocatepe member as determined in this study.

In a broad sense, Kapanboğazı formation (Görür *et al.*, 1993) and Yemişliçay formation (Görür, 1993) of northern Pontide basins, Karadağ (Akyürek *et al.*, 1984)

and Ilıcapınar formation (Norman, 1972) of the Kırıkkale-Bala Basin, Yaylaçayı formation (Yoldaş, 1982; Tüysüz *et al.*, 1995) of the Çankırı Basin, Göynük volcanoclastic olistostrome (Göncüoğlu and Köksal, 1997) of the Ayhan-Büyükkışla Basin, Kartal formation (Arıkan, 1975; Görür *et al.*, 1984) of the Tuzgölü Basin, and Aktaştepe formation (Demirtaşlı *et al.*, 1973) of the Ulukışla Basin might be considered as the equivalent of the Haymana formation in the region.

2.2.1.2 Beyobası Formation

The formation is named by Ünalın *et al.* (1976) and exposed around Beyobası, Kavakköy, Devecipınarı and Küçükyağcı villages at the core of anticlines (see Figure 2.1b and Appendix A for locations). Its contacts with the underlying Haymana and overlying Kartal and Yeşilyurt formations is described as both gradational.

The entire section of the formation is observed at the east of Beyobası village, therefore, a 92-m-thick stratigraphic section is measured in that locality (Figure 2.8 and see Figure 2.1 for location); 10-m-thick grey to light green, massive mudstone layer occurs at the base of the section; sandy mudstone–sandstone alternation with 8-m-thick conglomerate layer from rest of the section. Conchoidal fracturing, carbonate concentration and yellowish color define the mudstone layer of the section and mark the differences between turbiditic layers of the Haymana Formation. Sandy mudstone horizons of the formation are observed as up to 5-m-thick layers but they are generally interrupted by 10 to 50-cm-thick channel-type sandstone and conglomerate layers. Carbonate matrix and excessive fossil assemblages (mainly cyclolites and hippurites) are the common characteristics of these layers. Conglomerate layers are generally poorly graded and composed of semi-rounded basalt, serpentinite, andesite, chert, white quartz, schist and re-crystallized limestone pebbles; re-worked fossil traces are also common within these layers. It is thought that the formation represents the shallow-marine equivalent of the Haymana formation due to its gradational contact, fossil content, and coarser grain distribution.

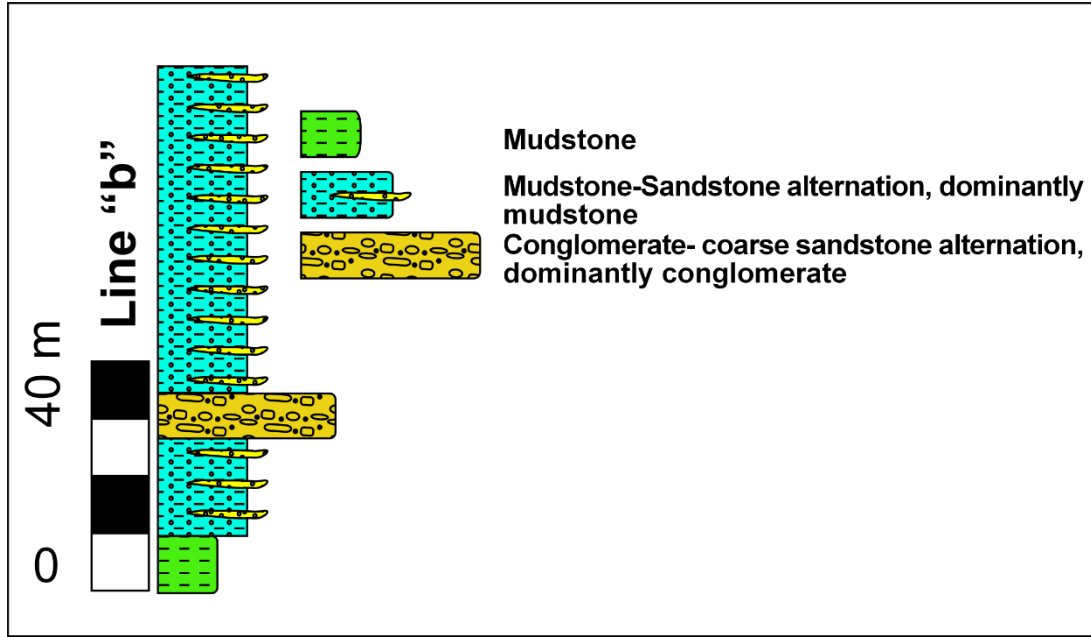


Figure 2.8: Measured stratigraphic sections of Beyobası formation. See text for explanations. (see Figure 2.1 for location).

Based on benthic fossil assemblages, the age of the formation was determined as Maastrichtian (Sirel and Gündüz, 1976), Maastrichtian–ate Maastrichtian (Dellaloğlu and Aksu, 1991), and late Maastrichtian (Özcan and Altıner, 1997).

Yapraklı formation (Birgili *et al.*, 1974) of the Çankırı Basin, Asmaboğazı formation (Rigo de Righi and Cortesini, 1959; Görür *et al.*, 1984) of the Tuzgölü Basin, and Bölükdağ (Norman, 1972) or Samanlık (Akyürek *et al.*, 1984) formations of the Kırıkkale-Bala Basin might be thought as the equivalent of the Beyobası formation.

2.2.2 Second Cycle

Paleocene Kartal, Çaldağ and Yeşilyurt formations form this cycle. Continental red clastic rocks represent the Kartal formation while Çaldağ formation is characterized by reefal limestone and Yeşilyurt formation, by deeper marine deposits.

2.2.2.1 Kartal Formation

Rigo de Righi and Cortesini (1959) named the formation, and same nomenclature were used by various authors since then. The unit is exposed around Eskiköseler, Sarıhalil,

Karahamzalı, and Kavakköy villages, generally at the core of anticlines (see Figure 2.1b and Appendix A for locations). Its contact relationship with underlying Beyobası and Haymana formations is observed as vertically gradational, and also same contact relationship with overlying Çaldağ, Yeşilyurt and Kırkkavak formations is noted (Figure 2.9).



Figure 2.9: GoogleEarth image showing vertical transition between Kartal and Kırkkavak formations. Location: South of Eskiköseler village (see Figure 2.1 for location).

The entire section of the unit is exposed in the area between Beyobası and Kırkkavak formations around Eskiköseler village located at the less deformed NW part of the study area, therefore, a stratigraphic section was measured at this locality (Figure 2.10 and see Figure 2.1 for location). In addition to first section, another stratigraphic section is also measured around Karahamzalı village at the east part of the study area. The first section shows vertical transition of the Kartal to overlying Kırkkavak formation along a 100-m-thick zone. The lowermost ~500 m of the Kartal formation is not added to the first stratigraphic section due to dense vegetation and extensive cover (not allowing measurement of a continuous section), the main descriptive characteristics the section are claret red mudstone with 5-20-m-thick sandstone and/or conglomerate levels. The total thickness of the formation is 950 m and 302m along first and second section, respectively. Through the first section, thick mudstone–

sandstone layers of the first 500 m are truncated by up to 5-m-thick conglomerate layers. Claret red, unsorted, poorly cemented, ungraded, sandy matrix-supported conglomerate layers of the formation mainly contain angular to semi-rounded ophiolitic fragments, limestone and rarely marble pebbles; the size of the fragments may reach up to 10 cm in diameter. A familiar thick conglomerate horizon is also repeated in the upper part of the section. Thin conglomeratic horizons (<20 cm thick) are also common along the section. Besides, up to 20-m-thick massive sandstone levels, reddish sandy mudstone–sandstone–mudstone alternation form the rest of the section. Reddish to greyish, carbonate nodules (up to 10 cm in diameter) and caliche formations are the main characteristics of medium- to fine-grained sandstone layers. The characteristic features of the mudstone layers are their claret red color and high amount of carbonate concentrations. The second section share similar characteristics as the first one, but; (i) it has ~ 40-m-thick sandy limestone–sandstone alternation without macro fossil content, (ii) gradual reduce in grain sizes and (iii) is being lighter colored towards the upper levels. The deposits of the formation was considered, based on common caliche horizons, dominant red color, channel type conglomerate–sandstone layers and rare shallow-marine foraminifers, as continental to shallow-marine clastic rocks as inferred by Ünalán *et al.* (1976)

The age of the formation is, based on benthic foraminifers, early Paleocene (Sirel, 1975; Ünalán *et al.*, 1976). This time span is also supported by underlying (upper Cretaceous), and overlying (upper Paleocene) sequences and also same age of shallow or deeper marine equivalents (Çaldağ and Yeşilyurt formations).

The equivalents of the Kartal formation is thought as lower part of the Hacıhalil formation (Kaymakcı *et al.*, 2009) of the Çankırı Basin, the Baraklı formation (Kara and Dönmez, 1990) of the Çiçekdağ-Yozgat Basin, center part of the Yeşilöz formation (Advokaat *et al.*, 2014) of the Ayhan-Büyükkışla Basin, and the Kalkankaya member of the Aktaştepe formation (Clark and Robertson, 2005) of the Ulukışla Basin.

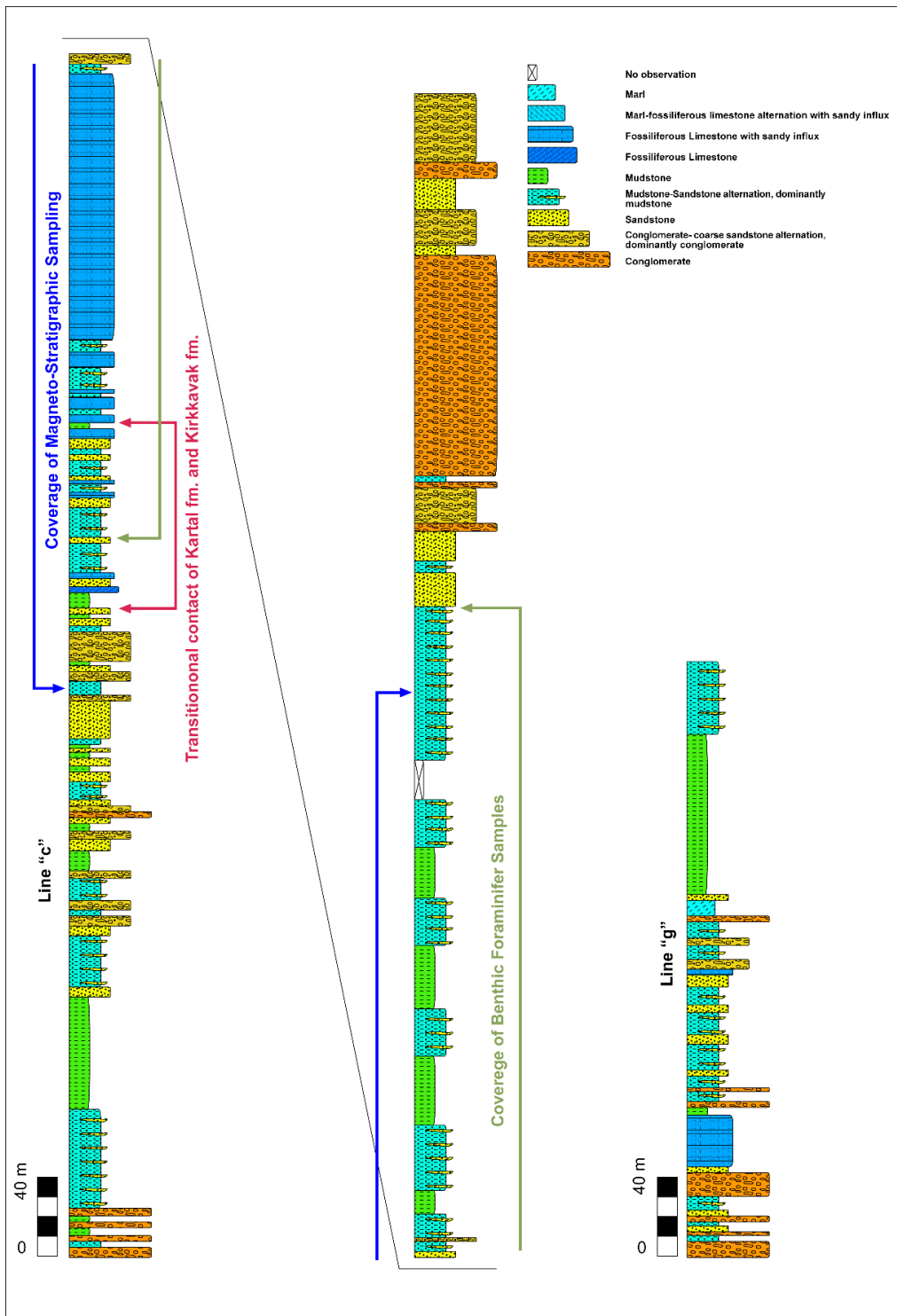


Figure 2.10: Measured stratigraphic sections of the Kartal formation. Note the transition between the Kartal and Kirkkavak formations along the line "c". See text for explanations (see Figure 2.1 for locations).

2.2.2.2 *Çaldağ Formation*

The formation is named by Rigo de Righi and Cortesini (1959); the Çaldağ formation is also adopted used for Jurassic platform sequences exposed in the study area (Sirel, 1975). Outcrops of the unit are generally observed at the flanks of anticlines around Babayakup, Ahırlıkuyu, and Saatli villages as NW–SE and E–W trends at the NW and SE part of the study area, respectively (see Figure 2.1b and Appendix A for locations). It has vertically gradational contacts with underlying Haymana, and overlying Kırkkavak formations, and also it laterally passes into the Kartal and Yeşilyurt formations.

The entire section of the unit is exposed in the area between Haymana and Yeşilyurt formations in the south of Ahırlıkuyu village. Detailed studies of Ünalan *et al.* (1976), and Sirel *et al.* (1986), suggest 1187 m thickness for the formation in this locality. This study confirms gradual transition from grainstone to wackestone as described in the literature. Up to 3-m-thick yellowish to white grainstone levels alternate with up to 1-m-thick blue marl levels at the base of the unit. Grainstone horizons are composed mainly of moderately-sorted and commonly fractured algae, coral, echinoderm, foraminifer (commonly miliolidae) and shell fragments but towards upper levels, grainstone and fossil content decrease. The unit is then dominated by intercalations of yellowish to orange, lenticular packstone and greyish to yellowish wackestone layers with a fine-grained clastic influx. The fossil content of the unit suggests a shallow-marine low energy environment (reef), but existence of grainstones and packstones with fractured fossil particles indicates a slope environment. It is therefore, inferred that some levels of the unit was deposited on slope and fed from reef platform or lagoon.

Benthic foraminifers suggest Selandian–Thanetian time interval for the deposition of the formation (Sirel and Gündüz, 1976; Meriç and Görür, 1981; Sirel *et al.*, 1986).

Dizilitaşlar formation (Norman, 1972; Kaymakçı *et al.* 2009) of the Kırıkkale-Bala and Çankırı basins, Çaldağ formation (Görür *et al.*, 1984) of the Tuzgölü Basin, and

Güneydağı member of the Aktaştepe formation (Clark and Robertson, 2005) of the Ulukışla Basin might be considered as equivalent of the formation.

2.2.2.3 Yeşilyurt Formation

Yeşilyurt formation is considered as a part of Çaldağ formation by some studies like Rigo de Righi and Cortesini (1959), and Yüksel (1970). Ünalán *et al.* (1976) named the formation, by considering its depositional facies characteristics. Exposures of the unit are generally observed in E-W trends around Yeşilyurt, Kesikkavak, Tabaklı, and Soğulca villages (see Figure 2.1b and Appendix A for locations). It laterally grades into Çaldağ formation, and has vertically gradational contact with underlying Haymana and overlying Kırkkavak formations.

The entire section of the formation is observed around Yeşilköy village and a stratigraphic section was measured in this location (Figure 2.11 and see figure 2.1 for location). The thickness of the unit is 274 m. The bottom of the formation is represented by 3-m-thick yellowish to grey algal limestone layer; and these layers are commonly repeated within dark green color mudstone or sandy mudstone–sandstone packages, in the upper part of the section, these layers get thinner and grades into sandy limestone horizons with clastic influx towards upper levels. Also, coarsening-upward sequences and a decrease in carbonate concentration are also observed along the section. High amount of carbonate concentration, grey to green color, and ~20 cm thick, grey, graded sandstone–sandy limestone levels form main characteristics of mudstone packages (up to 50-m-thick) of the formation. Similar characteristics are also valid for the sandy mudstone–sandstone packages, except for up to 3-m-thick channel type sandstone layers with scattered angular limestone clasts (up to 1 cm in diameter) (form Çaldağ formation, noted by Ünalán *et al.* 1976). Its gradual transition with the Çaldağ formation, existence of re-worked reef limestone clasts, alternation of mudstone–sandstone–sandy mudstone layers in thick packages, and previously defined pelagic fossil assemblages (Ünalán *et al.*, 1976) indicate turbidity currents-related sedimentation in front of a carbonate shelf. As a conclusion, it is inferred that the Yeşilyurt formation is deeper marine equivalent of Çaldağ formation as mentioned by Ünalán *et al.* (1976).

Based on pelagic fossil assemblages, age of the Yeşilyurt formation is assigned as Danian by Ünalın *et al.* (1976) and Selandian by Sirel and Gündüz (1975). Danian to Thanetian time interval is, however, considered as the age of this formation in this study due to its lateral and vertical relationships with the Çaldağ and Haymana formations.

Yeşilyurt formation is defined uniquely in the Haymana Basin, but its equivalents in the region might be considered as turbiditic or calci-turbiditic levels of the Dizilitaşlar formation (Norman, 1972; Kaymakcı *et al.*, 2009) of the Kırıkkale-Bala and Çankırı basins, the Çaldağ formation (Görür *et al.*, 1984) of the Tuzgölü Basin, and Ömerli member of the Aktaştepe formation (Clark and Robertson, 2005) of the Ulukışla Basin.

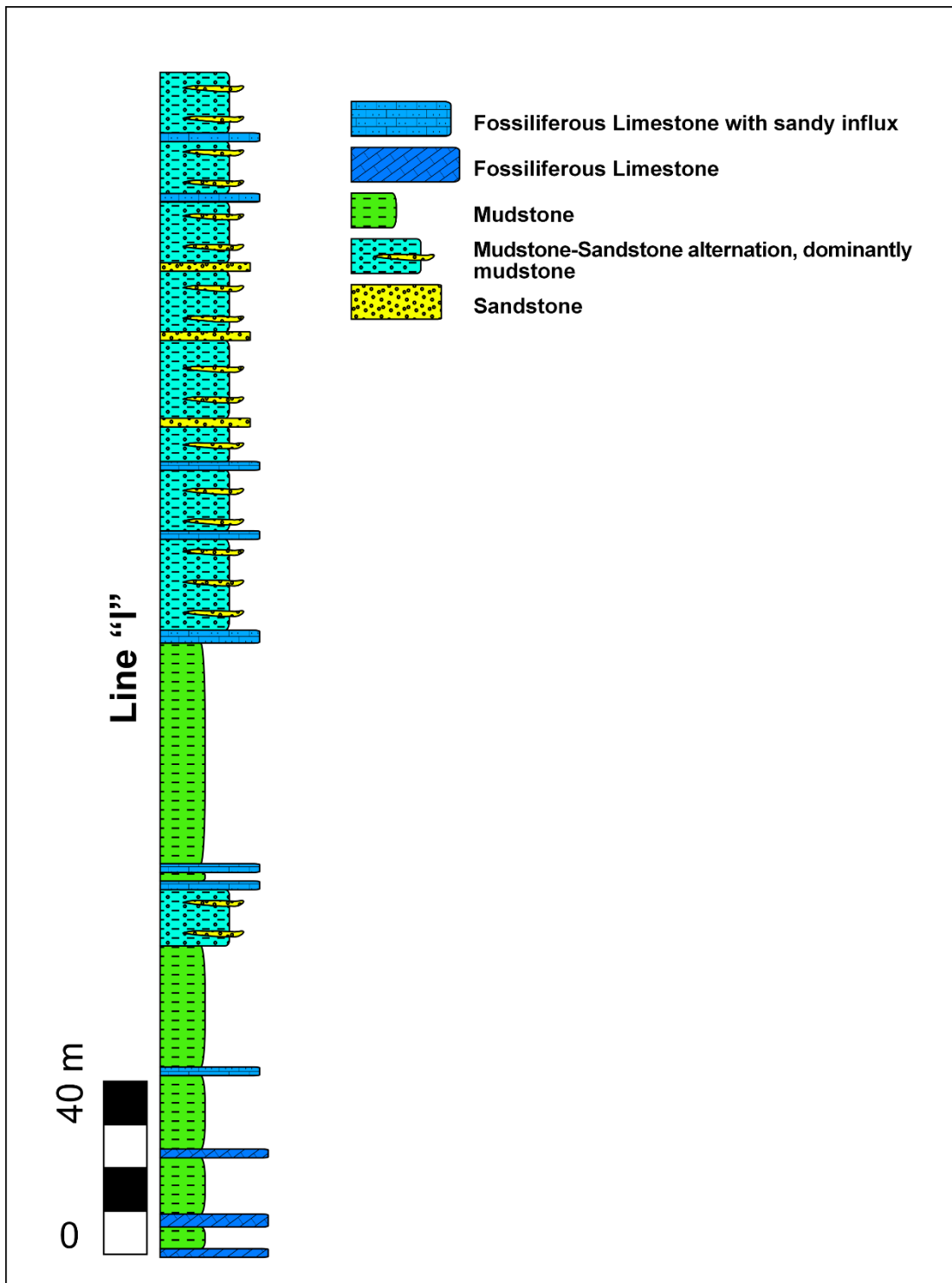


Figure 2.11: Measured stratigraphic sections of the Yeşilyurt formation. See text for explanations (see Figure 2.1 for location).

2.2.3 Third Cycle

Upper Paleocene–lower Eocene Kırkkavak, Eskipolatlı and Ilgınlıkdere formations represent the third cycle. Kırkkavak formation is composed of shallow-marine deposits associated with continental clastics, whereas Ilgınlıkdere and Eskipolatlı formations, by slope and slope front deep-marine deposits, respectively.

2.2.3.1 *Kırkkavak Formation*

The formation is named by Rigo de Righi and Cortesini (1959). It covers large areas in the north of the study area around Kuşcu, Kayabaşı and Sarıgöl villages, and smaller areas in the south around Sarıhalil, Karahamzalı, and Soğulca villages (see Figure 2.1b and Appendix A for locations). The contact relationship between Kırkkavak and underlying Kartal formation is described as unconformity at northern margin of the study area as inferred by Nairn *et al.* (2013), but in general, it has a gradational contacts with underlying Yeşilyurt, Çaldağ and Kartal formations, and laterally grades into Ilgınlıkdere formation.

The entire section of the unit is exposed between Kartal and Ilgınlıkdere formations at the west of Eskiköseler village, therefore, a stratigraphic section is measured in this locality where its gradational contact with the underlying Kartal formation is well exposed (Figure 2.10 and see Figure 2.1 for location). Another stratigraphic section is also measured in the western part of the study area around Karahamzalı village (Figure 2.12 and see figure 2.1 for location); two section show a sharp decrease in the thickness of the formation from 900 m to 320 m. Light greenish to white thick bedded (up to 5 m) fossiliferous sandy limestone–thin bedded reddish to orange sandstone and mudstone intercalation characterize the gradual 100-m-thick transition zone between the Kartal and Kırkkavak formations and the zone ends up with light green to gray 10-m-thick fossiliferous marl layer along the first section. Along the first section, coarsening-upward sequence was noted by gradual transition from marl–mudstone–sandy mudstone–sandstone–reef limestone alternation, to a sandy limestone–sandstone with scattered conglomeratic grains–conglomerate alternation. Light green to gray color at the base and dark green to green color at the top of the section,

concoidal fracturing, and moderate lamination are the main characteristics of the fossiliferous marl and sandy mudstone layers of the formation. Grey to green sandstone layers are generally observed as up to 20-cm-thick channels within marl and sandy mudstone levels. Towards upper parts of the section, they form up to 10-m-thick massive layers and include up to 50-cm-thick conglomerate channels. Semi-rounded, ungraded, poorly sorted limestone (probably from Çaldağ formation), macro fossil, and rarely ophiolitic fragments (up to 5 cm in diameter) within sandy matrix form the matrix-supported channel type conglomeratic levels. Lens-shaped limestone layers are also determined as two packages along the first and second sections: (1) at the base levels of the formation, 2) at the middle levels of the formation (see Figure 2.10 and 2.12 for intervals). The first one is composed of up to 3-m-thick yellowish to white grainstone with coral, echinoderm, foraminifera and shell fragments. Differently from the first one, the second package is represented by intercalations of yellowish to orange, thin-bedded fossiliferous sandy limestone, greyish to yellowish thin-bedded marl, and thick-bedded algal limestone layers. A decrease in limestone and an increase in mudstone layers with shallow marine fossil assemblages are observed towards eastern and southern part of the study area as described by Ünalán *et al.*, 1976. Similar characteristics are also described for the second section. As a result, it is inferred that; (1) base level of the formation is deposited in back reef settings in association with continental clastics; (2) algal limestone layers were formed along reef ridge; (3) conglomeratic upper levels are the deposits of reef front or deeper marine environment; (4) out crops of the formation located in the southern and eastern parts of the basin does not fit this reef-related model. Transition between continental clastics and Kırkkavak formation with shallow marine environment fossil assemblages within the study area, however, indicates shallow-marine deposition for the formation; and (5) the reason for the widely extended shallow-marine deposition within the basin for this time interval might be explained by Paleocene-Eocene thermal (maximum) event as stated in Nairn (2011) together with local uplift histories of the basement.

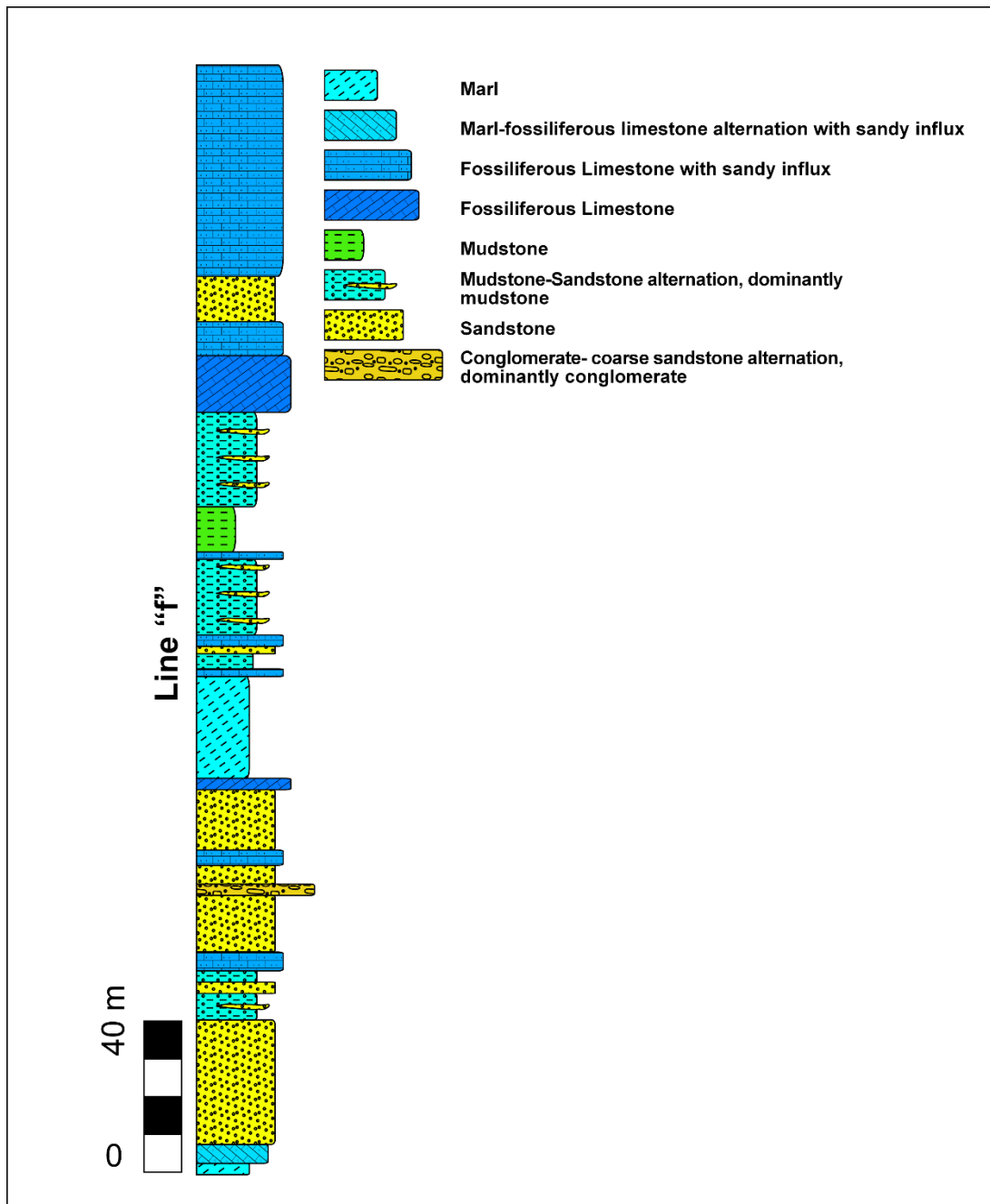


Figure 2.12: Measured stratigraphic sections of the Kırkkavak formation. See text for explanations (see Figure 2.1 for location).

Based on benthic foraminifers, the age of the formation is suggested as Thanetian to Ilerdian (Sirel and Gündüz, 1976; Sirel, 1998; and Özcan *et al.*, 2001). In addition to these ages, early Thanetian to late Paleocene time interval is also assigned, based on benthic foraminifer samples collected within the context of the study along the first

section (see figure 2.10 for interval), for the base and middle levels of the formation (Ercan Özcan, personal communication, 2014). The fossil assemblages of the samples are; *Glomalveolina primaevera reichel*, 1937, *Miscellanea yvettae leppig*, 1988, *Orbitoclypeus seunesi seunesi douville*, 1922, and *Operculina heberti*, 1937. In addition to paleontological dating techniques, 637 magneto-stratigraphy core samples were taken from 220 different stations located on the first section. The distance between sample stations were determined by considering 3 m steps on true thickness of the unit and totally 700 m of the formation is covered in terms of magneto-stratigraphy (see figure 2.10 for interval). First 50 m of magneto-stratigraphic section forms underlying Kartal formation, following 100 m represents the transition zone of Kartal and Kırkkavak formations and the rest represents the Kırkkavak formation. Based on unpublished data of Özkaptan (2015) and its correlation with the paleontological data; (i) 60,7 to 58,2 Ma time interval and 6 cm/kyr sedimentation rate were proposed for the first 150 m of this section, and (ii) 58,2 to 52,7 Ma time interval and 9,2 cm/kyr sedimentation rate were suggested for the rest of the section.

Badiğın formation and upper levels of the Dizilitaşlar Formation (Kaymakcı *et al.*, 2009; Norman, 1792) of the Çankırı and the Kırkkale-Bala basins, the Çaldağ and the Kırkkavak formations (Çemen *et al.*, 1999; and Görür *et al.*, 1984) of the Tuzgölü Basin, and middle levels of the Halkapınar formation (Clark and Robertson, 2005) of the Ulukışla Basin might be considered as the equivalent of the Kırkkavak formation.

2.2.3.2 Ilgınlıkdere Formation

The formation is named by Ünalan *et al.* (1976) but it is also considered as a member of lower Eocene Eskipolatlı formation by Dinçer (1977), Derman (1978) and Dellaloğlu and Aksu (1991). The unit crops out widely at the northern and northwestern part of the study area around Karaömerli, Esen, Kargalı, and Karahoca villages (see Figure 2.1b and Appendix A for locations). Its contact relationship with underlying Kırkkavak and overlying Eskipolatlı formations are observed as gradational.

A stratigraphic section covering the first 113 m of the formation was measured at the southwest of Çayraz village (Figure 2.13 and see Figure 2.1 for location). Although the entire section of the formation is not covered along the measured section due to Quaternary cover, this locality was chosen because of and its contact relationship with the underlying and the overlying units in order to understand the main characteristics of the formation in the northern margin of the basin. The base level of the section is represented by green to grey laminated sandy mudstone layers with up to 30-cm-thick, grey, lenticular sandstone horizons while the upper levels are composed of alternations of up to 5-m-thick lenticular conglomerate-thick grey sandstone-dark green, monotonous mudstone and sandy mudstone layers with pelagic and benthic foraminifer assemblages. Although the rest 150 m of the section is covered by recent sediments, a transition zone between overlying Eskipolatlı formation was documented and also 60-m-thick dark grey to green sandstone layers with up to 2-m-thick conglomerate channels of the Ilgınlıkdere formation was measured before the contact (Figure 2.14). The thickness of the formation might, therefore be considered as 323 m for this locality. Ungraded, unsorted and sandy matrix-supported and mainly channel type conglomerate horizons contain semi-angular to angular ophiolitic, limestone (probably originally from Kırkkavak or Çaldağ formations), and macro fossil (mainly large gastropoda) fragments (maximum 5 cm in diameter). Sole structures are rarely observed within the grey, sometimes graded and laminated sandstone horizons. By considering, its fossil and re-worked limestone content, association with the reef-related deposits of the Kırkkavak formation, which is widely observed in the study area, and monotonous, laminated, graded mudstone–sandy mudstone–sandstone alternations, it is inferred that Ilgınlıkdere formation was deposited in a range covering shallow-marine (fore reef at some part) to moderately deeper-marine environment (slope) under the influences of turbidity currents.

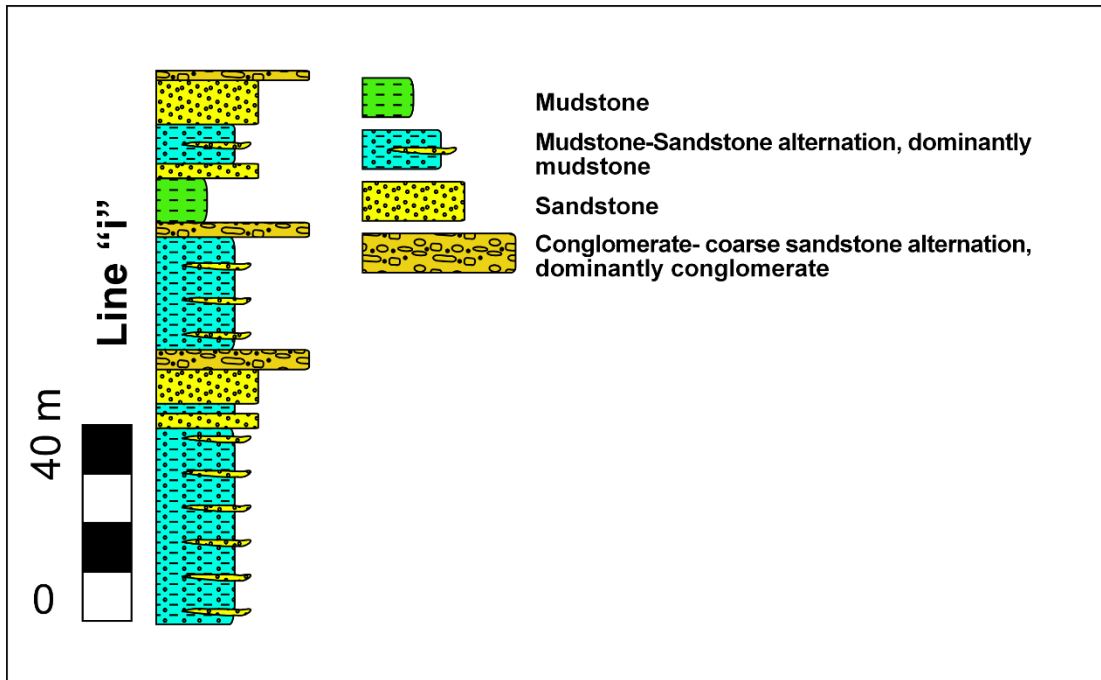


Figure 2.13: Measured stratigraphic section of Iğnıkdere formation. See text for explanations (see Figure 2.1 for location).



Figure 2.14: GoogleEarth image showing contacts between Iğnıkdere, Eskipolatlı, Kırkkavak and Çayraz formations. Note the unmeasured zone of Iğnıkdere formation. Location: West of Çayraz village (see Figure 2.1 for location and see text for further explanation).

The age of the formation is assigned as Ilerdian (Sirel and Gündüz, 1976) and late Paleocene–early Eocene (Dellaloğlu and Aksu, 1991) by focusing on benthic and pelagic foraminifers. These ages are also conformable with age of its shallow-marine equivalent, Kırkkavak formation.

The formation is defined locally by considering facies characteristics and their importance for the stratigraphic model of the Haymana Basin, but some levels with similar characteristics to the Ilgınlıkdere formation, can be equivalent to the units of the Central Anatolian basins: Yoncalı formation (Aziz, 1973; and Kaymakcı *et al.* 2009) of the Çankırı Basin, Hacıbalı formation (Norman, 1972) of the Kırkkale-Bala Basin, the Karapınaryaylası formation and the Eskipolatlı formation (Dellaloğlu and Aksu, 1984; and Görür *et al.*, 1984) of the Tuzgölü Basin.

2.2.3.3 Eskipolatlı Formation

Rigo de Righi and Cortesini (1959) named the formation and same terminology was widely used by various authors since then. The exposures of the units are observed throughout the study area around Eskipolatlı, Sarıgöl, Evcı, Evliyafakı, and Küçükyavaşçı villages (see Figure 2.1b and Appendix A for locations). It has gradational contacts with the Ilgınlıkdere and the Kırkkavak, and overlying Çayraz, Beldede and Yamak formations, however, at the northern margin of the basin an angular relationship between Eskipolatlı and overlying Çayraz was determined (Figure 2.15).

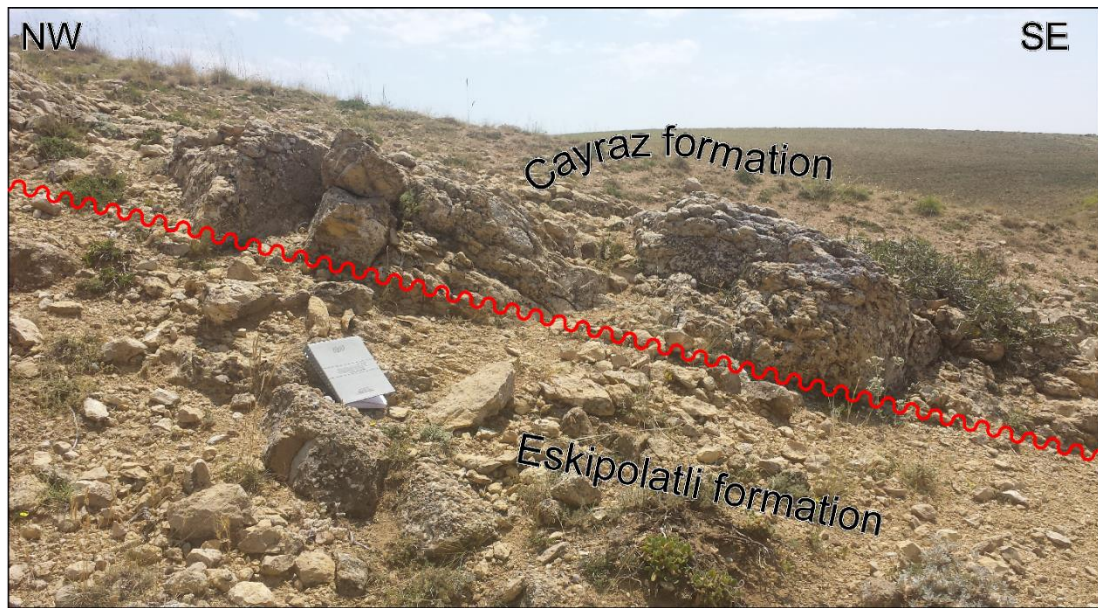


Figure 2.15: Angular relationship between the Çayraz and the Eskipolatlı formations. Location: South of Sarıgöl Village (see Figure 2.1 for location).

The entire section of the unit is exposed in the area between Iğnıkdere and Çayraz formations at the east of Sarıdeğirmen village, a stratigraphic section was therefore, measured at this locality. 437 m thickness was determined for the formation along the line (Figure 2.16 and see Figure 2.1 for location). Because the top of the formation is covered by Neogene deposits, another stratigraphic section was measured in the western part of the study area at the south of Eskipolatlı village (Figure 2.16 and see Figure 2.1 for location) in order to understand changing in depositional settings (if there is a change), and as a result, increasing in the thickness of the formation (520 m) and coarsening in grain size were noted. Alternation of, up to ~ 140-m-thick, dark green, laminated mudstone layers with up to ~50-cm-thick well-sorted, graded sandstone-sandy mudstone layers, and up to 15-m-thick, lenticular, grey to light green, graded, channel-type sandstone horizons characterize the first section. Primary sedimentary structures can be grouped as widely noted ripple marks, erosive base, load structures for the sandstone levels, and rare burrowing, flute/groove casts, and lamination for the mudstone-sandy mudstone layers. Another important characteristics of the first section is the existence of nummulite fragments together with increasing in carbonate concentration towards upper levels. The second section

is represented by similar features as described in the first section, except for an increase in grain size and up to 20-m-thick, lenticular, graded, generally matrix-supported and channel-type conglomerate levels. The pebbles of the conglomerate layers are composed mainly of semi-rounded limestone (probably Jurassic), chert, basic volcanic and plutonic clasts. Maximum pebble size which is 5 cm in diameter in lower conglomeratic levels increases up to 50 cm in upper horizons. Although there is no study arguing the presence of pelagic fossil assemblages and related depositional environment of the formation, continental slope to deep-marine and shallow-marine environments might be suggested for the deposition of base and top levels of the formation, respectively. Existence of classical turbidity currents related sedimentary structures (lamination, load structures, grading etc.), its lateral transition with Ilgınlıkdere formation, and increase in carbonate concentration and benthic fossil assemblages towards upper levels forms the criteria for the depositional setting.

The age of the formation is assigned based on benthic fossil assemblages, as Ilerdian to Cuisian (Ünalın *et al.*, 1976), Dellalođlu and Aksu (1991) also suggested, based on calcareous nanofossils, late Paleocene to early Eocene age. These ages are also in agreement with the age of Ilgınlıkdere and Kırkkavak formations which are considered as its lateral equivalents.

Upper levels of the Halkapınar formation (Clark and Robertson, 2005) of the Ulukışla Basin, the Yoncalı formation (Aziz, 1973 and Kaymakcı *et al.*, 2009) of the Çankırı Basin, the Keçili formation (Norman, 1972) of the Kırkkale-Bala Basin, the Karapınaryaylası formation and the Eskipolatlı formations (Dellalođlu and Aksu, 1984; and Görür *et al.*, 1984) of the Tuzgölü Basin are considered as the equivalents of the Eskipolatlı formation in the Central Anatolian basins.

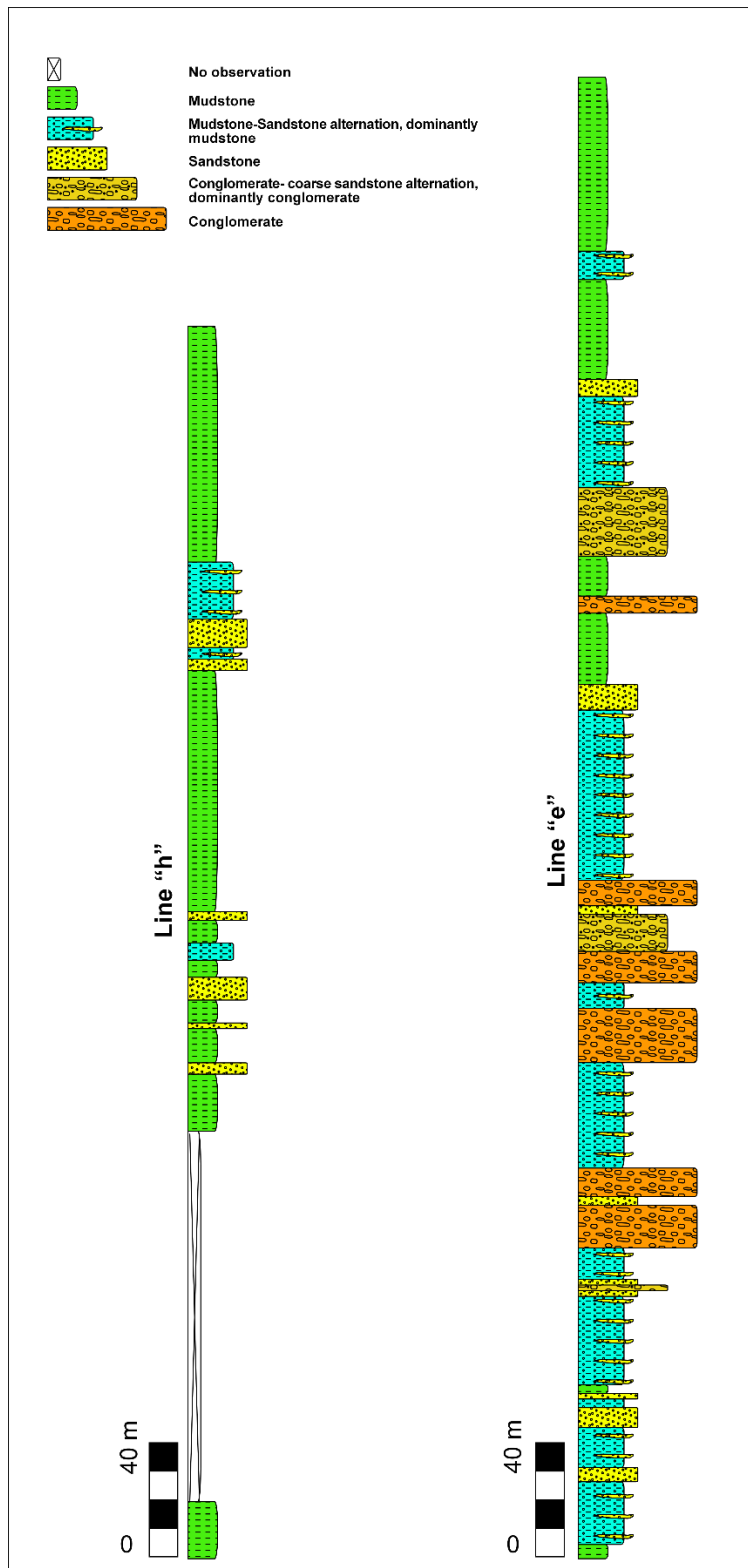


Figure 2.16: Measured stratigraphic sections of the Eskipolatlı formation. See text for explanations. (see Figure 2.1 for locations).

2.2.4 Fourth Cycle

Lower to middle Eocene Beldede, Çayraz and Yamak formations define the fourth cycle. Beldede formation is represented by continental red clastics while Çayraz and Yamak formations, by its shallow-marine and deeper-marine equivalents.

2.2.4.1 Beldede Formation

The formation is named by Ünalán *et al.* (1976). The exposures of the unit are widely observed at NW part of the study area around Kargalı village and Polatlı town (see Figure 2.1b and Appendix A for locations). It has boundaries only with the underlying Eskipolatlı formation and overlying Neogene deposits. These contact relationships are observed as vertically gradational and unconformable with the underlying and the Neogene deposits, respectively.

Although the outcrops of the unit are randomly distributed as patches, and the top of the formation is covered by Neogene deposits, a stratigraphic section representing the first 475 m of the formation is measured at the west of Kargalı village (Figure 2.17 and see Figure 2.1 for location). The section is represented dominantly by red sandstone–sandy mudstone–mudstone alternation, sandy mudstone with up to 50-cm-thick sandstone horizons and up to 10-m-thick channel-type conglomerate levels, and red thin- to thick-bedded (10 to 100 cm), red mudstone levels, at the base, center and top of the section, respectively. Angular to semi-rounded ophiolitic fragments (Up to 5 cm in diameter), limestone pebbles and high amount of gastropods and nummulites (possibly intraformationally re-worked) form the highly oxidized, red, sandy matrix-supported, poorly-sorted, ungraded, poorly-cemented, lens-shaped conglomerate levels of the formation. Lens-shaped, ungraded, thick-bedded (up to 10m) sandstone layers with erosive base are mainly represented by red color and contains randomly distributed pebble size polygenetic clasts and fossil fragments (mainly nummulites and rarely *Alveolina*). Cross-bedding showing multi-directional current are also common in these horizons. Monotonous red mudstone–sandy mudstone layers of the unit are frequently truncated by up to 50-cm-thick channel-type sandstone layer; rare thin (up to 50cm) limestone horizons (towards upper levels), and fossil fragments are also

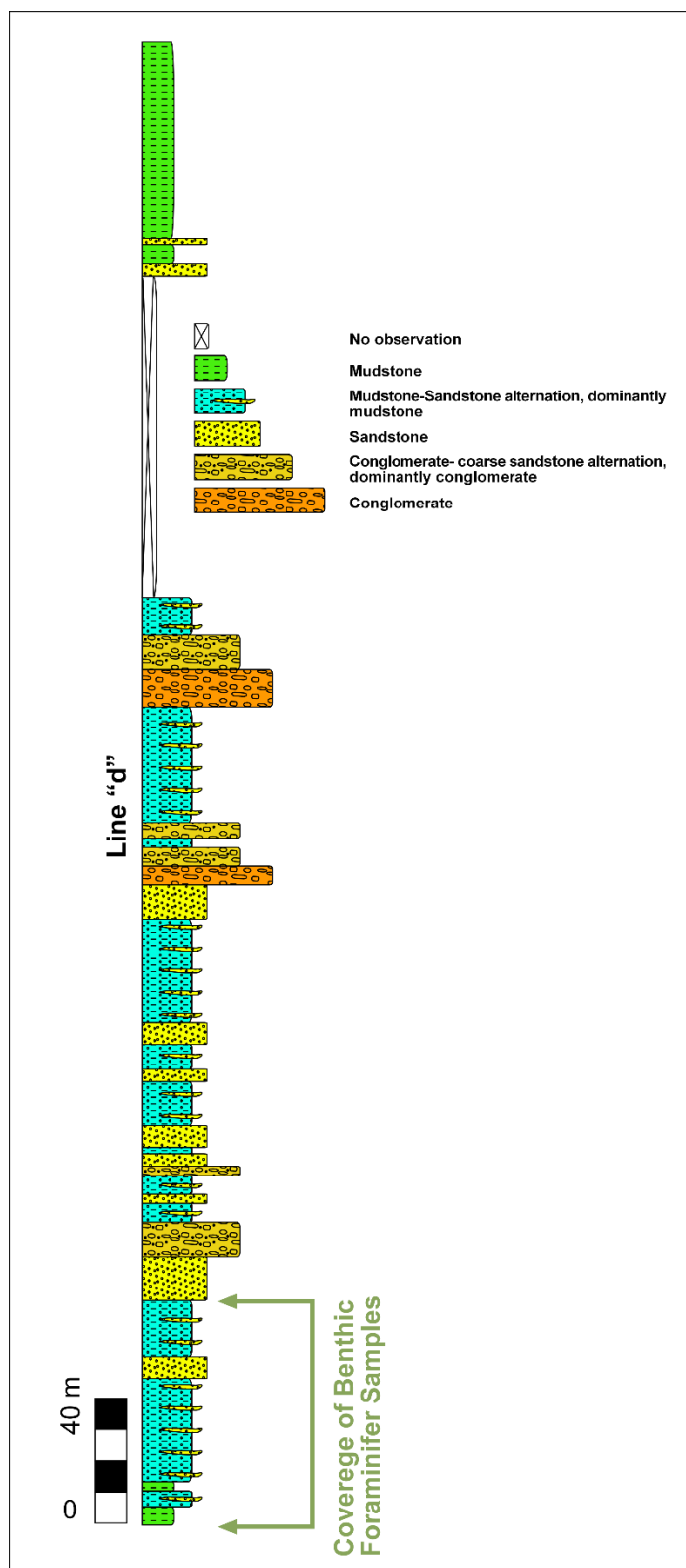


Figure 2.17: Measured stratigraphic sections of the Beldede formation. See text for explanations (see Figure 2.1 for location).

observed. The most important feature of the mudstone layers is an increase in carbonate concentrations together with nodular carbonate aggregations towards upper levels along the section. It is inferred that the formation was deposited in continental to shallow-marine settings (as inferred by Ünalán *et al.*, 1976); sedimentary features of the formation indicate a fluvial system and the shallow-marine fossil assemblages form the base of this interpretation

The age of the formation is assigned, based on benthic large foraminifers collected from limestone horizons located at the upper levels of the unit, as Cuisian by Ünalán *et al.* (1976). Middle Ilerdian age is also determined, based on an index large foraminifer, such as *Alveolina leupoldi hottinger* 1960 (see Figure 2.17 for sampling interval), for the lower levels of the formation (Ercan Özcan, personal communication, 2014). The fossil ages indicate Middle Ilerdian to Cuisian time interval, but the age of the unit can be extended to latest Cuisian or early Lutetian because of its gradual transition with the underlying Ilgınlıkdere formation.

The formation was defined locally in the Haymana Basin, but shallow-marine or continental deposits, exposed in the Central Anatolian basins might be considered as the equivalent of this unit. These formations include; the Karagüney formation (Norman, 1972) of the Kırıkkale-Bala Basin, the Karabalçık and the Osmankahya formations (Birgili *et al.*, 1974; Dellaloğlu *et al.*, 1992) of the Çankırı Basin, uppermost part of the Yeşilöz formation (Advokaat *et al.*, 2014) of the Ayhan-Büyükkışla Basin, upper levels of the Baraklı formation (Kara and Dönmez, 1990) of the Yozgat-Çiçekdağ Basin.

2.2.4.2 Çayraz Formation

The formation is named by Schmidt (1960) and this name has widely been used by various authors since then. The unit crops out only at the northern part of the study area around Çayraz and Yeşilyurt villages (see Figure 2.1b and Appendix A for locations). Its contact relationship with the almost same aged Beldede and Yamak formations is not exposed in the study area but it displays a boundary with the underlying Eskipolatlı formation. This boundary is observed conformable at the west

of Çayraz village whereas it is noted as an angular unconformity at the south of Sarıgöl village (see Figure 2.15). Also Neogene units unconformably cover the unit.

The exposures trend in E–W direction and its thickness decreases from ~400 m to ~20 m along the southern and northern limbs of a syncline at the north of Çayraz village, respectively (Figure 2.1b). The top of the formation is not observed in the study area; a stratigraphic section representing the first 390 m of the formation is measured along the southern limb of the syncline (Figure 2.18 and see figure 2.1 for location). Thick bedded (up to 10 m) laminated green sandstone with laminated mudstone horizons, mudstone with up to 20-cm-thick sandstone bands and fossiliferous sandy limestone layers form the first 25 m of the section; these horizons represent the abrupt transition between Eskipolatlı and Çayraz formations. The rest of the section is composed of mainly by grey to yellow fossiliferous marl–sandy limestone and limestone alternation. Along the section, four different sub-sequences are described. These sequences, from bottom to top are; (1) ~70-m-thick limestone–sandy limestone alternation, 2) ~90-m-thick limestone–sandy limestone–marl alternation, 3) ~110-m-thick monotonous marl horizon and 4) ~150-m-thick limestone–sandy limestone–marl alternation. The thickness of the third sequence decreases westwards to ~20 m. Thick-bedded (up to 10 m), lens-shaped, highly fossiliferous (mainly large benthic foraminifers), grey sandy limestone and limestone levels of the unit contain up to 1-m-thick blue marl horizons. The limestone layers may be classified as grainstones because their main components are large (up to 3 cm in diameter) foraminifers, especially nummulite and alveolina but gastropod and echinoderm particles are also present. Whereas sandy limestone and marl layers may be defined as packstones and wackestones, respectively. Well-bedded marl horizons with sandy limestone levels (up to 50-cm-thick) form up to ~150-m-thick monotonous intervals along the section but these levels rarely contain large foraminifers or other large fossil fragments with respect to limestone levels. The nummulitic limestone levels of the formation were described as nummulite banks (inferred by Çiner *et al.*,1996) (cf. Arni 1965) due to high amount of nummulite

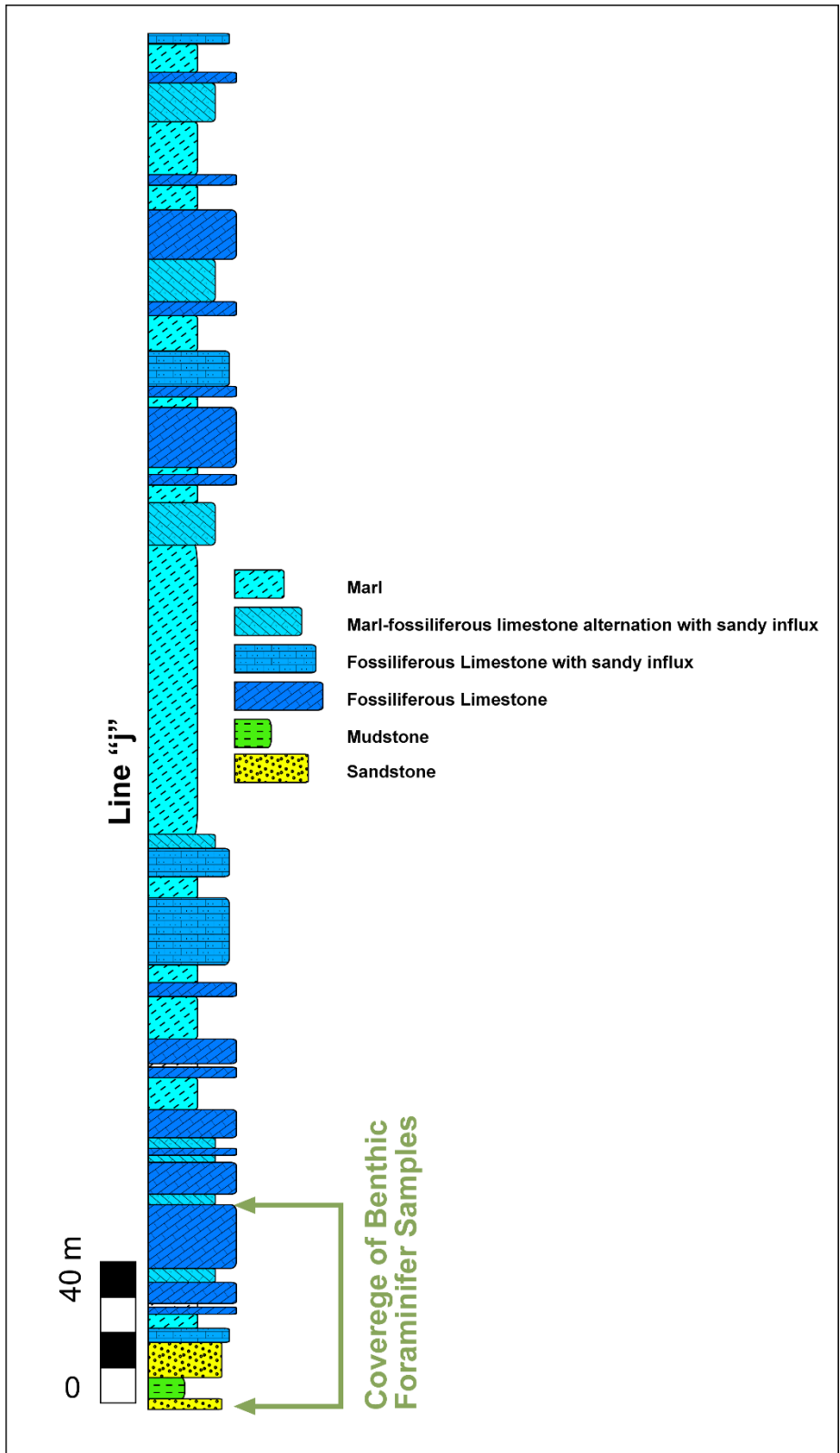


Figure 2.18: Measured stratigraphic sections of the Çayraz formation. See text for explanations (see Figure 2-1 for location).

Accumulation. Marl horizons are interpreted as distal equivalent of shallow-marine limestone levels due to lack of large fossil assemblages and clastic detritus. Green mudstone–sandstone–conglomerate alternations with clastic detritus and rare fossil fragments (nummulites), which is conformably covered by up to ~10-m-thick nummulitic limestone level along the northern limb of the syncline, was observed and considered as proximal equivalent of the marl horizons. As a conclusion, it is inferred that; (1) shallow-marine, shallow-marine to slope, slope front and another shallow-marine to slope environments deposits occur along the section from bottom to top as noted by four different sequences, (2) the unit represents the northernmost margin of the basin during its formation because of its shallow-marine character and limited E-W-trending outcrops located at the north of the basin, and (3) basin side of the system was located at S–SE because of thinning of the nummulitic limestone levels and increase in clastic detritus towards N–NW direction.

The age of the formation is assigned, based on large benthic foraminifers, as Cuisian to Lutetian by Sirel and Gündüz (1976) and Cuisian to lowermost Lutetian by Özcan, (2002). In addition to these ages, early Cuisian age is also assigned, based on an index large foraminifera, *Alveolina canavari*, for the lowermost level of the formation (see Figure 2.18 for sampling interval) (Ercan Özcan, personal communication, 2014)

Kocaçay formation (Birgili *et al.*, 1974) of the Çankırı and the Yozgat-Çiçekdağı basins, the Hasangazi formation (Demirtaşlı *et al.*, 1973) of the Ulukışla Basin, the Bahşili or the Mahmutlar formation (Norman, 1972; and Akyürek *et al.* 1984) of the Kırıkkale-Bala Basin, the Çayraz formation (Görür *et al.*, 1984) of the Tuzgölü Basin, and the Mucur formation (Göncüoğlu *et al.*, 1993) of the Ayhan-Büyükkişla Basin are considered as the equivalents of this formation.

2.2.4.3 Yamak Formation

The unit is named by Ünalın *et al.* (1976) and exposed generally at the SE part of the study area around Yamak, Söğüttepe, Yaprakbayırı, and Sırçasaray villages (see Figure 2.1b and Appendix A for locations). The unit does not have any direct contact with the almost same age Çayraz and Beldede formations. It forms E–W trending

exposures and conformably overlies underlying Eskipolatlı formation at the flanks of synclines. It also displays an angular contact relationship with the overlying Neogene deposits.

A stratigraphic section representing the first 1150 m of the formation is measured along its N–S trending outcrops in its type locality as defined around the Yamak village by Ünalın *et al.* (1976) (Figure 2.19 and see Figure 2.1 for location). Along the section, two fining- (at the bottom) and one coarsening-upward (at the top) sequences are described as ~400-m-thick cycles, although the section generally shows a shallowing upwards character (see Figure 2.19 for intervals). Green to brownish sandstone–sandy mudstone–mudstone alternation with rare up to 10-m-thick channel-type conglomerate levels dominate the formation. Dark green to black massive shale horizons (757–827 m and 517–541 m intervals) also occur and they terminate the fining-upward sequences. Sandstone levels are grouped as thick-bedded (up to 10 m) channel-types and thin-bedded (5 to 50 cm) turbiditic horizons. Green to grey, graded, medium- to coarse-grained channel-type sandstone levels show erosive base above mudstone and sandstone levels. Conglomerate pebbles (up to 5 cm in diameter) scattered within these intervals particularly are also common, at their base. Thin-bedded turbiditic sandstone horizons and their alternation with concoidally fractured, laminated, green mudstone–sandy mudstone levels forms ~%75 of the section. Flute-groove cast and graded bedding are syn-sedimentary features of these sandstone beds. Based on these primary structures, the main paleo-current direction was proposed as towards SSE (Çiner *et al.*, 1996) and E–W (for the middle levels of the formation by Çetin *et al.*, 1986). Unsorted, and grain-supported channel-type conglomerate layers are composed of limestone, ophiolitic, quartz, and rarely found volcanic pebbles.

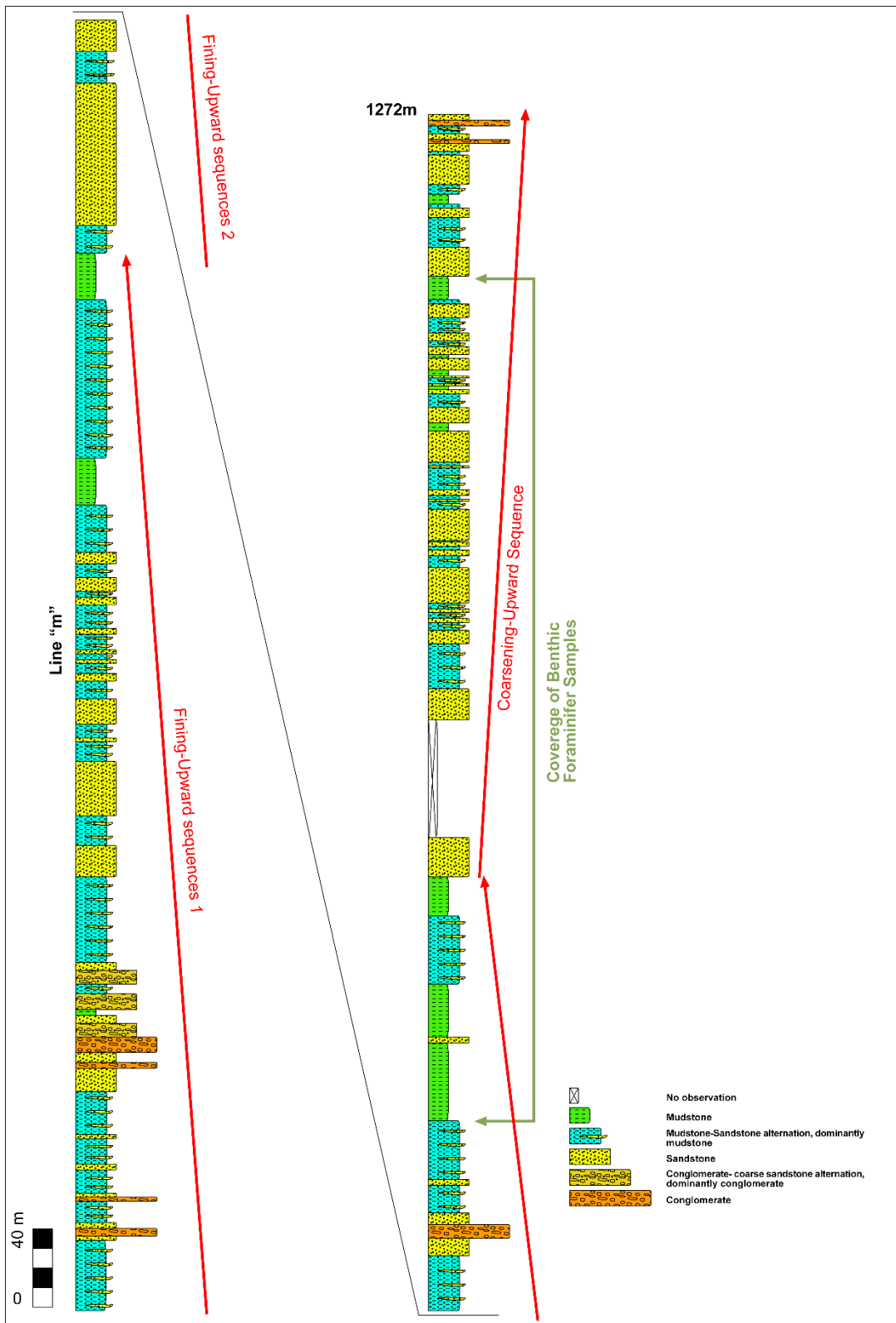


Figure 2.19: Measured stratigraphic sections of the Yamak formation. See text for explanations (see Figure 2.1 for location).

Maximum pebble size is <30 cm at the base and it gradually decreases upwards and they are <5 cm in diameter at the middle parts. Channel-type sandstone and conglomerate, dominant turbiditic and also massive shale levels suggest; Four different slope–slope front (deep sea) depositional environments for each fining-upward sequences. It is inferred that channel-type conglomerate and thick sandstone horizons represent upper and middle slope whereas turbiditic levels and black shale horizons, lower slope and slope front environments, respectively. The interpretation about upper and middle slope environment seems to be compatible with the coarsening-upward sequence (top levels of the section). Similar to our inferences, studies of Ünalán *et al.* (1976), Gökçen and Kelling (1983), and Çiner *et al.* (1996) suggested sub-marine fan-related deposition for the Yamak formation.

The age of the unit is assigned, based on benthic foraminifers found in the upper levels of the unit and its lateral relationship with the Çayraz formation, as Cuisian-Lutetian by Ünalán *et al.* (1976). Additionally, middle Lutetian age is also supplied, based on large benthic foraminifer assemblages; *Discocyclina spliti spliti butterlin and chrowicz, 1971*, for the middle to upper levels (see Figure 2.19 for sampling interval) of the formation (Ercan Özcan, personal communication, 2014)

Upper levels of the Yoncalı formation (Aziz, 1973) of the Çankırı Basin, the Bozbeltepe formation (Demirtaşlı *et al.*, 1973) of the Ulukışla Basin, and the Karapınaryaylası or the Eskipolathlı formation (Çemen *et al.*, 1999; Görür *et al.*, 1984) of the Tuzgölü Basin are considered as equivalent units in the region. The Çayraz and Beldede formations are also considered as the time equivalent of the Yamak formation due to its lateral relationships with these formations.

2.3 Neogene Units and Quaternary Alluvium

Neogene units are exposed mainly in the southern and northwestern part of the study area and comprise continental and lacustrine environment deposits together with post–Oligocene volcanic and pyroclastic rocks. The contact relationship between Neogene deposits and underlying basinfill is an angular unconformity exposed at several part of the study area (Figure 2.20). Alluvial deposits are mainly exposed along NW–SE- and

NE–SW-trending major stream valleys. Quaternary Alluvium together with Neogene units are out of scope of the study so no detailed work was carried out.



Figure 2.20: GoogleEarth image showing angular relationship between the Neogene units and basin infill. Location: East of İnlr village. Note 3x vertical exaggeration in the image (see Figure 2.1 for location).

CHAPTER 3

STRUCTURAL CHARACTERISTICS OF THE BASIN

Fold analyses, cross-section constructions and paleo-stress inversion analyses were conducted within the context of the structural studies in order to understand the spatio-temporal characteristics of deformation phases and related structures observed in the study area, under the concept of regional tectonic settings,. A structural map is given in Figure 3.1.

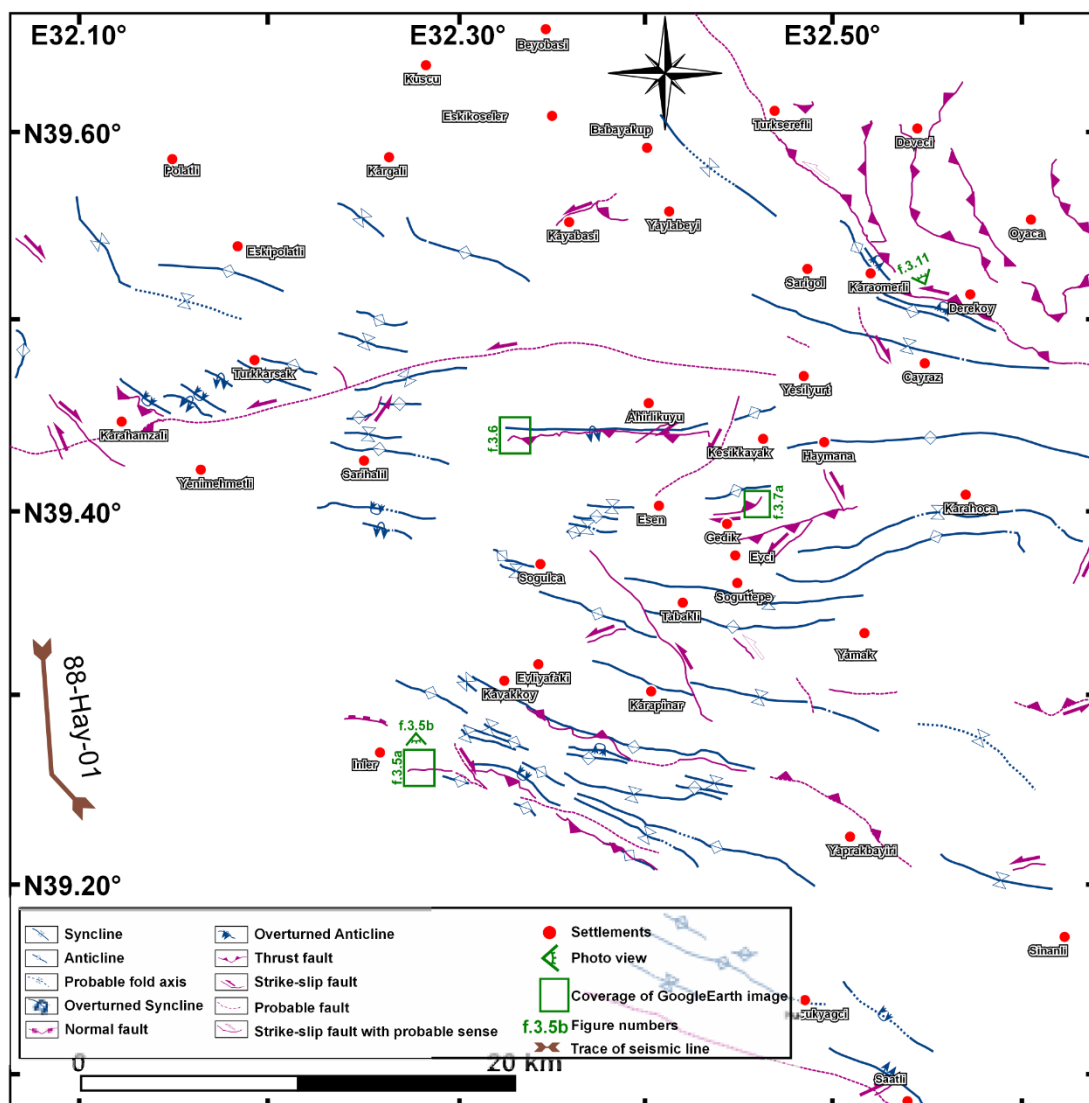


Figure 3.1: Structural map of the Haymana Basin (see Appendix A for name of the structures)

3.1 Folds and Bedding

In order to understand the characteristics and spatial distribution of the folds, 2823 bedding attitude measurements were collected and gathered from the literature (Appendix A). The rose diagram of the bedding strikes indicate two main directions, N65°W and N85°W (Figure 3.2a). Histogram of dip amounts also shows main concentration between 30° to 50° (Figure 3.2b). In keeping with the orientation of bedding planes, folds trend in two different directions: E–W and NW–SE in the south–southeast and north–northwest parts of the study area, respectively. 46 major folds

affecting the basinfill are mapped in the study area. Seventeen of them trend in NW–SE direction whereas the rest trend in E–W. Except for eight folds, which are considered as the product of intra-basinal strike-slip system, in the western part of the study area around Karahamzalı and Gündoğan villages, folds are mainly developed parallel to the basin margins. This implies that development of the folds might be related to activity of the basin-bounding faults and their continuation in the basin.

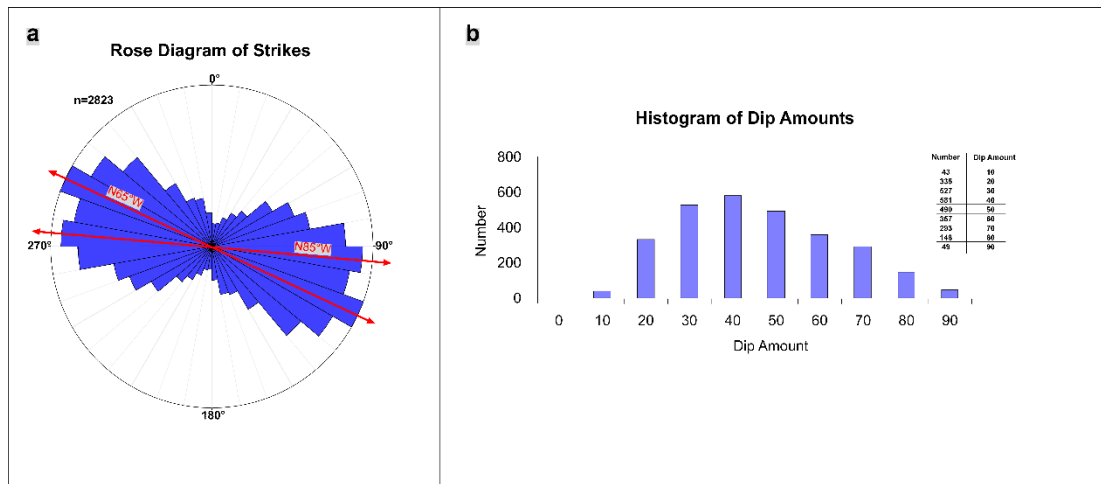


Figure 3.2: (a) rose diagram of strikes of bedding attitudes; (b) histogram of dip amounts of bedding planes

In addition to general interpretation of all fold structures, nine major and representative folds were also analyzed by using systematically collected 1017 bedding attitude measurements for detailed interpretations. Seven are from north to south Eskipolath anticline, Çayraz syncline, Haymana anticline, Ahırlıkuyu anticline, Sarıhalil anticline, Karapınar syncline, and Demirözü syncline, and they are attributed to product of the basin margin-related faults (or their continuation in the basin) and two of them (Türkkarsak and Yayladağ anticlines) were considered as related to intra-basinal strike-slip system. The β - and $-\pi$ diagrams of these folds are prepared by Stereonet 8 software using the algorithms of Allmendinger *et al.* (2012). Contour diagrams are plotted by considering %1 area contouring and; attitudes of hinge lines and axial planes are calculated by using mean pole directions of each limb of the folds.

The results of the β - and $-\pi$ diagrams are shown in Table 3.1, and Figure 3.3.

Table 3.1 Results of fold analyses.

Name of the Fold	n	n (overturned)	Fold axis	Axial plane	Interlimb angle	Pole of limb1	Pole of limb2
Eskipolatlı Anticline	127	0	287°N/07°	N74°W,88°NE	140°	174°N/70°	033°N/67°
Çayraz Syncline	189	0	110°N/04°	N70°W,89°NE	119°	205°N/58°	013°N/57°
Haymana Anticline	144	0	278°N/06°	N84°W,89°NE	80°	179°N/55°	016°N/54°
Ahrlıkuyu Anticline	283	20	263°N/07°	N84°E,83°SE	104°	163°N/53°	001°N/50°
Sarıhalil Anticline	58	6	101°N/13°	N77°W,83°NE	87°	209°N/51°	001°N/39°
Karapınar Syncline	75	0	105°N/12°	N73°W,78°NE	130°	235°N/73°	359°N/52°
Demirözü Syncline	64	10	104°N/04°	N76°W,81°NE	73°	202°N/62°	009°N/44°
Türkkarsak Anticline	40	0	293°N/07°	N74°W,68°SW	113°	189°N/63°	030°N/49°
Yayladağ Anticline	37	4	306°N/23°	N28°W,57°SW	82°	186°N/50°	055°N/38°

The β - and $-\pi$ diagrams also support the basin margin parallel folding with hinge line attitudes (E–W & NW–SE). The other important outcomes of the results are; (1) the plunges of the folds are gentle and mainly towards E–W -or NW (2) by considering the inter-limb angles, they are gently open (or close) folds where the basement or older units are exposed at their limbs or cores otherwise they are gentle folds. This implies that tightness of the folds is controlled by faults with tips reaching the surface (or close to the surface), (3) attitude of fold axial planes show upright fold character at the north of the study area whereas they indicate gently inclined (towards south) folds (except from Türkkarsak and Yayladağ anticline, towards north). This implies that general trend of the vergence is due south, however, the existence of south dipping overturned folds at the southern part of the basin (İnler and Köpekgediği overturned synclines, see Figure 3.1 for locations) also indicate northward vergence, and (4) Türkkarsak and Yayladağ anticlines together with parallel trending (NW–SE) fold series located at the southwestward (Figure 3.1) seems to be en échelon fold-pattern created by left-lateral strike-slip fault system.

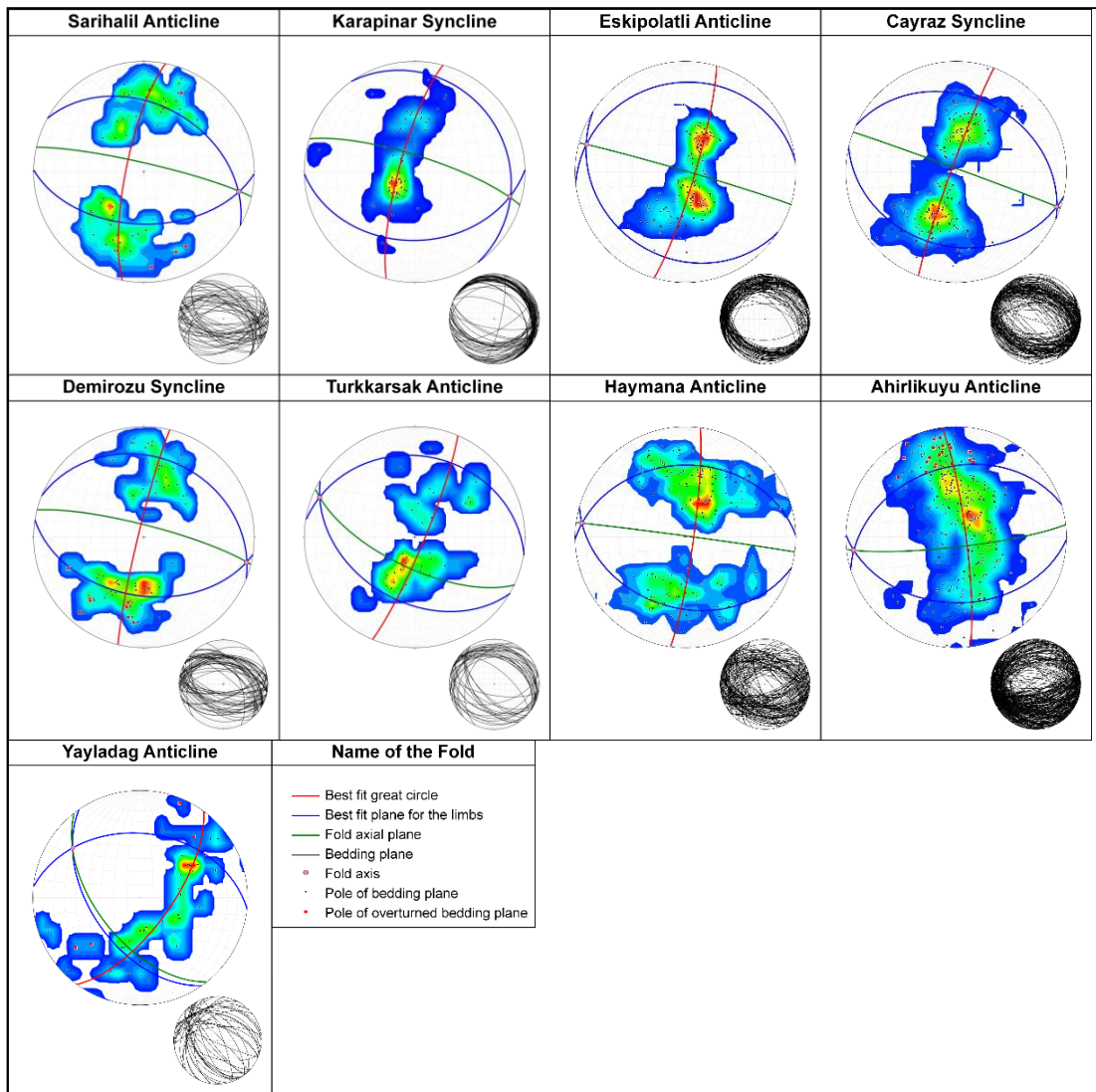


Figure 3.3: β - and $-\pi$ diagrams of the major folds of the Haymana basin. See Figure 3.1 for locations of the folds

possibly resulting in offset in the basement, due to increase in plunge (due NW) amounts and being overturned towards southwest.

3.2 Faults

The major structures controlling the deformation in the basin are thrust (or reverse) faults. Strike-slip faults are also common and together with major thrusts, they gave way to shape today's geometry of the basin. Seven major thrust, sixteen strike-slip and one normal faults were recognized in the study area and they were delineated on the

map (Figure 3.1). Although the length-weighted rose diagrams of the all structures, folds, and thrusts faults indicate two main trends (E–W and ENE–WSW), the main trends of strike-slip faults are WSW–ENE, E–W and NW–SE (Figure 3.4a, b, c, d). This implies that, (1) dominant structures are thrusts and folds, aligning in E–W and ENE–WSW directions, (2) formation of thrusts and folds are the products of possibly the same deformation phase, (3) formation of the some of the strike-slip faults may be related to same deformation phase with thrusts and folds, and (4) some of the strike-slip faults might be products of different (probably later) phase.

The basin is structurally bounded by two major thrust and reverse faults; they are north-dipping Dereköy Thrust (DT) and south-dipping İner reverse fault (İT).

DT is observed as curvilinear uplifted basement front creating a structural contact between ophiolitic mélangé and basinfill. E–W– to NW–SE- trending DT extends from Çingirli to Türkşerefli (~ 25km) villages and is covered by Neogene deposits. The key feature indicating thrusting is the presence of overturned basinfill beneath the highly deformed Upper Cretaceous ophiolitic units (Figure 3.5). The youngest unit affected by DT is the Çayraz formation, the latest activity of DT is therefore, constraint between Cuisian to Neogene time interval. Although the main fault plane is not observed in the field, mesoscopic- to small- scale faults trending parallel to the main fault indicate left-lateral slip motion together with main upward sense. The average dip amount of the main fault plane varies between 50° and 70° measured on small-scale fault plane outcrops. The minimum offset for that fault is, based on stratigraphic thickness of basinfill units older than Çayraz formation and approximate dip amount of the fault plane calculated during cross-section balancing, considered as ~5 km.

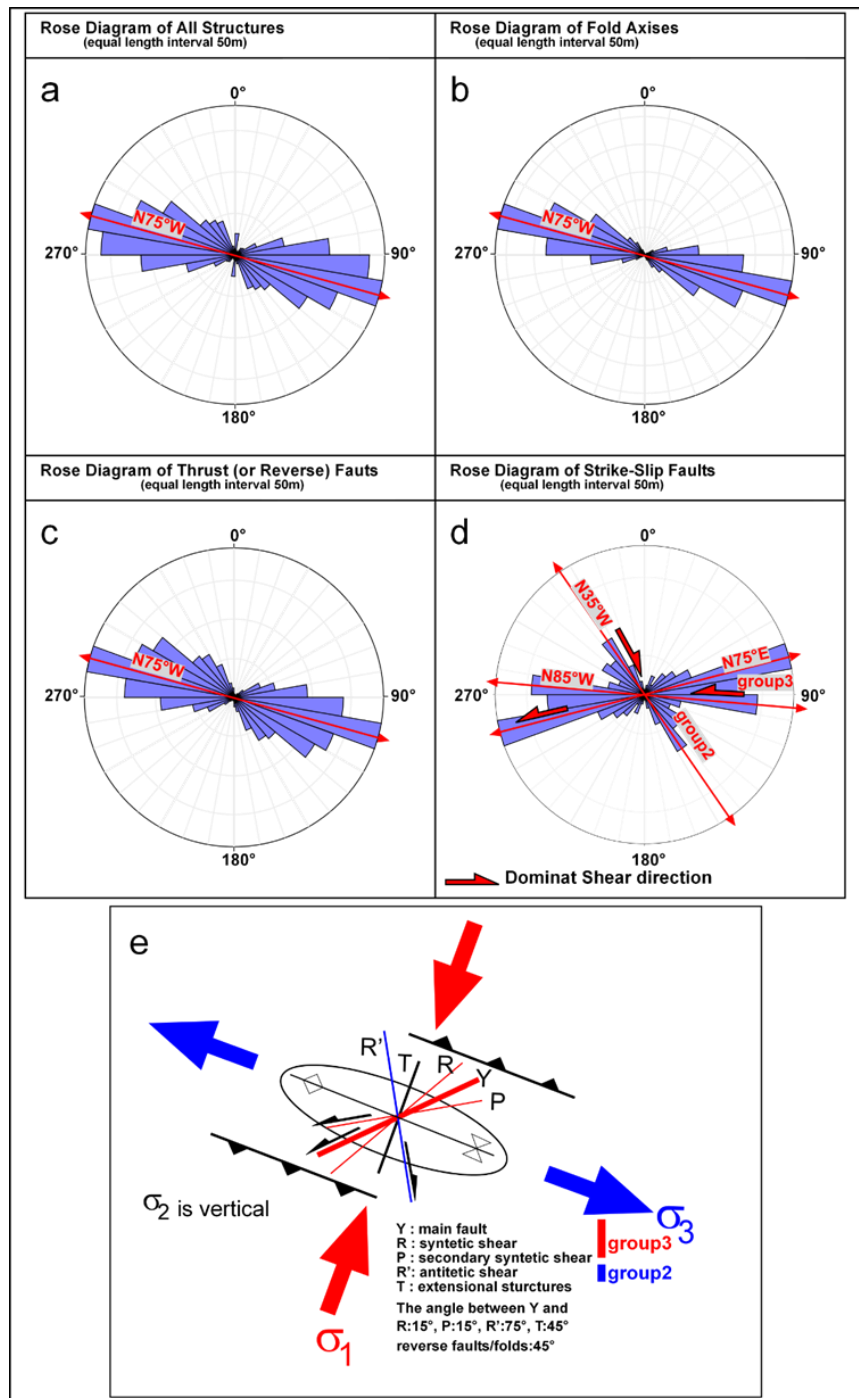


Figure 3.4: (a) Length-weighted rose diagram of all structures of the Haymana Basin; (b) length-weighted rose diagram of folds of the Haymana Basin; (c) length-weighted rose diagram of thrust (or reverse) faults of the Haymana Basin; (d) length-weighted rose diagram of strike-slip faults of the Haymana Basin, see text for explanations; (e) left-lateral Riedel shear diagram developed by ~015°N oriented maximum principle stress direction (σ_1), indicating possible trends of the structures in the Haymana Basin (see text for explanations).

NW–SE-oriented İnlere reverse fault defines the southern boundary of the basin and forms the contact between Jurassic platform carbonates and basinfill (Figure 3.5). Curvilinear İT is observed between İnlere village and Toptepe ridge (~13 km) and probably jumps to south and elongates with same trend from Yeşilöz to Saatli villages under the Neogene deposits (Figure 3.1b). The youngest unit affected by İT is early Eocene Iğnıkdere formation. In addition to the main reverse sense, left-lateral slip motion is also determined based on the small-scale fault plane measurements. Based on fault plane measurements, the average dip amount of the İT varies between 55° and 70°. According to a balanced cross-section crossing İT, the minimum offset is calculated as > ~1 km.

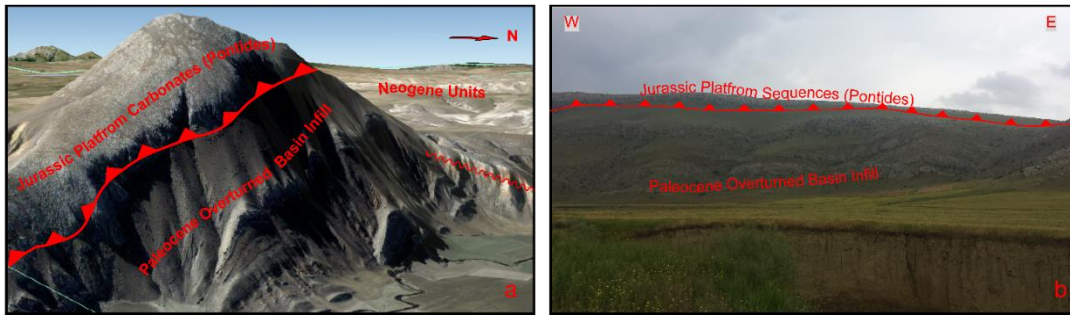


Figure 3.5: (a) GoogleEarth image showing fault contact between basin infill and platform sequences along the İnlere reverse fault. Location: East of İnlere village. Note 3x vertical exaggeration in the image; (b) a view of İnlere reverse fault and affected units. Location: west of İnlere village (see Figure 3.1 for locations).

In addition to these basin-bounding faults, almost same trending reverse faults are also identified at the central parts of the basin. From north to south, these faults are named as Ahırlıkuyu, Gedik, Topkaya, and Türbetepe faults (see Figure 3.1 for locations). Approximately 9-km-long Ahırlıkuyu fault is observed at the core of Ahırlıkuyu anticline and elongates almost parallel to its hinge line. The fault plane of Ahırlıkuyu fault was is not observed in the study area due to mostly dissolved limestone host rock (Çaldağ formation), but the dip of the plane and minimum offset are considered as >~70° towards S and >70 m, respectively; these inferences are based on a section view showing offset occurred along the fault (Figure 3.6).

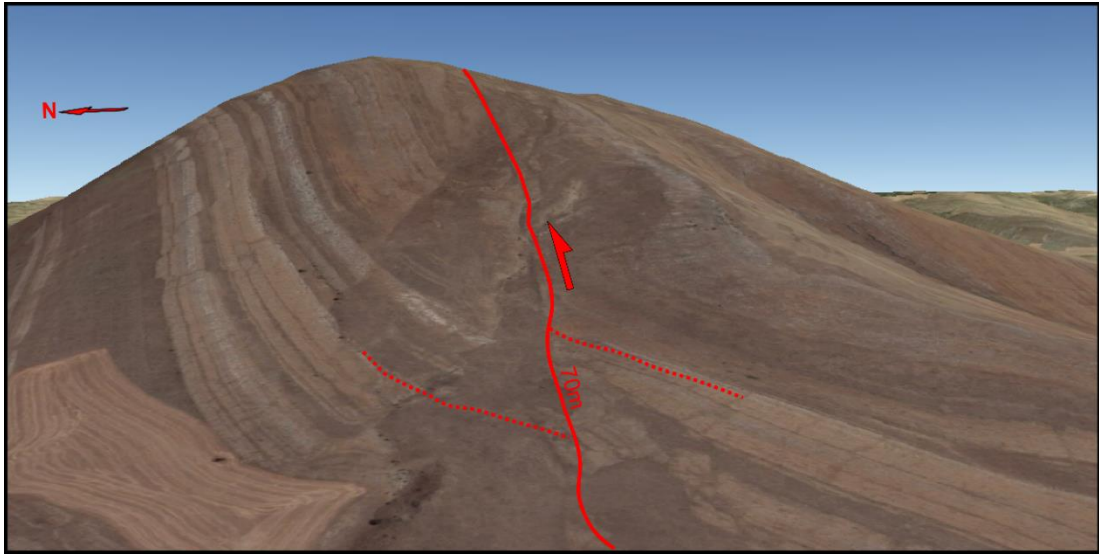


Figure 3.6: GoogleEarth image showing offset in the Çaldağ formation along Ahırlıkuyu reverse fault. Location: west of Ahırlıkuyu Village. Note 2x vertical exaggeration in the image (see Figure 3.1 for location).

Gedik fault is observed along the southern limb of the Gedik anticline (north of Gedik Village) and elongates parallel to its hinge line towards west but become oblique towards east. Iğnıkdere, Kırkkavak and Çaldağ formation are displaced by ~2.5-km-long Gedik fault but any unit covering this fault is not noted in the field. Therefore the age of the fault cannot be assigned. The type of the fault is determined, based on fault plane measurements, as dextral with reverse component (Figure 3.7).



Figure 3.7: (a) Two dimensional view of a GoogleEarth image showing offset in the Çaldağ formation along the Gedik fault. Location: South of Gedik Village; (b) fault plane of the Gedik fault, see Figure 3.7a for the location and view direction of the photo (see Figure 3.1 for location).

~5-km-long almost linear south-dipping Topkaya fault trends along Topkaya ridge. Upper Cretaceous to middle Eocene basinfill are displaced by this fault, which is covered by the Neogene units. According to balanced sections and fault plane measurements, $\sim 60^\circ$ for fault dip and ~ 1100 m minimum offset (resulting in a fault contact between upper Cretaceous Haymana formation and middle Eocene basinfill) are suggested for the Topkaya fault. North-dipping Türbetepe fault creates a fault contact between Jurassic platform carbonates and basinfill and is covered by Neogene units. ~12-km-long Türbetepe fault elongates from south of Kavakköy village to Bahçecik village (Figure 3.1b). It is suggested that Türbetepe fault terminates towards east beneath middle Eocene Yamak formation due to abrupt changes in dip directions of the units and possible ellipsoid geometry of the fault plane. The minimum offset and dip amounts of the fault plane for that fault was considered as ~ 800 m and 60° - 80° , respectively, according to fault plane measurements and balanced sections.

Strike-slip faults were traced by using combination of fault plane measurements, observable offsets in the field and satellite images, one of them (SS4) was, however,

delineated on the map as a probable fault by considering the orientations of the fold axes (see previous section for details). The faults are labelled as SS1 to SS16 (see Figure 3.1 for locations). The maximum offset along these faults is measured as 1100 m along SS10. By considering their trends and slip motions, these faults are categorized into four groups; (1) NW–SE (or WNW–ESE) -trending left-lateral (SS3, and SS10), (2) NW–SE (or WNW–ESE) -trending right-lateral (SS1, SS2, SS6, SS8, and SS16) (3) NE–SW (or ENE–WSW) -trending left-lateral (SS4, SS5, SS7, SS9, SS11, SS12 and SS13) and (4) NE–SW (or ENE–WSW) -trending right-laterals (SS14, and SS15) faults. In addition to them, almost E–W- or WNW–ESE-trending reverse (or thrust) faults (except Gedik Fault) with strike-slip motion have left-lateral components.

In order to relatively date the strike-slip faults, offsets of the sedimentary units and structures are considered, and except for group1 and group4 faults, any offset is not observed on the Neogene units or structures deforming them. It is therefore suggested that faults of group 1 and group 4 are relatively younger than faults of group 2 and group 3. it must , however, be taken into account that some of the faults of group 2 and group 3 may be related to younger deformation phases without observable offsets on Neogene units or related structures. Faults of group 2 and group 3 may be the result of the same deformation phase that formed folds and reverse faults. In this case, orientation of the faults of group 2, group 3, folds and reverse faults may be explained by left-lateral Riedel shear diagram developed by $\sim 015^\circ\text{N}$ oriented maximum principle stress direction (σ_1) (Figure 3.4e). In this regard, the faults of group 2, group 3 and folds/reverse faults correspond to the Riedel antithetic (R'), Riedel synthetics (Y,P,R), and compressional setting-related structure zones of the diagram, respectively. Although the line length rose diagrams of the structures is not exactly fit this diagram with $\sim \pm 10^\circ$ deviations, these diagrams can be considered as supportive statistical results because the results of the small deviations may well be ascribed to post local vertical block rotations and rheological differences. Besides this deformation phase, faults of the group 1, group 4, and Çirkintepe fault can be considered as the products of the Neogene transcurrent tectonic regime, which is out of the scope of the study.

3.3 Fault Kinematics (Paleostress Inversion)

In order to understand the paleostress configuration of the basin during its evolution, a detailed fault kinematic analysis is conducted.

3.3.1 Method and Data

Determining the principal stress orientations of an individual deformation phase is the main aim of the paleostress analyses. Various methods have been suggested for this inverse solution (e.g. Carey and Brunier., 1974; Angelier, 1979; 1984; 1989; 1994; Armijo *et al.*, 1982; Etchecopar *et al.*, 1981; Hardcastle, 1989; Will and Powell, 1991; Shan *et al.*, 2003; Sato and Yamaji, 2000) and they all assume that the direction of maximum shear stress is parallel to direction of movement on the fault plane, and that movement along a fault is independent of the other faults of same tectonic regime. Defining the orientation of σ_1 (maximum), σ_2 (intermediate), and σ_3 (minimum) principle stress axes and also calculating the shape ratio of the principle stress differences ($\Phi = (\sigma_2 - \sigma_3) / (\sigma_1 - \sigma_3)$) are the main results of these analyses. The results are used for defining the stress regime, which is basically defined as extensional where σ_1 close to vertical, strike-slip where σ_2 close to vertical, or compressional where σ_3 close to vertical. In addition to these basic (pure) regimes, being trans-tensional, trans-pressive, radial extensional, or radial-compressional are also possible. In order to understand such kind of impure possibilities, Delvaux *et al.* (1997) suggested another numeric index (Φ') calculated from (Φ), where Φ' ranges from 0 to 3, as;

$$\Phi' = \Phi \quad \text{where } \sigma_1 \text{ close to vertical}$$

$$\Phi' = 2 - \Phi \quad \text{where } \sigma_2 \text{ close to vertical}$$

$$\Phi' = 2 + \Phi \quad \text{where } \sigma_3 \text{ close to vertical}$$

They also suggested Φ' values for different tectonic settings as; radial extensional ($0 < \Phi' < 0.25$), pure extensional ($0.25 < \Phi' < 0.75$), trans-tensional ($0.75 < \Phi' < 1.25$), pure strike-slip ($1.25 < \Phi' < 1.75$), trans-pressive ($1.75 < \Phi' < 2.25$), pure compressional ($2.25 < \Phi' < 2.75$) and radial compressional ($2.75 < \Phi' < 3$).

In order to unravel principle stress orientations, fault plane attitudes and rake of slip lines are measured in the field. In this study, T-TECTO 3.0 software, using Gauss Method (Zalohar and Vrabec, 2007) is used for processing the data because of its effectiveness on separating deformation phases in heterogeneous fault system and its option allowing for defining separation parameters before calculation. The calculation process of the method mainly requires pre-defined values of three parameters, these are;

- (1) Parameter (s): Dispersion parameter of the distribution of angular misfits between the actual and resolved direction of slip along the fault. In the study, parameter (s) were chosen as 20° in order to keep the possible irrelevant data out of the calculations.
- (2) Parameter (d): Represent a threshold value for compatibility measure calculated by considering both misfit angle between actual and predicted direction of movement on the fault, and the position fault slip datum on Mohr diagram (the ratio of normal and shear stress on fault plane). The range for that parameter is suggested as $>60^{\circ}$ for highly heterogeneous stress field and $>30^{\circ}$ for less inhomogeneous stress fields by Zalohar and Vrabec (2007). In the study, this parameter was assigned as 45° due to the high possibility of having moderately heterogeneous stress filed in the sites.
- (3) Parameter q1 and q2: (q1) defines the maximum residual frictional angle for activating pre-existing fractures whereas (q2) represents the angle of internal friction angle of an intact rock which will be fractured. In the study, (q1) and (q2) was assigned as 60° and 20° in order to create a corridor covering 40° space in Mohr diagram which allowed for taking into account the possible re-activated fractures or the intact rocks having different internal friction angles.

Although fault plane attitudes and rake of slip lines are the main requirements of paleostress analyses, during data collection processes, displacement of the units, slip senses, and overprinting or cross-cutting relationships are also noted in order to differentiate deformation phases. After this separation, the data from individual sites are processed by considering the restrictions (parameters) mentioned above. After

processing each site, if there are any residual measurements, they are re-processed, if the residual data satisfies the requirements of the processes, otherwise they are deleted.

623 fault-slip measurements from 73 localities are collected under the context of kinematic studies. From these sites, 82 paleostress analyses are conducted and based on (Φ') index, 6 radial extensional, 9 pure extensional, 7 trans-tensional, 11 strike-slip, 20 trans-compressive, 23 pure compressional, and 7 radial compressive stress orientations are interpreted. Only less than 2.5% of the measurements are determined as incompatible during calculation process and they are deleted. The results of these studies are summarized in Table 3.2 and Figure 3.8. Although the data collection in the field is not performed systematically due to randomly distributed (exposed) fault plane outcrops (resulting in random data collection and related bias in the results), statistical analyses are conducted on fault plane measurements in order to clarify the characteristics of the data. Basically, the results of the analyses (Figure 3.9) indicate that; (1) measurement of the strike-slip faults ($\text{rake} < 45^\circ$) dominates all data, (2) distribution of dip amounts of the fault planes are compatible with the natural fault plane patterns, and (3) compressional setting-related faults are mainly controlled by reverse faults rather than thrusts.

Table 3.2: Locations and the results of paleostress analyses (see Figure 3.12 for locations).

ID	Longitude	Latitude	σ_1	σ_2	σ_3	Φ	Φ'	n
HY1	32.58519	39.39156	266/31	163/21	055/52	0.7	2.7	7
HY2	32.60343	39.41228	003/54	175/35	268/03	0.3	0.3	8
HY3	32.60587	39.41369	131/23	272/61	034/17	0.4	1.6	7
HY4	32.61143	39.41863	088/02	357/36	181/54	0.2	2.2	7
HY5 PH1	32.61317	39.42111	113/02	022/36	206/54	0.1	2.1	6
HY5 PH2	32.61317	39.42111	215/55	348/26	089/23	0.5	0.5	2
HY6 PH1	32.56972	39.47018	079/34	335/20	220/60	0.5	2.5	7
HY6 PH2	32.56972	39.47018	337/12	241/23	093/63	0.7	2.7	2
HY7	32.53521	39.43755	015/02	105/02	240/87	0.3	2.3	10
HY8	32.51289	39.54457	351/13	084/12	215/73	0.3	2.3	7
HY9	32.51173	39.54109	030/13	298/12	166/73	0.5	2.5	10
HY10	32.35841	39.5787	196/23	056/61	293/17	0.3	1.7	5

Table 3-2 (continued)

ID	Longitude	Latitude	σ_1	σ_2	σ_3	Φ	Φ'	n
HY11	32.34941	39.57535	351/13	084/12	215/73	0.2	2.2	7
HY12	32.10503	39.44738	027/02	291/72	118/18	0.3	1.7	7
HY13	32.10526	39.45166	351/13	084/12	215/73	0.1	2.1	6
HY14	32.13187	39.44851	185/55	012/35	280/03	1	1	9
HY15	32.13423	39.45285	236/02	326/02	101/87	0.8	2.8	7
HY16	32.13182	39.45945	309/13	214/23	065/63	0.6	2.6	8
HY17	32.17432	39.52801	098/34	309/52	198/15	0.9	1.1	7
HY18	32.53072	39.48464	196/23	090/33	314/48	0.2	2.2	5
HY19	32.51121	39.48075	347/34	250/10	146/55	0.8	2.8	7
HY20	32.51158	39.48759	212/23	099/43	321/38	0.6	1.4	4
HY21	32.52891	39.38742	019/23	118/22	247/57	0	2	7
HY22	32.52964	39.38796	027/02	135/84	297/06	0.2	1.8	6
HY23 PH1	32.43514	39.0011	346/02	080/60	255/30	0	2	11
HY23 PH2	32.43514	39.0011	083/23	352/02	258/67	0.2	2.2	2
HY24 PH1	32.51193	39.52666	094/55	344/14	245/32	0.1	0.1	7
HY24 PH2	32.51193	39.52666	115/23	021/11	267/64	0.4	2.4	10
HY25 PH1	32.56693	39.50942	030/13	298/12	166/73	0.5	2.5	18
HY25 PH2	32.56693	39.50942	094/55	322/26	220/23	0.6	0.6	5
HY26 PH1	32.49576	39.42484	196/33	291/11	044/64	0.1	2.1	13
HY26 PH2	32.49576	39.42484	156/12	057/35	262/52	0.9	2.9	4
HY27 PH1	32.50717	39.53027	327/34	059/02	151/56	0.5	2.5	13
HY27 PH2	32.50717	39.53027	196/33	296/22	065/57	0.4	2.4	5
HY28	32.84805	38.67389	226/76	351/08	083/12	0.3	0.3	8
HY29	32.55808	39.47286	045/65	245/24	152/08	1	1	6
HY30	32.53761	39.48336	003/34	241/38	119/34	0	2	10
HY31	32.48119	39.43528	194/34	285/02	017/56	0.1	2.1	12
HY32	32.47419	39.44008	337/12	241/23	093/63	1	3	15
HY33	32.37788	39.38725	002/86	094/00	185/04	0.4	0.4	15
HY34	32.37644	39.39714	035/23	254/61	132/17	0.6	1.4	20
HY35	32.26222	39.39058	348/65	201/21	106/12	0.4	0.4	6
HY36 PH1	32.20064	39.47947	044/13	140/23	288/63	0.3	2.3	15
HY36 PH2	32.20064	39.47947	323/13	219/47	064/41	0.2	1.8	7
HY37	32.08536	39.469	260/02	169/36	353/54	0.3	2.3	12
HY38 PH1	32.07489	39.44928	213/34	002/52	113/15	0.2	1.8	9
HY38 PH2	32.07489	39.44928	100/13	193/12	325/73	0.6	2.6	5
HY39	32.46051	39.49542	002/76	213/13	122/07	0.3	0.3	4
HY40	32.45285	39.49978	002/02	272/24	097/66	0.1	2.1	9
HY41	32.45506	39.49873	022/24	113/02	205/56	0.5	2.5	6
HY42	32.4605	39.49251	357/23	262/11	149/64	0.1	2.1	4
HY43	32.45386	39.50393	089/65	314/18	218/16	0.2	0.2	4

Table 3-2 (continued)

ID	Longitude	Latitude	σ_1	σ_2	σ_3	Φ	Φ'	n
HY44	32.45412	39.49211	262/65	025/14	120/20	0.5	0.5	6
HY45	32.46272	39.4948	035/23	289/33	153/48	0.1	2.1	5
HY46	32.47155	39.4775	327/34	059/02	151/56	0.5	2.5	4
HY47	32.52271	39.48405	015/02	266/84	105/06	0.4	1.6	9
HY48	32.52044	39.47393	067/23	336/02	242/67	1	3	4
HY49	32.47553	39.39523	305/65	204/05	112/24	0.2	0.2	4
HY50	32.47788	39.38468	088/02	358/02	223/87	0.7	2.7	5
HY51	32.48101	39.38454	002/23	143/61	265/17	0.4	1.6	5
HY52	32.482	39.38541	284/44	096/46	190/04	0.8	1.2	6
HY53	32.44642	39.38607	213/34	101/29	340/42	0.6	2.6	5
HY54	32.44297	39.38319	002/65	251/10	156/23	0.2	0.2	5
HY55	32.45021	39.38538	262/65	014/10	108/23	0.2	0.2	9
HY56	32.45224	39.39777	187/02	093/60	278/30	0.6	1.4	10
HY57	32.45404	39.39821	260/02	170/12	360/78	0.2	2.2	7
HY58	32.48194	39.38493	039/02	306/60	130/30	0.1	1.9	6
HY59	32.42166	39.26821	019/23	118/22	247/57	0.3	2.3	4
HY60	32.42194	39.26996	212/23	117/11	004/64	0.7	2.7	4
HY61	32.41907	39.26763	346/02	078/36	253/54	0.5	2.5	4
HY62	32.39074	39.27128	273/86	074/04	165/01	0.5	0.5	4
HY63	32.39186	39.27266	219/65	330/10	065/23	0.2	0.2	4
HY64	32.38865	39.27005	358/02	089/24	264/66	0.4	2.4	4
HY65	32.38898	39.26874	002/86	213/03	122/02	0.8	0.8	5
HY66	32.3842	39.27821	322/02	052/24	227/66	1	3	4
HY67	32.31789	39.25719	187/02	090/72	277/18	0.1	1.9	33
HY68	32.31792	39.25849	255/13	133/12	001/73	0.8	1.2	7
HY69	32.25637	39.28368	175/65	063/13	329/23	0.4	0.4	6
HY70	32.27339	39.26793	334/02	243/24	068/66	0.8	2.8	6
HY71	32.85627	38.63961	125/02	234/84	035/06	0.3	1.7	10
HY72	32.3592	39.42932	117/34	267/52	017/15	0.5	1.5	6
HY73	32.36069	39.43148	300/75	102/14	183/04	0.8	0.8	4

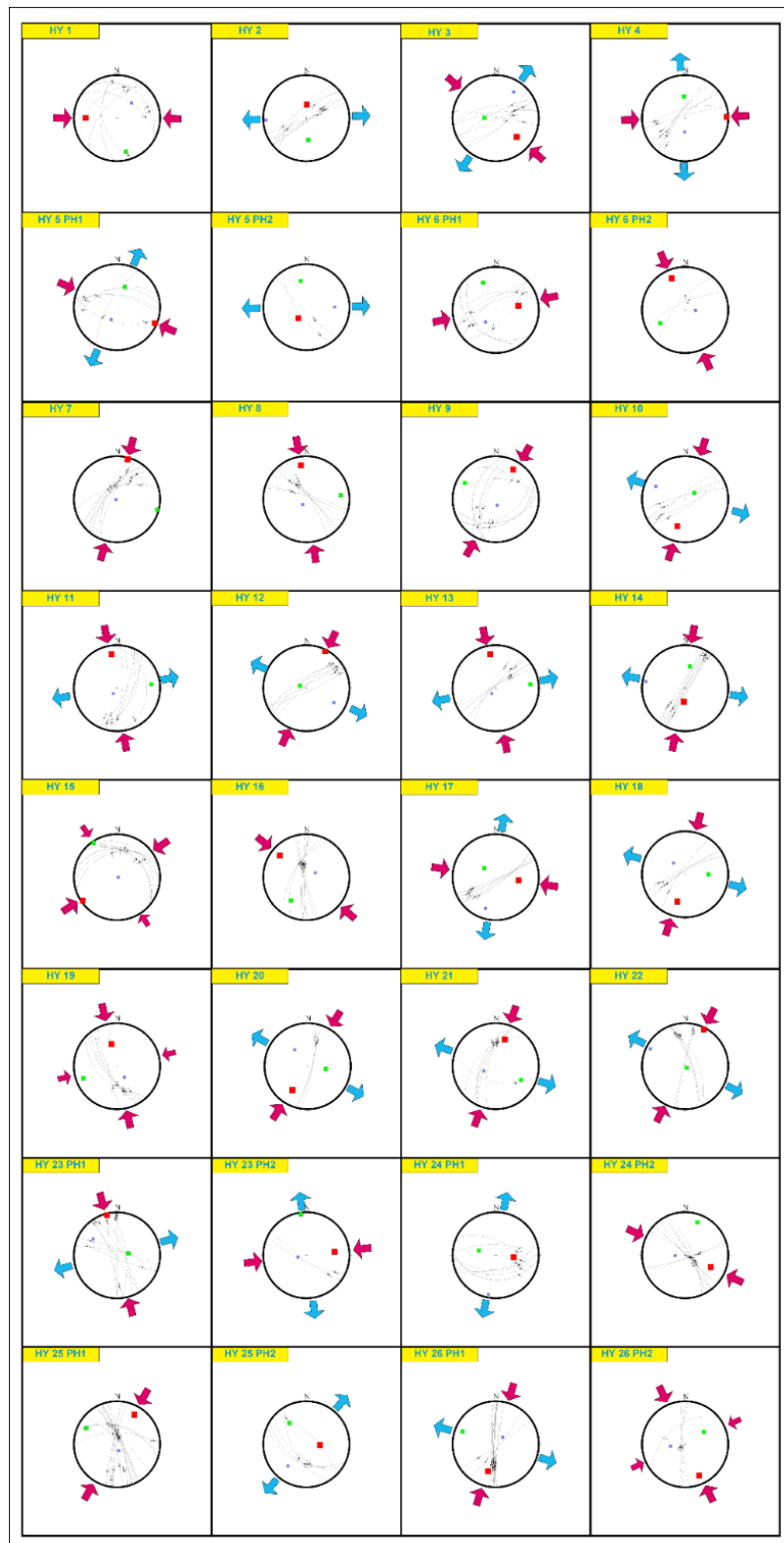


Figure 3.8: Cyclographic traces, slickensides and constructed paleostress configurations of the Haymana Basin fault plane measurements.

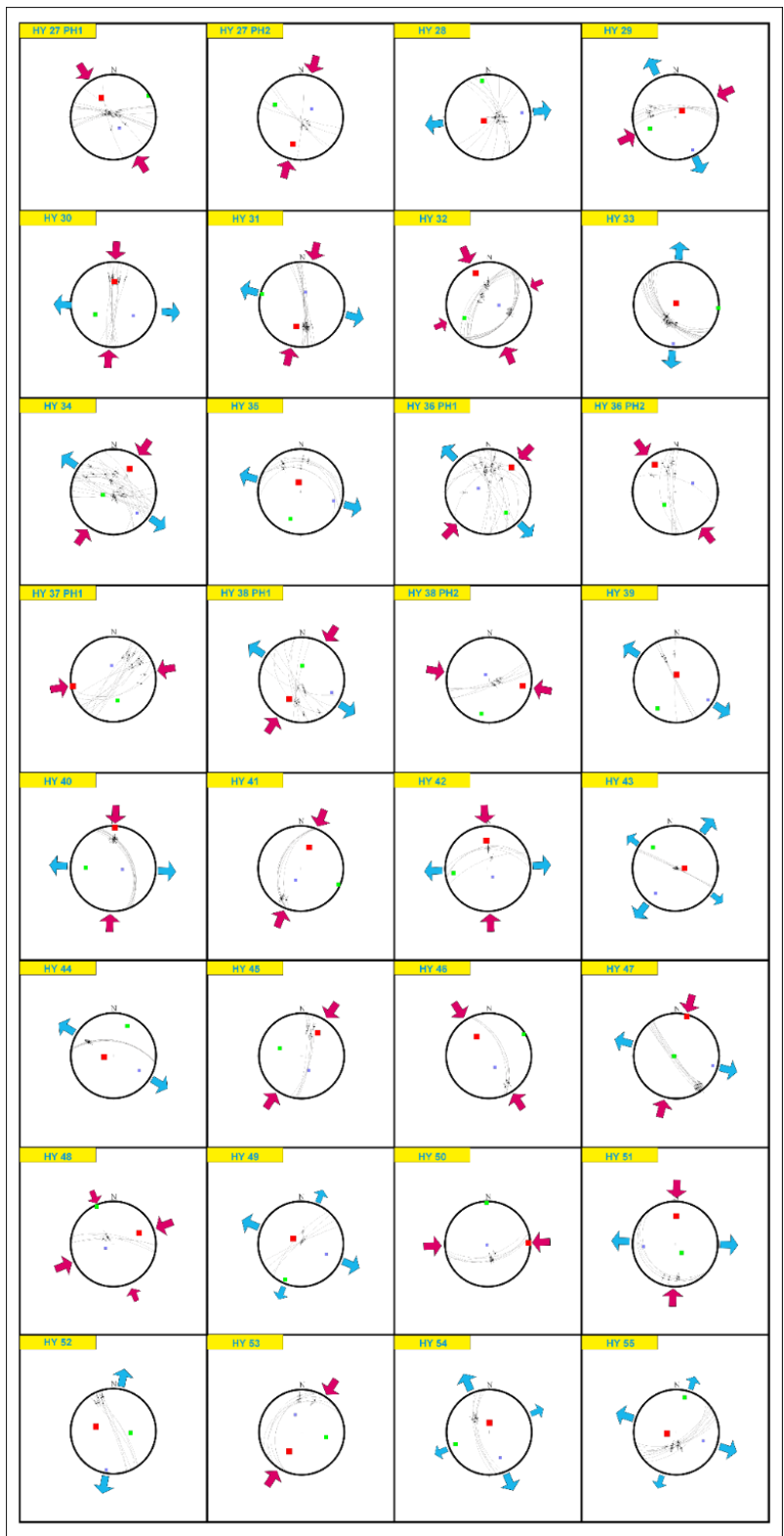


Figure 3.8 (continued)

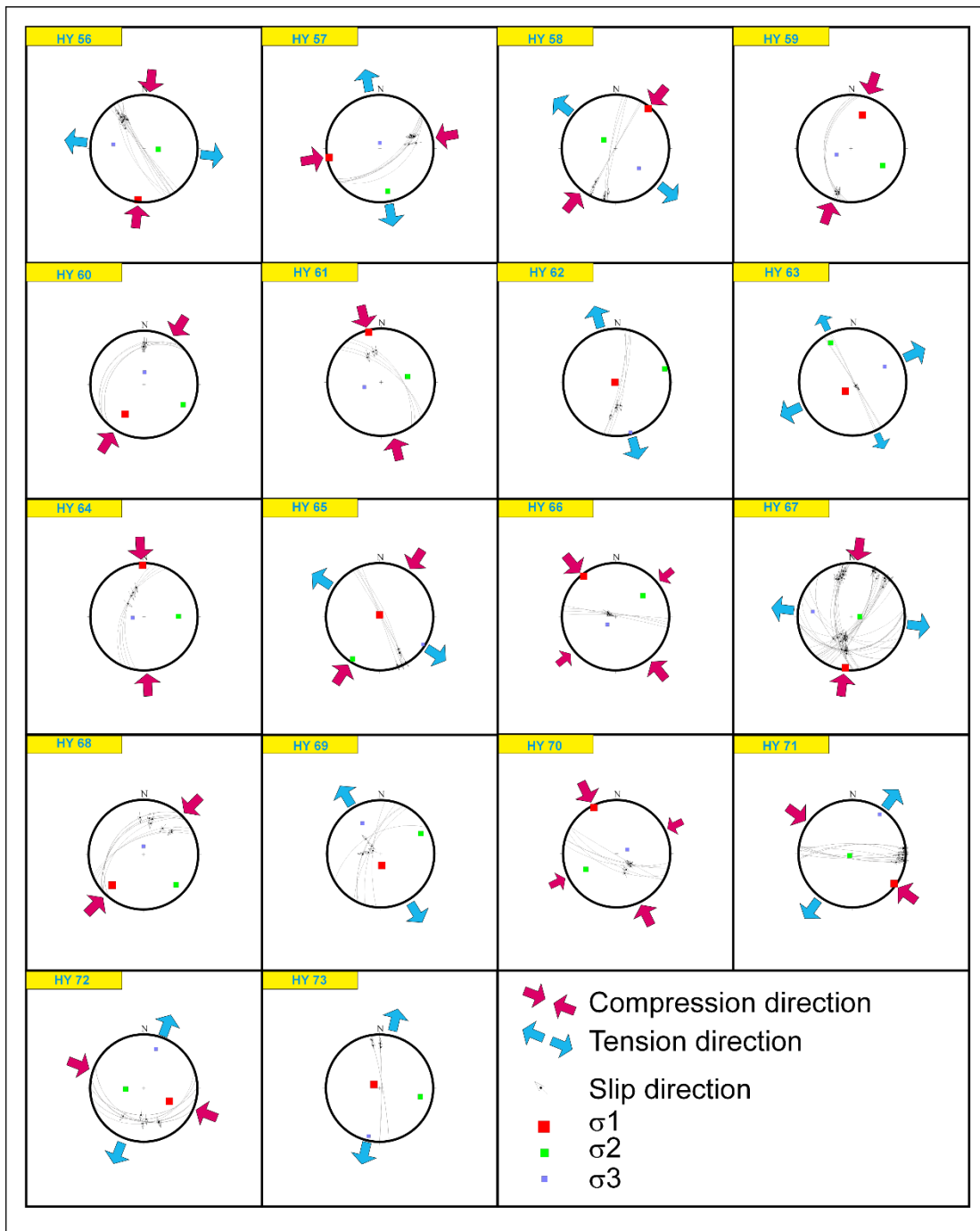


Figure 3.8 (continued)

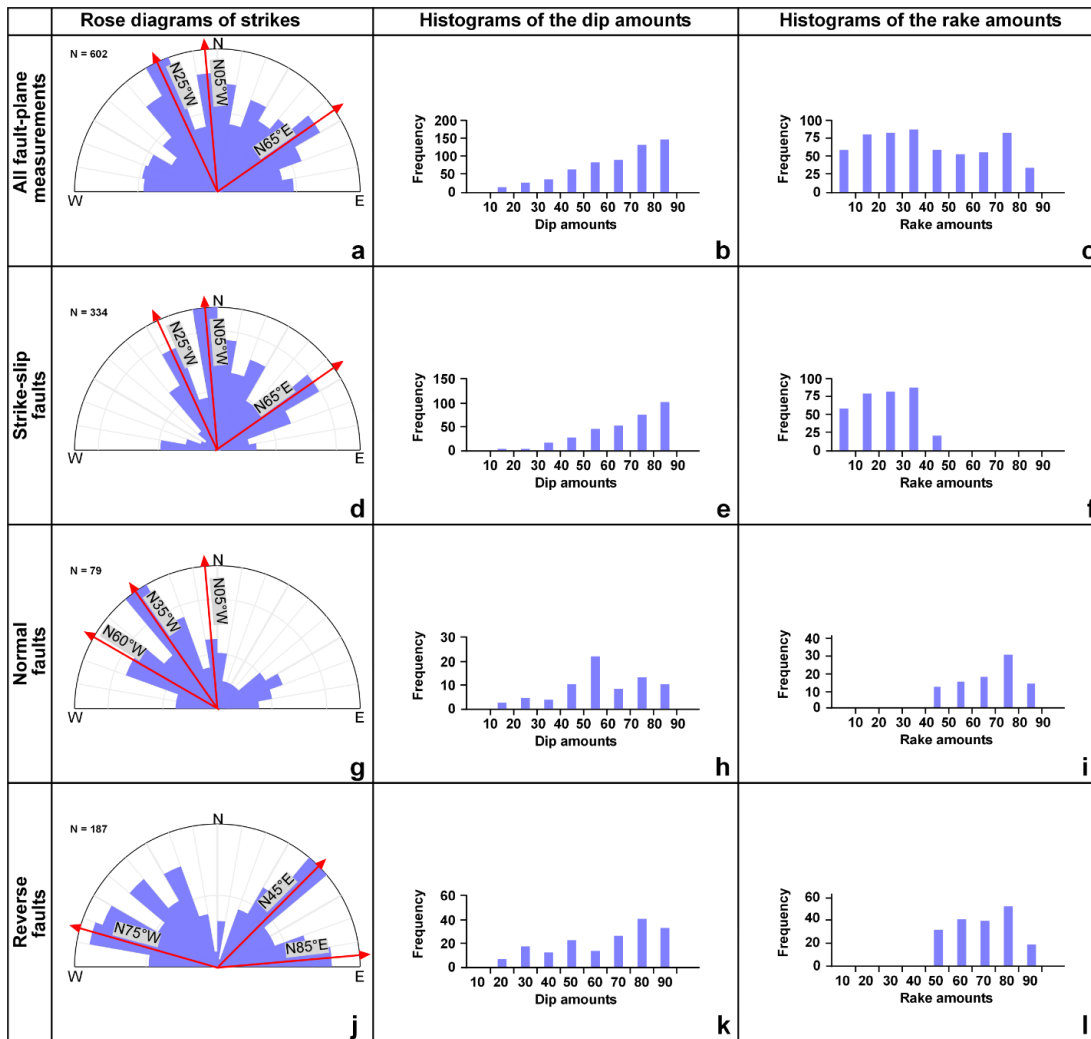


Figure 3.9: Statistical analyses of fault plane measurements. Rose diagrams of strike of the fault planes, histograms of dip amount of fault planes and rake amounts for all fault plane measurements (a,b,c); for strike-slip faults (d,e,f); for normal faults (g,h,i); for reverse/thrust faults (j,k,l). See text for explanation.

3.3.2 Spatio-Temporal Characteristics of Paleostress Inversion Solutions

During the data collection processes, three different deformation phases are determined by geological observations (e.g., displacement of the units, slip senses, and overprinting or cross-cutting relationships). Because such kind of observations was not possible for the most of the measurement sites, the sites with critical observations are therefore used as references during analyses. Together with the field observations and (Φ') values, three phase of deformation are determined.

The first phase is represented by 7 sites (HY 24, 25, 33, 52, 54, 55, and 73) and group 1 stress orientations (tensional). The average orientations of (σ_1), (σ_2), (σ_3) and the Φ' value are 357°N/84°, 031°N/61°, 178°N/14° and 0.5, respectively (Figure 3.10). Almost vertical (σ_1), N–S-trending horizontal component of almost horizontal (σ_3) and average amount of the Φ' indicate obvious normal faulting related to a N–S extension in the region. Although relative dating is not possible for all the sites of the phase, it is noted that the age of youngest unit in which the phase-related measurements is middle Paleocene. Observed overprinted slicken-lines (Figure 3.11) and the trend of the fault planes which are mainly parallel to compressional setting structures indicate re-work potential of the faults during later phases. Spatially, the measurements of the phase are distributed at the northern part of the study area (Figure 3.12b).

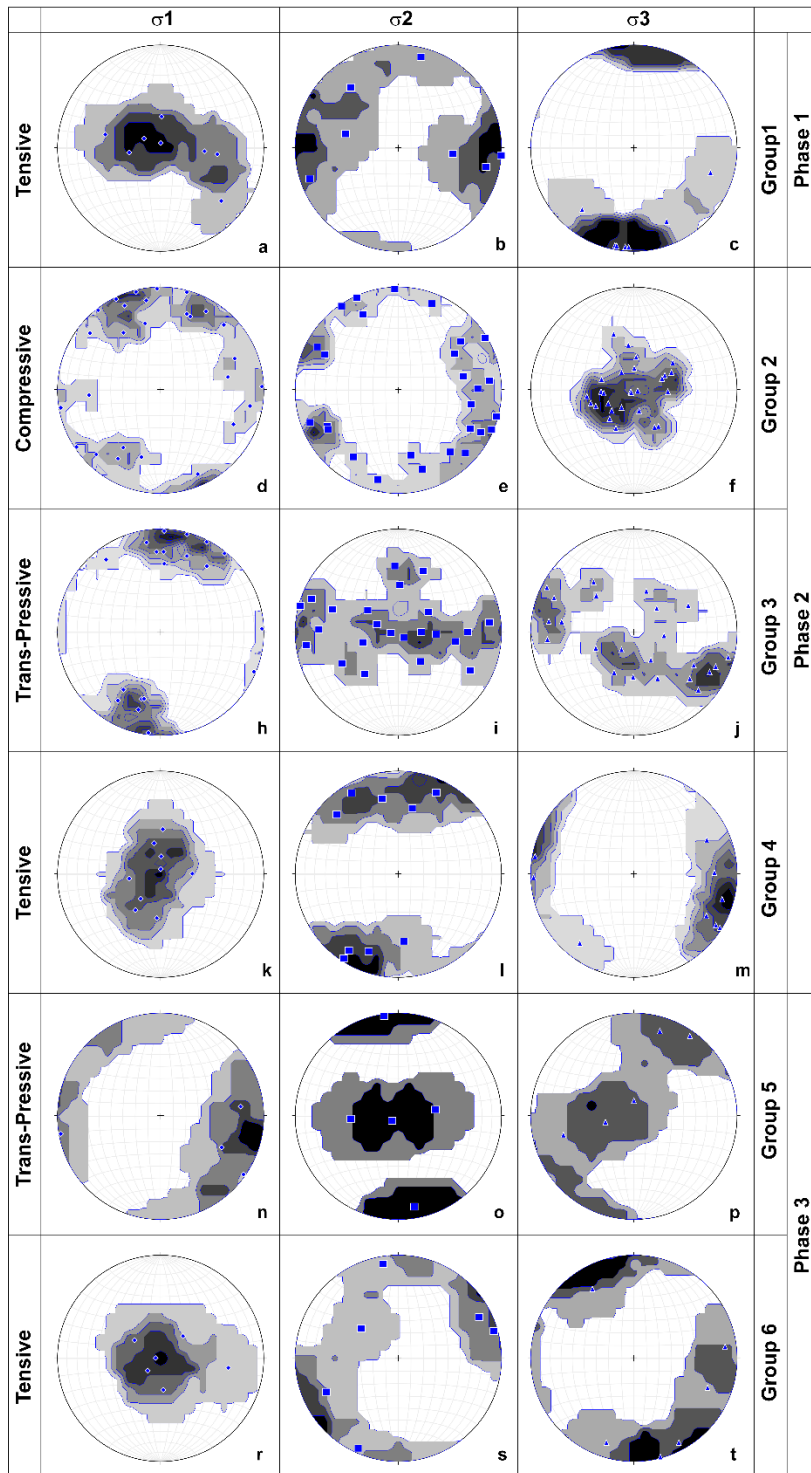


Figure 3.10: Contour diagrams of the principle stress orientations of deformation phases. Phase 1 group 1 stress orientations (a,b,c); phase 2 group 2 stress orientations (d,e,f); phase 2 group 3 (h,i,j); phase 2 group 4 stress orientations (k,l,m); phase 3 group 5 stress orientations (n,o,p); phase 3 group 6 stress orientations (r,s,t). See text for explanation.

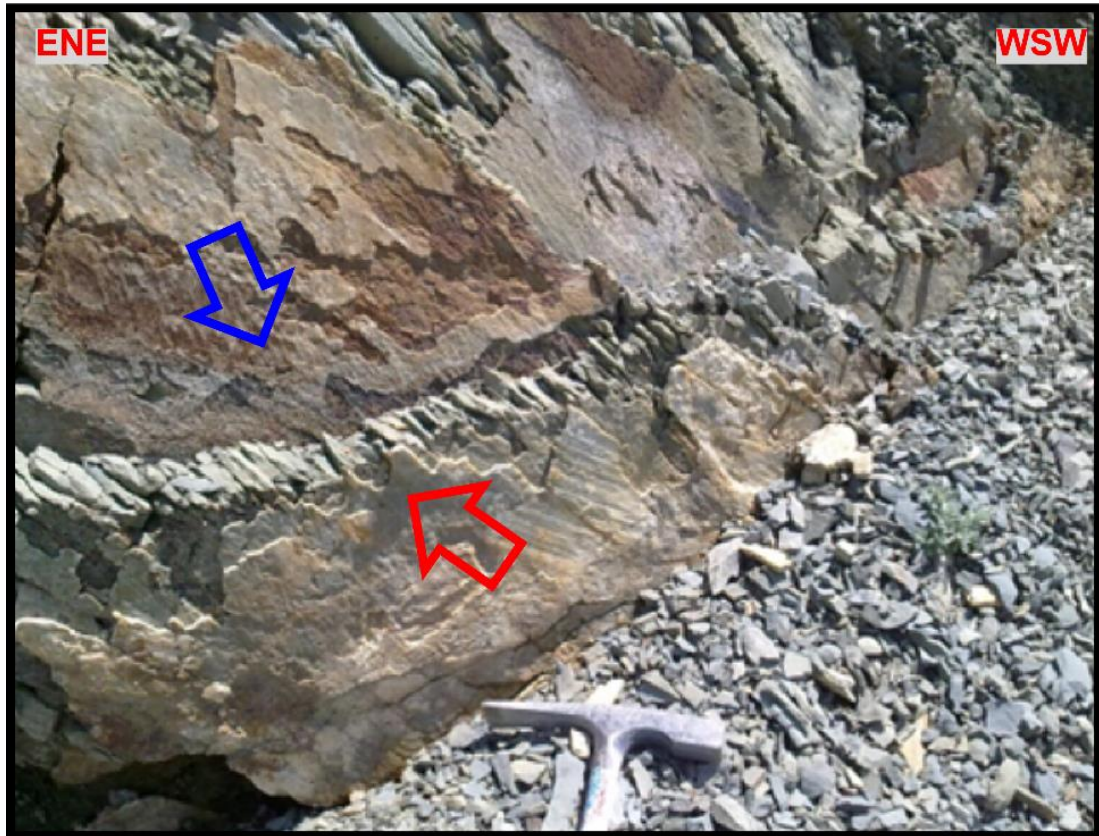


Figure 3.11: Overprinting slickensides observed in the deformation zone of the Dereköy thrust fault. View: towards NNW. Note that first movement (blue arrow) is normal indicated by striations, the second movement (red arrow) is reverse as indicated by calcite fibers (see Figure 3.1 for location).

The second phase comprises three different stress orientations of the same regime which are compressional (group 2) represented by 28 sites (HY 1, 6, 7, 8, 9, 15, 16, 19, 24, 25, 26, 27, 32, 36, 37, 38, 41, 46, 48, 50, 53, 59, 60, 61, 64, 66, 68, and 70), trans-compressional (group 3), 24 sites (HY 4, 5, 10, 11, 12, 13, 18, 20, 21, 22, 26, 30, 31, 34, 36, 38, 40, 42, 45, 47, 51, 56, 58, and 67) and tensional (group 4), 9 sites (HY 2, 5, 14, 35, 39, 43, 44, 63, 65) (Figure 3.10, see Figure 3.12 a and b for locations).

The mean vectors of the principle stresses of the group 2 are determined as $352^{\circ}\text{N}/16^{\circ}$ (σ_1), $089^{\circ}\text{N}/16^{\circ}$ (σ_2) and $229^{\circ}\text{N}/64^{\circ}$ (σ_3), and the average Φ' , as 2.6. Although the results of the paleostress analyses of that group clearly indicate N–S compressional setting with N–S oriented almost horizontal (σ_1) and vertical (σ_3), the spatial distribution of the solutions also indicate NNE–SSW compressional setting in the

north and northwestern part of the study area where the strikes of the folds and reverse faults become WNW–ESE oriented. It is therefore inferred that the solutions of that group is consistent with the structures observed in the basin (Figure 3.12a).

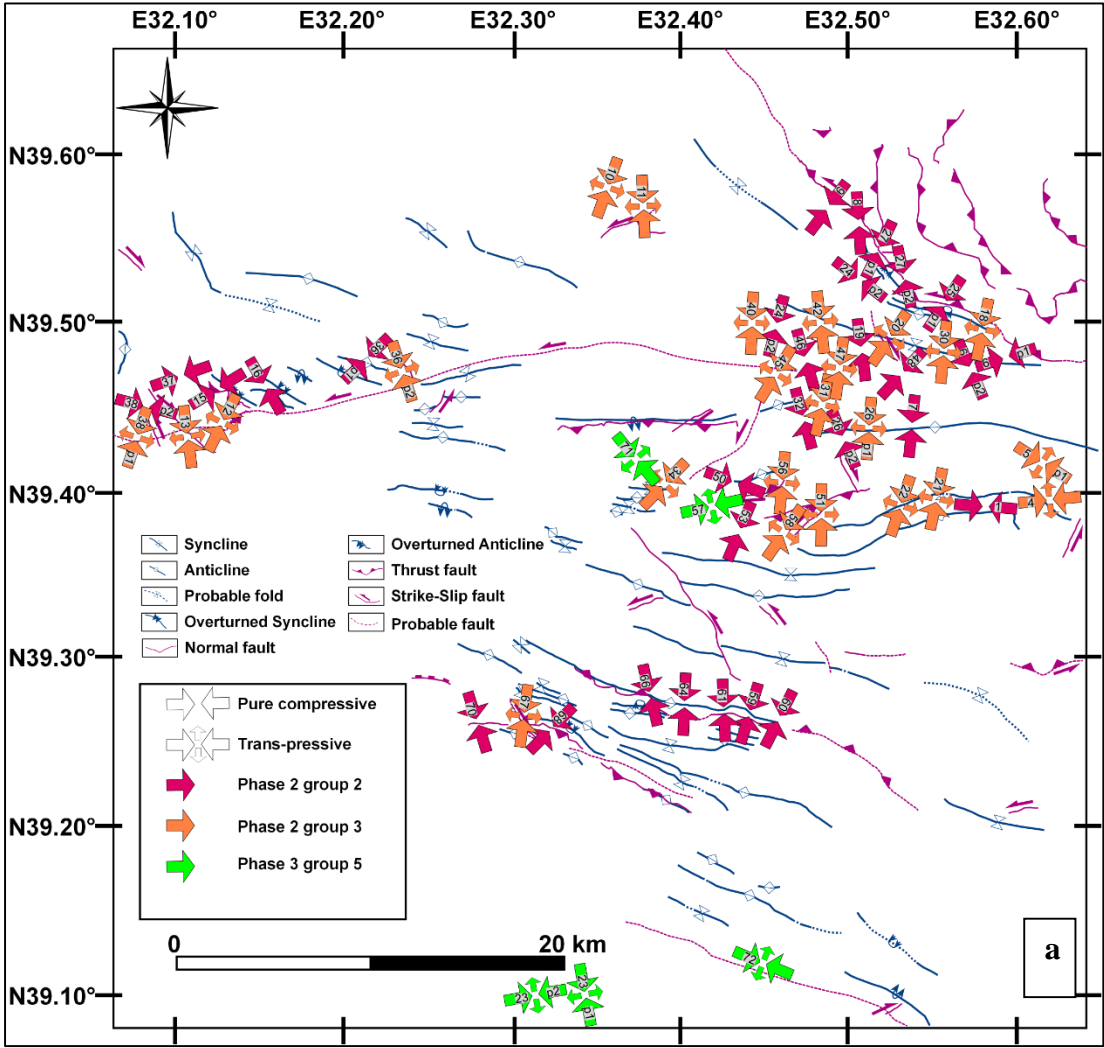


Figure 3.12: Major structures and paleostress orientations. (a) Paleostress orientations of group 2, 3, and 5; (b) Paleostress orientations of group 1, 4, and 6. See text for explanation. See Figure 3.1 for legend.

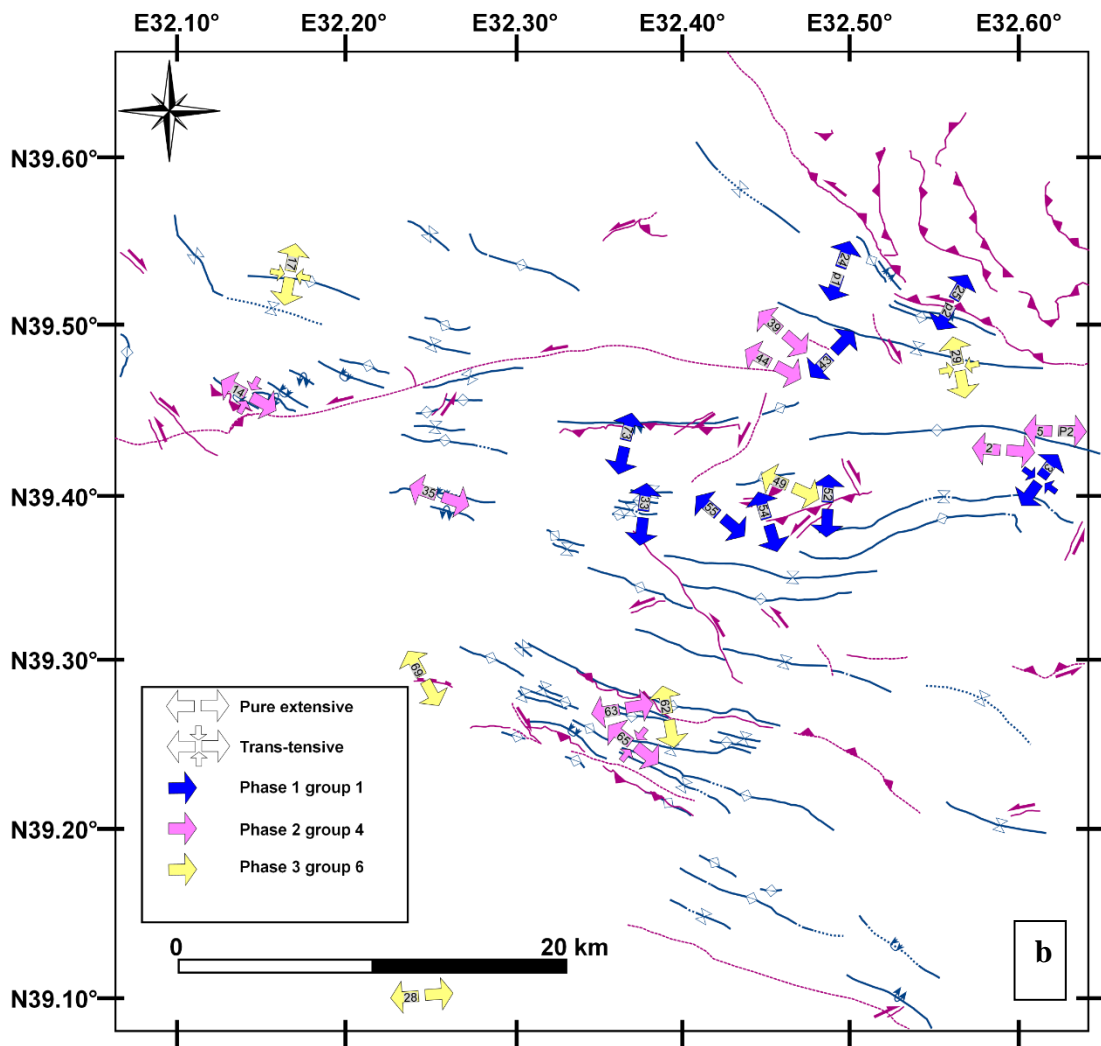


Figure 3.12: (Continued)

The average orientations of (σ_1) , (σ_2) , (σ_3) and Φ' value of group 3 are $023^\circ\text{N}/16^\circ$, $336^\circ\text{N}/43^\circ$, $173^\circ\text{N}/40^\circ$ and 1.9, respectively. The paleostress solutions suggest obvious NNW–SSE-directed compressional regime-related strike-slip fault development. Spatial distribution of these results are consistent with the strike-slip faults observed in the study area (Figure 3.12a).

$261^\circ\text{N}/65^\circ$ (σ_1), $289^\circ\text{N}/20^\circ$ (σ_2) and $127^\circ\text{N}/12^\circ$ (σ_3) are the average direction of the principle stresses of group 4 and 0.5 is Φ' value. Almost vertical (σ_1) and WNW–ESE-oriented horizontal component of (σ_3) together with Φ' value indicate a clear WNW–ESE-directed extension. The orientation of the strikes of faults of the group 4 are almost $\sim 70^\circ\text{--}100^\circ$, oblique to the main trends of the reverse faults and fold. By

considering this angular relationship, mean extension direction of the group and the stratigraphic levels of the measurements, it is suggested that this group and related small-scale (unmappable) normal faults are the natural products of N–S- and NNE–SSW-directed main compressional deformation phase (phase 2).

Phase 3 covers the Neogene deformation of the basin and is represented by group 5 (trans-pressure) structures observed at 4 sites (HY 23, 57, 71, 72) and group 6 (tensional) structures occurring at 6 sites (HY 17, 28, 29, 49, 62, 69) (Figure 3.12 a and b). The fault-slip are collected mainly from almost horizontal and less deformed Neogene units. Because this phase is out of scope of the study, there are small number of sites representing this phase and less representative with respect to the other phases. It may be suggested that: (1) group 5 is mainly controlled by WNW–ESE-directed compressional regime and this is inferred by average principle stress orientations and Φ' value ($091^{\circ}\text{N}/12^{\circ}$ for σ_1 , $276^{\circ}\text{N}/42^{\circ}$ for σ_2 , $347^{\circ}\text{N}/40^{\circ}$ for σ_3 and 1.9 for Φ), (2) The main stress orientation controlling group 6 is almost NW–SE-directed tensional stress regime. These results are supported by the average (σ_1) ($091^{\circ}\text{N}/65^{\circ}$), (σ_2) ($357^{\circ}\text{N}/18^{\circ}$), and (σ_3) ($141^{\circ}\text{N}/14^{\circ}$) orientations and average Φ' (0.6) value.

There is no field observation above relative timing of group 5 and group 6 stress orientations of phase 3, group 5 is considered older due to possibility of being continuation of older compressional phase, and existence of compressional regime-related structures observed at the lower levels of the Neogene units as determined along a seismic line, crossing the Neogene units (Figure 3.13 and see Figure 3.1 for location).

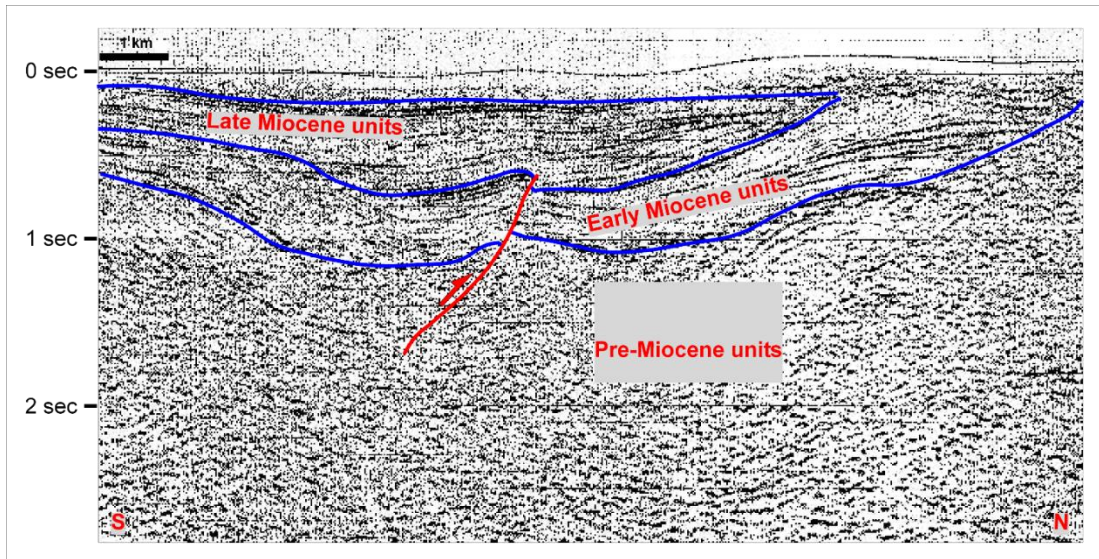


Figure 3.13: Seismic line (88-Hay-01) showing compressional deformation over Miocene units (see Figure 3-1 for location). Seismic line is gathered from seismic department of T.P.A.O and interpreted in this study. Note: The boundaries of the units were assigned by considering deformation phases discussed in this section and Chapter 4 and 5.

A summary of the temporal relationships of the deformation phases is shown in Figure 3.14.

Age	Unit	Phase	Main directions of the stresses					
			1	2	3	4	5	6
Neogene	Neogene Units	Phase 3						
Paleogene		Phase 2						
Cretaceous	Basement	Phase 1						

Figure 3.14: Summary of temporal relationships of the deformation phases.

3.4 Cross-Sections and Balancing

In order to reveal the three dimensional geometry of the basin, six cross-sections (see Figure 3.15 for the locations) are constructed and then balanced to precisely calculate shortening rates in different parts of the basin.

3.4.1 Methods and Data

Bedding attitudes, boundaries of stratigraphic cycles, locations and types of the structures, and digital elevation model of the study area are used as base data for constructing cross-sections. The trends of the sections are determined by considering the orientations of the main structures and the locations of the slightly and highly deformed zones within the basin in order to calculate maximum and minimum shortening rates in the region.

During construction, ~300 bedding measurements from 2-km-wide buffer zones of the section traces are used. Projection of the measurements in the buffer zones to the section traces are performed by considering the apparent dip attitudes. The reason for using the boundaries of the stratigraphic cycles rather than formation boundaries is the fact that the locations of the transitions lateral facies changes between the same age formations in subsurface are unpredictable. The use of the stratigraphic cycle boundaries are therefore considered as solution to overcome this problem because they are thought as continuous lines tracing same time interval below the surface. 30-m resolution digital elevation model is taken from USGS open sources and it is used to extract topographic elevations along the section traces.

Academic version of Midland Valley Move 2015.1 is also used to construct sections and balancing. During construction processes six steps are followed;

- (1) Grouping the projected dips by considering the faults intersecting the section line;
- (2) Creating a template horizon based on 1B fold classes (parallel folding) of Ramsey (1967), by using isogons of separated dips where it is possible

otherwise the gaps are filled by considering the locations of the folds with respect to sections;

- (3) Creating horizon (boundaries of the cycles) lines based on constant bed height by using created template horizon.
- (4) Determining the bed heights by considering outcrops widths of the cycles and stratigraphic thicknesses;
- (5) Repeating first four steps for each separated dip groups;
- (6) Fitting the sections on the topography and the geological map by considering possible fixed offsets created by the faults.

Note: Offsets are taken as fixed distances due to lack of subsurface data, such as seismic lines.

After these processes, constructed cross-sections are balanced. In order to validate the section, four main steps are followed; these are unfolding, validation (balancing) of original section, movement on fault plane and calculation of shortening amount.

The procedure outlined below is followed for unfolding part of section balancing:

- (1) Separating the sections by considering the locations of the folds and faults;
- (2) Defining unfolding algorithm of the software. In the study, flexural-slip unfolding algorithm is used, so that the thickness of the stratigraphic cycles, and line-length of the upper most horizon (first-created horizon during section construction) are preserved. The algorithm assumes that internal deformation occurs mostly by layer-parallel slip and the amount of slip increases away from hinge lines of the folds. Based on these assumptions, software construct a slip-system parallel to a selected template horizon and resulted slip-system is used for unfolding the other horizons of the folds during calculations. This procedure may briefly be explained by rotating the horizons to the horizontal by removing the flexural slip components of the fold;
- (3) Defining a pin line following the trace of the axial planes on cross-sections. This line is used as rotation axis during unfolding calculations;
- (4) Defining a template horizon used for creating a slip-system;

- (5) Defining passive objects (horizons and structures) to be unfolded by considering template horizon;
- (6) Repeating first five steps for all separated parts of the section.

Validation of the initially created section is required during unfolding procedure because the attitude of the previously determined faults and offsets affect the shapes of the unfolded layers by creating thickness variations between horizons. These effects are recognized during unfolding procedure and problematic fault plane attitudes and offsets are corrected in initial section in order to allow for geometrically consistent backward modelling.

After validations separated segments of the sections are joined by moving on the fault planes based on the fixed offsets occurred between horizons.

Shortening rates are calculated, based on the lengths of the validated and unfolded sections, in percentage and formulated by $100(L'-L)/L'$ where L' equals to length of unfolded section and L , length of validated section.

Note: The reason for selecting flexural-slip unfolding procedure and 1B class of Ramsey, (1967) during cross-section construction is the possible occurrence of post-depositional deformation in the basin (see thermo-chronology chapter for details) that produce almost any important change in the thickness of the horizons.

Although the locations of the sections are tried to be determined by considering the attitudes of the structures, and amount of deformation, the limiting factors are amount and continuation of the bedding attitude measurements and good quality subsurface data. Only six cross-sections can therefore be conducted and three dimensional block models of the basin cannot be constructed.

3.4.2 Characteristics of the Balanced Cross-Sections

The results of the balanced sections and shortening ratio calculations are given in Figure 3.15 and 3.16, respectively. Correlation of the cross-section in fence diagram is also given in Figure 3.17.

By analyzing these sections, it is possible to suggest that;

(1) N and NW parts of the study area are the least deformed sections of the basin (average 3% shortening ratio);

(2) The total true thickness of the units reaches up to 6 km which is consistent with the measured stratigraphic sections;

(3) Complexity and deformation amounts (average 24% shortening ratio) dramatically increases towards E-SE part of the basin;

(4) Basinfill is thick in the north and but thin in the south (wedge like geometry);

(5) Development of the folds are related to reverse faults, and

(6) The main deformation in the basin is controlled by reverse or thrust faults.

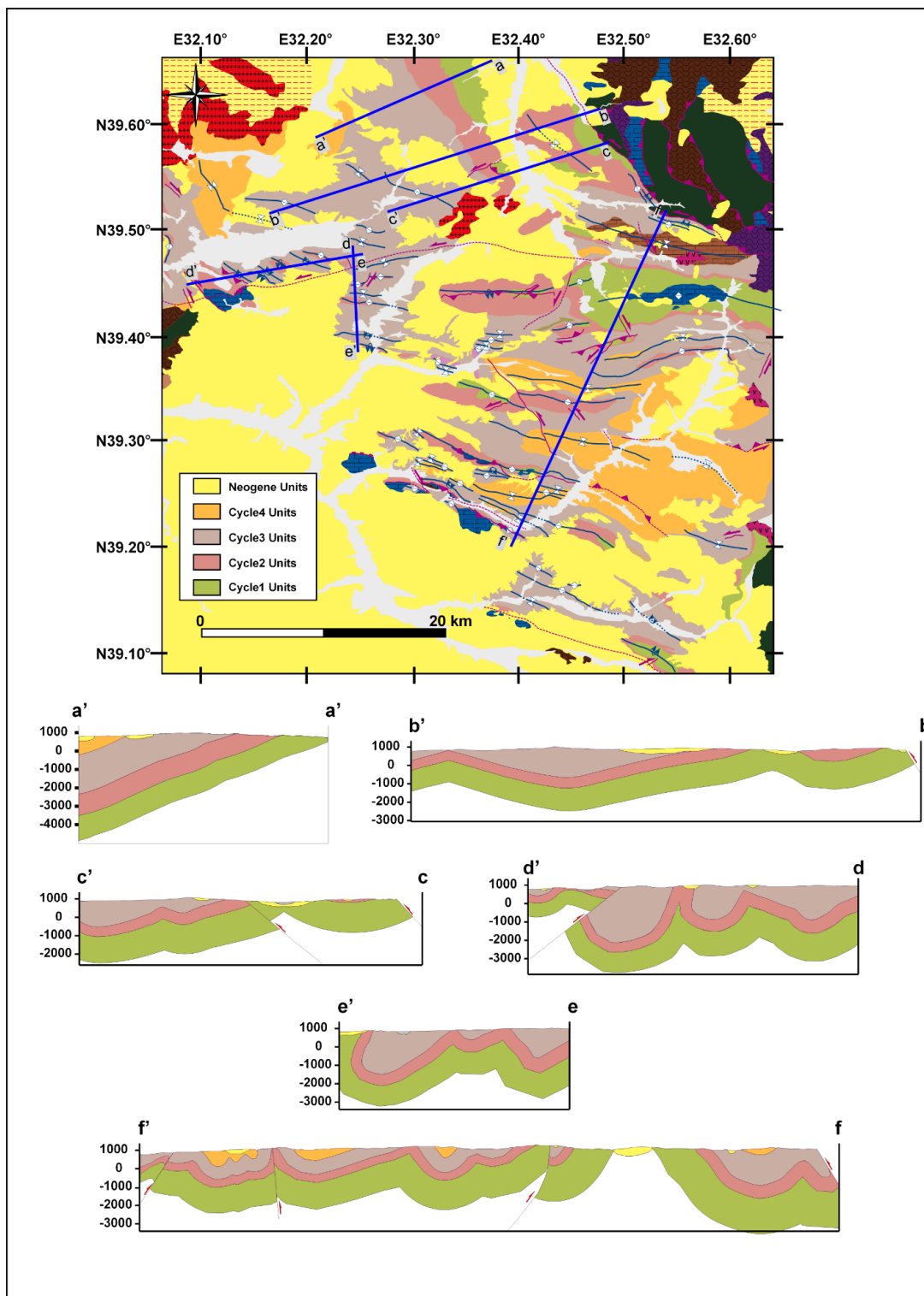


Figure 3.15: Locations of the balanced cross-section lines and results of balanced cross-sections (see Figure 2.1 and 3.1 for legend).

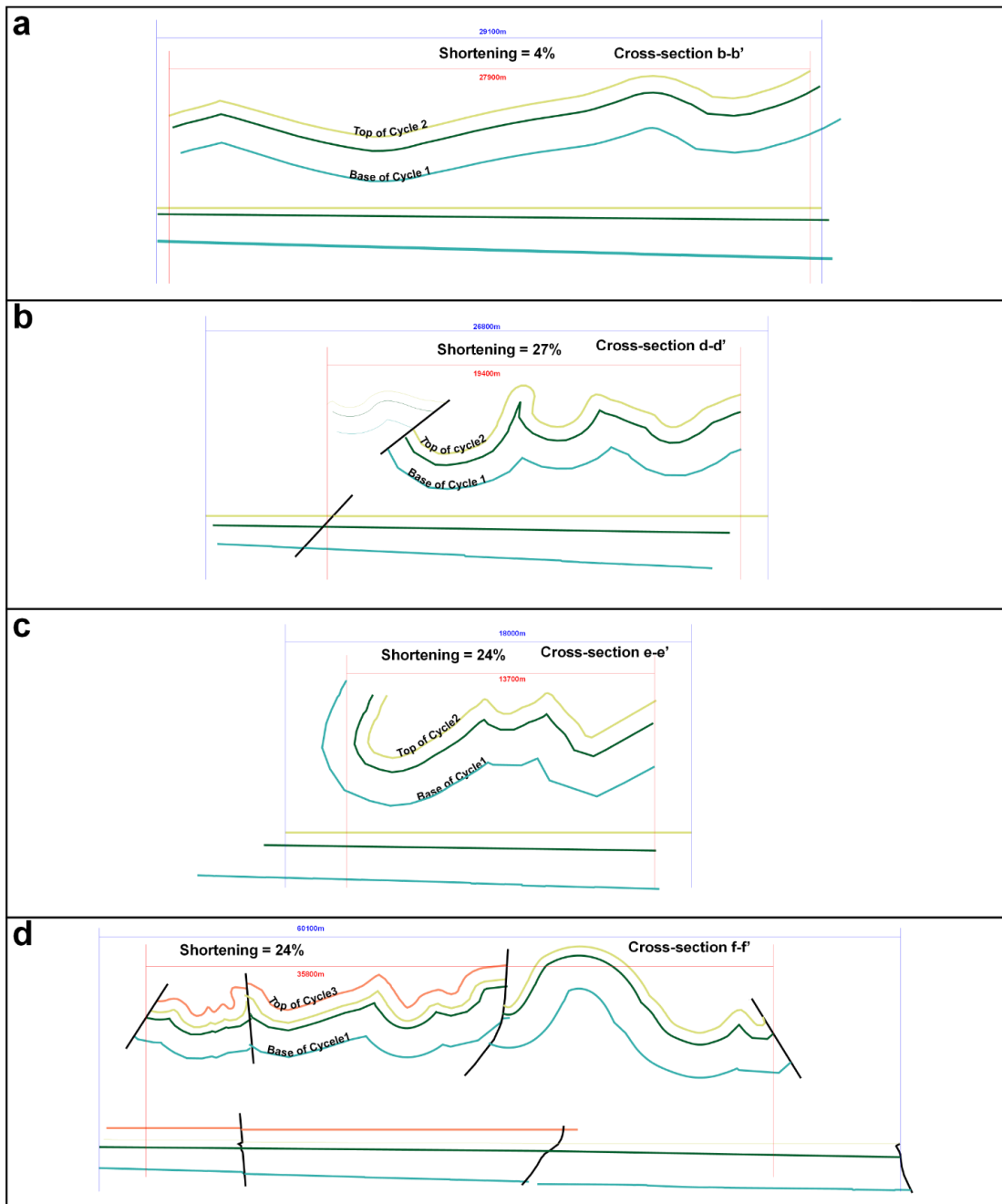


Figure 3.16: Shortening ratio calculations. Note that blue lines indicate initial (expected) length of the horizons and the red lines indicate the length of deformed horizons. a) Shortening calculation of cross-section line b-b'; (b) shortening calculation of cross-section line d-d'; (c) shortening calculation of cross-section line e-e'; (d) shortening calculation of cross-section line f-f'. See text for explanation.

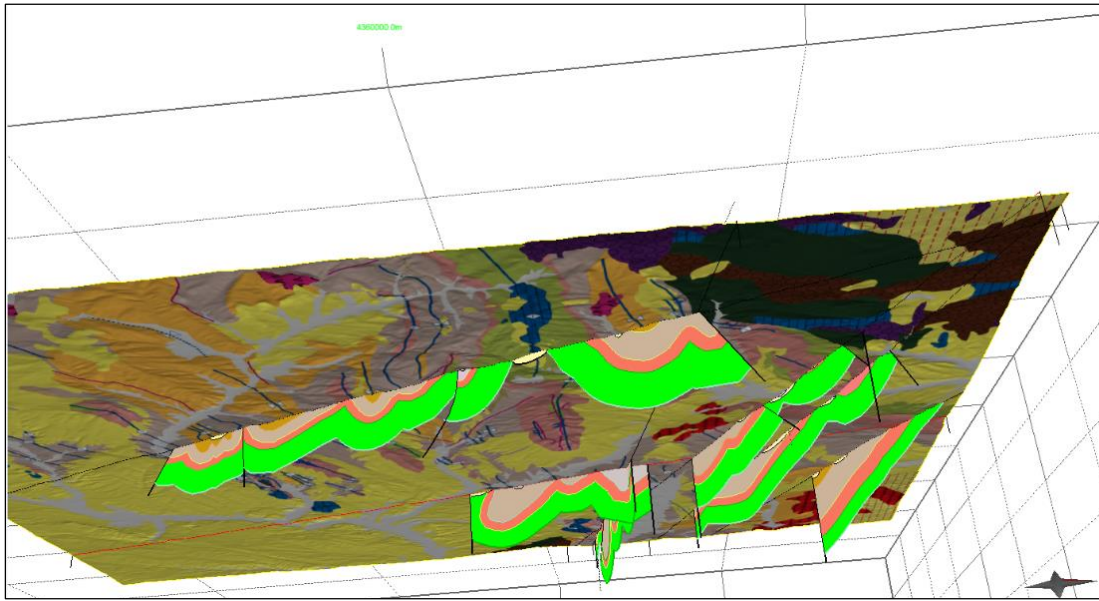


Figure 3.17: Fence diagram showing the correlation of the balanced cross-sections and increase in deformation towards eastern and southeastern part of the Haymana Basin.

CHAPTER 4

THERMO-CHRONOLOGY (AHe DATING)

An ideal chronological history of an individual magmatic grain in a sedimentary unit may represent crystallization, uplift, erosion, deposition, subsidence (re-heating) and secondary uplift (re-cooling). In this part of the study, last two stages were studied by using detrital AHe (apatite-helium) low temperature dating technique in order to date the subsidence and exhumation taken place in the basin and create a link with previously described deformation phases. In addition to the dating, the length of fission tracks in apatite grains are also measured to understand re-heating and re-cooling paths of the sedimentary units and the possible tectonic scenarios affecting these paths. Determining the potential of petroleum maturation might also be defined as another outcome of this study.

4.1 Method and Data

Methods comprises two different techniques. The first one is AHe dating and the second one, fission track length measurements.

4.1.1 AHe dating

Simply, thermo-chronology may be defined as dating a time span in which a mineral passes through an individual temperature which is called as closure temperature (T_c) (Dodson, 1973). By using some minerals with known closure temperatures, cooling (uplift) paths of them and also their host rocks can be understood.

The main idea behind AHe dating technique bases on the ratio between the decay of uranium and thorium, and the amount of helium product (U-Th/He); the age results of this method are, however, generally younger than formation or sedimentation ages and the reason for getting younger ages are explained by loss of helium products during

cooling in the temperatures higher than T_c . $\sim 68 \pm 5^\circ\text{C}$ is considered, based on step wise heating diffusion experiments, as closure temperature for apatite-helium systems (Farley, 2000).

The source of ^4He (α particles) are considered as the products of radioactive decay of ^{238}U , ^{235}U and ^{232}Th and the resultant products are determined as stable ^{206}Pb , ^{207}Pb and ^{208}Pb . The basic equation for AHe dating is determined by considering the present day atoms of ^4He , ^{238}U , ^{235}U and ^{232}Th , and their decay constants (λ s) by Farley, (2002), and Reiners, (2002); the equation assumes no initial ^4He in the apatite grain and is formulated as:

$$^4\text{He} = 8^{238}\text{U}(\exp(\lambda_{238}t) - 1) + 7^{235}\text{U}(\exp(\lambda_{235}t) - 1) + 6^{232}\text{Th}(\exp(\lambda_{232}t) - 1), \quad (1)$$

Where “ t ” is the helium age.

Loss or addition of extra helium to the system after T_c are the problematic side of the age calculations; these effects can, however, be corrected during picking apatite crystals and after calculations. During picking stage, apatite crystals with fluid or mineral inclusions are separated and the effects of helium addition is minimized. The α ejection is defined as the source of the helium loss and the reason for the ejection is explained by the travel distance (or stopping distance) of the α particles exceeding the wall of the apatite crystals (Farley *et al.*, 1996). On the other hand, implantation of α particles to the apatite crystals from another source as neighbor crystals is also possible but these effects are negligible during calculations due to common distribution of the crystals in the rock allowing large spacing (Farley *et al.*, 1996). Although the α decay of U and Th series have specific energy, the stopping distance is controlled by the characteristics of the materials (especially density and zoning) in which an α decay is occur (Zeigler, 1977). For apatites the stopping distance is determined as $\sim 20 \mu\text{m}$ by Farley *et al.* (1996). In order to minimize the effects of the α ejection during age calculations, requirement of a correction factor (F_T parameter) taking into account measured grain geometries and sizes are proposed by Farley *et al.* (1996). The F_T parameter is defined as surface to volume ratio of the crystals and the corrected ages are calculated by dividing the measured ages to F_T parameter. In order to determine F_T

parameter for each grain, the length and width of the apatite crystals must be measured and also the shapes of the crystal terminations must be noted as flat, parallel, pyramidal or irregular. In the study, F_T parameters of each grain are calculated by 10.2.2012 version of Flojt software using the criteria's of Ketcham *et al.* (2011) and Gautheron and Tassan-Got (2010).

4.1.1.1 Sampling Strategies and Separation

Rock samples are collected only from sedimentary units, the dated grains are therefore detrital. During sampling procedure, rock samples are taken from bedded fresh sandstone layers by considering the main structures, spatial and stratigraphic characteristics of the basin. In this sense, samples from the areas within the main structures exposed are not taken. Sampling locations are distributed in the basin to cover whole stratigraphy and 2D geometry of the basin.

Samples are separated so that one can pick individual apatite crystals. In the study, separation procedure is conducted in the fission track laboratories of the University of Glasgow. This procedure comprises six steps;

- (1) Crashing: Approximately 4kg sandstone samples are crashed until they get into an individual grain;
- (2) Sieving: Crashed samples are sieved to separate 200–500 micron grains from the bulk of grains because this interval corresponds to ideal apatite crystal size;
- (3) Shaking table: This table is used for separating pre-sieved material by considering density as fine, light, medium and heavy. As a result, the grains with $> \sim 2.5 \text{ gr/cm}^3$ density are separated for the next steps because the density of the apatite is 3.18 gr/cm^3 ;
- (4) Magnetic separator: Apatite together with sphene, andalusite, monzonite etc. respond the magnetic field in 1.2A and 5° inclined surface but some other heavy minerals as magnetite, garnet, olivine etc. respond magnetic field in lower amperes and higher slopes, therefore, magnetic separation is conducted by following a step-wise procedure;

- (5) Heavy liquid: Using heavy liquids is a density separation technique. In the study, LST (concentrated solution of lithium heteropolytungstates in water with 2.95g/mL density at 25°C) is used as heavy liquid;
- (6) Picking: Apatite crystals are picked from pre-separated bulk of heavy grains under the binocular microscope at magnifications up to 100x by avoiding possible fluid or mineral inclusions.

4.1.1.2 Age Calculation Procedure

Facilities of Scottish Universities Environmental Research Centre (SUERC) are used for age calculations.

Age calculation requires helium, uranium and thorium concentrations in an apatite grain. In order to measure these concentrations two steps are followed;

- (1) Measuring helium concentration: Picked apatite grains are loaded in a platinum capsule, then, loaded capsules are heated up to 950°C for 5 minutes by a pointed laser beam in order to liberate the helium gas. After heating, helium concentration is measured by a quadrupole mass spectrometer (Hiden HALF3F) but same grain is reheated in order to check possible unfree helium in the sample and this procedure is repeated until getting same results with the blank level of the system;
- (2) Measuring uranium and thorium concentrations: After helium concentration measurements, the capsules are dissolved in %5 HNO₃ and ~3ng ²³⁰Th and ²³⁵U added to the capsule and the concentrations are measured by inductively coupled plasma mass spectrometry (ICP-MS).

The equation given above (equation 1), AHe ages without F_t correction are calculated by using these concentrations.

4.2 Fission Track Lengths and Their Measurements

The lengths of the fission tracks occurred in the minerals with same composition at same temperature are almost similar, in an individual sample, these track lengths are ,

however, mostly variable and the reason for the length variation is explained by differential temperature history of the sample as shorter lengths at higher and longer lengths at lower temperatures (Green *et al.*, 1986; Laslett *et al.*, 1987; Duddy *et al.*, 1988; Green *et al.*, 1989; and Gallagher, 1995). Additionally, temperature also limits the variation of the track lengths, and this limitation zone for apatite is determined as $\sim 110^{\circ}\text{C} - \sim 80^{\circ}\text{C}$ temperature interval because in apatite crystals, tracks disappear after $\sim 110^{\circ}\text{C}$ and retain with almost fixed lengths below $\sim 80^{\circ}\text{C}$ due to its material properties (Wagner, 1968; Naeser and Faul, 1969; Naeser, 1981; Burbank and Anderson, 2001). This limitation zone is termed as partial annealing zone (PAZ) (Gleadow and Fitzgerald, 1987). The usage of statistical analyses of the track lengths together with the known stratigraphic and AHe ages of an individual sample is an important tool for determining the possible thermal history of a given sample and its host rock. In the study, these analyses are conducted by using 1.7.4.55 version of HeFTy software, by Apatite to Zircon Inc. (2011).

The lengths of the fission tracks are measured in the fission track laboratories of the University of Glasgow. Before measurements two steps are followed for sample preparation:

- (1) Mounting and polishing: Previously separated apatite grains are mounted to the lamellae and latterly polished;
- (2) Etching: Polished grains are etched in HNO_3 for 20 seconds at 21°C in order to make the tracks visible and enlarge. See Laslett *et al.* (1984), Watt and Durani (1985), Crowley *et al.* (1991) and Donelick *et al.* (2005) for further details about etching parameters.

After sample preparation, only confined tracks in the crystals polished parallel to the C-axis are measured because these tracks are entirely found in the crystals with both ends which *enable* to accurate measurements (Laslett *et al.*, 1982; Gleadow *et al.*, 1986; Donelick *et al.*, 2005). During measurements, the **length** and also width (Dpar) of the confined tracks are digitized under the high magnification but these measurements need to be corrected according to the inclination angle between the tracks and the C-axis of the crystals because the tracks perpendicular to the c-axis tend to be shorter

than parallel ones (Gleadow *et al.*, 1986). In the study, these corrections are conducted according to the criteria's determined by Ketcham *et al.* (2007).

4.3 AHe Age Results

Eleven thermo-chronology samples are collected from the coarse sandstone levels of the basinfill (see Figure 4.1 for locations); only five of them are, however, used for detrital AHe dating due to insufficient amount of high quality apatite grains without fluid or mineral inclusions.

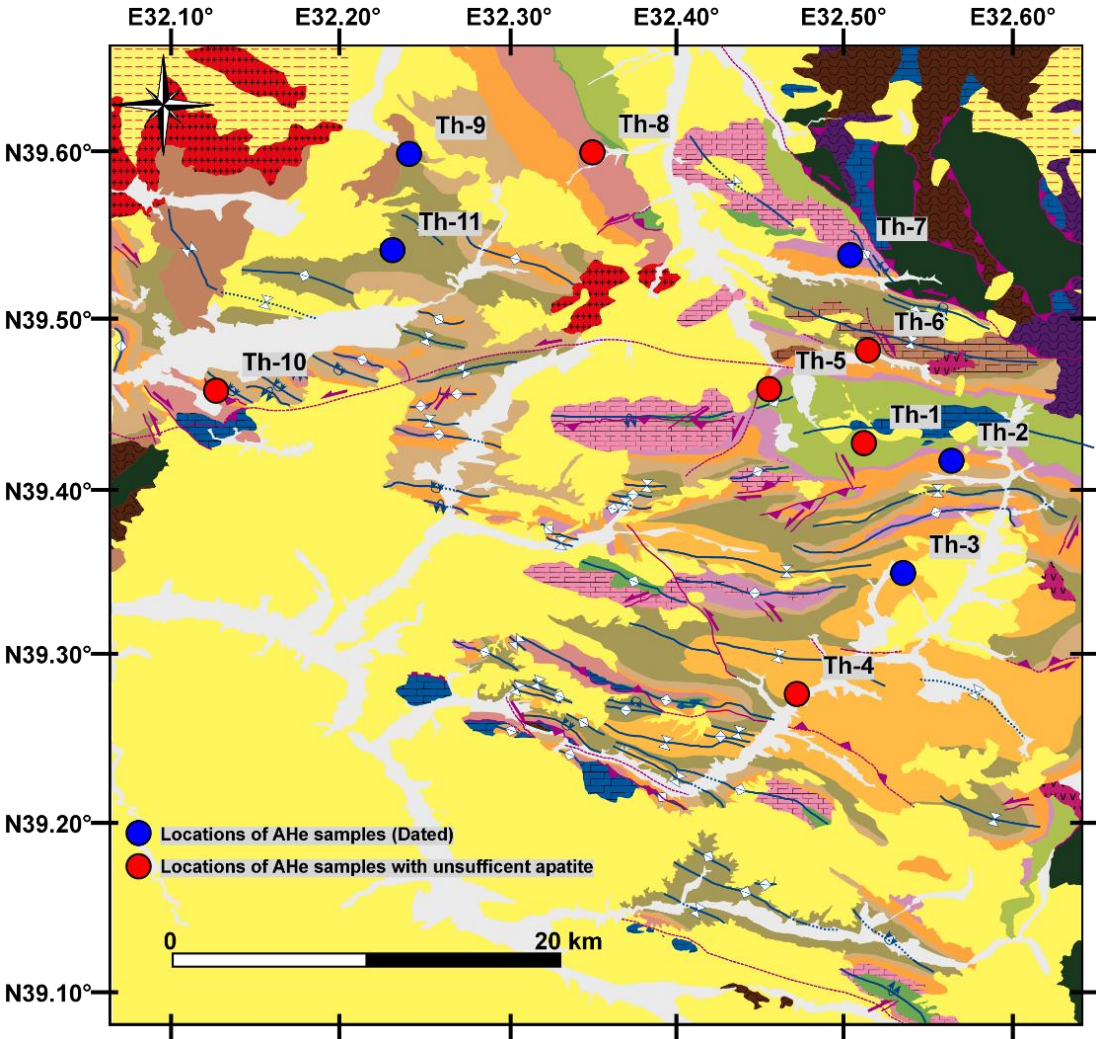


Figure 4.1: Geological map of the Haymana Basin, and locations of the thermo-chronology samples (see Figure 2.1 and 3.1 for legend).

During age calculations, 27 apatite grains separated from 5 samples are used (Figure 4.2). Additionally, three Durango grains with known AHe ages (32.0 ± 1.0 Ma) (Farley, 2002) are also analyzed in order to check the quality of the measurement; 29.77 ± 3 Ma average age is calculated. The results of the age calculations are shown in Table 4.1.


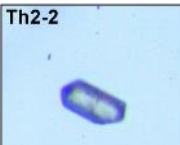

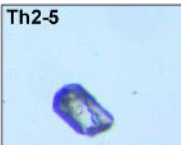
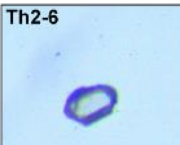

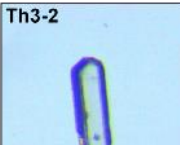
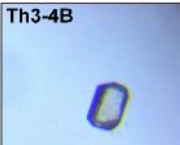
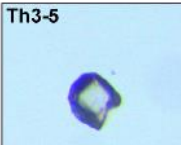
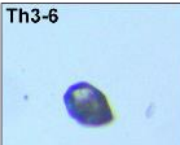
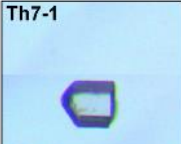





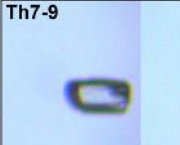
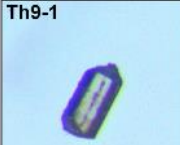
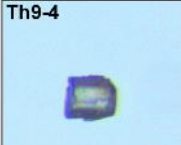



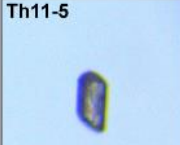
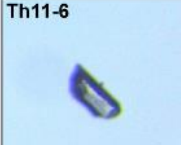
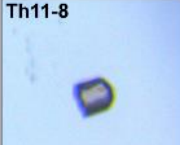


 D: 125 μ m L: 276 μ m FT: 0.855	 D: 099 μ m L: 201 μ m FT: 0.803	 D: 122 μ m L: 207 μ m FT: 0.862	 D: 115 μ m L: 192 μ m FT: 0.853	 D: 114 μ m L: 167 μ m FT: 0.845
 D: 105 μ m L: 138 μ m FT: 0.826	 D: 089 μ m L: 260 μ m FT: 0.835	 D: 089 μ m L: 126 μ m FT: 0.802	 D: 121 μ m L: 135 μ m FT: 0.839	 D: 099 μ m L: 130 μ m FT: 0.806
 D: 122 μ m L: 138 μ m FT: 0.785	 D: 117 μ m L: 154 μ m FT: 0.843	 D: 117 μ m L: 168 μ m FT: 0.848	 D: 103 μ m L: 177 μ m FT: 0.821	 D: 095 μ m L: 142 μ m FT: 0.817
 D: 120 μ m L: 144 μ m FT: 0.795	 D: 087 μ m L: 154 μ m FT: 0.812	 D: 106 μ m L: 214 μ m FT: 0.840	 D: 119 μ m L: 134 μ m FT: 0.836	 D: 070 μ m L: 132 μ m FT: 0.774
 D: 104 μ m L: 100 μ m FT: 0.800	 D: 077 μ m L: 121 μ m FT: 0.781	 D: 081 μ m L: 163 μ m FT: 0.792	 D: 069 μ m L: 161 μ m FT: 0.773	 D: 084 μ m L: 088 μ m FT: 0.750
 D: 058 μ m L: 168 μ m FT: 0.758	 D: 086 μ m L: 087 μ m FT: 0.766	Th : Grain ID D : Diameter of the grain L : Length of the grain FT : Calculated FT parameter		

Figure 4.2: Pictures of apatite grains used for AHe dating and their dimensions used for calculation of F_T correction parameter. See Figure 4.1 for sample locations.

During calculations two different methods are used for determining age of an individual sample which is represented by more than one apatite grain. The first method is arithmetic mean and the second one is pooling. Terminology of the pooled age is suggested by Vermeesch, (2008) for multi-grain age calculations instead of averaging ages. The slope of the best-fit line drawn by considering helium production rates (P) and helium abundances of individual grains, summed production rate of helium (P total) and total helium abundances of all measurements, are also considered in determining the pooled age of a sample. The graphics showing the pooled age calculations is given in Figure 4.3 and the data used in the graphics are shown in Table 4.1. In the study, pooled ages are considered as the age of the samples rather than average ages due to more realistic approach of the pooling method (Vermeesch, 2008).

Table 4.1: Results of AHe age calculations (see Figure 4.1 for sample locations

Sample ID	238U (mol)	235U (mol)	232Th (mol)	4He (mol)	P(He mol/ma)	P (total)	He mol (total)	AHe age (ma)	AHe age (Ft Corrected) (Ma)	Average AHe Age (Ma)	Pooled Age (Ma)	Pooled Age (Ft corrected) (Ma)
Th2-1	333.32	2.45	1533.29	33.24	0.89			37.40	43.80 +/- 4.4			
Th2-2	102.37	0.75	511.01	8.06	0.28	3.42	92.33	28.30	35.30 +/- 3.5	32.70 +/- 3.3	26.80	31.53 +/- 3.2
Th2-4	310.39	2.28	1794.47	19.72	0.93			21.10	24.50 +/- 2.4			
Th2-5	96.83	0.71	536.45	7.96	0.28			27.90	33.10 +/- 3.3			
Th2-6	266.37	1.96	2319.06	23.36	1.03			22.60	26.80 +/- 2.6			
Th3-1	144.33	1.06	1948.52	36.19	0.76			47.20	57.20 +/- 5.7			
Th3-2	89.75	0.66	747.02	7.98	0.34			23.60	28.30 +/- 2.8	28.70 +/- 2.9	29.18	35.29 +/- 3.5
Th3-4B	211.36	1.55	1037.61	6.59	0.58	2.19	60.29	11.30	14.10 +/- 1.4			
Th3-5	116.19	0.85	697.50	7.11	0.36			19.90	23.70 +/- 2.4			
Th3-6	55.14	0.41	259.06	2.42	0.15			16.30	20.20 +/- 2.0			
Th7-1	199.14	1.46	572.37	13.31	0.43			31.10	39.60 +/- 4.0			
Th7-2	142.93	1.05	594.08	10.58	0.36			29.30	34.70 +/- 3.4			
Th7-3	149.28	1.10	963.33	9.84	0.48			20.50	24.20 +/- 2.4			
Th7-5	172.03	1.26	822.29	9.04	0.47	2.78	65.59	19.40	23.60 +/- 2.4	29.01 +/- 2.9	23.56	28.84 +/- 2.9
Th7-6	169.93	1.25	446.29	8.53	0.35			24.20	29.60 +/- 3.0			
Th7-7	129.07	0.95	634.61	6.28	0.36			17.70	22.20 +/- 2.2			
Th7-9	124.57	0.91	594.50	8.00	0.34			23.70	29.20 +/- 2.9			
Th9-1	125.22	0.92	625.05	5.91	0.35			17.00	20.20 +/- 2.0	23.30 +/- 2.3	17.77	21.20 +/- 2.1
Th9-4	74.10	0.54	514.20	5.49	0.25	0.60	11.40	22.10	26.40 +/- 2.6			
Th11-2	39.25	0.29	572.57	2.50	0.22			11.30	14.70 +/- 1.5			
Th11-3	64.48	0.47	336.22	1.61	0.18			8.80	11.00 +/- 1.1			
Th11-4	75.42	0.55	346.06	3.72	0.20			18.60	24.40 +/- 2.4			
Th11-5	347.13	2.55	899.65	6.20	0.72			8.70	10.90 +/- 1.1	26.16 +/- 2.6	16.83	21.83 +/- 2.2
Th11-6	51.29	0.38	158.42	2.78	0.11	2.18	38.58	24.50	31.70 +/- 3.2			
Th11-8	105.55	0.78	220.99	5.31	0.20			26.30	35.00 +/- 3.5			
Th11-9	141.73	1.04	467.21	7.59	0.32			23.60	31.10 +/- 3.1			
Th11-10	48.32	0.35	558.95	8.86	0.23			38.70	50.50 +/- 5.5			
Du-4	1937.61	14.23	39177.39	438.83	14.13			31.00	31.00 +/- 3.1	29.77 +/- 3.0	29.46	29.46 +/- 2.9
Du-5	1874.68	13.77	42409.37	420.37	15.01	30.56	902.31	28.00	28.00 +/- 2.8			
Du-7	196.32	1.44	3935.12	43.12	1.42			30.30	30.30 +/- 3.0			

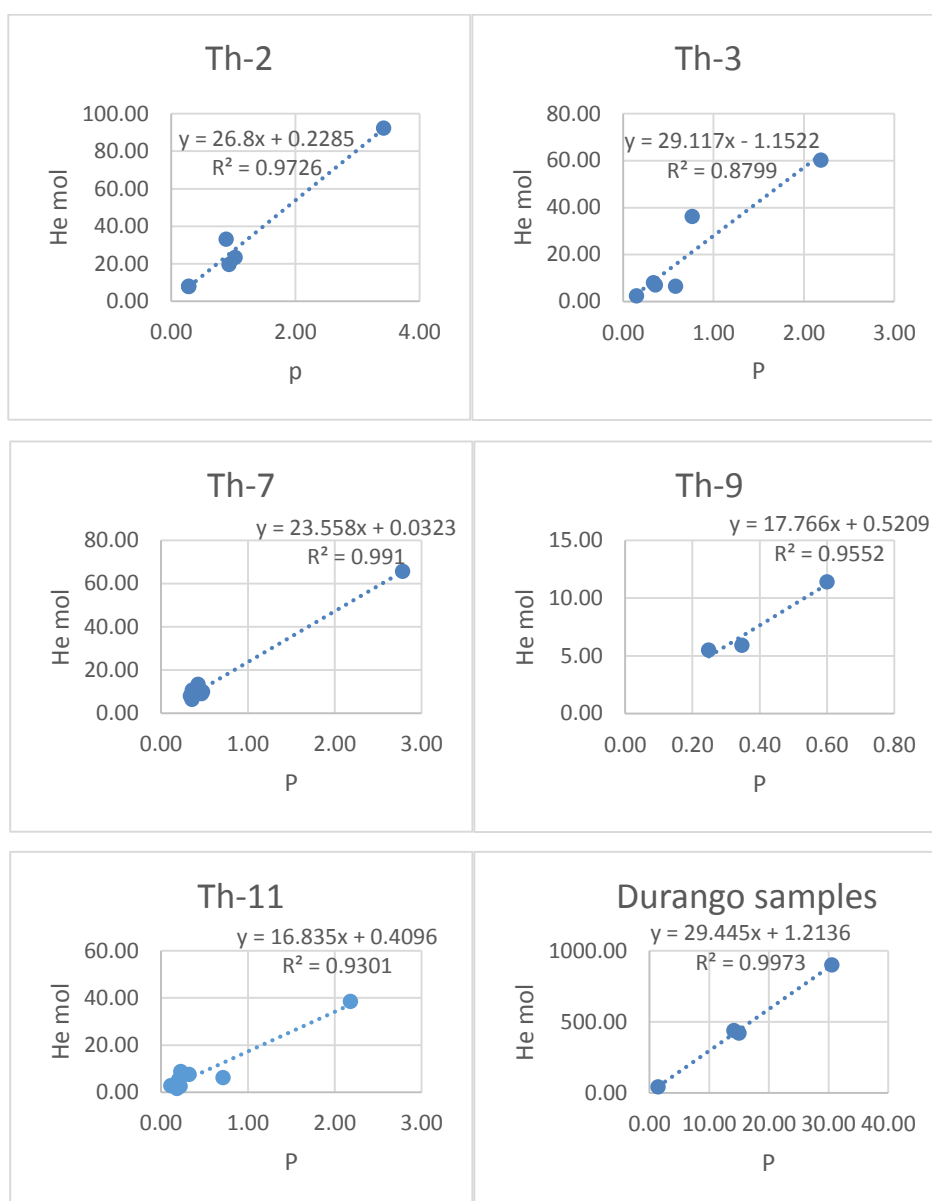


Figure 4.3: Graphics of pooled age calculations. Horizontal axes represent production rate (P) of He (for 1ma) and vertical axes, measured He concentrations (He mol) for each grain. Note that the highest values of P and He mol of each graphics represent the sum of P and He mol values of each sample.

The age variation within the grains of the same samples is explained by artefact of unobservable helium-rich fluid or mineral inclusions (for the grains with older ages with respect to average ages as Th2-1; Th3-1; Th7-1; and Th11-10) or artefact of high amount of α ejection, which cannot be calculated during Ft calculations due to possible inhomogeneous distribution of the α radiations (for the grains with younger ages with

respect to average ages as Th3-4b; Th11-2; Th11;3 and Th11-5). Although these unexpected ages seems to be outlier for the age calculations, they were added to pooled age calculations in order to get statistically more confident results because the statistical results of the pooled ages with the problematic grains show almost confident result with the coefficient of determination (R^2) higher than 0,9 (Figure 4.3).

4.3.1 Spatio-Temporal Characteristics of AHe Ages

Middle Eocene Beldede and Yamak formations, lower Eocene Yamak formation, middle Paleocene Kırkkavak, and lower Paleocene Yeşilyurt formation are the host rocks of the samples Th9, Th3, Th11, Th2, and Th7, respectively. By considering the temporal (stratigraphic) distribution of the samples, older AHe ages are expected for the samples of upper stratigraphic levels because they are thought to reach closure temperature ($\sim 70^\circ\text{C}$) earlier than these from lower level samples, during cooling processes. In the basin; this ideal AHe age distribution is, however, not observed in the processed samples because Th9 and Th11 yield youngest AHe ages (21.20 ± 2.1 Ma and 21.83 ± 2.2 Ma) are hosted by younger units (Figure 4.1). Therefore, spatial distribution of the samples must also be taken into account in addition to the temporal distribution. In this sense, the samples can spatio-temporally be grouped in two as the western group comprising Th9 and Th11 and the eastern group comprising samples Th3, Th2, and Th7 (Figure 4.4). In this case, an ideal AHe age distribution may be suggested for the eastern group because AHe ages get older towards upper stratigraphic levels; for the western group, such kind of suggestion cannot be proposed because AHe and stratigraphic ages of Th9 and Th11 are very close to each other.

AHe ages indicate that the basinfill units exposed in the eastern part of the basin started their cooling (uplift) histories at least sometime before 35.29 ± 3.5 Ma and lower stratigraphic levels exhumed at least sometime after 28.84 ± 2.9 Ma, whereas in the western part of the basin cooling started at least sometime before $\sim 21 \pm 2.1$ Ma and uplift of the lower stratigraphic levels must be younger than this age. These different uplift ages also indicate differential uplift histories for the western and eastern parts of the basin and a ~ 14 Ma older initiation of the uplift in the east (see location of Th9 and Th3 in Figure 4.4).

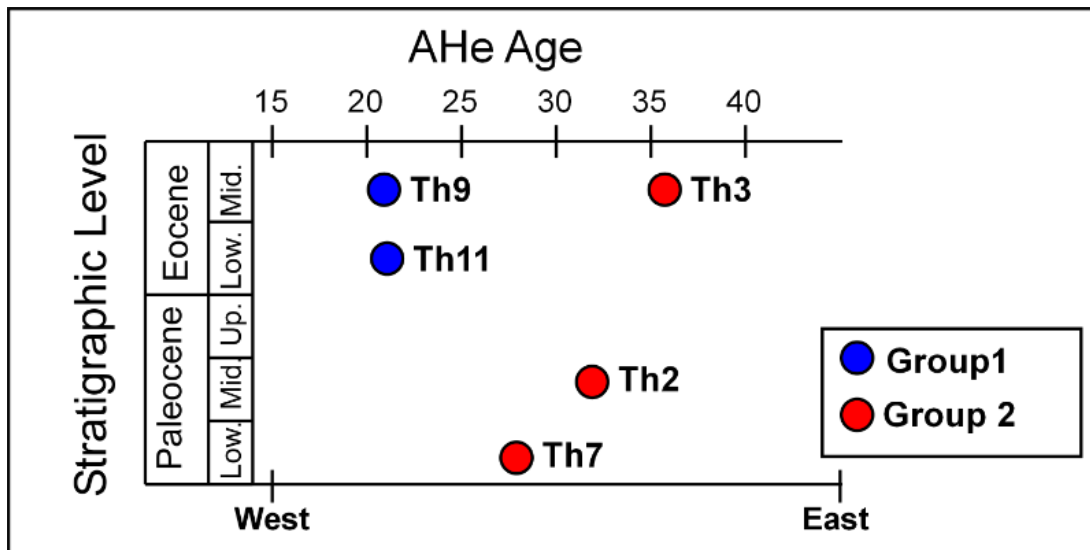


Figure 4.4: Graphic showing the relationship between the AHe ages and sedimentation ages. Note that AHe ages obtained from eastern part of the Haymana Basin is older than western part. AHe ages of the eastern part also decrease towards lower stratigraphic levels, which indicates gradual uplift in that part. See text for further explanation.

4.4 Results of Fission Track Length Measurements and Time-Temperature Modelling

All the samples are checked for fission track length measurements, but only two of them have statistically sufficient confined tracks. These samples are Th2 with 51 tracks from the eastern part of the basin and Th9 with 71 tracks from the western part of the basin. Histograms of the measured track lengths and related time-temperature (T-t) models of the samples are shown in Figure 4.5.

An ideal time-temperature history of an individual apatite grain with a AHe younger age than the stratigraphic age of the host unit can basically be summarized by three steps: (1) deposition at surface temperature; (2) subsidence and heating during the rocks experienced temperature higher than $\sim 70^{\circ}\text{C}$; (3) uplift and cooling and arrival to the surface temperature. In addition to these steps, (i) heating up to temperatures higher than the temperature interval of partial annealing zone, which can be signed by variation in track lengths (Gleadow *et al.*, 1986; Hurford, 1986; Moore *et al.*, 1986), and (ii) re-heating (or re-burial) after exhumation, which can be signed by existence

of the unconformities, must be considered for T-t models. Five time–temperature constraints are therefore determined for each sample; They include; (I) stratigraphic age of the unit and depositional temperature (SA), (ii) possible time interval for partial annealing zone in which the sample passed through (PPAZI), (iii) AHe ages (AHeI), possible time line of unconformities covering the host rocks of the samples and thickness of covering units (UT), and (iv) recent temperature of the region (RT). Intervals of the constraints are shown in Table 4.2.

Table 4.2: Constraints of time–temperature modellings.

	Th2				Th9			
	First Point		End Point		First Point		End Point	
	Time (Ma)	Temperature	Time (Ma)	Temperature	Time (Ma)	Temperature	Time (Ma)	Temperature
SA	62	18°C	56	35°C	48	18°C	41	35°C°
PPAZI	56	18°C	35	115°C	41	18°C	24	115°C
AHeI	35	18°C	26	75°C	24	18°C	18	75°C
UT	12	18°C	5	45°C	12	18°C	5	45°C
RT	5	18°C	0	35°C	5	18°C	0	35°C

SA: Stratigraphic age of the sample. PPAZI: Possible time interval for partial annealing zone. AHeI: AHe age. UT: Time line of unconformities. RT: Recent temperature.

During T–t model calculations, intervals of the constraints are taken as large as possible in order to test every possible T–t paths of the samples. During computing processes, 20000 possible T–t paths are tried for each sample, and acceptable, good, mean and best fit paths were exported (Figure 4.5).

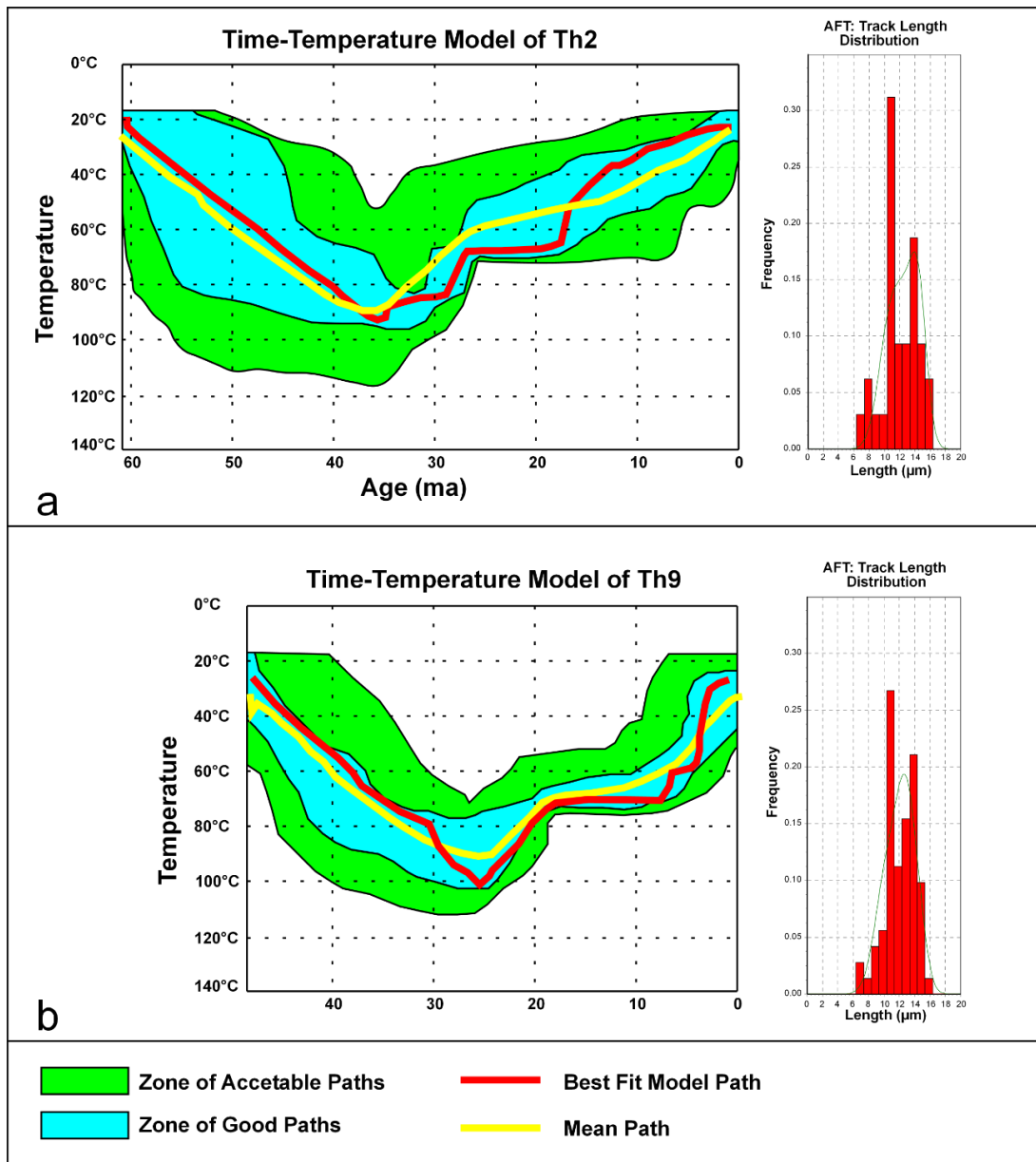


Figure 4.5: Time–temperature models of samples Th2 (a) and Th9 (b). Note that Th2 represents the eastern part of the Haymana Basin while Th9 represents western part of the basin. See text for explanations and Table 4.3 for uplift and subsidence rates calculated from these models.

4.4.1 Interpretation of Time–Temperature Models

T–t history of the samples Th2 and Th9 are represented by four time intervals; (1) depositional age (~60 Ma) to ~35 Ma for Th2, and depositional age (~48 Ma) to ~24

Ma for Th9, (2) ~35 Ma to ~28 Ma for Th2 and ~24 Ma to ~18 Ma for Th9, (3) ~28 Ma to ~18 Ma for Th2 and ~18 Ma to ~8 Ma for Th9, and lastly (4) ~18 Ma to recent for Th2 and ~8 Ma to recent for Th9. The first intervals represents the gradual burial of the samples whereas the others, the differential uplift histories. The average burial (subsidence) and uplift rates of the intervals are calculated according to average 1°C temperature differences in 33 m (normal geothermal gradient) and the mean T–t paths of the samples. The results of the calculations are shown in Table 4.3.

Table 4.3: Subsidence and uplift rate calculations.

	Th2				Th9			
	Int.1	Int.2	Int.3	Int.4	Int.1	Int.2	Int.3	Int.4
TD (ma)	~25	~7	~10	~18	~24	~6	~10	~8
tD (°C)	~70	~30	~10	~30	~60	~18	~12	~30
PDD (m)	2310	990	330	990	1980	594	396	990
Average rate m/kyr	9.24	14.1	3.3	5.5	8.25	9.9	3.96	12.38
TD: Time differences, tD: Temperature differences, PDD: Possible depth differences								

According to the results of T–t models and subsidence/uplift rate calculations, it might be suggested that;

- (1) There are at least ~11 Ma differences (~35 Ma and ~24 Ma) between the initiations of the uplift of the samples. Although this time interval is not equal to 14 Ma differences as determined for the western and eastern parts of the basin by AHe results, it may be proposed that the results of the T–t models are compatible with the AHe ages because the differences in stratigraphic levels of the Th2 and Th9 may result in narrower time interval;
- (2) The reason for the rapid uplift in the second time intervals of the T–t models may be attributed to the activity of the thrust faults and the second deformation phase;
- (3) Miocene deposition may result in dramatic decrease in uplift rate during third time interval of the T–t models. It may also be inferred that the effects of the tectonic activity was higher than sedimentation rate in that time interval because T–t models do not indicate any re-heating signature in the samples;

- (4) Spatial differentiation in tectonic regime during Neogene may result in relatively higher uplift rates in the western part of the basin during fourth time interval of the T-t models.

CHAPTER 5

DISCUSSION

Tectono–stratigraphic evolution of the Haymana Basin will be discussed by considering the information given in Chapters 2, 3 and 4. The tectonic position of the basin in a spatio–temporal concept will also be discussed; the evolutionary scenarios of the other sedimentary basins and non-sedimentary units discussed in the first chapter form the base of this discussion.

5.1 Summary of Stratigraphic, Structural and Thermal Characteristics of the Haymana Basin

Previously discussed stratigraphic, structural and thermal characteristics of the basin will be summarized.

5.1.1 Characteristics of the Stratigraphical Data

The initiation of the northward subduction of the Neotethyan oceanic crust beneath the Central Pontides around the Haymana region is considered as post–Cenomanian due to the existence of Turonian to Paleocene (mainly Campanian) arc-related magmatism in the Central Pontides, and late Cretaceous to middle Paleocene back–arc or fore–arc setting-related sequences in the north and south of the Central Pontides, respectively (see also Chapter 1). It has been stated in Chapter 2, that the basement of the Haymana basin is represented by imbricated units of the southernmost parts of the central Pontides and the oldest basinfill unit covering the basement is Santonian to late Campanian in age.

As presented in Chapter 2, basinfill of the Haymana Basin is divided, based on their facies characteristics, into four stratigraphic cycles. The first cycle comprises Santonian to late Campanian Haymana and Beyobaşı formations. Lower–Middle

Paleocene Kartal, Çaldağ and Yeşilyurt formations from the second cycle. Upper Paleocene–lower Eocene Kırkkavak, Iğnıkdere and Eskipolatlı formations belong to the third cycle. Lastly, lower to middle Eocene Beldede, Çayraz and Yamak formations from the rock units of the youngest cycle. Lateral and vertical correlation of these units and the cycles is the main concern of the following part of this section.

The sharp (onlap) contact between the Haymana formation and the imbricated complex basement and fragments of Haymana formations found in this complex in the southernmost margin of the basin indicates that the deposition of the Haymana formation and imbrication in the basement were coeval at least in the southernmost part of the basin. Haymana formation was mainly fed from northerly derived clastics (mainly mélangé related) and deposited in a slope or slope front environment under the influences of fore–arc settings whereas the Beyobası formation was deposited in shallower environment as a time equivalent of the Haymana formation. Gradual shallowing and differential uplift in the basin are indicated by vertical gradation of the Haymana formation to the reefal Çaldağ formation or its time and distal equivalent of the calci-turbiditic Yeşilyurt formation. Also, the existence of the detritus of the Çaldağ formation within the younger basinfill units supports the local uplift histories in the region. The reason for uplift in the basin during the deposition of these units may be explained by growth of subduction complex (accretionary wedge) beneath the basin (sensu Dickinson and Seely, 1979). The Kartal formation was deposited as proximal and time equivalent of the Çaldağ and Yeşilyurt formations. The units of the second cycle grade laterally and vertically into the units of third cycle which are Kırkkavak, Iğnıkdere and Eskipolatlı formations. Proximal part of the cycle 3 is represented by Kırkkavak formation due to its association with the continental clastics, and reefal origin whereas Iğnıkdere and Eskipolatlı formations represent the distal parts with their turbidity currents related deeper marine deposits. Existence of a local unconformity between the second and third cycle units, which is defined in the northern margin of the study area (proximal), observation of this relationship as also gradational in distal parts of the basin, and also the detritus of the second cycle found in the third cycle support formation of syn-depositional unconformities in the proximal, which might be considered as the result of coupling of sedimentation and

tectonic activity in the region. Also, the reason for wide distribution (northernmost to southernmost margins of the basin) of the shallow-marine and continental deposits of the second and third cycles may be explained by this tectonic activity and the Paleocene–Eocene thermal maximum event. The fourth cycle comprises continental clastic rocks of the Beldede formation, sequence of nummulitic bank deposits of the Çayraz formation, and basinal turbiditic sequences of the Yamak formation. Although any contact relationship between these units is exposed in the study area, it is thought that these units are laterally gradational because of their almost same depositional ages. The transition from third to fourth cycle may be defined as same the one observed between second and third cycles, so coupling of tectonic and sedimentation may also be suggested for that time interval. In addition to these inferences, it is also possible suggest that a regional uplift or progressive shallowing and subsequent erosion took place in the basin. The reason for this interpretation is explained by gradual shallowing of deep-marine deposits of the Eskipolatlı and the Yamak formations, limited outcrop distribution of continental and shallow-marine deposits of fourth cycle (located only northern part of the study area) and lack of younger age marine deposits in the basin. 3D geometry of the Çayraz formation and the locations of the Beldede formation at the proximal (north) and the Yamak formation at the distal (south) suggest a source area (continent) at the north/northwest. The existence of bi-directional paleo-currents noted from the Yamak formation and very coarse sub-angular ophiolitic pebbles (<30 cm in diameter) in the upper levels of the formation, however, indicate that unit may also be fed from E–SE located ophiolitic source, besides the northerly located source (Figure 5.1).

Distribution of outcrops of the cycles mainly shows that: (1) units of the first three cycle are getting thicker in the north and thinner towards south (this observation is also supported by balanced cross-sections given in Chapter 3; (2) in spite of the existence of smaller outcrops of the first cycle in the south, they cover large areas in the north whereas younger cycles dominate the southern part of the study area and (3) units of the third cycle dominate study area whereas the fourth cycle is only exposed at the core of synclines mainly at the eastern part of the study area (Figure 5.1). These observations indicate; (i) wedge-like distribution of the units, (ii) general younging

direction of the basin infill (N to S) (Figure 5.1), and (iii) main erosional period and the possibility of easterly located source, respectively.

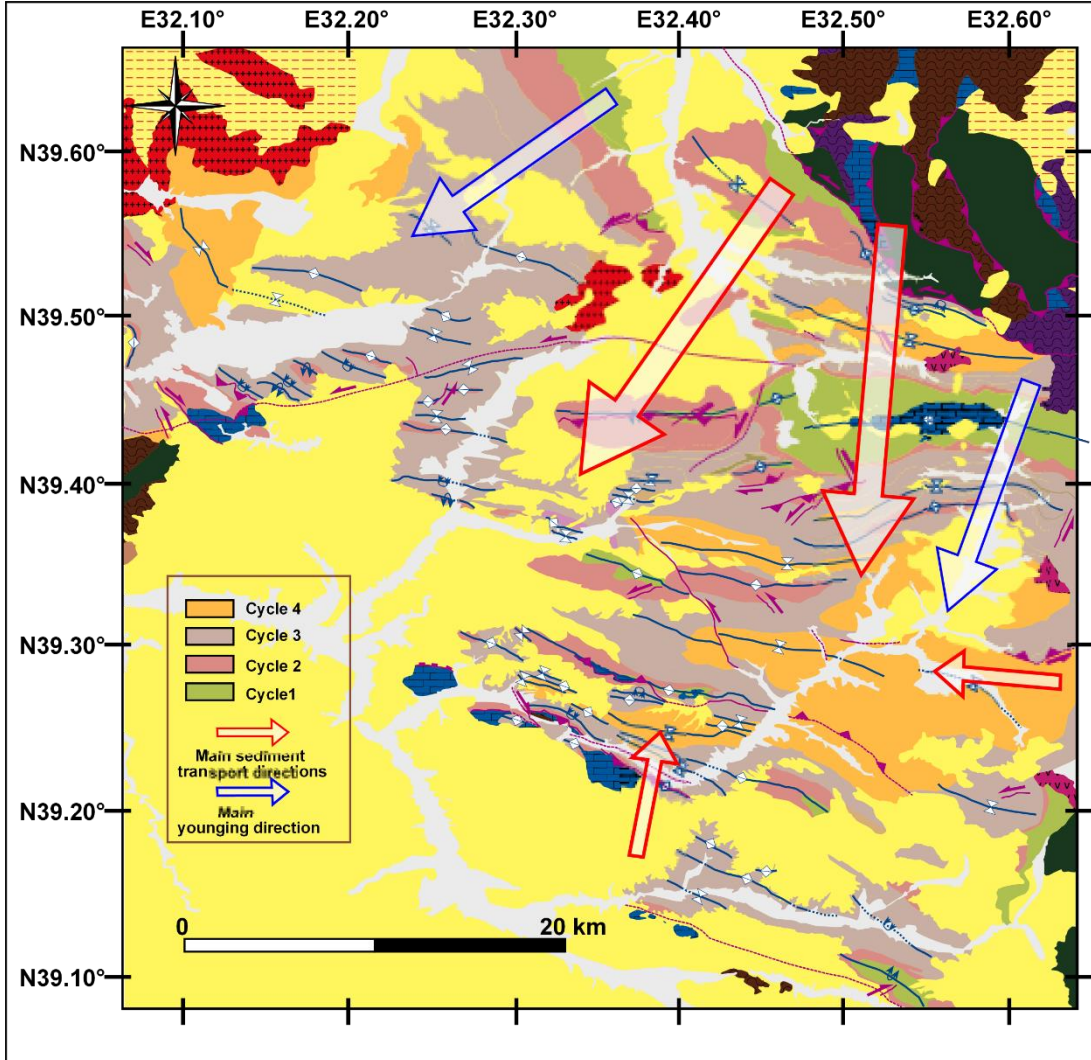


Figure 5.1: Geological map showing distribution of stratigraphic cycles and main younging and sediment transport directions (see Figure 2.1 and 3.1 for legend). Note: Sediment transport directions are representative and mainly based on Çetin *et al.* (1986) and Çiner *et al.* (1996).

Depositional period of the first cycle mainly corresponds to back-arc sequences of northern and intra-to fore-arc sequences of southern Pontides, fore-arc or intra-oceanic fore-arc settings related deposits of the Kırıkkale-Bala and Çankırı basins, extensional setting-related deposits of the Ayhan-Büyükkişla Basin and extensional or fore-arc settings related sequences of the Tuzgölü and the Ulukışla basins. In contrast to

complex equivalents of the first cycle, the depositional period of the rest of the cycles mainly correspond to compressional and collision settings-related sequences of the Central Pontides and Central Anatolian basins (see section on ‘Cretaceous–Paleogene basins around the Haymana Basin’ in Chapter 1 for further explanations).

By considering the correlation of the Haymana Basin with the surrounding basins, the imbricated Pontide basement, lack of volcano-sedimentary sequences, lateral-vertical relationships of the stratigraphical cycles, wedge-like distribution of the units, N to S younging direction, the existence of local unconformities between the cycles at the northern margin of the basin, and the general coarsening-upward trends in the units of third and fourth cycles, it is possible to suggest that; (1) the Haymana basin started its evolution in fore-arc setting during which the units of the first cycle was deposited, (2) growth of accretionary prisms gave way to differential uplift histories in the basin and deposition of the shallow-marine units of the second and third cycles towards southern margin of the basin and (3) the units of the last two cycles were deposited in compressional settings.

5.1.2 Characteristics of the Structural Data and Paleostress Results

Haymana Basin is regionally bounded by Pontides in the north, Kırşehir Block in the east and Tauride Anatolide Platform in the south (Figure 1.1). Relative movements of these blocks during the closure of Neotethys, collision taken place within the blocks, and the post-collisional tectonic activity in the region are the main reasons for the deformation recorded in the upper Cretaceous to middle Eocene deposits of the Haymana Basin.

Temporally, deformation history of the basin is explained by three different phases as discussed in Chapter 3. The first phase is represented by N–S extension and signed by fault plane measurements collected from the pre–middle Paleocene units. This deformation phase corresponds to the deposition of the first two stratigraphic cycles and may be result of extensional faulting during fore-arc basin development due to the location of the trench and angle of the slap which allow extension (or thinning) perpendicular to the basin margins in the fore-arc region. The second phase is the main

deformation phase that shape the Haymana Basin and is represented by N–S compressional regime. This phase is compensated by coevally developed E–W-and NW–SE-trending thrusts/reverse faults and folds. In addition to the these pure compressional structures, almost N–S-trending extensional structures together with NW–SE-trending right-lateral and NE–SW-trending left-lateral strike-slip faults form the major structures of this phase. The association of these structures is explained by left-lateral Riedel shear diagram developed by a $\sim 015^\circ\text{N}$ -oriented maximum principle stress direction (σ_1). Paleostress analyses of fault-slip data from pre–late Eocene units indicating N–S pure compressional, E–W pure extensional and N–S transpressive stress orientations supports this assertion. The last phase defines the Neogene deformation of the basin and it is represented by extensional and transcurrent tectonics.

By considering the dramatic increase in shortening amounts towards eastern part of the basin (from 3% to 24%), calculated along balanced cross-sections, and changing in the trends of the structures as being E–W-directed in the east and becoming NW–SE-directed in the west and northwest parts of the basin, structurally the Haymana Basin can be divided into two segments and the boundary of these segments can be determined by SS4 (see Figure 3.1 for location) strike-slip fault. The reason for the structural segmentation is explained by the orientations, movements and effective zones of the basin-bounding Dereköy and İner thrust faults which allowed differentiation in the trends of the structures and shortening amounts.

In a regional concept, it is possible to suggest that the folds and the structures located in the Kırıkkale-Bala, Tuzgölü and Central Pontide basins follow the outline of the Kırşehir block (Figure 5.2). This indicates that the trend and the characteristics of the structures located on both Central Pontides and Taurides are affected by the north and northwest movement and indentation of the Kırşehir Block into the Pontides and Taurides (Kaymakcı, 2000; and Lefebvre *et al.*, 2013). Although the Haymana Basin seems not to be affected from this indentation, the Dereköy thrust with left-lateral sense appear to be continuation of the transform fault defined by Lefebvre *et al.* (2013) that dissects the Kırşehir block (Hirfanlar-Hacıbektas fault zone, see Figure 5.2 for location). In this sense, it is possible suggest that deformation in the Haymana Basin

was not only controlled by relative movements of the Pontides and Taurides, it was also affected by the indentation of the Kırşehir Block. The timing of the indentation of the Kırşehir Block was determined as post–Paleocene (Özkaptan, 2015, studied, vertical block rotations in the central Pontides, at the western margin of the Kırşehir Block and the Haymana basin; he proposes differential vertical block rotations for the western and eastern structural segments of the Haymana basin as $\sim 35^\circ$ and $\sim 75^\circ$ counterclockwise, respectively). Briefly, it may be proposed that deformation in the Haymana Basin is controlled by closure of the Neotethys Ocean between Pontides and Taurides at least until the end of Paleocene. The collision between these continents and the indentation of the Kırşehir Block that gave way to development of fold and thrust belt, and differentiation in the trends of the structures by vertical block rotations.

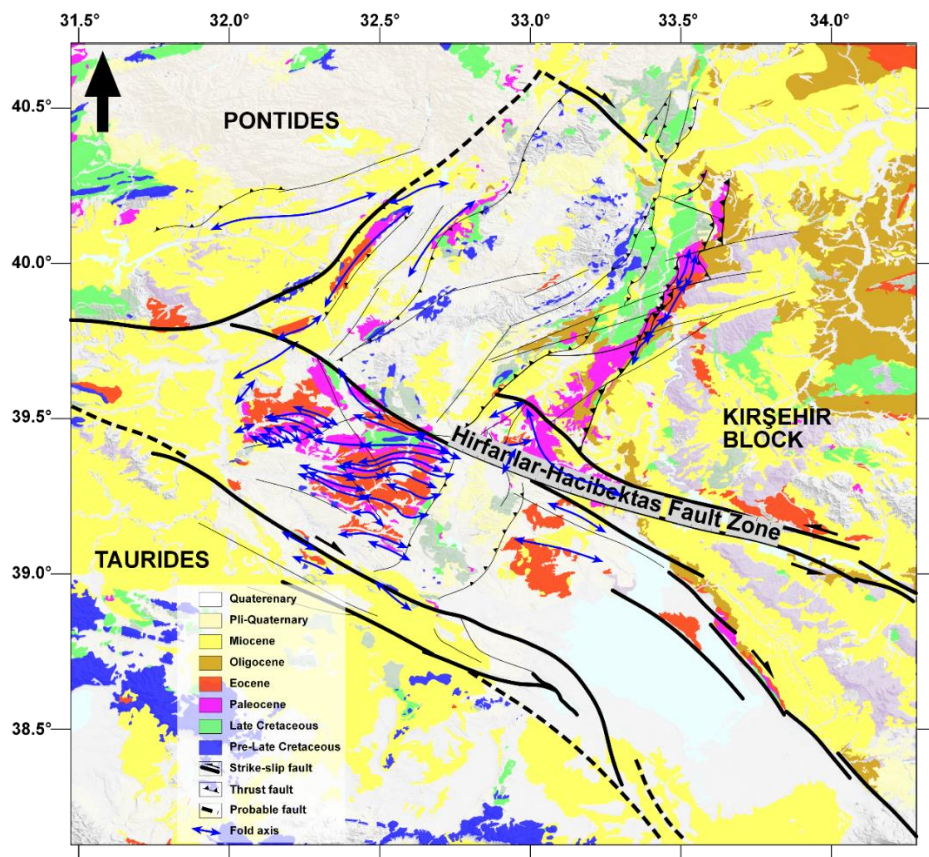


Figure 5.2: Geological map of Central Anatolia showing the elongation of the main structures. Note that orientations of the structures follows the outline of the Kırşehir Block, and westward extension of Hirfanlar-Hacıbektaş fault zone corresponds to Dereköy thrust in the Haymana Basin.

5.1.3 Characteristics of Thermo-Chronological Data

AHe ages suggest that initiation of the uplift in eastern structural segment of the basin must be older than 35.29 ± 3.5 Ma whereas in the western segment, it must be older than 21 ± 2.1 Ma. This implies that the main uplift events in the basin occurred in accordance with the structural development of the basin. Therefore, it is possible to propose that the movement and related effective zone of the Dereköy basin-bounding thrust also resulted in the older uplift ages in the eastern structural segment of the basin by being relatively more active in the east during relatively older time intervals. As discussed in Chapter 4, thermal models of samples Th2 and Th9 are comfortable with the AHe age results. Additionally, thermal models also suggest that the maximum uplift rates for the eastern segment of the basin is 14.1 m/kyr between 35 to 28 Ma, and 9.9 m/kyr between 25 to 19 Ma for the western segment. These time intervals correspond to the main vertical block rotation events and also the deformation phase2 determined in Chapter3.

In a regional sense, it may be suggested that the main uplift events in the Haymana Basin was mainly affected by the collision of the Pontides and Taurides and also the indentation of the Kırşehir Block because the post-middle Paleocene initiation and pre– early Miocene termination of these events (Kaymakcı *et al.* 2000 and 2009) have resulted in the peak uplifts events in the Haymana region during late Eocene to early Miocene time interval.

5.2 Spatio-Temporal Association of Neotethyan Central Pontide and Central Anatolian Basins, and the Haymana Basin

Progressive closure of Neotethys and collision along İAESZ and ITSZ are the main controlling structural features to understand the linkage between Neotethyan Central Pontide and Central Anatolian basins and the Haymana Basin. In order to better understand this linkage, spatial and temporal discriminations must be taken into account. For this purpose the basins were spatially discriminated by considering subductions of Neotethys and debatable ITO beneath the Pontides and Kırşehir Block, respectively. As a result, basins located on the central Pontides are grouped as northern

and southern Pontide basins by considering the possible location of the subduction-related arc magmatics. Central Anatolian basins were classified as the basins developed between Kırşehir Block and Taurides, and just on Kırşehir Block. For temporal classifications, commencement of subduction (closure) and collisional stages are considered as the basic criteria. In respect to this spatio-temporal classification criteria: (1) the position of the Haymana Basin with respect to subduction along İAESZ and related basin evolutions; (2) the position of the Haymana Basin with respect to subduction along ITO and related basin developments; (3) the position of the Haymana Basin with respect to collision between Pontides and Kırşehir Block or Taurides and related basin evolutions, and finally 4) the position of the Haymana Basin with respect to collision between Kırşehir Block and Taurides and related basin evolutions form the subgroups of this section.

Tectono-stratigraphic columnar sections and correlations of the major Tertiary basins of which evolution histories related to İAESZ and ITO are illustrated in Figure 5.3. A conceptual model showing the possible tectonic positions of the Haymana Basin with respect to İAESZ and ITO is given in Figure 5.4.

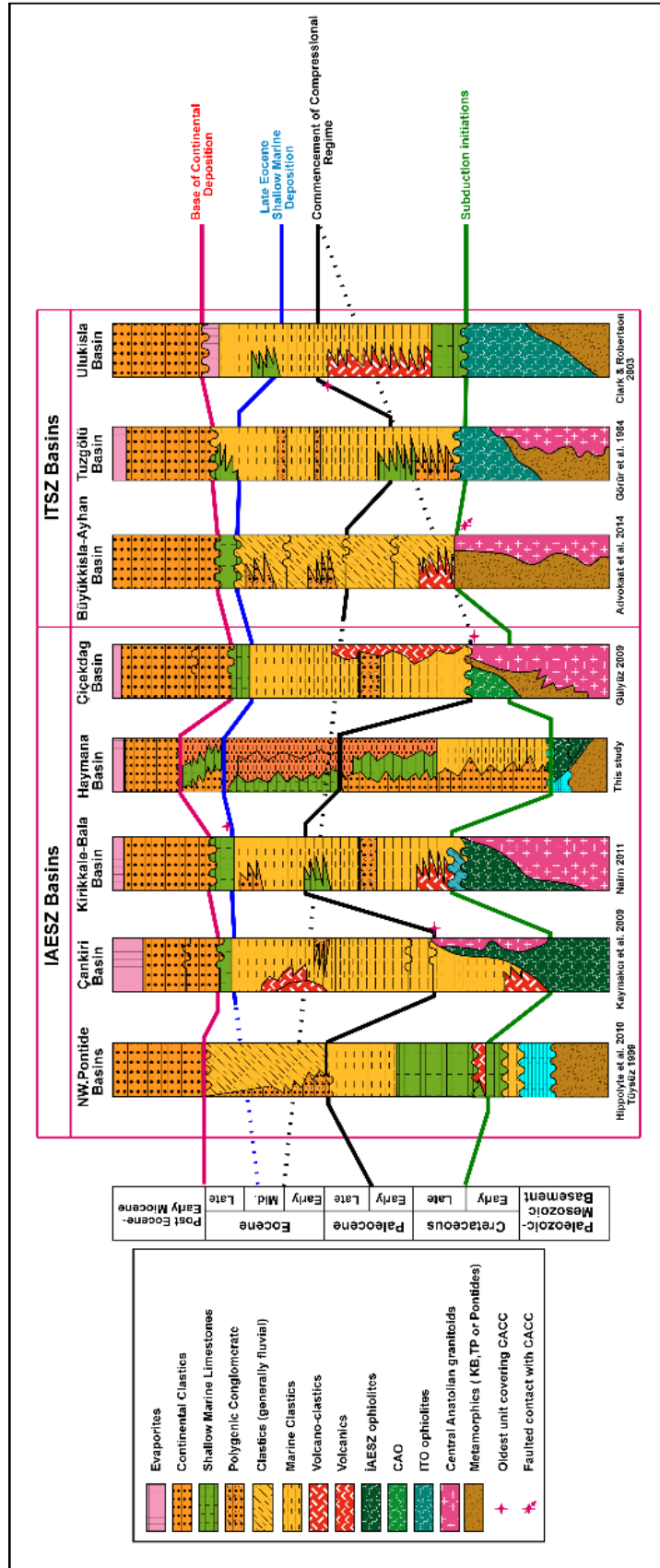


Figure 5.3: Correlation of IAESZ and ITSZ related basins and main tectonic events in these basins

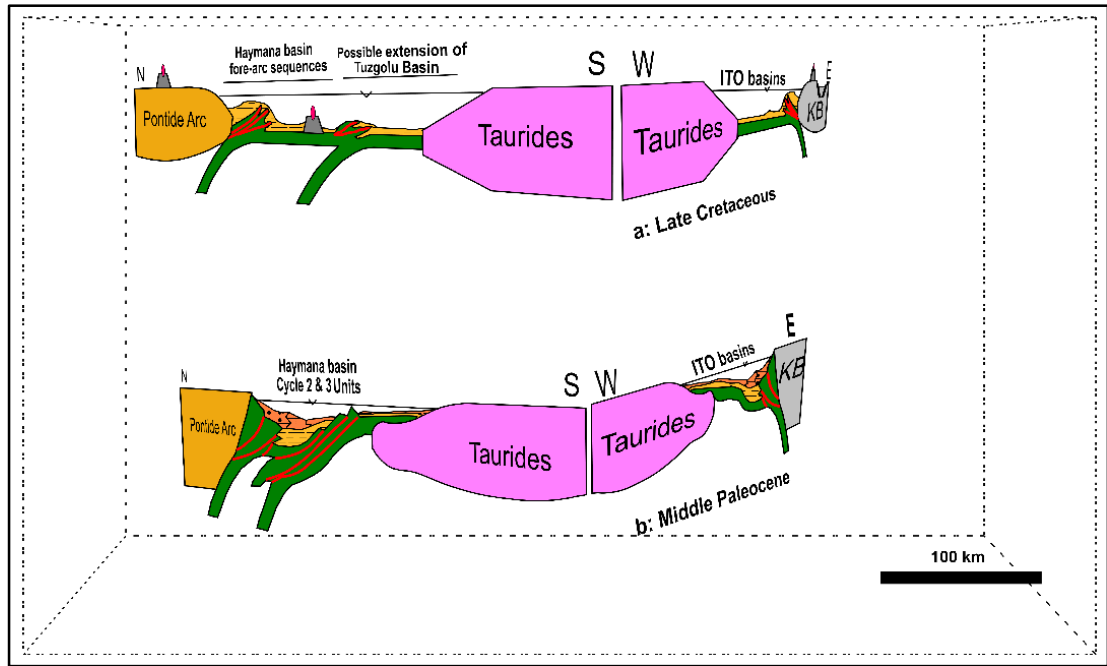


Figure 5.4: Conceptual model showing tectonic position of the Haymana Basin during late Cretaceous (a) and middle Paleocene (b) with respect to İAESZ and ITSZ.

5.2.1 The Position of the Haymana Basin with respect to Subduction Along İAESZ

In the Central Pontides, inceptions of; (1) an intra oceanic subduction, (2) an ocean to continent subduction, (3) continent to continent collision, and (4) an ocean to continent subduction for the closure of Neotethys is determined as; (1) Middle–Late Jurassic (179–166,9 Ma) (Dilek and Thy, 2006; Meijers *et al.*, 2010; Çelik *et al.*, 2011; Okay *et al.*, 2013) by dating amphibolites, plagiogranites and arc volcanics in the northernmost Pontides and also in the Crimea; (2) Late Valanginian–Early Barremian (Tüysüz and Tekin, 2007) by dating radiolarites from the matrix of a mélangé located in the central Pontides; (3) Albian (107 Ma) (Okay *et al.*, 2006; 2013) by dating eclogites or blueschists and (4) late Cretaceous (Tüysüz *et al.*, 1995; Kaymakçı 2000, Koçyiğit *et al.*, 2003; Rice *et al.*, 2006; 2009) by dating arc related magmatics or volcano-sedimentary sequences. These successively occurred tectonic events roughly within 70 Ma may be explained by three different subduction zone development or

southward retreat of a single slab, determining the characteristics of these tectonic events except from the last one was, however, considered as out of scope of the study because their timing and sedimentary records are not correlative with the post-Late Cretaceous basinfill and deformation history of the Haymana Basin. Pre-late Cretaceous units and late Cretaceous subduction were therefore thought as the basement of the study and initiation of the subduction along southern margin of the Pontides, respectively.

Turonian to Paleocene (mainly Campanian) age arc-related intrusives and coeval volcano-sedimentary, back-arc, and fore-arc sequences of the Pontides are considered as the product of this subduction. Spatial distribution of these sequences is defined by the location of the arc-related intrusives and volcanics (see ‘Pontide arc’ section of Chapter 1, for further explanations). Temporally, it is possible to suggest that Turonian to Campanian deposits of both back-arc or fore-arc regions unconformably cover lower Cretaceous platform sequences, and/or accreted ophiolitic mélanges of İAESZ (Görür, 1997; Koçyiğit, 1991; 2003; Rojay, 1991; 1995; Rojay and Süzen, 1997; Tüysüz *et al.*, 1999; Kaymakcı *et al.*, 2009; Nairn, 2011). This relationship may also be proposed for the Haymana Basin and the deposits of the first cycle units. Therefore, in addition to the stratigraphic characteristics of the first cycle units and the Pontide basement of the basin, this regional concept also suggests that the Haymana Basin started its evolution in the southernmost tip of the Pontides as a fore-arc basin. Additionally, the presence of an SSZ-type ophiolites proposed by Önen (2003), and Çelik and Delaloye (2006) and intra-oceanic subduction zone proposed by (Rojay, 2013) in the south of the Haymana Basin must be taken into account because this event may result in N–S extension as deformation phase 1 (see Chapter 3).

5.2.2 The Position of the Haymana Basin with respect to Subduction along ITO

It is believed that debatable Inner Tauride Ocean is located between Tauride Platform and Kırşehir Block (Görür *et al.*, 1984). Two different suggestions are proposed for the existence of the ITO. According to the first one, five different but correlative suggestions that indicate the existence of the Inner Tauride Ocean are proposed. These include; (1) development of the Tuzgözü and Ulukışla basins is related to fore-arc

settings created by a subduction of Inner Tauride Ocean (Görür *et al.*, 1984); (2) the ophiolites found on the Taurides are the product of a supra-subduction zone occurred in the Inner Tauride Ocean and they were emplaced southwards onto Tauride Platform during late Cretaceous to Eocene time interval as nappes (Lytwyn and Casey, 1995; Dilek *et al.*, 1999; Parlak and Delaloye, 1999; Robertson, 2002; Robertson and Andrew, 2002); (3) the metamorphic belt of Anatolides and decrease in metamorphic grade from north to south cannot be explained by only the subduction of Taurides beneath Pontides because this belt also follows the outline of the Kırşehir Block, so westward subduction of Tauride block beneath Kırşehir Block during late Cretaceous must be taken into account in order to reconstruct this metamorphic belt (Pourteau, 2011); (4) the origin of the late Cretaceous Central Anatolian granitoids is related to arc magmatism and their location parallel to the western margin of the Kırşehir Block indicates the existence of a subduction beneath the western margin of the Kırşehir Block (Görür *et al.*, 1984; 1998; Tüysüz *et al.*, 1994; Erdogan *et al.*, 1996; Kadioğlu *et al.*, 2006) and (5) sedimentation in the Ayhan-Büyükkişla Basin started during Campanian in back-arc extensional setting consequent to westward subduction beneath Kırşehir Block (Advokaat *et al.*, 2014). In contrast to first suggestion, the second one proposes two different but correlative suggestions which might indicate inexistence of the Inner Tauride Ocean and related subduction; (1) development of the Tuzgölü and Ulukışla basins during late Cretaceous is related to the basin margin parallel extensional faults; this has also resulted in the exhumation of the Niğde Massif (Çemen *et al.*, 1999; Dirik and Erol, 2000; Aydemir and Ateş, 2006; Gautier *et al.*, 2002; 2008); and (2) the origin of the Central Anatolian granitoids is related to collisional settings, and they are products of crustal thickening resulted from arc to arc or arc to continent collision between Pontides and Kırşehir Block (Göncüoğlu *et al.* 1986; 1992). In addition to the previous suggestions indicating existence of Inner Tauride Ocean, also by considering the new findings of Pourteau (2011), and Advokaat *et al.* (2014), subduction of Inner Tauride Ocean beneath the Kırşehir Block at least during late Cretaceous time interval was considered as the reason for the development of the Tuzgölü, Ulukışla and Ayhan-Büyükkişla basins (Görür *et al.*, 1984; 1998; Kadioğlu *et al.* 2006; Pourteau, 2011; Advokaat *et al.*, 2014). In this sense, it is

possible to suggest that first cycle units of the Haymana Basin was deposited in almost same time interval and tectonic settings with the upper Cretaceous fore-arc sequences of the Tuzgölü and Ulukışla basins, in different but most probably hydraulically connected fore-arc regions while sedimentation in the Ayhan-Büyükkışla Basin was controlling in back-arc settings.

5.2.3 The Position of the Haymana Basin with respect to Collision between Pontides and KB or Taurides

Although Paleocene to pre-early Miocene time interval is proposed as the collisional period of the Pontides and Kırşehir Block (Koçyiğit *et al.*, 1988; Koçyiğit, 1991; Rojay, 1995; Kaymakçı, 2000; Kaymakçı *et al.*, 2009; Hippolyte *et al.*, 2010), timing of the collision of Pontides and Taurides around the Haymana region is not known. Post-early Paleocene age can, however, be inferred as the initiation age of the collision; the youngest peak metamorphic age (Pourteau, 2011) from the metamorphic rocks of the Tauride Platform forms the main evidence. This time interval is represented by compressional setting-related structures and retro-arc foreland or collisional-setting related deposition in the northern Central Pontides and southern Central Pontides, respectively (Koçyiğit *et al.*, 1988; Koçyiğit, 1991; Rojay, 1991; 1995; Tüysüz, 1999; Kaymakçı, 2000; Kaymakçı *et al.*, 2009; Hippolyte *et al.*, 2010, Şen 2013; Espurt *et al.*, 2014). This implies that the collision between Pontides and Kırşehir Block or Taurides affected not only the basins located along the southern margin of the central Pontides, but also the basins along the northern margin of the central Pontides. It may therefore be suggested that post-Early Paleocene evolution of the Haymana basin can be correlated with all of these basins. In this sense, it is proposed that the last two cycle units of the Haymana Basin are deposited in almost the same settings with the other central Pontide basins. This suggestion is also supported by the stratigraphic and sedimentological characteristics of the last two cycle units of the basin and the characteristics of the deformation phase 2, that indicate N-S compression and related fold and thrust belt development for that time interval. Additionally, by considering the thermal models discussed in Chapter 4, it may also be suggested that effects of the collision lasts at least to early Miocene in the Haymana

region. Additionally, studies of Özsayın and Dirik (2007 and 2011), and Özsayın *et al.* (2013) support this suggestion by indicating pre–early Miocene compressional deformation phase for the western part of the Tuzgölü basin.

5.2.4 The Position of the Haymana Basin with respect to Collision between KB and Taurides

The initiation and the termination of development of the collisional-setting related structures in Tuzgölü, Ulukışla and Ayhan-Büyükkişla basins is proposed as middle Eocene (Görür *et al.*, 1984; 1998; Çemen *et al.*, 1999; Dirik and Erol, 2000; Clark and Robertson, 2003) to middle Miocene (Advokaat *et al.*, 2014). It may therefore be suggested that collision of Tauride Platform and Kırşehir Block is younger than the one between Tauride Platform and Pontides. This implies different evolutionary histories for the Haymana and the other basins located between Tauride Platform and Kırşehir Block for that time interval; middle Eocene shallow-marine units of these basins are, however, correlatable which indicates probability of hydraulic connection of the basins or a thermal maximum event for that time span. Structurally, it may be proposed that effects of the collision and possible post-collisional convergent period on Kırşehir Block may enhance the vertical block rotations and uplift rates in the Haymana region.

CHAPTER 6

CONCLUSIONS

This study has reached following conclusions.

A. Stratigraphical and sedimentological studies have revealed that;

- i. Santonian to middle Eocene continuous deposits of the Haymana Basin comprises four depositional sequences, as represented by contemporaneous sedimentation in continental to deep marine environment.
 - The first sequence includes Santonian to upper Campanian fore-arc deposits of the Beyobası and its distal equivalent the Haymana formations. Danian to lower Thanetian deposits of continental Kartal, shallow-marine Çaldağ and calci-turbiditic Yeşilyurt formations form the second cycle. Upper Paleocene-lower Eocene shallow-marine limestones of Kırkavak, slope front deposits of the Iğnıkdere and turbiditic the Eskipolatlı formations represent the third cycle. Early to middle Eocene continental Beldede, nummulitic bank deposits of the Çayraz and turbiditic Yamak formations define the fourth cycle.
- ii. Units and sequences are laterally and vertically gradational at the southern part of the basin (distal to the northern margin) whereas local syn-sedimentary unconformities between second, third and fourth sequences are present at the northern part of the basin (proximal to the northern margin) that indicate local uplift histories in the basin.
- iii. Dominant sediment transportation direction in the basin is due south for all sequences, except for the youngest sequence where the dominant transportation is due west.

- iv. The units of last two sequences are regressive in nature and all basinfill units have wedge-like geometries, thicker in the north and thinner in the south.
- v. The last marine products of the basin is represented by middle Eocene Çayraz and Yamak formations.
- vi. Post-middle Eocene time interval in the basin is represented by non-deposition or an erosional period until Neogene during which continental fluvio-lacustrine deposition prevailed in the region.

B. Structural and paleostress inversion studies have revealed that;

- i. The Haymana Basin is segmented into two parts as northwestern segment and southeastern segment. The boundary between these segments is defined as a strike-slip fault (SS4).
 - The northwestern segment is represented by NW–SE-trending folds and reverse/thrust faults which resulted in ~3% to %5 shortening of the basin.
 - The second segment is represented by dominantly E–W-trending folds and reverse/thrust faults which resulted in ~25% shortening of the basin.
- ii. Fault and fold analyses indicate earlier south- and later north-directed tectonic transport.
- iii. Approximately, 015°N oriented σ_1 and vertical σ_3 gave way to the development of E–W- to WNW–ESE-oriented folds, reverse/thrusts faults, and NNW–SSE-oriented right-lateral and NE–SW- to ENE–WSW-oriented left lateral strike-slip faults.
- iv. Paleostress inversion studies indicate that the Haymana Basin experienced three phase of deformation which were active during pre–middle Paleocene, middle Paleocene to late Eocene and post–late Eocene time intervals, respectively. The first phase is characterized by extensional deformation with sub-vertical σ_1 and approximately N–S-oriented sub-horizontal σ_3 . The second phase is characterized by complex stress pattern

during which reverse, normal and strike-slip faults with reverse components developed in different parts of the study area. The third phase represents the Neogene deformation of the basin and is characterized by extensional and transcurrent tectonics in places.

C. Thermo-chronometric and thermal modelling studies have revealed that;

- i. The northwestern of the basin started to uplift at least sometime before 21.83 ± 2.2 Ma whereas the southeastern segment started to uplift at least sometime before 35.29 ± 3.5 Ma.
- ii. Thermal modelling studies have also revealed that the Haymana basin subjected to four successive thermal events in the northwestern/southeastern structural segments; each of these events are approximately 14 Ma older in the northwestern/southeastern segment of the basin. The first event represents the gradual burial of the basin with mean 8.5m/kyr subsidence rate, which is consistent with the 9.2 m/kyr sedimentation rates as calculated by magneto-stratigraphy studies (Özkaptan, 2015) whereas the others represent the differential uplift histories of the basin. The second event is represented by 9.9 m/kyr and 14.1 m/kyr rapid uplift rates in both segments of the basin. Mean slow uplift rates of 3.5 m/kyr represent the third cooling event in the basin. The latest thermal event is represented by rapid uplift rate (12.38 m/kyr) in the southeastern segment of the basin whereas in the northwestern segment, uplift rate for the fourth thermal event is 5.5 m/kyr.

D. Integration of the results of this study conducted on the Haymana Basin and literature information led to following conclusions;

- i. Haymana Basin was developed on southernmost tip of the Central Pontides and comprises two distinct episodes of tectonic development: (1) fore-arc basin phase: the Haymana Basin developed on both Ankara imbricate zone and accretionary wedge of the Northern Neotethys Ocean during Santonian

to middle Paleocene time interval; (2) foreland basin phase related to the progressive collision of Pontides and Anatolides that gave way to the Ankara imbricate zone and ophiolite obduction on to Taurides along the western part of the Inner Tauride Ocean during middle Paleocene to late Eocene time interval.

- ii. Haymana, Tuzgölü and Ulukışla basins were hydrologically connected at least until middle Eocene, however, the Haymana Basin was evolved between the Pontides and Tauride Platform whereas Tuzgölü and Ulukışla basins, between Kırşehir and Tauride Platform.
- iii. The collision between Pontides and Tauride Platform is the main factor for the uplift and exhumation of the Haymana Basin during post–middle Eocene to middle Miocene time interval.

REFERENCES

- Advokaat, E.L., van Hinsbergen, D.D.J., Kaymakçı, N., Vissers, R.L.M., and Hendriks, B.W.H., 2014. Late Cretaceous extension and Palaeogene rotation related contraction in Central Anatolia recorded in the Ayhan-Büyükkişla basin. *International Geology Review*, 56, 1813-1836.
- Akarsu, İ., 1971. II. Bölge AR/TPO/747 nolu sahanın terk raporu. Pet. İş. Gen. Md., Ankara (Unpublished).
- Akıl, B., 2008. Structural Evolution of İnönü-Eskişehir Fault System between Günyüzü (Eskişehir) and Yeniceoba (Konya-Turkey). Ph.D. Thesis, University of Hacettepe, 113 p.
- Akyürek, B., Bilginer, E., Akbaş, B., Hepşen, N., Pehlivan, Ş., Sunu, O., Soysal, Y., Dağer, Z., Çatal, E., Sözeri, Z., Yıldırım, H., and Hakyemez, Y., 1984. The geology of the Ankara-Elmadağ-Kalecik region. *Jeoloji Mühendisliği Dergisi*, 20, 31-46.
- Allmendinger, R.W., Cardozo, N.C., and Fisher, D., 2012. *Structural Geology Algorithms: Vectors & Tensors*. Cambridge, England, Cambridge University Press, 289 pp.
- Altner, D., Koçyiğit, A., Farinacci, A., Nicosia, U., and Conti, M.A., 1991. Jurassic-Lower Cretaceous stratigraphy and paleogeographic evolution of the southern part of NW Anatolia, Turkey. *Geologica Romana*, 27, 13-80.
- Andrew, T., and Robertson, A.H.F., 2002. The Beyşehir-Hoyran-Hadim nappes: genesis and emplacement of Mesozoic marginal and oceanic units of the northern Neotethys in southern Turkey. *Journal of the Geological Society of London*, 159, 529-543.
- Angelier, J., 1979. Determination of mean principal direction of stress for a given fault population. *Tectonophysics*, 56, 17-26.

Angelier, J., 1984, Tectonic analysis of fault slip data sets. *Journal of Geophysical Research*, 89, 5835-5848.

Angelier, J., 1989. From orientation to magnitudes in paleostress determinations using fault slip data. *Journal of Structural Geology*, 11, 37-50.

Angelier, J., 1994. Fault slip analysis and paleostress reconstruction. In: P.L. Hancock (Editor), *Continental deformation*. Pergamon Press, Oxford, 53-101.

Arıkan, Y., 1975. Tuzgölü havzasının jeolojisi ve petrol imkanları. *MTA Bülteni*, 85, 17-38.

Armijo, R., Carey, E., and Cisternas, A., 1982. The inverse problem in microtectonics and the separation of tectonic phases. *Tectonophysics*, 82, 145-160.

Arni, P., 1965. L'évolution des nummulitinae en tant que facteur de modification des depots littoraux. *Coloque International de Micropaléontologie (Daker), Mémoires du BRGM*, 32, 7-20.

Arslan, M., Aslan, Z., Sen, C., and Hoskin, P.W.O., 2000. Constraints on Petrology and Petrogenesis of Tertiary Volcanism in the Eastern Pontide Paleo-Arc System, NE Turkey. *Journal of Conference Abstracts, Cambridge Publications*, 5(2),157

Arslan, M., Temizel, İ., Abdioğlu, E., Kolaylı, H., Yücel, C., Boztuğ, D., and Şen, C., 2013. ⁴⁰Ar–³⁹Ar dating, whole-rock and Sr–Nd–Pb isotope geochemistry of post-collisional Eocene volcanic rocks in the southern part of the Eastern Pontides (NE Turkey): implications for magma evolution in extension-induced origin. *Contributions to Mineralogy and Petrography*, 166,113–142.

Aydemir, A., Ates, A., 2006. Structural interpretation of the Tuzgolu and Haymana Basins, Central Anatolia, Turkey, using seismic, gravity and aeromagnetic data. *Earth, Planets and Space*, 58, 951–961.

Aydın, M., Demir, O., Özçelik, Y., Terzioğlu, N., Satır, M., 1995. A geological revision of İnebolu, Devrekani, Ağlı and Küre areas: new observations in Paleo-Tethys

- Neo-Tethys sedimentary successions. In: Erler, A., Ercan, T., Bingöl, E., Örçen, S. (Eds.), *Geology of the Black Sea Region*. MTA Bülteni, Özel baskı, 33–38.

Aziz, A. 1975. İskilip civarı ile güney ve güneybatısının detay jeolojisi ve petrol olanakları. M.T.A. Ars., Rap. No: 6132 (unpublished).

Bailey, E.B., McCallien, W.J., 1950. The Ankara mélangé and the Anatolian thrust. MTA Bülteni, 40, 17-21.

Batman, B., 1978. Haymana kuzeyinin jeolojik evrimi ve yöredeki melanjın incelenmesi - stratigrafi birimleri. Hacettepe University, Earth Sciences , 4, 95-124

Bingöl, E., 1974. Discussions on the metamorphic map of Turkey in a scale of 1:2,500,000 and geotectonic evolution of some metamorphic belts. MTA Bülteni, 83, 119–131.

Birgili, S., Yoldaş, R., and Ünalın, G., 1974. Çankırı-Çorum Havzası jeolojisi ve petrol olanakları ön raporu. TPAO Rap. No: 1216 (unpublished).

Boccaletti, M., Gocev, P., and Manetti, P., 1974. Mesozoic isotopic zones in the Black Sea region. *Società Geologica Italiana, Bollettino*, 93, 547-565.

Boztuğ, D., Harlavan, Y., 2007. K-Ar ages of granitoids unravel the stages of Neo-Tethyan convergence in the eastern Pontides and central Anatolia, Turkey. *International Journal of Earth Sciences*, 97, 585-599.

Boztuğ, D., G.A. Wagner, A.İ. Erçin, D. Göc , Z. Yeğingil, A. İskenderoğlu, M. K. Kuruçelik, İ. Kömür, and Y. Güngör., 2002. Sphene and zircon fission-track geochronology unravelling subduction-and collision related magma surges in the composite Kaçkar Batholith, Eastern Black Sea region, Turkey. 1st International Symposium of the Faculty of Mines (İTÜ) on Earth Sciences and Engineering, 16–18 May 2002, Istanbul, Turkey, Abstracts, p. 121.

Bragin, N.J., Tekin, K., 1996. Age of radiolarian-chert blocks from the Senonian ophiolitic mélangé (Ankara, Turkey). *Island Arc*, 5, 114–122.

Burbank, D.W., and Anderson, R.S., 2001. *Tectonic Geomorphology*. Blackwell Science, Massachusetts, 274 p.

Candan, O., Cetinkaplan, M., Oberhänsli, R., Rimmelé, G., and Akal, C., 2005. Alpine high Pressure low-Temperature metamorphism of the Afyon Zone and implications for the metamorphic evolution of Western Anatolia, Turkey. *Lithos* 84(1-2), 102-124.

Carey, E., and Brunier, B., 1974. Analyse théorique et numérique d'un modèle mécanique élémentaire appliqué à l'étude d'une population de failles: C. R. hebd. Séanc. Acad. Sci. Paris, D, v. 279, p. 891-894.

Cater, J.M.L., Hanna, S.S., Ries, A.C, and Turner, P., 1991. Tertiary evolution of the Sivas Basin, central Turkey. *Tectonophysics*, 195, 29-46.

Chaput, E., 1932. Observations géologiques en Asie Mineure: Le Crétacé supérieur dans l'Anatolie Centrale. C. R. A. S., 194, 1960-1961.

Chaput, E., 1935a. L'Eocene du plateau de Galatie (Anatolie Centrale). C. R. A. S., 200, 767-768.

Chaput, E., 1935b. Les plissements Tertiaire de l'Anatolie Centrale. C. R. A. S., 201, 1404-1405.

Chaput, E., 1936. Voyages d'études géologiques et géomorphologiques en Turquie. *Mém. Inst. Français D'Archéol. İstanbul*, II, 312 p.

Clark, M., Robertson, A., 2002. The role of the Early Tertiary Ulukışla Basin, southern Turkey, in suturing of the Mesozoic Tethys Ocean. *Journal of the Geological Society*, 159(6), 673-690.

Clark, M. and Robertson, A., 2005. Uppermost Cretaceous–Lower Cenozoic Ulukışla Basin, south-central Turkey: sedimentary evolution of part of a unified basin complex within an evolving Neotethyan suture zone. *Sedimentary Geology*, 173, 15–51.

Crowley, K.D., Cameron, M., and Schaefer, R.L., 1991. Experimental studies of annealing of etched fission tracks in fluorapatite. *Geochimica Et Cosmochimica Acta*, 55, 1449-1465.

Çelik, Ö.F., Delaloye, M., 2006. Characteristics of ophiolite-related metamorphic rocks in the Beyşehir ophiolitic mélangé (Central Taurides, Turkey), deduced from whole rock and mineral chemistry. *Journal of Asian Earth Sciences*, 26, 461–476.

Çelik, Ö. F., Marzoli, A., Marschik, R., Chiaradia, M., Neubauer, F. and Öz, I., 2011. Early–Middle Jurassic intra-oceanic subduction in the Izmir-Ankara-Erzincan Ocean, Northern Turkey. *Tectonophysics*, 509, 120–134.

Çemen, İ., Göncüoğlu, M.C., and Dirik, K., 1999. Structural evolution of the Tuzgölü Basin in Central Anatolia, Turkey. *Journal of Geology*, 107, 693–706.

Çetin, H., Demirel, İ. H., and Gökçen, S.L., 1986. Haymana'nın (SW Ankara) doğusu ve batısındaki Üst Kretase-Alt Tersiyer istifinin sedimantolojik ve sedimanter petrolojik incelemesi. *TJK Bülteni* , 29/2, 21-33.

Çetinkaplan, M., Candan, O., Oberhänsli, R., Bousquet, R., 2008. Pressure-temperature evolution of lawsonite eclogite in Sivrihisar; Tavşanlı Zone-Turkey. *Lithos*, 104, 12–32.

Çiner, A., Deynoux, M., Ricou, S., and Koşun, E. 1996a. Cyclicity in the middle Eocene Çayraz Carbonate Formation, Haymana Basin, Central Anatolia. *Palaeogeography, Palaeoclimatology, Palaeoecology*, 121, 313-329.

Çiner, A., Deynoux, M., and Koşun, E., 1996b. Cyclicity in the Middle Eocene Yamak turbidite complex of the Haymana basin, Central Anatolia, Turkey. *Geologische Rundschau*, 85, 669-682.

Delaloye, M., and Bingöl, E., 2000. Granitoids from Western and Northwestern Anatolia: Geochemistry and modeling of geodynamic evolution. *International Geology Review*, 42(3), 241- 268.

Dellalođlu, A. A., Tüysüz, O., Kaya, O.H., and Harput, B., 1992. Kalecik (Ankara) – Eldivan - Yapraklı(Çankırı) - İskilip(Çorum) ve Devrez Çayı arasındaki alanın jeolojisi ve petrol olanakları. TPAO Rap. No. 3194 (unpublished).

Dellalođlu, A.A., and Aksu, R., 1984. Polatlı, Haymana, Yenice, Yeniceoba ve Cihanbeyli dolaylarının Ayrıntılı Jeoloji ön raporu. TPAO rapor no.2006 (unpublished)

Dellalođlu, A.A., and Aksu, R., 1986. Eređli (Konya)-Ulukışla-Çiftehan-Çamardı(Niğde) dolayının jeolojisi ve petrol olanakları. TPAO rapor no.2205 (unpublished)

Dellalođlu, A.A., and Aksu, R., 1991. Ankara-Temelli-Haymana-Kulu-Kırıkkale arasındaki alanın jeolojisi ve petrol olanakları. TPAO rapor no.3006 (Unpublished).

Delvaux, D., Moeys, R., Stapel, G., Petit, C., Levi, K., Miroshenko, A., Ruzhich, V., and Sankov, V., 1997. Paleostress reconstructions and geodynamics of the Baikal region, Central Asia, Part 2. Cenozoic rifting. *Tectonophysics*, 282, 1–38.

Demirtaşlı, E., Bilgin, A.Z., Erenler, F., Işlar, S., Sanlı, D., Selim, N. and Turhan, N., 1973. Bolcardağlarının Jeolojisi. Cumhuriyetin 50. yılı Yerbilimleri Kongresi, Tebliğler, MTA Yayını, Ankara, 608 p.

Derman, A.S., 1978. Tuzgölü ve Kuzeyinin Jeolojisi. TPAO rapor no 1512 (unpublished).

Dickinson, W.R., and Seely, D.R., 1979. Structure and stratigraphy of forearc regions. *AAPG Bulletin*, 63, 2–31.

Dilek, Y. and Thy, P., 2006. Age and petrogenesis of palgiogranite intrusions in the Ankara mélangé, central Turkey. *Island Arc*, 15, 44-57.

Dilek, Y., Thy, P., Hacker, B. & Grundvig, S., 1999. Structure and petrology of Tauride ophiolites and mafic dike intrusions (Turkey): implications for the Neotethyan Ocean. *Bull. Geol. Soc. Am.* 111, 1192-1216.

Dinçer, A., 1977. Haymana-Kulu yöresinin jeolojisi ve petrol olanakları. TPAO rapor no.1314 (unpublished)

Dirik, K., and Erol, O., 2000. Tuzgölü ve civarının tektonomorfolojik evrimi [Tectonomorphologic evolution of Tuzgölü and surrounding area]. Haymana-Tuzgölü-Ulukışla Basenleri Uygulamalı Çalışması, Aksaray, Abstracts, p. 7–8.

Dirik, K., and Erol, O., 2003. Tuzgölü ve civarının tektonomorfolojik evrimi, Orta Anadolu-Türkiye.TPJD Özel sayı, 27-46.

Dirik, K., and Göncüoğlu, M.C., 1996. Neotectonic characteristics of central Anatolia. International Geology Review, 38, 807–817.

Dodson, M.H., 1973. Closure temperature in cooling geochronological and petrological systems. Contributions to Mineralogy and Petrology, 40, 259-274.

Donelick, R.A., O'Sullivan, P.B., and Ketcham, R.A., 2005. Apatite Fission-Track analysis. Reviews in Mineralogy and Geochemistry, 58, 49-94.

Duddy, I.R., Green, P.F., and Laslett, G.M., 1988. Thermal annealing of fission tracks in apatite, 3. Variable temperature behavior. Chemical Geology (Isotope Geoscience Section), 73, 25–38 .

Eichenseer, H., and Luterbacher, H., 1992. The Marine Paleogene of the Tremp Region (NE Spain) - Depositional sequences, facies history, biostratigraphy and controlling factors. Facies, 27, 119-152.

Erdoğan, B., Akay, E., and Uğur, M.S., 1996. Geology of the Yozgat region and evolution of the collisional Çankiri Basin. International Geology Review, 38, 788-806.

Erler, A., and Göncüoğlu, M.C., 1996. Geologic and tectonic setting of the Yozgat batholith, Northern Central Anatolian Crystalline Complex, Turkey. International Geology Review, 38 (8), 714-726.

Erler, A., Akıman, O., Unan, C., Dalkılıç, F., Dalkılıç, B., Geven, A., and Önen, P., 1991. Kaman (Kırşehir) ve Yozgat yörelerinde Kırşehir masifi magmatik kayaçlarının petrolojisi ve jeokimyası: TÜBİTAK, Doga-Tr. J. of Eng. and Env. Sc., 15, 76-100.

Espurt, N., Hippolyte, J.-C., Kaymakci, J.C.N., and Sangu, E., 2014. Lithospheric structural control on inversion of the southern margin of the Black Sea Basin, Central Pontides, Turkey. *Lithosphere*, 6, 26–34.

Etchecopar, A., Vasseur, G., Daigniers, M., 1981. An inverse problem in microtectonics for the determination of stress tensors from fault striation analysis. *Journal of Structural Geology*, 3, 51-65.

Farley, K.A., Wolf, R.A., and Silver, L.T., 1996. The effects of long-alpha-stopping distances on (U–Th)/ He ages. *Geochimica et Cosmochimica Acta*, 60, 4223–4229.

Farley, K.A., 2000. Helium diffusion from apatite: general behaviour as illustrated by Durango fluorapatite. *Journal of Geophysical Research*, 105, 2903–2914.

Fayon, A.K., Whitney, D.L., Teyssier, C., Garver, J.I., and Dilek, Y., 2001. Effects of plate convergence obliquity on timing and mechanisms of exhumation of a mid-crustal terrain, the Central Anatolian Crystalline Complex. *Earth and Planetary Science Letters*, 192, 191–205.

Fernandez-Blanco, D., Bertotti, G., and Çiner, T.A., 2013. Cenozoic tectonics of the Tuzgölü basin (Central Anatolian Plateau, Turkey). *Turkish Journal of Earth Science*, 22, 715-738.

Gallagher, K., 1995. Evolving temperature histories from apatite fission-track data. *Earth and Planetary Science Letters*, 136, 421–435.

Gautheron, C., and Tassan-Got, L., 2010. A Monte Carlo approach to diffusion applied to noble gas/helium thermochronology. *Chemical Geology*, 273, 212–224.

Gautier, P., Bozkurt, E., Bosse, V., Hallot, E., Dirik, K., 2008. Coeval extensional shearing and lateral underflow during Late Cretaceous core complex development in the Niğde Massif, Central Anatolia, Turkey. *Tectonics*, 27, TC1003

Gautier, P., Bozkurt, E., Hallot, E., Dirik, K., 2002. Dating the exhumation of a metamorphic dome: geological evidence for pre-Eocene unroofing of the Niğde Massif (Central Anatolia, Turkey). *Geological Magazine*, 139(5), 559-576.

Gleadow, A.J.W., and Fitzgerald, P.G., 1987. Uplift history and structure of the Transantarctic Mountains: new evidence from fission track dating of basement apatites in the Dry Valleys area, southern Victoria Land. *Earth and Planetary Science Letters*, 82, 1-14.

Gleadow, A.J.W., Duddy, I.R., Green, P.F., and Lovering, J., 1986b. Confined fission track lengths in apatite: a diagnostic tool for thermal history analysis. *Contribution Mineralogy Petrology*, 94, 405-415.

Gökçen, S.L., 1976. Haymana güneyinin sedimentolojik incelemesi. I. Stratigrafik birimler ve tektonik. *Yerbilimleri*, 2, 161-201.

Gökçen, S.L., Kelling, G., 1983. The Paleogene Yamak sand-rich submarine fan complex, Haymana basin, Turkey. *Sedimentary Geology*, 34, 219-243.

Göncüoğlu, M.C., and Türeli, K., 1993. Orta Anadolu Ofiyoliti plajiyogranitlerinin petrolojisi ve jeodinamik yorumu (Aksaray-Türkiye). *Turkish Journal of Earth Sciences*, 2, 195-203.

Köksal, S., and Göncüoğlu, M.C., 1997. İdiş Dağı-Avanos alanının jeolojisi (Nevşehir-Orta Anadolu). *MTA Bülteni*, 119, 73-89.

Göncüoğlu, M.C., 1997. İdiş Dağı-Avanos Alanının Jeolojisi (Nevşehir-Orta Anadolu): *MTA Bülteni*, 119, 73-87.

Göncüoğlu, M.C., Sayit, K., and Tekin, U.K., 2010. Oceanization of the northern Neotethys: Geochemical evidence from ophiolitic mélangé basalts within the Izmir-Ankara suture belt, NW Turkey. *Lithos*, 116, 175-187.

Göncüoğlu, M.C., 1986. Orta Anadolu Masifinin güney ucundan jeokronolojik yaş bulguları. *MTA Bülteni*, 105/106, 111-124.

Göncüoğlu, M.C., Toprak, V., Kuşcu, I., Erler, A., and Olgun, E., 1991. Orta Anadolu Masifinin orta bölümünün jeolojisi - bölüm 1: Güney kesim. TPAO Rapor no.2909, 140 p (unpublished).

Göncüoğlu, M.C., 1977. *Geologie des westlichen Niğde Massivs*. Phd Thesis, Bonn University, 181 pp.

Göncüoğlu, M.C., Erler, A., Toprak, V., Olgun, E., Yaliniz, K.M., Kuşcu, I., Dirik, K., 1993. Orta Anadolu Masifinin orta bölümünün jeolojisi - bölüm 3: Orta Kızılırmak Tersiyer Baseninin jeolojik evrimi. TPAO Rapor no.3313, 104 pp (unpublished).

Görür, N., Tüysüz, O., Aykol, A., Sakinc, M., Yiğitbaş, E.ö and Akkök, R.ö 1993. Cretaceous red pelagic carbonates of northern Turkey: their place in the opening history of the Black Sea. *Eclogae Geology Helvetica*, 86, 819-838.

Görür, N., 1997. Cretaceous Syn- to Post-rift Sedimentation on the Southern Continental Margin of the Western Black Sea Basin. In A. G. Robinson (Ed.), *Regional and petroleum geology of the Black Sea and surrounding region*. AAPG Memoir, 68, 227-240.

Görür, N., Oktay, F.Y., Seymen, I., and Şengör, A.M.C., 1984. Palaeotectonic evolution of the Tuzgölü basin complex, Central Turkey: sedimentary record of a Neo-Tethyan closure. *Journal of the Geological Society of London Special Publications*, 17(1), 467-482.

Görür, N., Tüysüz, O., and Şengör, A.M.C., 1998. Tectonic Evolution of the Central Anatolian Basins. *International Geology Review*, 40, 831-850.

Green, P.E., Duddy, I.R., Gleadow, A.J.W., Tingate, P.R., and Laslett, G.M., 1986. Thermal annealing of fission tracks in apatite 1. A qualitative description. *Chem. Geol. (hot. Geosci. Sect.)*, 59:236-253

Green, P.E., Duddy, I.R., Laslett, G.M., Hegarty, K.A., Gleadow, A.J.W., and Lovering, J.E., 1989. Thermal annealing of fission tracks in apatite: 4. Quantitative modelling techniques and extension to geological time scales. *Chem. Geol. (Isot. Geosci. Sect.)*, 79:155-182.

Gülyüz, E., Kaymakci, N., Meijers, M.J.M., van Hinsbergen, D. J.J., Lefebvre, C.J.C., Vissers, R.L.M., Hendriks, B.W.H., and Peynircioğlu, A.A., 2013. Late Eocene evolution of the Çiçekdağı Basin (central Turkey): Syn-sedimentary compression during microcontinent–continent collision in central Anatolia. *Tectonophysics*, 602, 286–299.

Gürbüz, E., and Evans, C., 1991. A seismic refraction study of the western Tuzgolu Basin, central Turkey. *Geophysical Journal International*, 106, 239–251.

Gürer, Ö.F., and Aldanmaz, E., 2002. Origin of the Upper Cretaceous–Tertiary sedimentary basins within the Tauride–Anatolide platform in Turkey. *Geological Magazine*, 139, 191-197.

Hardcastle, K. C., 1989. Possible paleostress tensor configurations derived from fault-slip data in eastern Vermont and western New Hampshire. *Tectonics*, 8, 265-284.

Hippolyte, J.-C., Müller, C., Kaymakci, N., and Sangu, E., 2010. Nannoplankton dating in the Black Sea inverted margin of Central Pontides (Turkey) reveals two episodes of rifting. In M. Sosson, N. Kaymakci, R. A. Stephenson, V. Starostenko & F. Bergerat (Eds.), *Sedimentary basin tectonics from the Black Sea and Caucasus to the Arabian Platform*.). Geological Society of London, 340, 13-136.

Hurford, A.J. 1986. Cooling and uplift patterns in the Lepontine Alps, South Central Switzerland and an age of vertical movement on the Insubric fault line. *Contributions to Mineralogy and Petrology*, 92, 413-427.

İlbeyli, N., and Kibici, Y., 2009. Collision-related granite magma genesis, potential sources and tectono-magmatic evolution: comparison between central, northwestern and western Anatolia (Turkey). *International Geology Review*, 51, 252-278.

Kadiođlu, Y.K., Dilek, Y., and Foland, K.A., 2006. Slab break-off and syn-collisional origin of the Late Cretaceous magmatism in the Central Anatolian crystalline complex, Turkey. *Geological Society of America Special Paper*, 409, 381–415.

Kara, H., and Dönmez, M., 1990. 1/100.000 ölçekli açınısama nitelikli Türkiye jeolojisi haritalar serisi: Kırşehir G-17 paftası. MTA Raporu.

Kaygusuz, A., Aydınçakır, E., 2009. Mineralogy, whole-rock and Sr-Nd isotope geochemistry of mafic microgranular enclaves in Cretaceous Dagbaşı granitoids, eastern Pontides, NE Turkey: evidence of magma mixing, mingling and chemical equilibration. *Chemie der Erde*, 69, 247-277.

Kaygusuz, A., Siebel, W., İlbeyli, N., Arslan, M., Satır, M., Şen, C., 2010. Insight into magma genesis at convergent plate margins e a case study from the eastern Pontides (NE Turkey). *Journal of Mineralogy and Geochemistry*, 187 (3), 265-287.

Kaygusuz, A., Sipahi, F., İlbeyli, N., Arslan, M., Chen, B., Aydınçakır, E., 2013. Petrogenesis of the Late Cretaceous Turnagöl intrusion in the eastern Pontides: implications for magma genesis in the arc setting. *Geoscience Frontiers*, 4, 423–438.

Kaymakci, N., 2000. Tectono-stratigraphical evolution of the Cankiri Basin (Central Anatolia, Turkey). *Geologica Ultraiectina*, 190, 1-247.

Kaymakci, N., Özçelik, Y., White, S.H., and Van Dijk, P.M., 2009. Tectono-stratigraphy of the Çankiri Basin: late Cretaceous to early Miocene evolution of the Neotethyan suture zone in Turkey. *Journal of the Geological Society of London Special Publications*, 311, 67-106.

Keskin, M., Genç, S.C., and Tüysüz, O., 2008. Petrology and geochemistry of post-collisional Middle Eocene volcanic units in North-Central Turkey: Evidence for

magma generation by slab breakoff following the closure of the Northern Neotethys Ocean. *Lithos*, 104, 267-305.

Ketcham, R.A., Carter, A., Donelick, R.A., Barbarand, J., and Hurford, A.J., 2007a. Improved measurement of fission-track annealing in apatite using c-axis projection. *American Mineralogist*, 92, 789–798.

Ketcham, R.A., Gautheron, C., and Tassan-Got, L., 2011. Accounting for long alpha-particle stopping distances in (U-Th-Sm)/He geochronology. Refinement of the baseline case. *Geochimica et Cosmochimica Acta*, 75, 7779-7791.

Ketin, I., 1966. Tectonic units of Anatolia (Asia Minor). *MTA Bülteni*, 66, 23-34.

Kibici, Y., Ilbeyli, N., Yıldız, A., and Bağcı, M., 2008. Petrology and geochemistry of the Günyüzü pluton, Northwest Anatolia, Turkey. *International Geology Review*, 50, 931–947.

Koçyiğit, A., 1987. Hasanoğlan (Ankara) yöresinin tektonostratigrafisi: Karakaya orojenik kuşağının evrimi. *Yerbilimleri*, 14, 269-293.

Koçyiğit, A., 1991. An example of an accretionary forearc basin from Central Anatolia and its implications for the history of subduction of Neo-Tethys in Turkey. *Geological Society of America Bulletin*, 103, 22-36.

Koçyiğit, A., Özkan, S., Rojay, B., 1988. Examples of the forearc basin remnants at the active margin of northern Neo-Tethys: development and emplacement ages of the Anatolian Nappe, Turkey. *Middle East Technical University Journal of Pure and Applied Sciences*, 3, 183-210.

Koçyiğit, A., Winchester, J.A., Bozkurt, E. and Holland, G., 2003. Saraçköy Volcanic Suite: implications for the subductional phase of arc evolution in the Galatean Arc Complex, Ankara-Turkey. *Geological Journal*, 37, 1–14.

Köksal, S., and Göncüoğlu, M.C., 1997. Geology of the İdiş Dağı - Avanos area (Nevşehir - Central Anatolia). *MTA Bülteni*, 119, 41-58.

Laslett, G.M., Green, P.F., Duddy, I.R., and Gleadow, A.J.W., 1987. Thermal annealing of fission tracks in apatite 2. A quantitative analysis. *Chemical Geology, Isotope Geoscience Section*, 65, 1–13.

Laslett, G. M., Kendall, W. S., Gleadow, A. J. W. and Duddy, I. R., 1982. Bias in measurement of fission-track length distributions. *Nucl. Tracks*, 6, 79-85.

Laslett, G.M., Gleadow, A.J.W. and Duddy, I.R., 1984. The relationship between fission track length and track density in apatite. *Nucl. Tracks*, 9, 29-37.

Lefebvre, C.J.C., Meijers, M.J.M., Kaymakçı, N., Peynircioğlu, A.A., Langereis, C.G., and Van Hinsbergen, D.J.J., 2013. Reconstructing the geometry of central Anatolia during the late Cretaceous: Large-scale Cenozoic rotations and deformation between the Pontides and Taurides. *Earth and Planetary Science Letters*, 366, 83-98.

Loucks R.G., Moody R.T.J., Bellis, J.K, Brown, A.A., 1998. Regional depositional setting and pore network systems of the El Garia Formation (Metlaoui Group, Lower Eocene), offshore Tunisia. *Journal of the Geological Society of London Special Publications*, 132, 355–374.

Lytwyn, J.N., and Casey, J.F., 1995. The geochemistry of postkinematic mafic dike swarms and subophiolitic metabasites, Pozanti-Karsanti ophiolite, Turkey. Evidence for ridge subduction. *Geological Society of America Bulletin*, 107, 830-850.

Meijers, M.J.M., Kaymakci, N., Hinsbergen, D.J.J. v., Langereis, C.G., Stephenson, R.A., and Hippolyte, J.-C. (2010a). Late Cretaceous to Paleocene oroclinal bending in the central Pontides (Turkey). *Tectonics*, 29, TC4016.

Meijers, M.J.M., Langereis, C.G., van Hinsbergen, D.J.J., Kaymakçı, N., Stephenson, R.A. and Altıner, D., 2010b. Jurassic-Cretaceous low paleolatitudes from the circum-Black Sea region (Crimea and Pontides) due to True Polar Wander, *Earth and Planetary Science Letters*, 296, 210–226.

Meriç, E., Görür, N., 1981. Haymana-Polatlı havzasındaki Çaldağ kireçtaşının kireçtaşının yaş konağı. *MTA Bülteni*, 93, 137-142.

- Moores, E.M., 1981. Ancient suture zones within continents. *Science*, 213, 41–46.
- Naeser, C.W. and Faul, H., 1969. Fission track annealing in apatite and sphene. *Journal of Geophysical Research*, 74, 705-710.
- Naeser, C.W., 1981. The fading of fission tracks in the geologic environment-data from deep drill holes. *Nuclear Tracks*, 5, 248-50.
- Nairn, S., 2011. Testing alternative models of continental collision in Central Turkey by a study of the sedimentology, provenance and tectonic setting of Late Cretaceous-Early Cenozoic syn-tectonic sedimentary basins. University of Edinburgh, PhD. Thesis, 395 p.
- Nairn, S.P., Robertson, A.H.F., Ünlügenç, U.C., İnan, N., Taslı, K., 2013. Tectonostratigraphic evolution of the Upper Cretaceous-Cenozoic central Anatolian basins: an integrated model of diachronous ocean basin closure and continental collision. *Journal of the Geological Society of London Special Publication*, 372, 343–384.
- Norman, T., 1973. Ankara Yahşihan bölgesinde Üst Kretase-Alt Tersiyer sedimantasyonu. *TJK Bülteni*, 16, 41-66.
- Norman, T.N., 1972. Ankara Yahşihan bölgesinde Üst Kretase-Alt Tersiyer istifinin stratigrafisi. *TJK Bülteni*, 15, 180-276.
- Okay, A.I., 1984. Distribution and characteristics of the northwest Turkish blueschists. *Journal of the Geological Society of London Special Publications*, 17, 455-466.
- Okay, A. I., 2002. Jadeite-chloritoid-glaucophane-lawsonite blueschists in north-west Turkey: unusually high P/T ratios in continental crust. *Journal of Metamorphic Geology*, 20, 757-768.
- Okay, A.I., Monod, O., and Monie, P., 2002. Triassic blueschists and eclogites from northwest Turkey: vestiges of the Paleo-Tethyan subduction. *Lithos*, 64(3-4), 155-178.

Okay, A.I., Harris, N. B.W., and Kelley, S.P., 1998. Exhumation of blueschists along a Tethyan suture in northwest Turkey. *Tectonophysics*, 285, 275-299.

Okay, A.I., and Şahintürk, Ö., 1997. Geology of the Eastern Pontides. In A. G. Robinson (Ed.), *Regional and petroleum geology of the Black Sea and surrounding region*. AAPG Memoir, 68, 291-311.

Okay, A.I., and Satır, M., 2006. Geochronology of Eocene plutonism and metamorphism in northwest Turkey: evidence for a possible magmatic arc. *Geodinamica Acta*, 19, 251-266.

Okay, A.I., Satır, M., Maluski, H., Siyako, M., Monié, P., Metzger, R., and Akyüz, S., 1996. Paleo- and Neo-Tethyan events in northwestern Turkey: geologic and geochronologic constraints. In A. Yin & T. M. Harrison (Eds.), *The tectonic evolution of Asia*, Cambridge University Press, 420-441

Okay, A. I., Tansel, I., and Tüysüz, O., 2001. Obduction, subduction and collision as reflected in the Upper Cretaceous–Lower Eocene sedimentary record of western Turkey. *Geological Magazine*, 138, 117-142.

Okay, A.I., Tüysüz, O., Satır, M., Özkan-Altınır, S., Altınır, D., Sherlock, S., and Eren, R.H., 2006. Cretaceous and Triassic subduction-accretion, HP/LT metamorphism and continental growth in the Central Pontides, Turkey. *Geological Society of America Bulletin*, 118, 1247-1269.

Okay, A.I., Sunal, G., Sherlock, S., Altınır, D., Tüysüz, O., Kylander-Clark, A.R.C., and Aygül, M., 2013. Early Cretaceous sedimentation and orogeny on the southern active margin of Eurasia: Central Pontides, Turkey. *Tectonics*, 32, 1247–1271.

Önen, A.P., 2003. Neotethyan ophiolitic rocks of the Anatolides of NW Turkey and comparison with Tauride ophiolites. *Journal of the Geological Society of London*, 160, 947-962.

Özcan, E., Sirel, E., Özkan-Altınır, S., Çolakoğlu, S., 2001. Late Paleocene Orthophragminae (foraminifera) from the Haymana-Polatlı Basin, Central Turkey and

description of a new taxon, *Orbitoclypeus haymanaensis*. *Micropaleontology*, 47/4, 339-357.

Özcan, E., Özkan-Altın, S., 1997. Late Campanian-Maastrichtian evolution of orbitoid foraminifera in Haymana basin succession (Ankara, Central Turkey). *Revue de Paléobiologie*, 16/1, 271-290.

Özcan, E., 2002. Cuisian orthophragminid assemblages (*Discocyclina*, *Orbitoclypeus* and *Nemkovella*) from the Haymana-Polatlı Basin (Central Turkey): biometry and description of two new taxa. *Eclogae geol. Helv.*, 95, 75-97.

Özgül, N., 1984. Stratigraphy and tectonic evolution of the Central Taurides. in Tekeli, O. and Göncüoğlu, M.C. (eds): *Geology of the Taurus Belt*. MTA Bülteni, Özel Sayı, 78-90.

Özkaptan, M., 2015. Paleomagnetism of Central Anatolia, Turkey, PhD. Thesis, Middle East Technical University, Ankara, Inpress.

Özsayın, E. & Dirik, K., 2007. Quaternary activity of Cihanbeyli Fault Zone (southern segment of Eskişehir-Sultanhanı Fault System), Central Anatolia, Türkiye. *Turkish Journal of Earth Sciences*, 16, 471-492.

Özsayın, E. & Dirik, K., 2011. The role of oroclinal bending in the structural evolution of the Central Anatolian Plateau: Evidence from a regional changeover of shortening to extension. *Geologica Carpathica*, 62-4, 345-359.

Özsayın, E., Çiner, T.A., Rojay, F.B., Dirik, R.K., Melnick, D., Fernandez-Blanco, D., Bertotti, G., Schildgen, T.F., Garcin, Y., Strecker, M.R., Sudo, M., 2013. Plio-Quaternary Extensional Tectonics of the Central Anatolian Plateau: A case study from the Tuz Gölü Basin, Turkey. *Turkish Journal of Earth Sciences*, 22, 691-714.

Öztürk, Y.Y., Helvacı, C., and Satır, M., 2012. Geochemical and Isotopic Constraints on Petrogenesis of the Beypazarı Granitoid, NW Ankara, Western Central Anatolia, Turkey. *Turkish Journal of Earth Science*, 21, 53-77.

Parlak, O. and Delaloye, M., 1999. Precise $^{40}\text{Ar}/^{39}\text{Ar}$ ages from the metamorphic sole of the Mersin Ophiolite (southern Turkey). *Tectonophysics*, 301, 145–58.

Poisson, A., Guezou, J., Ozturk, A., Inan, S., Temiz, H., Gürsöy, H., and Özden, S., 1996. Tectonic Setting and Evolution of the Sivas Basin, Central Anatolia, Turkey. *International Geology Review*, 38(9), 838 – 853.

Pollak, A., 1958. 1957 yılında Akdağmadeni-Yıldızeli sahasında yapılan prospeksiyon hakkında rapor. M.T.A. Rap., no. 2679.

Pourteau, A., 2011. Closure of the Neotethys Ocean in Anatolia: structural, petrologic & geochronologic insights from low-grade high-pressure metasediments, Afyon Zone. PhD Thesis. Potsdam University, 106 p.

Ramsay, J. G., 1967. *Folding and Fracturing of rocks*. MacGraw Hill, New York, 1-568

Reckamp, J., U., Özbey, S., 1960. Petroleum geology of Temelli and Kuştepe structures, Polatlı area. *Pet. İş. Gen. Md.*, Ankara.

Reiners P.W., 2002. (U-Th)/He chronometry experiences a renaissance. *EOS, Trans Am Geophys Union*, 83: 21, 26-27.

Rice, S.P., Robertson, A.H.F., and Ustaömer, T., 2006. Late Cretaceous-Early Cenozoic tectonic evolution of the Eurasian active margin in the Central and Eastern Pontides, northern Turkey. *Journal of the Geological Society of London Special Publications*, 260, 413-445.

Rice, S.P., Roberson, A.H.F., Ustaömer, T., Inan, T., Taslı, K., 2009. Late Cretaceous-Early Eocene tectonic development of the Tethyan Suture Zone in the Erzincan area, eastern Pontides, Turkey. *Geological Magazine*, 146(4), 567-590.

Rigo de Righi, M., and Cortesini, A., 1959. Regional studies in central Anatolian basin. Progress Report 1, Turkish Gulf Oil Co., *Pet. İş. Gen. Md.*, Ankara.

Clark, M., and Robertson, A. 2002. The role of the Early Tertiary Ulukışla Basin, southern Turkey, in suturing of the Mesozoic Tethys Ocean. *Journal of the Geological Society*, 159(6), 673-690.

Robertson, A.H.F., 2002. Overview of the genesis and emplacement of Mesozoic ophiolites in the Eastern Mediterranean Tethyan region. *Lithos*, 65, 1-67.

Robertson, A.H.F., and Dixon, J.E., 1984. Aspects of the geological evolution of the Eastern Mediterranean. *Journal of the Geological Society of London Special Publications*, 17, 1-74.

Rojay, B., 1991. Tectonostratigraphy and neotectonic characteristics of the southern margin of Merzifon-Suluova Basin (Central Pontides, Amasya). PhD. Thesis, Middle East Technical University, Ankara, 105 p.

Rojay, B., 1995. Post-Triassic evolution of Central Pontides: evidence from Amasya region, Northern Anatolia. *Geologica Romana* 31, 329–350.

Rojay, B., and Altıner, D., 1998. Middle Jurassic–Lower Cretaceous biostratigraphy in the Central Pontides (Turkey): remarks on the paleogeography and tectonic evolution. *Rivista Italiana di Paleontologia e Stratigrafia*, 104 (2), 167–180.

Rojay, B., Süzen, L., 1997. Tectonostratigraphic evolution of an arc-trench basin on accretionary ophiolitic mélangé prism, central Anatolia, Turkey. *Association of Turkish Petroleum Geologist Bulletin*, 9, 1–12.

Rojay, B., Yalınız, K., Altıner, D., 2001. Age and origin of some pillow basalts from Ankara mélangé and their tectonic implications to the evolution of northern branch of Neotethys, Central Anatolia. *Turkish Journal of Earth Science* 10 (3), 93–102.

Rojay, B., Altıner, D., Özkan Altıner, S., Önen, P., James, S., and Thirwall, M., 2004. Geodynamic significance of the Cretaceous pillow basalts from North Anatolian Ophiolitic Mélangé Belt (Central Anatolia, Turkey): geochemical and paleontological constrains. *Geodinamica Acta*, 17 (5), 349–361.

Rojay, B., 2013. Tectonic evolution of the Cretaceous Ankara ophiolitic mélangé during the Late Cretaceous to pre-Miocene interval in Central Anatolia, Turkey. *Journal of Geodynamics*, 65, 6–81.

Sarifakioglu, E., Dilek, Y., and Sevin, M., 2014. Jurassic–Paleogene intra-oceanic magmatic evolution of the Ankara Mélangé, north-central Anatolia, Turkey. *Solid Earth*, 5, 77–108.

Saner, S., 1980. Batı Pontidler'in ve komşu havzaların oluşumlarının levha tektoniği kuramıyla açıklanması, kuzeybatı Türkiye. *MTA Dergisi*, 93/94 1-19.

Schmidt, G., C., 1960. AR/MEM/365-266-367 sahalarının nihai terk raporu. Pet. İş. Gen. Md., Ankara

Seaton N.C.A., Whitney D.L., Teyssier C., Toraman E., and Heizler M.T., 2009. Recrystallization of high-pressure marble (Sivrihisar, Turkey). *Tectonophysics*, 479(3-4), 241-253.

Şengor, A.M.C., and Yilmaz, Y., 1981. Tethyan Evolution of Turkey - a Plate Tectonic Approach. *Tectonophysics*, 75(3-4), 181-241.

Seymen, I., 1981. Stratigraphy and metamorphism of the Kırşehir Massif around Kaman (Kırşehir - Turkey). *Bulletin of Geological Society of Turkey*, 24, 7-14.

Seymen, I., 1982. Kaman Dolayında Kırşehir masifi'nin Jeolojisi. . ITÜ Maden Fakültesi, Doçentlik Tezi, İstanbul, 164 p.

Shan, Y., Suen, H., and Lin, G., 2003. Separation of polyphase fault/slip data: an objectivefunction algorithm based on hard division. *Journal of Structural Geology*, 25(6), 829-840.

Sherlock, S., Kelley, S., Inger, S., Harris, N., and Okay, A.I., 1999. $^{40}\text{Ar}/^{39}\text{Ar}$ and Rb-Sr geochronology of high-pressure metamorphism and exhumation history of the Tavsanli Zone, NW Turkey. *Contributions to Mineralogy and Petrology*, 137, 46-58.

Sirel, E., 1975. Polatlı (GB Ankara) güneyinin stratigrafisi. TJK Bülteni, 18/2, 181-192 .

Sirel, E., and Gündüz, H., 1976. Description and stratigraphic distribution of some species the genera Nummulites, Assilina and Alveolina from the Ilerdian, Cuisian and Lutetian of Haymana region. TJK Bülteni, 19, 33-44.

Sirel, E., Dağ, Z., and Sözeri, B., 1986. Some biostratigraphic and paleogeographic observations on the Cretaceous-Tertiary boundary in the Haymana-Polatlı region (Central Turkey) in Walliser O. (ed) Global Bioevents. Lecture Notes in Earth Sciences, 8, 385-396.

Sirel, E., 1998. Foraminiferal description and biostratigraphy of the Paleocene-Lower Eocene shallow-water limestones and discussion on the Cretaceous-Tertiary boundary in Turkey. General Directorate of the Mineral Research and Exploration, Monography Series, 2, 117 p.

Speciale, P.A., Catlos, E.J., Yıldız, G.O., Shina, T.A., and Black, K.N., 2014, Zircon ages from the Beypazarı granitoid pluton (north central Turkey): tectonic implications, *Geodinamica Acta*, 25:3-4, 162-182.

Sunal, G., and Tüysüz, O., 2002. Palaeostress analysis of Tertiary post-collisional structures in the Western Pontides, northern Turkey. *Geological Magazine*, 139, 343-359.

Tankut, A., Dilek, Y., and Önen, A.P., 1998. Petrology and geochemistry of the Neo-Tethyan volcanism as revealed in the Ankara mélange, Turkey. *Journal of Volcanology and Geothermal Research*, 85, 265-284.

Tekeli O., 1981. Subduction complex of pre-Jurassic age, northern Anatolia, Turkey. *Geology*, 9(2), 68-72.

Temizel, İ., Arslan, M., 2008. Petrology and geochemistry of Tertiary volcanic rocks from the İkizce (Ordu) area, NE Turkey: implications for the evolution of the eastern Pontide paleomagmatic arc. *Journal of Asian Earth Sciences*, 31, 439–463.

- Toprak, V., Savascı, Y., Güleç, N., and Tankut, A., 1996. Structure of the Galetean Volcanic Province, Turkey. *International Geology Review*, 38, 747-758.
- Topuz, G., Altherr, R., Kalt, A., Satir, M., Werner, O., and Schwarz, W. H., 2004a. Aluminous granulites from the Pular complex, NE Turkey: a case of partial melting, efficient melt extraction and crystallisation. *Lithos*, 72, 183-207.
- Topuz, G., Altherr, R., Satir, M., and Schwarz, W.H. 2004b. Low-grade metamorphic rocks from the Pular complex, NE Turkey: implications for the pre-Liassic evolution of the Eastern Pontides. *International Journal of Earth Sciences*, 93, 72-91.
- Tüysüz, O., 1999. Geology of the Cretaceous sedimentary basins of the Western Pontides. *Geological Journal*, 34, 75-93.
- Tüysüz, O., and Tekin, U.K., 2007. Timing of imbrication of an active continental margin facing the northern branch of Neotethys, Kargı Massif, northern Turkey. *Cretaceous Research*, 28, 754-764.
- Tüysüz, O., Dellaloğlu, A.A., and Terzioğlu, N., 1995. A magmatic belt within the Neo-Tethyan suture zone and its role in the tectonic evolution of Northern Turkey. *Tectonophysics*, 243, 173-191.
- Ünalın, G., Yüksel, V., Tekeli, T., Gönenç, O., Seyirt, Z., and Hüseyin, S., 1976. Haymana-Polatlı yöresinin (Güneybatı Ankara) Üst Kretase-Alt Tersiyer stratigrafisi ve paleocoğrafik evrimi. *TJK Bülteni*, 19, 159-176.
- Vermeesch, P., 2008. Three new ways to calculate average (U-Th)/He ages, *Chemical Geology*, 249, 339-347.
- Wagner G.A., 1968. Fission track dating of apatites. *Earth and Planetary Science Letters*, 4, 411-415.
- Watt, S., Durrani, S.A., 1985. Thermal stability of fission tracks in apatite and sphene: using confined track-length measurements. *Nuclear Tracks*, 10, 349-357.

Whitney, D. L., and Davis, P.B., 2006. Why is lawsonite eclogite so rare? Metamorphism and preservation of lawsonite eclogite, Sivrihisar, Turkey. *Geology*, 34, 473-476.

Whitney, D.L., Teyssier, C., Dilek, Y., and Fayon, A.K., 2001. Metamorphism of the Central Anatolian Crystalline Complex, Turkey: influence of orogen-normal collision vs wrench-dominated tectonics on P-T-t paths. *Journal of Metamorphic Geology*, 19, 411-432.

Whitney, D.L., Teyssier, C., Fayon, A.K., Hamilton, M.A., and Heizler, M., 2003. Tectonic controls on metamorphism, partial melting, and intrusion: timing and duration of regional metamorphism and magmatism in the Nigde Massif, Turkey. *Tectonophysics*, 376, 37-60.

Will, T.M., Powell, R., 1991. A robust approach to the calculation of paleostress fields from fault plane data. *Journal of Structural Geology*, 13, 813-821.

Yaliniz, M.K., 2008. A Geochemical Attempt to Distinguish Forearc and Back Arc Ophiolites from the "Supra-Subduction" Central Anatolian Ophiolites (Turkey) by Comparison with Modern Oceanic Analogues. *Ofioliti*, 33(2), 119-134.

Yaliniz, K.M., and Göncüoğlu, M C., 1998. General geological characteristics and distribution of the Central anatolian Ophiolites. *Yerbilimleri* , 20, 19-30.

Yalınz, M.K., Floyd, P.A. and Göncüoğlu, M.C., 1996. Supra-subduction zone ophiolites of Central Anatolia : geochemical evidence from the Sarıkaraman ophiolite, Aksaray. Turkey. *Mineralogical Magazine*, 60, 697-710.

Yaliniz, K.M., Güncüoğlu, M. C., and Özkan-Altiner, S., 2000. Formation and emplacement ages of the SSZ-type Neotethyan ophiolites in Central Anatolia, Turkey: palaeotectonic implications. *Geological Journal*, 35, 53-68.

Yoldaş, R.,1982. Tosya (Kastamonu) ile Bayat (Çorum)arasındaki bölgenin jeolojisi. PhD. Thesis. University of İstanbul (unpublished).

Yüksel, S., 1970. Etude geologique de la region d'Haymana (Turquie central): PhD. Thesis. Fac. Sci. Univ. Nancy, France, 179 p.

Žalohar, J., Vrabec, M., 2007. Paleostress analysis of heterogeneous fault-slip data: the Gauss method. *Journal of Structural Geology*, 29, 1798–1810.

Ziegler, J.F., 1977. Helium: Stopping Powers and Ranges in all Elemental Matter. Pergamon, New York, 1-367.

APPENDIX A

MAPS

Geological and structural maps of Haymana Basin are presented on the following pages.

CURRICULUM VITAE

PERSONAL INFORMATION

Surname, Name: Gülyüz, Erhan
Nationality: Turkish (TC)
Date and Place of Birth: 13 June 1981, İstanbul
Marital Status: Married
Phone: +90 507 232 16 20
Fax: +90 312 210 57 50
email: gulyuzerhan@gmail.com

EDUCATION

Degree	Institution	Graduation Year
MS	METU Geological Engineering	2010
BS	Kocaeli University Geological Engineering	2004
High School	B.Paşa Ana. Mah. İdareler Meslek Lisesi	1999

WORK EXPERIENCE

Year	Place	Enrollment
2006-Present	METU Department of Geological Engineering	Research Assistant
2005-2006	Major Drilling Company	Geo. Engineer
2004-2005	European Nickel Company	Geo. Engineer

FOREIGN LANGUAGES

Fluent English

PUBLICATIONS

Gülyüz, E., Kaymakci, N., Meijers, M.J.M., van Hinsbergen, D. J.J., Lefebvre, C.J.C., Vissers, R.L.M., Hendriks, B.W.H., and Peynircioğlu, A.A., 2013. Late Eocene evolution of the Çiçekdağı Basin (central Turkey): Syn-sedimentary compression during microcontinent–continent collision in central Anatolia. *Tectonophysics*, 602, 286–299.

HOBBIES

Basketball, Fishing, Football, Table Tennis, Cinema

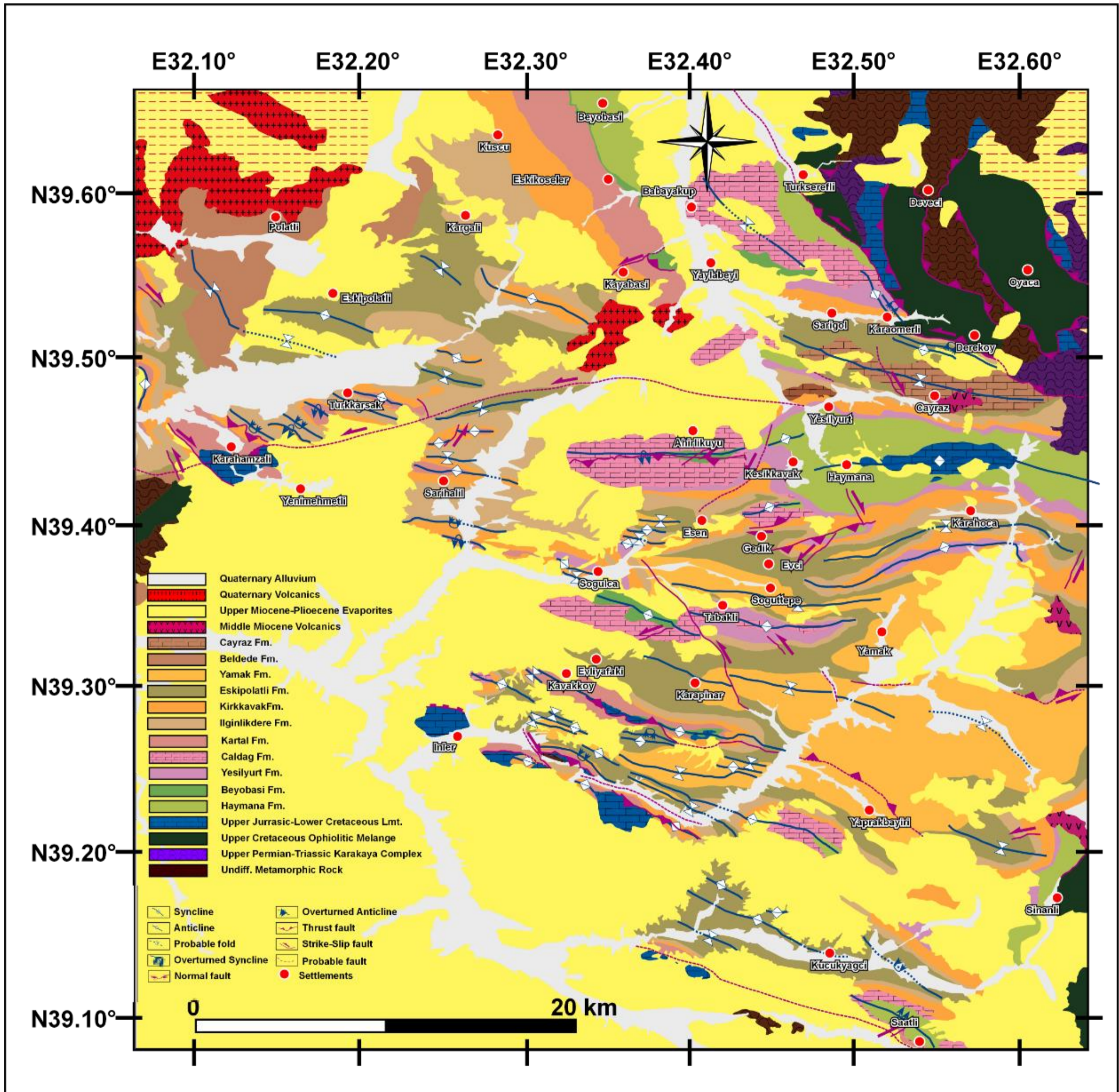


Figure A.1: Geological Map of the Haymana Basin

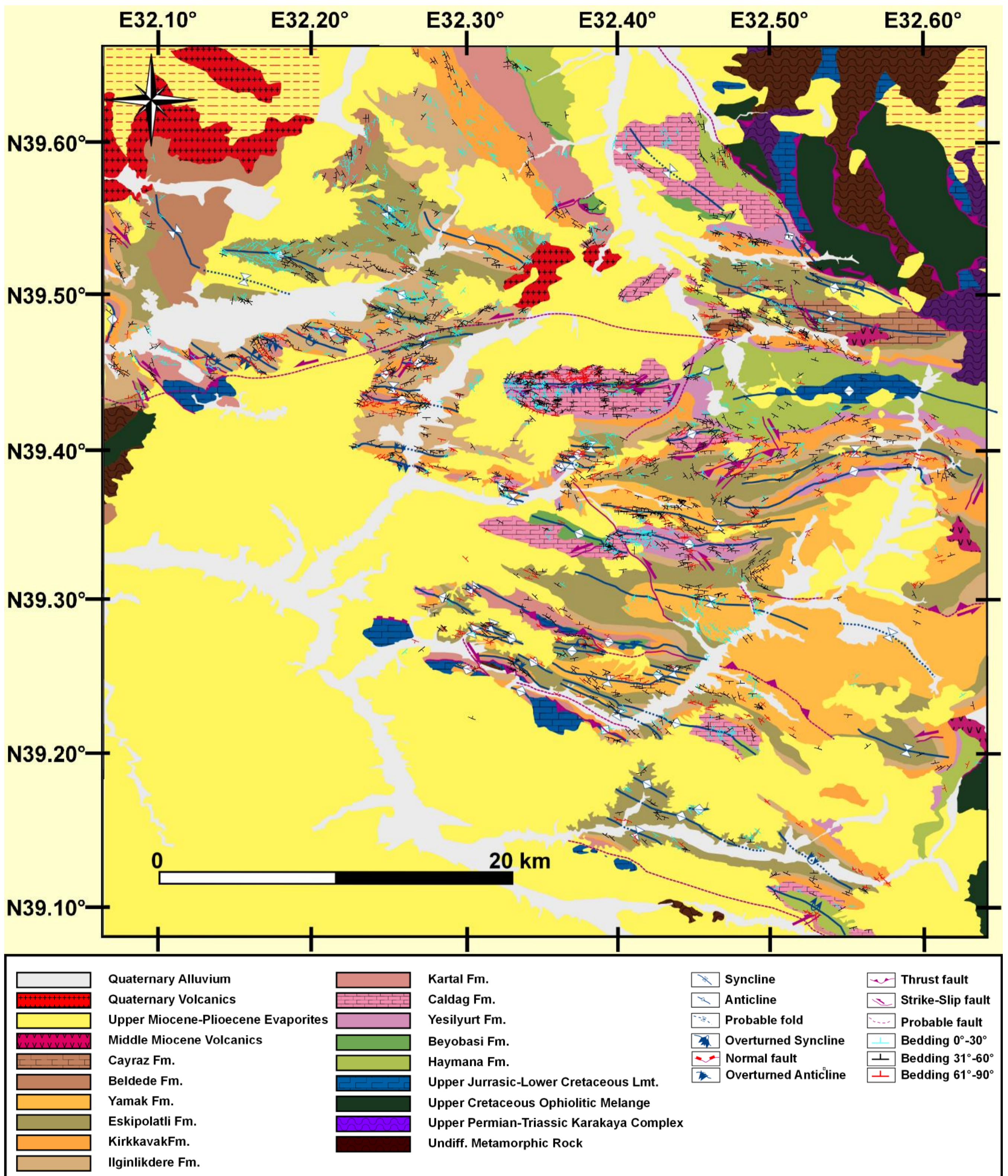


Figure A.2: Geological map of the Haymana Basin with bedding plane measurements

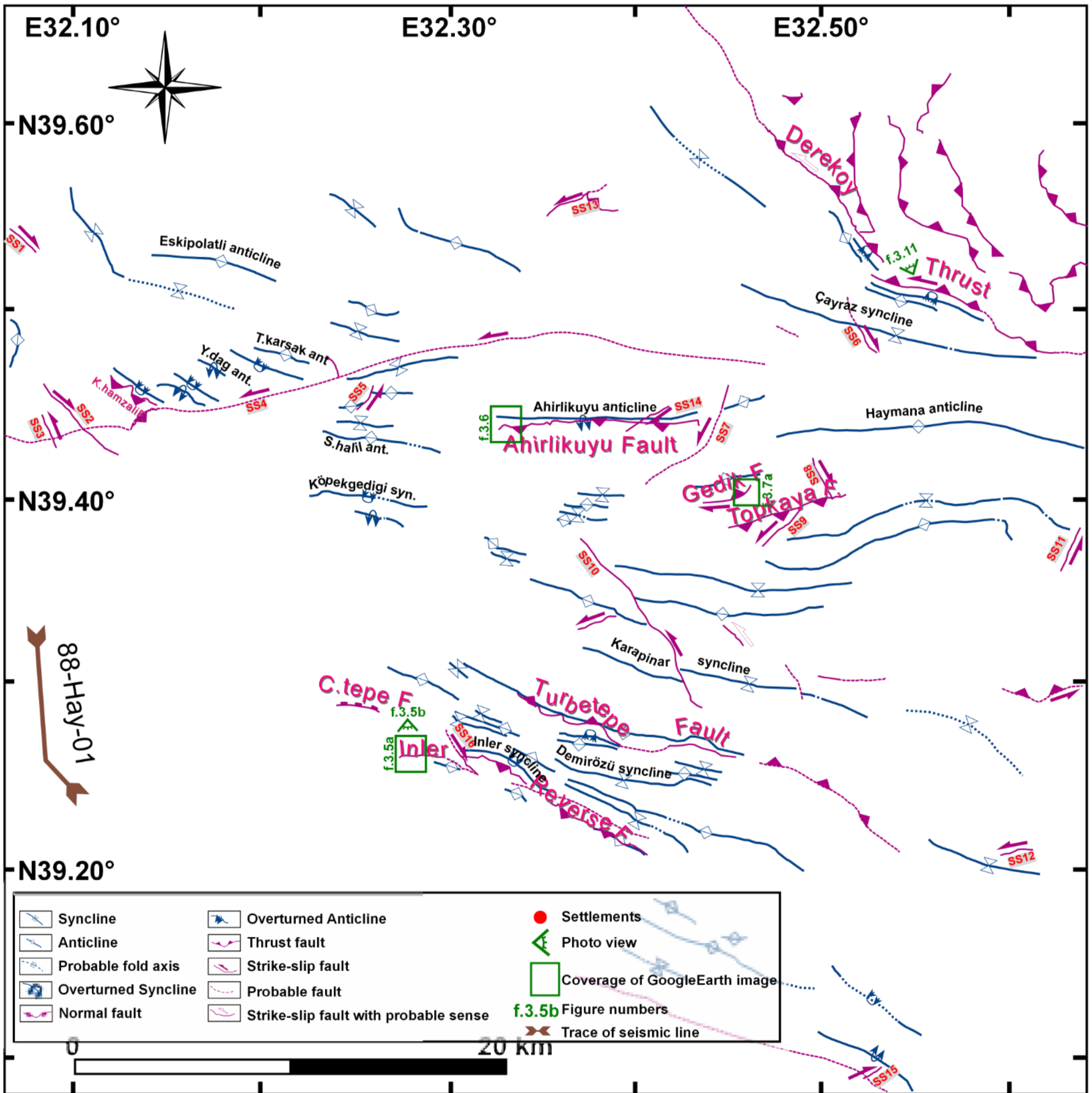


Figure A.3: Structural Map of the Haymana Basin